NUMERICAL STUDIES ON DYNAMIC BEHAVIOR OF REINFORCED SOIL RETAINING WALLS

A Thesis Submitted

in Partial Fulfillment of the Requirements

for the Degree of

DOCTOR OF PHILOSOPHY

by

ARUP BHATTACHARJEE

DEPARTMENT OF CIVIL ENGINEERING
INDIAN INSTITUTE OF TECHNOLOGY GUWAHATI
GUWAHATI

JULY 2014

CERTIFICATE

This is to certify that the thesis entitled "**Numerical Studies on Dynamic Behavior of Reinforced Soil Retaining Walls**" submitted by **Arup Bhattacharjee** (Roll No.08610406), to the Indian Institute of Technology Guwahati, for the award of degree of Doctor of Philosophy in Civil Engineering is a record of bonafide research work carried out by him under my supervision and guidance. The thesis work, in my opinion, has reached the requisite standard fulfilling the requirement for the degree of Doctor of Philosophy.

The results contained in this thesis have not been submitted in part or full to any other University or Institute for award of any degree or diploma.

Dr. A. Murali Krishna
Associate Professor
Department of Civil Engineering
Indian Institute of Technology Guwahati
Guwahati-781039, India

STATEMENT

I do hereby declare that the matter embodied in this thesis is the result of investigations carried out by me in the Department of Civil Engineering, Indian Institute of Technology Guwahati, Guwahati, Assam, India.

In keeping with the general practice of reporting scientific observations, due acknowledgements have been made wherever the work described is based on findings of other investigators.

Arup Bhattacharjee

Guwahati
Date :

ACKNOWLEDGEMENTS

I owe sincere gratitude to many people for having the pleasure of submitting the Thesis.

I have great pleasure in expressing my deep sense of gratitude to my thesis supervisor and research guide, ***Dr. A. Murali Krishna*** *for his inspiring guidance and constant encouragement throughout the course of my research work. I am grateful to him for sparing his valuable time and effort at all stages of the work. I am very much obliged to him for all the help, affection and kind suggestions, which helped me to complete the work successfully.*

I wish to express my sincere thanks to the Commissioner (Education), Govt. of Assam, Dispur, Assam (India) for permitting me to pursue research work in IIT Guwahati as a Part Time Student. I also wish to thank the Principal, Jorhat Engineering College, and HOD, Civil Engineering, Jorhat Engineering College to allow me to pursue research work with regular academic and administrative work during this period.

I am thankful to Prof. Arup Kumar Sarma, Head of Civil Engineering Department and Prof. Anjan Dutta and Prof. Sajal K. Deb, former Heads' of Civil Engineering, IIT Guwahati, for their support and permission to pursue this research programme. My thanks due to the Civil Engineering office staff for their constant help.

I am indebted to Doctoral Committee members Prof. Anjan Dutta, Dr. Sreedeep. S and Dr. K.S.R.Krishna Murthy for sparing their valuable time in reviewing my work and valuable suggestions.

My sincere thanks to my friends Animesh, Pranab, Trptimoni, Abhijit, Arghadeep, Shiv, Bali Reddy, Pawan, Awadesh, Prashant, Chandan, Bablu for their companionship and constant encouragement.

I am extremely grateful to my parents for their encouragement and moral support throughout my education life, without which I could not have seen the light of the day.

The most important factors to acknowledge are the greatest support and love I received from my wife, Anosua and our loving daughter, Ayantika (Diti).

Finally, I thank the Almighty for providing strength with blessings in every step taken by me.

Arup Bhattacharjee

ABSTRACT

Applications of reinforced soil retaining walls have increased enormously in last three decades. Satisfactory performances of reinforced soil retaining structures during recent earthquakes, in comparison with conventional retaining walls, are reported by several researchers. However, some failures of reinforced soil structures during earthquake are also reported. Thus, dynamic behavior of reinforced soil retaining walls is of research interest to several researchers. Most studies conducted by different researchers, using small scale laboratory studies and numerical analyses, mainly focused on parameters like: wall displacements, backfill settlements, lateral earth pressures, reinforcement loads and acceleration amplifications. But, very little was reported in literature on the strain behavior of soil and reinforcement. The objective of the present research programme is to investigate the seismic response of reinforced soil retaining walls (RSRW) through numerical simulations to provide insight on their behavior with different wall configurations subjected to different excitations. The main focus is to determine the strains developed in backfill soil and reinforcement members and to compare with horizontal and vertical displacements along the backfill for determining probable deformation zones within the backfill.

To achieve the objective, numerical models for two types of reinforced soil wall systems are developed using a finite difference method software FLAC^{3D} (Fast Lagrangian Analysis of Continua 3D). Flexible wrap-faced and full height rigid-faced walls are considered for the study. Initially, numerical models of laboratory scale walls, reported in literature, are developed for validation. Validated numerical models are then extended for simulating full scale models for extensive parametric studies with idealized sinusoidal excitations. Parametric studies are conducted to study the

influence of different parameters like reinforcement length, reinforcement stiffness, number of reinforcing layers and backfill soil parameters on response of wall, backfill and reinforcement. The wall behavior has been presented in terms of displacements, accelerations and horizontal pressures. Strain behavior of RSRW in terms of octahedral shear strains developed in backfill soil; and axial strains developed in reinforcements have been analyzed. The strains determined are compared with the horizontal and vertical displacements along the length of wall to observe the deformation zones in backfill soil. The probable location of deformation zones based on octahedral shear strain developed on backfill soil. Studies are also conducted for both the wall models subjected to real earthquake excitations to observe the effect of frequency content on response.

The models developed were sensitive to different material properties like backfill friction and dilation angles, stiffness of reinforcement material and soil-reinforcement interface parameters. From the full scale model studies, it is observed that, three distinct modes of deformation zones: shear deformation within reinforced zones, relative compaction near the end of reinforcements and compound deformation zones extending to the retained backfill zone, are prominent for wrap-faced wall. The length of compound deformation zones depend on length of reinforcement and backfill soil friction angles. The shear deformations within reinforced zone depend on reinforcement stiffness and number of layer of reinforcement. The strains developed in reinforcements are influenced by strain developed within soil element, extent of compound deformation zones into retained backfill, interaction between soil and reinforcement, reinforcement stiffness and inertia force developed within reinforced zone. Providing longer reinforcement in the top 1/3 to ½ height of the wall showed the performance similar to the one will full height longer reinforcement.

In full height rigid-faced wall models two types of strained zones: high strain zone near the wall facing; and low strained zone extending into the retained backfill. Larger localised vertical and horizontal displacements near the wall facing indicate high strain zone (about 1 to 2%); low strain zone was marked by the extent of the retained backfill experiencing elastic strain level (around 0.3%). These zones differ from the zones identified in flexible wrap-faced wall model. The soils near the wall facing are settled due to development of high strain near facing and increase in horizontal and vertical displacements in rigid faced walls. The length of reinforcement, number of layers of reinforcements and reinforcement stiffness and backfill soil do not change significantly the deformation zones, other than small changes in vertical settlement near the wall facing. The reinforced soil walls deformation modes and strains in reinforcement depend on type and flexibility of facing. When a reinforced retaining wall is being subjected to real earthquake excitation, which contains different frequency content, amplitudes at frequency close to the fundamental frequency of the wall will be amplified by the most. The maximum displacement of the structure and horizontal pressure on wall and its time of occurrence during earthquake excitation and deformation zones formed subjected to different earthquake excitation are different based on frequency content of the earthquakes. Type of facing plays significant role on the response of reinforced soil retailing structures. The results compared for wrap-faced and rigid-faced walls; and rigid-faced walls with different facing stiffness values support this observation.

TABLE OF CONTENTS

Abstract ……i

Table of Contents……...iv

List of Figures ……viii

List of Tables……....xvii

Notation and Abbreviations……...xviii

Chapter 1. Introduction **1**

1.1 Reinforced Soil Retaining Structures 1

1.2 Seismic Performance of GRS Retaining Walls 3

1.3 Objectives of the Present Study 4

1.4 Organization of thesis 5

Chapter 2. Literature Review **7**

2.1 Introduction 7

2.2 Reinforced Soil Structures: Behavior, Analysis and Design 7

2.3 Static Studies on GRS Retaining Walls 12

2.4 Dynamic Studies on GRS Retaining Walls 12

2.4.1 Physical model studies 13

2.4.2 Analytical studies 22

2.4.3 Numerical model studies 29

2.5 Critical Appraisal 41

2.6 Objectives and Detailed Scope of Work 42

2.7 Summary 44

Chapter 3. Description of Numerical Programme and Model Properties **45**

3.1 Introduction 45

3.2 Overview of FLAC^{3D} 45

3.2.1 FISH programming 47

3.2.2 Structural elements 48

3.2.3 Dynamic modeling in FLAC^{3D} 48

3.3 Material Models for Numerical Simulation 51

3.3.1 Backfill soil 51

3.3.2 Geosynthetic reinforcement 57

3.3.3 Facing elements 60

3.3.4 Interface elements 60

3.4 Soil-Reinforcement Interaction 61

3.4.1 Laboratory pullout tests 62

3.4.2 Numerical simulation of pullout tests 67

3.3 Summary 71

Chapter 4. Studies on Wrap-Faced Walls 73

4.1 Introduction 73

4.2 Developement of Numerical Models 73

4.2.1 Target physical model 74

4.2.2 Development of numerical grid 76

4.2.3 Selection of grid size 80

4.2.4 Sensitivity analysis 81

4.2.5 Validation of numerical model 87

4.2.6 Dynamic response of wrap-faced walls: displacements and strains 89

4.3 Seismic Behavior of Full Scale model 91

4.3.1 Response of full scale wall after dynamic excitation 92

4.4 Parametric Studies 98

4.4.1 Effect of length of reinforcement 99

4.4.2 Effect of number of reinforcing layers 105

4.4.3 Effect of backfill (angle of internal friction) 110

4.4.4 Effect of reinforcement stiffness 114

4.4.5 Effect of frequency of excitation 118

4.4.6 Effect of seismic acceleration 121

4.5 Response of Designed Wrap-Faced Wall Model 124

4.6 Summary 130

Chapter 5. Studies on Rigid-Faced Walls 132

5.1 Introduction 132

5.2 Developement of Numerical Models of Rigid-Faced Walls 132

5.2.1 Target physical model 132

5.2.2 Development of numerical grid 134

5.2.3 Validation of numerical model 139

5.2.4 Sensitivity analysis 142

5.2.5 Dynamic response of rigid-faced walls: Displacements and Strains 145

5.3 Seismic Respnse of Full Scale Rigid-Faced Wall Models 147

5.3.1 Rigid-faced wall subjected to dynamic excitation 147

5.4 Parametric Studies 152

5.4.1 Effect of backfill friction angle 153

5.4.2 Effect of reinforcement stiffness 155

5.4.3 Effect of length of reinforcing layers 157

5.4.4 Effect of number of reinforcing layers 159

5.4.5 Effect of facing stiffness 161

5.4.6 Effect of frequency of excitation 163

5.4.7 Effect of acceleration of dynamic excitation 165

5.5 Comparison of Wrap-Faced and Rigid-Faced Walls Behaviour 169

5.6 Summary 174

Chapter 6. Model Walls Subjected To Different Earthquake Motions 175

6.1 Introduction 175

6.2 Fundamental Frequency of Model Walls....177

6.3 Earthquake Ground Motions....178

6.4 Model Response for Earthquake Motions....179

6.5 Summary....197

Chapter 7. Concluding Remarks....198

7.1 Summary of the thesis....198

7.2 Conclusions....199

7.2.1 Studies on Wrap-Faced Reinforced Soil Walls....199

7.2.2 Studies on Rigid-Faced Reinforced Soil Walls....201

7.2.3 Reinforced soil wall subjected to different earthquake motions....202

7.3 Major contributions of the present study....203

7.4 Limitations of present study....204

7.5 Scope for Future Research....205

References....206

Appendix A. Hyperbolic Model Parameters of Sand....219

Appendix B. Stability Analysis of Reinforced Soil Walls....224

Appendix C. List of publications....232

LIST OF FIGURES

Fig. 1.1 Application of reinforced soil structures: (a) highways; (b) bridge abutments; and (c) slope stability (www.reinforcedearth.com) 2

Fig. 1.2 Typical system of reinforced soil structures: (a) wrap-faced wall (b) modular block wall and (c) full-height rigid-faced wall (redrawn from Holtz 2001).....2

Fig. 2.1 Potential external failure mechanism for reinforced soil wall (FHWA 2001)10

Fig. 2.2 Potential internal failure mechanism of reinforced soil wall (FHWA 2001) .10

Fig. 2.3 Cross-section of geogrid wall suffered some damage during 1995 Hyogo-ken Nanbu Earthquake (Tatsuoka et al. 1996).....13

Fig. 2.4 Large deformation in geosynthetic reinforced modular block wall during Chi-Chi (Taiwan) Earthquake (after Huang, 2000) 14

Fig. 2.5 Test setup and cross section of model wall considered by Ramakrishna et al. (1998).....16

Fig. 2.6 Different types of retaining wall model walls on level ground (after Watanabe et al. 2003) 17

Fig. 2.7 Reinforced wall model configuration (after El-Emam and Bathurst 2004) ..18

Fig. 2.8 Model configuration and instrumentation adopted for reduced scale RS walls (after El-Emam and Bathurst 2005).....18

Fig. 2.9 Test slope before and after shaking test (after Lo Grasso et al. 2005) 19

Fig. 2.10 Typical wall model configuration adopted by Ling et al. (2005a).....20

Fig. 2.11 Visual observation of deformation (a) surface cracking behind reinforced zone (b) settlement behind block facing (after Ling et al. 2005a).....20

Fig. 2.12 Schematic diagrams of typical test wall configurations and instrumentation adopted by Latha and Krishna (2008).....21

Fig. 2.13 Calculation of dynamic earth pressure under seismic loading (after Bathurst and Cai, 1995).....23

Fig. 2.14 Calculation of tensile load in a reinforcement layer due to dynamic earth pressure and wall inertia (after Bathurst and Cai, 1995) 23

Fig. 2.15 Direct sliding of reinforced soil retaining wall (after Ling, 2001) 24

Fig. 2.16 Failure mechanism and force equilibrium in multi-wedge method (after Huang and Wang, 2005) 26

Fig. 2.17 Reinforced wall with kinematics of deformation of the reinforcement (after Reddy et al., 2008) 27

Fig. 2.18 Finite element mesh for simulation of segmental retaining wall (after Cai and Bathurst, 1995) 32

Fig. 2.19 Finite difference mesh (using FLAC) of geosynthetic reinforced soil wall (after Bathurst and Hatami, 1998) 33

Fig. 2.20 Influence of reinforcement stiffness, reinforcement length and base condition on maximum wall displacement (after Bathurst and Hatami, 1998) 33

Fig. 2.21 Normalized maximum lateral displacement of wall crest with normalized frequency (after Hatami and Bathurst, 2000) 34

Fig. 2.22 Details of finite element mesh of segmental reinforced wall (after Helwany et al., 2001) 35

Fig. 2.23 Finite element mesh adopted by Ling et al. (2005b) 35

Fig. 2.24 Reinforcement loads of GRS walls subject to seismic loading at end of construction (EOC) and 10 years afterward (after Liu 2009) 36

Fig. 2.25 Finite element mesh used for numerical simulation of three wall models (after Lee et al. 2010) 36

Fig. 2.26 Wall face peak horizontal displacement comparison (after Lee et al. 2010) 37

Fig. 2.27 Plastic shear strains within soil for at peak acceleration and at end of shaking (after Liu et al. 2011) 38

Fig. 2.28 Plastic shear strain within soil for reinforcement length (L) 0.5H and L=1.0H (after Liu et al. 2011) 38

Fig. 2.29 Numerical grid considered for reinforced soil retaining wall model (after Krishna and Latha 2012) 39

Fig. 2.30 Finite element mesh of wrap-faced wall (after Liu and Ling 2012) 40

Fig. 2.31 Octahedral shear strain in reinforced soil walls with different types of sands as backfill (after Liu and Ling, 2012) 40

Fig. 3.1 Basic calculation sequence in FLAC^{3D} (Itasca 2008) 47

Fig. 3.2 Numerical model of triaxial test sample (dia 38 mm & height 76 mm) 53

Fig. 3.3 Comparison of results between numerical and physical triaxial tests at different confining pressure 54

Fig. 3.4 Behavior of soil in numerical triaxial compression 55

Fig. 3.5 Non-linear hysteretic stress-strain model of granular soil: (a) stress-strain cap; (b) unload-reload cycle (modified after Cai and Bathurst 1995) 56

Fig. 3.6 Stresses acting on geogrid surrounding a node (Itasca 2008) 59

Fig. 3.7 Grain size distribution of sand used in the study.....63

Fig. 3.8 Comparison numerical and physical triaxial test results on sand at different confining pressures 64

Fig. 3.9 Load elongation response of woven geotextile 65

Fig. 3.10 Pullout box along with instrumentation 66

Fig. 3.11 Pullout response of composite geotextile at different confining pressure....66

Fig. 3.12 Mesh for numerical model of pullout stress 69

Fig. 3.13 Pullout stress versus displacement for surcharge of (a) 20 kPa (b) 33 kPa and (c) 67 kPa for numerical result with different interface parameter and experimental result.....70

Fig. 3.14 Pullout stress versus displacement for surcharge of (a) 20 kPa (b) 33 kPa and (c) 67 kPa for numerical simulation with different angle of internal friction of soil.....71

Fig. 4.1 Physical model configuration of wrap-faced wall (after Krishna and Latha, 2007) 75

Fig. 4.2 Typical variation of horizontal displacements with time in physical model test (after Latha and Krishna, 2008).....75

Fig. 4.3 Accelerations at different elevations from the physical model test (after Krishna and Latha 2008).....76

Fig. 4.4 Development of numerical grid of wrap-faced wall.....77

Fig. 4.5 Boundary conditions of the model in X-Y plane and Z-X plane.....80

Fig. 4.6 Model wall with free field boundary condition before dynamic loading`.....80

Fig. 4.7 Sensitivity of grid size on model response 81

Fig. 4.8 Typical sinusoidal dynamic excitation components (a = 0.2g; f = 3 Hz).....83

Fig. 4.9 Typical displacement histories at different elevation for acceleration 0.2g and frequency 3Hz.....84

Fig. 4.10 Typical acceleration histories obtained in numerical simulation 84

Fig. 4.11 Sensitivity of numerical model with respect to backfill friction angle: a) Displacement profiles; b) Acceleration amplification factor; c) Incremental pressure 85

Fig. 4.12 Sensitivity of numerical model with respect to backfill dilation angle: a) Displacement profiles b) Acceleration amplification c) Incremental pressure 86

Fig. 4.13 Sensitivity of numerical model with respect to reinforcement stiffness: a) Displacement profiles b) Acceleration amplification c) Horizontal pressure..86

Fig. 4.14 Sensitivity of numerical model with respect to soil-reinforcement interface stiffness: a) Displacement profiles b) Acceleration amplification c) Horizontal pressure 87

Fig. 4.15 Comparison of results of numerical and physical model tests (a = 0.2g, L_{rein}/H =0.7, N_L =4) (a) horizontal displacement, (b) RMSA amplification factor and (c) incremental pressure.....90

Fig. 4.16 Comparison of results of numerical and physical model tests for different number of reinforcement layers (a = 0.2g, f = 3 Hz and L_{rein}/H=0.7) 90

Fig. 4.17 (a)Horizontal displacement and (b) vertical displacements along length of backfill after 20 cycles (a =0.2g, f =5Hz, L_{rein}/H=0.7, N_L=4).....91

Fig. 4.18 Variation of $\Delta\gamma_{oct}$ in soil along length of backfill (a) between two reinforcement layers (b) at reinforcement level (a =0.2g, f =5Hz, L_{rein}/H=0.7, N_L=4).....91

Fig. 4.19 Numerical grid for full scale wrap-faced wall (a) before support removal (b) after support removal 92

Fig. 4.20 Variation of (a) horizontal displacement (b) vertical displacement (c) RMSA amplification factor and (d) Horizontal pressure for wall subjected to dynamic excitation (a = 0.2g, f = 5Hz, N_L = 4 and L_{rein}/H = 0.7).....93

Fig. 4.21 Octahedral shear strain, horizontal displacement and vertical displacement along the length of backfill after 20 cycles of dynamic excitation (a =0.2g, f =5Hz, L_{rein}/H=0.7, N_L =6).....95

Fig. 4.22 Contour of octahedral shear strain after 20 cycles of dynamic excitation (a=0.2g, f=5Hz, L_{rein}/H=0.7, N_L=6) 96

Fig. 4.23 Deformation zones of wrap-faced reinforced soil retaining wall after dynamic excitation.....96

Fig. 4.24 Incremental Octahedral shear strain on soil element and incremental axial strain on reinforcement after 20 cycles of dynamic excitation (a = 0.2g, f = 5Hz, L_{rein}/H=0.7, N_L=6) 97

Fig. 4.25 Overburden pressure acting on reinforcement at different elevations.....98

Fig. 4.26 Response of model wall with length of reinforcement lengths (0.7H, 1.0H and 1.2H) after dynamic excitation (a = 0.2g, f = 5Hz and N_L= 6).....100

Fig. 4.27 Variation of $\Delta\gamma_{oct}$, u and v along the length of backfill after dynamic excitation for model wall with L_{rein}/H=1.0 (a=0.2g, f=5 Hz, N_L=6).....101

Fig. 4.28 Comparison of octahedral shear strain at backfill with reinforcement length 0.7*H*, 1.0*H* and 1.2*H* subjected to dynamic excitation (a = 0.2g, f = 5 Hz and N_L = 4).....102

Fig. 4.29 Deformation zones of wrap-faced walls with (a) L_{rein}/H=0.7 (b) L_{rein}/H=1.0 103

Fig. 4.30 Contours of octahedral shear strain after dynamic excitation (a = 0.2g, f =5Hz, N_L = 6) (a) L_{rein}=0.7*H* ; (b) L_{rein} = 1.0*H* and; (c) L_{rein} =1.2*H* 103

Fig. 4.31 Variation of $\Delta\varepsilon_{a\_rein}$ after dynamic excitation with L_{rein}/H=0.7, 1.0 and 1.2 (a = 0.2g, f = 5Hz, N_L = 6) 104

Fig. 4.32 Response of model walls with 4,6 and 8 layers of reinforcement subjected to dynamic excitation (a = 0.2g, f = 5Hz and L_{rein} = 0.7*H*).....106

Fig. 4.33 Variation of $\Delta\gamma_{oct}$, u and v along the length of backfill after dynamic excitation for N_L=4 (a=0.2g, f=5 Hz, L_{rein}/H=0.7*H*) 106

Fig. 4.34 Variation of $\Delta\gamma_{oct}$, u and v along the length of backfill after dynamic excitation for N_L=8 (a=0.2g, f=5 Hz, L_{rein}/H=0.7*H*) 107

Fig. 4.35 Comparison of $\Delta\gamma_{oct}$ for walls with 4, 6 and 8 layers of reinforcement (a = 0.2g, f = 5Hz and L_{rein}/H = 0.7).....108

Fig. 4.36 Contour of octahedral shear strain after 20 cycles of dynamic excitation (a = 0.2g, f = 5Hz and L_{rein}/H = 0.7) with (a) N_L = 4 (b) N_L = 6 (c) N_L = 8.....109

Fig. 4.37 Deformation zones of wrap-faced reinforced soil retaining wall after dynamic excitation with no. of reinforcing layer (a) 4 layers (b) 8 layers.....110

Fig. 4.38 Variation of $\Delta\varepsilon_{a\_rein}$ after dynamic excitation (a=0.2g, f=5Hz, L_{rein}/H=0.7) for walls with (a) N_L=4 (b) N_L=6 (c) N_L=8.....111

Fig. 4.39 Response of model walls with backfill friction angles 30°, 38° and 43° subjected to dynamic excitation (a = 0.2g, f = 5Hz, N_L = 6and L_{rein} = 0.7*H*) 112

Fig. 4.40 Comparison of $\Delta\gamma_{oct}$ for walls with backfill friction angle 30°, 38° and 43° after dynamic excitation (a = 0.2g, f = 5Hz and L_{rein}/H = 0.7) 113

Fig. 4.41 Incremental axial strain in reinforcement after dynamic excitation (a=0.2g, f=5Hz, L_{rein}/H=0.7) with backfill friction angle 30°, 38° and 43° 114

Fig. 4.42 Response of model walls with backfill different reinforcement stiffness subjected to dynamic excitation (a = 0.2g, f = 5Hz, N_L = 8 and L_{rein} = 0.7*H*) 115

Fig. 4.43 Octahedral shear strain, horizontal and vertical displacement along the length of backfill with reinforcement stiffness 5.2 kN/m (a=0.2g, f=5 Hz, L_{rein}/H=0.7*H*, N_L=8) 116

Fig. 4.44 Octahedral shear strain, horizontal and vertical displacement along the length of backfill with reinforcement stiffness 152 kN/m (a=0.2g, f=5 Hz, L_{rein}/H=0.7H, N_L=8) 116

Fig. 4.45 Comparison of $\Delta\gamma_{oct}$ at backfill for wall with reinforcement stiffness subjected to dynamic excitation (a = 0.2g, f = 5Hz and L_{rein}/H = 0.7, N_L=8) 117

Fig. 4.46 Incremental axial strain on reinforcement after dynamic excitation (a=0.2g, f=5Hz, L_{rein}/H=0.7, N_L=8) with reinforcement stiffness 5.2, 100 and 152 kN/m 118

Fig. 4.47 Response of model walls subjected to dynamic excitation at different frequencies (a = 0.2g, N_L = 6and L_{rein} = 0.7H) 119

Fig. 4.48 Comparison of octahedral shear strain at backfill for walls subjected to dynamic excitations of frequency 3 Hz, 5 Hz and 7 Hz (a = 0.2g and L_{rein}/H = 0.7) 120

Fig. 4.49 Incremental axial strain on reinforcement for walls subjected to dynamic excitation of 3 Hz, 5Hz, and 7 Hz frequencies (a = 0.2g and N_L = 6) 120

Fig. 4.50 Variation of (a) horizontal and (b) vertical displacement (c) RMSA amplification factor and (d) Horizontal pressure for walls subjected to dynamic excitation 0.2g, 0.3g and 0.4g (f=5 Hz, L_{rein}/H = 0.7, N_L = 6) 122

Fig. 4.51 Comparison of octahedral shear strain at backfill for walls subjected to dynamic excitations of acceleration 0.2g, 0.3g and 0.4g (f=5 Hz, L_{rein}/H = 0.7, N_L = 6) 123

Fig. 4.52 Incremental axial strain on reinforcement for walls subjected to dynamic excitations of acceleration 0.2g, 0.3g and 0.4g (f=5 Hz, L_{rein}/H = 0.7, N_L = 6) 123

Fig. 4.53 Octahedral shear strain, horizontal displacement and vertical displacement along the length of backfill after 20 cycles of dynamic excitation (a=0.2g, f=5 Hz, L_{rein}/H=0.7H, N_L=12) 126

Fig. 4.54 Incremental axial strain on reinforcement after dynamic excitation (a=0.2g, f=5Hz, L_{rein}/H=0.7, N_L = 12) 126

Fig. 4.55 Wrap-faced wall with reinforcement length (a) 0.7H (b) 1.0H and (c) top three layers 1.0H and other layers 0.7H (d) top seven layers 1.0H and others 0.7H 128

Fig. 4.56 Response of full height model walls with different reinforcement configurations subjected to dynamic excitation (a = 0.2g, f = 5Hz, N_L = 12) 129

Fig. 4.57 Comparison of octahedral shear strain at backfill for wall with reinforcement 0.7H, 1.0H , 2L-1.0H and 6L-1.0H subjected to dynamic excitation (a = 0.2g, f = 5Hz) 130

Fig. 5.1 Test arrangement of rigid face reinforced retaining wall in physical model tests (after Krishna and Latha 2009) 134

Fig. 5.2Typical horizontal displacements histories of unreinforced wall with number of cycles (after Krishna and Latha, 2009) 135

Fig. 5.3Typical acceleration histories of reinforced wall with number of cycles (after Krishna and Latha, 2009) 135

Fig. 5.4 Grid adopted for numerical simulation (a) static simulation (b) dynamic simulation 137

Fig. 5.5 Boundary conditions of the model (not to scale) in X-Y plane (plan) and Z-X plane (side elevation) 138

Fig. 5.6 Typical displacement histories at different elevations during dynamic excitation (a= 0.2g, f=3Hz, L_{rein}/H = 0.7 and N_L=4) 140

Fig. 5.7 Typical acceleration histories at different elevations in numerical simulation 140

Fig. 5.8 Comparison of results from numerical and physical model tests on unreinforced and reinforced (a = 0.2g, f= 3 Hz and N_L = 4): a) Displacement profiles b) Acceleration amplification and c) Incremental pressure 141

Fig. 5.9 Sensitivity of numerical model with respect to backfill friction angle: a) Displacement profiles b) Acceleration amplification c) Incremental pressure 143

Fig. 5.10 Sensitivity of numerical model with respect to backfill dilation angle: a) Displacement profiles b) Acceleration amplification c) Incremental pressure 143

Fig. 5.11 Sensitivity of numerical model with respect to stiffness of reinforcement: a) Displacement profiles b) Acceleration amplification c)Horizontal pressure. 144

Fig. 5.12 Sensitivity of numerical model with respect to number of reinforcing layers: a) Displacement profiles b) Acceleration amplification c) Incremental pressure 144

Fig. 5.13 $\Delta\gamma_{oct}$, u and v along length of backfill after dynamic excitation (a = 0.2g and f = 3Hz) for unreinforced wall 146

Fig. 5.14 $\Delta\gamma_{oct}$, u and v along length of backfill of dynamic excitation for reinforced wall (a = 0.2g and f = 3Hz, L_{rein}/H = 0.7 and N_L = 4) 146

Fig. 5.15 Typical displacement histories at different elevation of rigid-faced wall .. 149

Fig. 5.16 Horizontal, vertical displacements, RMSA amplification factor and horizontal pressure at different elevations after dynamic excitation (a=0.2g, f = 5Hz L_{rein}/H=0.7, N_L=4) 149

Fig. 5.17 $\Delta\gamma_{oct}$, u and v along the length of backfill after 20 cycles of dynamic excitation (a=0.2g, f=5Hz, L_{rein}/H=0.7, N_L=4).....150

Fig. 5.18 Incremental axial strain along length of reinforcement after dynamic excitation (a = 0.2g, f = 5Hz, L_{rein}/H = 0.7 and N_L = 4).....150

Fig. 5.19 Contour of octahedral shear strain after dynamic excitation.....152

Fig. 5.20 Deformation zones of rigid-faced reinforced soil retaining wall after dynamic excitation.....152

Fig. 5.21 Response of model walls with backfill friction angles 30°, 38° and 43° subjected to dynamic excitation (a = 0.2g, f = 5Hz and L_{rein}/H = 0.7, N_L=4) 154

Fig. 5.22 Comparison of $\Delta\gamma_{oct}$ at backfill for wall with backfill friction angle 30°, 38° and 43° after dynamic excitation (a = 0.2g, f = 5Hz and L_{rein}/H = 0.7, N_L=4) 154

Fig. 5.23 $\Delta\varepsilon_{a\_rein}$ on reinforcement after dynamic excitation (a=0.2g, f=5Hz and L_{rein}/H = 0.7) with backfill friction angle 30°, 38° and 43°.....155

Fig. 5.24 Comparison of $\Delta\gamma_{oct}$ for walls with reinforcement stiffness 5.2, 100 and 152 kN/m after dynamic excitation (a = 0.2g, f = 5Hz and L_{rein}/H = 0.7).....156

Fig. 5.25 Comparison of $\Delta\gamma_{oct}$ at backfill for wall with reinforcement stiffness 5.2, 100 and 152 kN/m after dynamic excitation (a = 0.2g, f = 5Hz and L_{rein}/H = 0.7, N_L=4).....156

Fig. 5.26 $\Delta\varepsilon_{a\_rein}$ on reinforcement after dynamic excitation (a=0.2g, f=5Hz and L_{rein}/H = 0.7) with reinforcement stiffness 5.2, 100 and 152 kN/m 157

Fig. 5.27 Response of model walls with L_{rein}/H = 0.7, 1.0 and 1.2 subjected to dynamic excitation (a = 0.2g, f = 5 Hz and N_L=4).....158

Fig. 5.28 Comparison of octahedral shear strain at backfill for wall with L_{rein}/H = 0.7 and 1.0 after dynamic excitation (a = 0.2g, f = 5 Hz and N_L=4).....159

Fig. 5.29 Response of model walls for wall with 4, 6 and 8 layers of reinforcement subjected to dynamic excitation (a = 0.2g, f = 5Hz and L_{rein}/H = 0.7) 160

Fig. 5.30 Comparison of $\Delta\gamma_{oct}$ at backfill for wall with 4, 6 and 8 layers of reinforcement after dynamic excitation (a = 0.2g, f = 5Hz and L_{rein}/H = 0.7) 161

Fig. 5.31 Response of model walls with backfill different facing stiffness 27.4 GPa and 15.2 after dynamic excitation (a = 0.2g, f = 5 Hz and L_{rein}/H = 0.7) 162

Fig. 5.32 Comparison of v at backfill for wall with facing stiffness 27.4 GPa and 15.2 GPa after dynamic excitation (a = 0.2g, f = 5Hz and L_{rein}/H = 0.7) 163

Fig. 5.33 Response of model walls with backfill different frequency of excitation (a = 0.2g and L_{rein}/H = 0.7).....164

Fig. 5.34 Comparison of $\Delta\gamma_{oct}$ at backfill for walls subjected to dynamic excitations of frequency 3 Hz, 5 Hz and 7 Hz (a = 0.2g and L_{rein}/H = 0.7) 165

Fig. 5.35 Input base stepped acceleration 165

Fig. 5.36 Horizontal and vertical displacement at different elevation for different input acceleration 167

Fig. 5.37 The octahedral shear strain on backfill soil after 2 sec dynamic excitation of (a) 0.2g (b) 0.4g (c) 0.5g and (d) 0.6g. (f = 3 Hz, L_{rein}/H = 0.7 and N_L= 4)...167

Fig. 5.38 $\Delta\gamma_{oct}$ along the length of backfill at different excitation level 168

Fig. 5.39 $\Delta\varepsilon_{a\_rein}$ along the length of reinforcement at different excitation level.....169

Fig. 5.40 Response of wrap and rigid-faced walls with after 20 cycles of dynamic excitation (a=0.2g, f = 5Hz L_{rein}/H=0.7, N_L=6).....170

Fig. 5.41 Octahedral shear strain, horizontal displacement and vertical displacement along the length of backfill for (a) wrap-faced wall and (b) rigid-faced wall after 20 cycles of dynamic excitation of 0.2g and 5Hz (a=0.2g, f=5Hz, L_{rein}/H=0.7, N_L=6).....172

Fig. 5.42 Axial stress along the length of reinforcement at different excitation level (a=0.2g, f=5 Hz, L_{rein}/H = 0.7 and N_L= 6).....173

Fig. 6.1 Earthquake ground motion records (a) Actual histories; (b) Scaled histories for 10 second duration and 0.3 g PGA and, (c) FFTs of the scaled ground motions.....180

Fig. 6.2 Acceleration applied at base of model (A0) and acceleration recorded at top of backfill (A3) for rigid and wrap-faced walls for different earthquakes 182

Fig. 6.3 Fast Fourier Transformation (FFT) of acceleration applied at base of model (A0); and recorded at top of backfill (A3) for rigid and wrap-faced walls for different earthquakes.....183

Fig. 6.4 Transfer functions between accelerations at base of wall (A0) and top of backfill (A3) for (a) Loma Prieta, (b) Parkfield and (c) Bhuj earthquakes....184

Fig. 6.5 Transfer function between accelerations at base of wrap-faced wall (A0) and top of backfill (A3) for (a) Loma Prieta and (b) Parkfield earthquakes 186

Fig. 6.6 Accelerations at base of model (A0) and at top of backfill (A2) and their corresponding FFTs of 3m high model subjected to scaled Bhuj earthquake motion 186

Fig. 6.7 Transfer function between accelerations at base of wall (A0) and top of backfill (A2) of 3 m high model subjected to scaled Bhuj earthquake motion 187

Fig. 6.8 Horizontal displacement, RMSA amplification factor and horizontal pressure for (a)rigid-faced wall (b)wrap-faced wall subjected to different scaled earthquake excitations.....189

Fig. 6.9 Comparison of displacement histories during dynamic excitation of different earthquakes for (a) rigid-faced walls (b) wrap-faced walls 192

Fig. 6.10 Comparison of incremental horizontal pressure on (a) rigid-faced wall (b) wrap-faced wall during dynamic excitation for different earthquakes 193

Fig. 6.11 Contours octahedral shear strains at the end of different excitations 195

Fig. 6.12 $\Delta\gamma_{oct}$ along the length of backfill of rigid-faced wall subjected to Kobe EQ and Parkfield EQ.....195

Fig. 6.13 Contours octahedral shear strains at the end of different excitations 196

Fig. 6.14 $\Delta\gamma_{oct}$ along the length of backfill of wrap-faced wall subjected to Kobe EQ and Parkfield EQ.....196

LIST OF TABLES

Table 2.1 Design codes for seismic design of GRS walls (modified after Koseki et al. 2006) 9

Table 2.2 Summary of numerical studies seismic behavior of RS retaining structures. 30

Table 3.1 Soil Physical Characteristics 63

Table 3.2 Hyperbolic model parameters obtained from triaxial test 64

Table 3.3 Material properties used in numerical model for pullout tests 68

Table 4.1 Material properties used in numerical simulation for sensitivity analysis 82

Table 4.2 Comparison of results from physical and numerical model 88

Table 4.3 List of parameters considered for parametric studies 99

Table 4.4 Static and dynamic Factors of safety values for full scale model 124

Table 5.1 Material properties used in numerical simulation 139

Table 5.2 Comparison of results from physical and numerical model 142

Table 5.3 Material properties used for sensitivity analysis 142

Table 5.4 Static and dynamic factors of safety for full scale rigid-faced model 147

Table 5.5 List of parameters considered for parametric studies 152

Table 6.1 Static and dynamic Factors of safety values for wrap and rigid-faced walls 176

Table 6.2 Fundamental frequency values of reinforced soil wall models 178

Table 6.3 Ground motion parameters of actual earthquake records 179

Table 6.4 Ground motion parameters and responses of scaled earthquake excitations 190

NOTATIONS AND ABBREVIATIONS

NOTATIONS

English symbols

a	Acceleration (m/s^2)
B	Length of backfill (m)
B_t	Tangent bulk modulus (kN/m^2)
c	cohesion (kN/m^2)
C_c	Coefficient of curvature (dimensionless)
C_p	Speed of p-wave propagation (m/s)
C_s	Speed of s-wave propagation (m/s)
C_u	Uniformity coefficient (dimensionless)
D_{10}	size such that10% of soil finer than the size (mm)
D_{50}	size such that 50%of soil finer than the size (mm)
D_{60}	size such that 60% of soil finer than the size (mm)
E_t	Stress dependent elastic modulus (kN/m^2)
f	Frequency (Hz)
$FS_{overturing}$	Factors of safety of overturning (dimensionless)
$FS_{pullout}$	Factors of safety of pullout (dimensionless)
$FS_{rupture}$	Factors of safety of rupture (dimensionless)
$FS_{sliding}$	Factors of safety of sliding (dimensionless)
G	Shear modulus (kN/m^2)
G_{max}	Initial shear modulus (kN/m^2)
H	Height of reinforced soil wall (m)
K	Bulk modulus (kN/m^2)
K_b	Bulk modulus constant (dimensionless)
K_n	Modulus number (dimensionless)
k_n	Normal stiffness of interface ($kN/m^2/m$)
k_s	Shear stiffness of interface ($kN/m^2/m$)
L_{rein}	Length of reinforcement (m)
M_w	Moment magnitude of earthquake (Dimensionless)
n	Modulus number (dimensionless)
N_L	Number of reinforcement layers (Dimensionless)
p_a	Atmospheric pressure (kN/m^2)
R_f	Failure ratio (Dimensionless)
TF	Transfer function (Dimensionless)
u	Horizontal displacement (mm)
v	Vertical displacement (mm)

Greek symbols

ρ	Density of soil (kg/m^3)
λ	Wave length (m)
ϕ	Angle of internal friction (degree)
σ_1	Major principal stress (kN/m^2)
σ_3	Minor principal stress (kN/m^2)
γ_{oct}	Octahedral shear strain (kN/m^2)
σ_{oct}	Octahedral normal stress (kN/m^2)
τ_{oct}	Octahedral shear stress (kN/m^2)
τ_{max_oct}	Maximum octahedral shear stress (kN/m^2)

$\Delta\gamma_{oct}$	Incremental octahedral shear strain (%)
γ_{u_oct}	Octahedral shear strain at starting point of unloading (kN/m^2)
γ_{r_oct}	Octahedral shear strain at starting point of reloading (kN/m^2)
γ_{ε_oct}	Octahedral shear strain at present state (%)
σ_m	Mean normal stress (kN/m^2)
γ_{min}	Minimum unit weight (kN/m^3)
γ_{max}	Maximum unit weight (kN/m^3)
δ	Interface friction angle (degree)
$\Delta\varepsilon_{a\_rein}$	Reinforcement axial strain (%)
Δl	largest zone dimension (m)

ABBREVIATIONS

2D	Two dimension
3D	Three dimension
AASHTO	American Association of State Highway and Transportation Officials
ASTM	American Standard for Testing Materials
BS	British Standard
CFEM	Canadian Foundation Engineering Manual
CHBDC	Canadian Highway Bridge Design Code
EC	Euro Code
EQ	Earthquake
FDM	Finite Difference Method
FEM	Finite Element Method
FF	Fundamental frequency
FHR	Full height rigid
FHWA	Federal Highway Administration
FLAC	Fast Lagrangian Analysis of Continua
GF	Shape factor
GRS	Geosynthetic reinforced soil
IS	Indian Standard
MSE	Mechanically stabilized wall
NCMA	National Concrete Masonry Association
PGA	Peak ground acceleration
PGD	Peak ground displacement
PGV	Peak ground velocity
PWRC	Public Works Research Center
RMSA	Root mean square amplification
RSRW	Reinforced soil retaining wall
RTA	Roads and Traffic Authority
RTRI	Railway Technical Research Institute

Chapter 1. INTRODUCTION

1.1 REINFORCED SOIL RETAINING STRUCTURES

Earth retaining structures are invariably used in various projects that include highways, bridge abutments and slopes to support vertical or nearly vertical slopes of earth masses. The retaining structures may be of gravity retaining walls, reinforced concrete cantilever walls and mechanically stabilized earth (MSE) walls. Koerner and Soong (2001) gave a perspective on evolution of reinforced soil retaining walls. Over the decades, the classical gravity retaining walls transitioned into reinforced concrete cantilever walls, with or without buttress and counter forts and of mechanically stabilized earth (MSE) walls. The MSE walls are referred as internally stabilized walls, because of reinforcement installed within the backfill soil (Vidal 1966). The initial walls developed were reinforced with steel strips and subsequently replaced by welded wire mesh. By 1980s, the MSE wall technology started to use polymeric reinforcement like geogrids, geotextiles and polymer strap etc. as an alternative to metallic reinforcement.

Applications of geosynthetic reinforced soil (GRS) retaining walls in major public infrastructure works are increasing tremendously due to rapid urbanization and demand of effective land space utilization. They offer improved performances, in addition to, advantages in ease and less cost of construction compared to conventional earth retaining systems. Fig. 1.1 shows several examples of reinforced soil structures.

The reinforced soil retaining structures have three main components: backfill, reinforcement and facing system. Sand and gravels are often recommended as backfill soil due to good drainage properties and better interaction with reinforcement.

Fig. 1.1 Application of reinforced soil structures: (a) highways; (b) bridge abutments; and (c) slope stability (www.reinforcedearth.com)

Reinforcing materials may be of relatively inextensible steel strips, sheet or relatively extensible polymer products like geotextiles and geogrids. Wall facing may include: wrap facing, full height rigid (FHR) facing, segmental block facing and modular block facing (Holtz 2001). The wrap-faced reinforced soil walls are with flexible facing, whereas, full height rigid-faced reinforced soil walls are with stiff facing. In segmental block facing and modular block facing reinforced soil walls, the facings are constructed with discrete panels or blocks and are semi-rigid in nature. Fig. 1.2 shows various types of reinforced soil retaining walls.

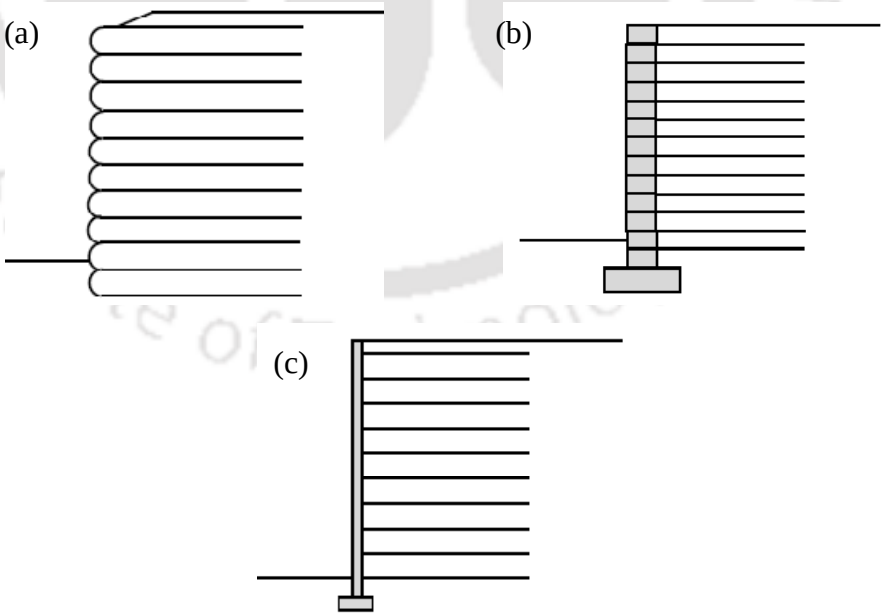

Fig. 1.2 Typical system of reinforced soil structures: (a) wrap-faced wall (b) modular block wall and (c) full-height rigid-faced wall (redrawn from Holtz 2001)

1.2 SEISMIC PERFORMANCE OF GRS RETAINING WALLS

Satisfactory performances of reinforced soil retaining structures during recent earthquakes, in comparison with conventional retaining walls, are reported by several researchers (e.g. Sandri 1997; Tatsuoka et al. 1995, 1997 and 2007; Kramer and Paulsen 2004; Koseki et al. 2006). However, some failures of reinforced soil structures during earthquake are also reported (Huang 2000; Ling et al. 2001; Pamuk et al. 2004; Ling and Leshchinsky 2005, Koerner and Koerner 2013). Koerner and Koerner (2013) analyzed 171 failed geosynthetic reinforced soil (GRS) retaining walls and highlighted that about 69 % of walls fall under design failure category. Analyzing the performance of retaining structures under static and seismic ground shaking conditions helps to understand better about their behavior during earthquakes and to design these structures more seismic efficient. Thus, dynamic behavior of reinforced soil retaining walls is of research interest to several researchers through different modes of studies like, physical model studies, analytical studies and numerical model studies. Examples of few such studies include: Cai and Bathurst (1995); Hatami and Bathurst (2000); Ling et al. (2004); Lee et al. (2010); Liu et al. (2011); Krishna and Latha (2012) etc. Most studies, conducted by different researchers, were based on small scale laboratory studies and numerical analyses, and mainly focused on parameters like: wall displacements, backfill settlements, lateral earth pressures, reinforcement loads and acceleration amplifications. But, very little was reported in literature on the deformation zones, strain behavior etc. on soil and reinforcement.

Some researchers observed slip surface, large deformations and surface cracks after seismic shaking. Matsuo et al. (1998) showed definite slip surface existed in GRS structures after conducting reduced scale shaking tables tests. However, no sign

of sliding deformation of geosynthetic reinforced soil (GRS) walls were reported after large scale shaking table tests (Ling et al. 2005a) and dynamic centrifuge test (Nova-Roessig and Sitar 2006). Large deformations and surface cracks were reported in the unreinforced zone and behind the facing of reinforced wall after seismic shaking 0.8g (Ling et al. 2005a). A small horizontal displacement and vertical settlement was reported in reinforced soil slopes after seismic shaking of 1.08g (Nova-Roessig and Sitar 2006). Liu and Ling (2012) reported that permanent deformation of reinforced soil structures were due to deformation within reinforced and unreinforced zone and reinforcement loads are directly related to strain-softening behavior of soil. The method to estimate the permanent displacement of reinforced soil structures are based on shear resistance on backfill soil which in turn leads to strain development in backfill soil and mobilization of reinforcement loads. So strain variations in the backfill soil and reinforcement will provide better understanding about the mechanism of formation of deformation zones soil and load variations in reinforcement members.

1.3 OBJECTIVES OF THE PRESENT STUDY

The objective of the present research programme is to investigate the dynamic response of reinforced soil retaining walls (RSRW) through numerical simulations. The study envisaged to get insight on their behavior with different wall configurations subjected to different excitations. The main focus of this research is to determine the strains developed in backfill soil and to compare with horizontal and vertical displacements along the backfill for determining probable deformation zones within the backfill. Another aspect of the present research work is to evaluate the effect of

different earthquake ground motions, which are rich in frequency contents, on behavior of reinforced soil walls.

1.4 ORGANIZATION OF THESIS

This thesis is organized into seven chapters.

Chapter 1 presented the introduction to the problem, objective of the research work. Organization of the thesis is also briefly described in this chapter.

In **Chapter 2**, literature on reinforced soil retaining walls, relevant to the present research work, are presented and discussed. Literature was reviewed in three parts: experimental studies, analytical studies and numerical studies related to seismic response of reinforced soil retaining walls. The chapter concludes with critical appraisal of the literature and detailed scope of the work.

Chapter 3 gives description of numerical program and model parameters required for modeling the reinforced soil retaining walls. A finite difference method based programme FLAC^{3D} (Fast Lagrangian Analysis of Continua) has been used to develop numerical models. Various components of numerical models of wrap and rigid-faced reinforced soil retaining walls and their model parameters are discussed. As the behavior of soil reinforced structures is mainly depends on soil-geosynthetic interaction behavior, numerical simulations of interaction through interface elements is validated with the laboratory test results.

Chapter 4 deals with the numerical simulations on wrap-faced reinforced soil wall models. Development of wrap-faced wall numerical model has been presented in detail. The results are presented in terms of displacements, strains; pressures and corresponding deformation zones are discussed. Variations of reinforcement strains along length of reinforcement at different layers are presented. Parametric studies are conducted to study the strain mobilization and deformation zones.

Chapter 5 covers the numerical simulations on full height rigid-faced reinforced soil wall models. Numerical simulations of laboratory scale shaking table tests on rigid-faced reinforced soil retaining walls are described. The location of deformation zones based on horizontal and vertical displacements and octahedral shear strains along the length of backfill are discussed. Parametric studies are conducted to study strain mobilization in backfill soil and reinforcement by varying different parameters.

Chapter 6 presents numerical model studies on both the wall models, subjected to different actual earthquake excitations, which are rich in frequency content. The chapter provides relative comparison between rigid-faced and wrap-faced walls and also describes the deformation modes under random excitations.

Chapter 7 summarizes the present study and presents the conclusions drawn from the research work. The limitations of the study and future scope of work are also discussed.

Chapter 2. LITERATURE REVIEW

2.1 INTRODUCTION

Studies related to behavior of the reinforced soil retaining structures subjected to seismic excitation are becoming popular day by day. A typical research work can be conducted through analytical frame work or/and model studies. Model studies are advantageous to simulate complex system and provide insight to the fundamental mechanism, operating within the system. Model studies in geotechnical engineering may be physical model studies in laboratory or numerical model studies simulating the actual field problem. Both of the studies gives insight into the model behavior and mechanism involved. The objective of the present study is to understand the seismic response of reinforced soil retaining structures, which is aimed through the numerical model studies. The following sections summarize the literature pertaining to the reinforced soil retaining structures and their seismic behavior.

2.2 REINFORCED SOIL STRUCTURES: BEHAVIOR, ANALYSIS AND DESIGN

The behavior of reinforced soil structures depends on three of its basic components: soil, reinforcement and facing and their interaction characteristics. Among these, backfill soil and its engineering behavior governs internal stress distribution, pullout resistance and failure surface shape (Federal Highway Administration, FHWA 2001). Based on the engineering properties and its interaction with reinforcement and drainage properties, granular soils are ideally suited for reinforced soil retaining wall structures (FHWA 2001, BS8006 2010). Major functions of the reinforcement members in GRS retaining structures are to sustain

tensile loads and deformation, if any developed, in the fill. The reinforcements are classified as extensible reinforcement like polymer products and inextensible reinforcement like metallic mat and strip etc. (FHWA 2001). In case of the extensible reinforcement, deformation of reinforcement is comparable or even greater than soil deformation, while in inextensible reinforcement deformation of reinforcement is much less than soil deformation of soil (FHWA 2001). Different types of facing components are being used, basically, to prevent the soil to slide away from the rows of reinforcements; and also to contribute in stability of the structure by maintaining reinforcement members to function together.

In reinforced soil structure design, soil-reinforcement interaction is an important factor, which governs the composite behavior of soil and reinforcement. The soil reinforcement interactions are controlled by two interaction mechanism namely pullout of reinforcement from soil (pullout mechanism) and soil sliding over the reinforcement (direct shear mechanism). Internal stability of reinforced soil retaining walls will be contributed by strength of geosynthetics and length of reinforcement required to prevent pullout (FHWA 2001). The pullout resistance offered by reinforcement is due to frictional force developed between the soil and reinforcement. Many researchers conducted pullout tests on geosynthetic reinforcement for the determination of interaction properties (Bergado et al. 1986; Juran et al. 1988; Farrag et al. 1993; Gurung and Iwao 1999; Palmeira 2004; Shahu 2007; Subaida et al. 2008).

Koseki et al. (2006) reviewed the design codes for seismic design of geosynthetic reinforced soil walls as listed in Table 2.1. Different agencies developed design guidelines for reinforced soil retaining walls. They are: Federal Highway

Administration (FHWA 2001 and 2010); British Standard (BS8006 2010) and National Concrete Masonry Association (NCMA, 1997 and 1998) etc.

Table 2.1 Design codes for seismic design of GRS walls (modified after Koseki et al. 2006)

Reference codes	**Title**	**Summery**
BS8006 (2010)	Code of practice for strengthened/reinforced soils and other fills	Based on limit states design format and guidelines for partial material factors and load factors for various applications
NCMA, 1997	Design manual for segmental retaining walls.	Based on allowable stress design method
AASHTO (2002)	Standard specification for highway bridges	Based on allowable stress design
AASHTO (2004)	LRFD bridge design specifications,	Based on limit state design factor called "load and resistance factor design – LRFD"
FHWA (2001)	Mechanically stabilized earth wall and reinforced soil slope: design and construction guide lines	Based on allowable stress design
FHWA (2010)		Based on limit state design
CHBDC (2000)	Canadian highway bridge design code	Gives no guidance on GRS wall for static and seismic design and recommends use of analytical limit state design methods and should be checked against accepted working stress design methods
CFEM (2006)	Canadian Foundation Engineering Manual	A description of Tie-back Wedge (Simplified)method for geosynthetic reinforced soil wall but no guidance on use of limit state design
RTA (2005)	Design of reinforced soil walls	Based on limit state design procedures within performance based framework 2.2.1
RTRI (2006)	Design standard for railway earth structures	
PWRC(2000)	Design and construction manual for geotextile reinforced soil structures	

Design of reinforced soil retaining walls involves external stability (Fig. 2.1) and internal stability (Fig. 2.2) considerations. External stability issues consider

sliding and overturning of the structure as a monolithic block; bearing capacity of the foundation soil against increased normal pressure near the toe; and a potential deep seated failure surface. External design ensures that the reinforced block provides enough gravity resistance against the external forces. Internal stability aspects verify geosynthetic performance against tie-back and pullout failure. One should estimate the anticipated reinforcement forces and the geometry of the potential sliding surface at limit state. Internal design ensures that the reinforced block is strong enough and maintains its structural integrity against external forces (i.e. horizontal pressure from the retained fill, traffic surcharge) and self-weight (FHWA, 2001).

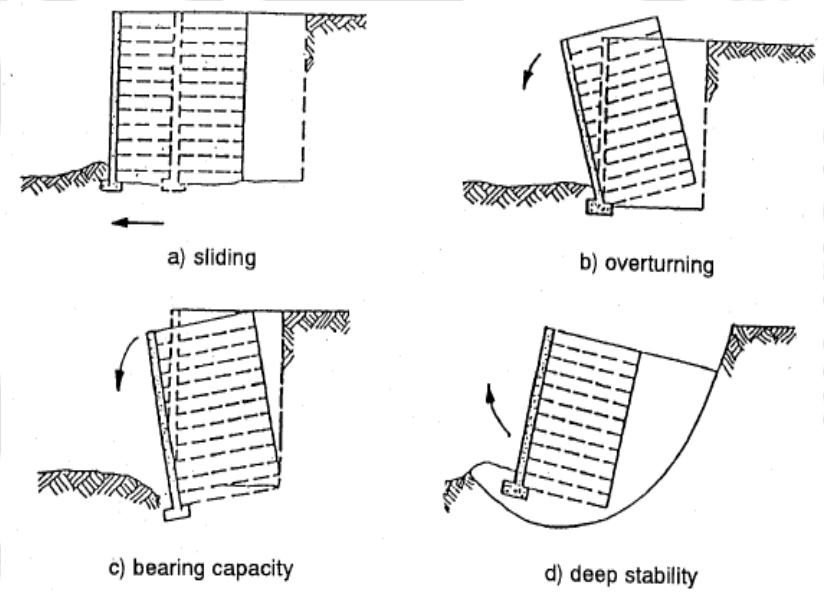

Fig. 2.1 Potential external failure mechanism for reinforced soil wall (FHWA 2001)

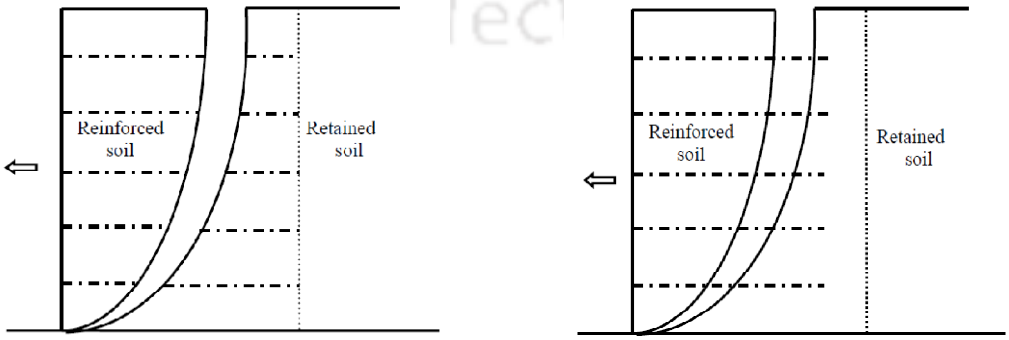

(a) Tie-back failure (b) Pullout failure

Fig. 2.2 Potential internal failure mechanism of reinforced soil wall (FHWA 2001)

The static and dynamic design of reinforced soil structures involves the estimation of external forces acting on the structures to evaluate external and internal stability. In static analysis, the force exerted on the reinforced block, by the retained soil is estimated using fundamental soil mechanics principles of lateral earth pressure (Coduto 2002). The soil retained behind the mechanically stabilized earth (MSE) wall is assumed to be in limit equilibrium. The force exerted, on the reinforced soil zone, by the retained soil is calculated by well known Rankine (1857) or Coulomb (1776) earth pressure theories. This force is assumed to be acting at one-third the wall height ($H/3$, where H is the total height of wall), corresponding to a triangular earth pressure distribution.

For areas with seismic hazards, stability under seismic forces is evaluated by considering two additional forces: the seismic thrust and horizontal inertia force. During an earthquake, the retained fill exerts a dynamic horizontal thrust in addition to static thrust on the reinforced soil wall, using Mononobe-Okabe (1929) method. The reinforced soil mass is also subjected to horizontal inertia force that arises from part of the reinforced soil block due to the horizontal acceleration. These two forces are evaluated using site specific peak horizontal ground acceleration value, obtained from relevant codal provisions (IS 1893; EC8). The external and internal stabilities of the reinforced soil wall, with the selected reinforced configurations (strength, length, spacing etc.), are evaluated from the lateral forces considered and corresponding resisting forces developed. Relevant factors of safety for various mechanisms considered in the stability analysis (FHWA 2001) must be ensured to complete the design process.

2.3 STATIC STUDIES ON GRS RETAINING WALLS

Many researchers worked on static performance of reinforced soil walls (Karpurapu and Bathurst, 1992; Ho and Rowe 1996; Rowe and Ho 1997; Rowe and Skinner 2001; Ling and Leshchinsky 2003; Hatami and Bathurst 2005 and 2006; Skinner and Rowe 2005; Yoo and Kim 2008). The effect of geometric parameters such as reinforcement length, number of layers of reinforcement, distribution of reinforcement and wall height on the static forces developed are analyzed. The stress distribution in soil and total resisting force developed on the reinforcement depends on reinforcement stiffness density, reinforcement/soil friction angle, facing/soil friction angle, backfill friction angle and facing rigidity (Rowe and Ho, 1997). The reinforced soil wall behavior is affected by the nature of foundation soil (Rowe and Skinner, 2001). Bathurst et al. (2005) established a working stress method for the calculation of reinforcement loads in GRS wall using database of instrumented and monitored full-scale field and laboratory walls.

2.4 DYNAMIC STUDIES ON GRS RETAINING WALLS

Bathurst et al. (2002) reviewed the work associated with the properties of cohesionless soil, geosynthetic reinforcement and facing component under cyclic loading. They concluded that the reinforced soil walls performed well during seismic shaking when located on competent foundation soil and above water table. The seismic performances of reinforced soil wall have been reported for recent major earthquakes such as: Loma Prieta earthquake 1989 (Eliahu and Watt 1991; Collin et al. 1992); North bridge USA earthquake 1994 (Sandri 1997; White and Holtz 1996); Hyogo-Ken Nanbu Japan earthquake 1995(Nishimura et al. 1996; Tatsuoka et al. 1997); Chi Chi Taiwan earthquake 1999 (Ling et al. 2001; Huang et al. 2003);

Koceli Turkey earthquake 1999 (Koseki et al., 2006); and El Salvador earthquake 2001 (Race and del Cid, 2001). In most of the cases GRS walls performed well. However, damages to reinforced soil walls during earthquakes were also reported in literature (Tatsuoka et al. 1996; Huang 2000; Ling and Leschinsky 2005) as depicted in Fig. 2.3 and Fig. 2.4. Increase in applications of reinforced soil walls and its satisfactory performances and few failures during earthquakes draw attention of researchers, to study behavior of reinforced soil retaining walls under seismic conditions.

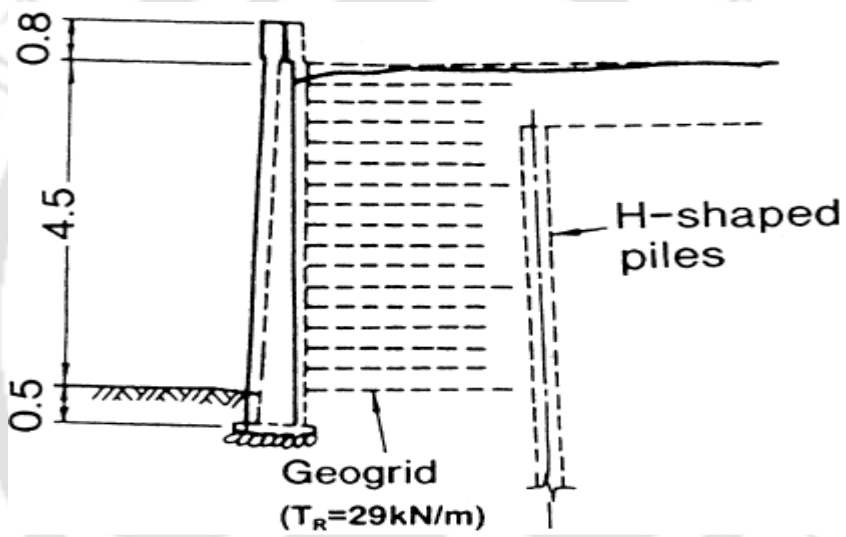

Fig. 2.3 Cross-section of geogrid wall suffered some damage during 1995 Hyogo-ken Nanbu Earthquake (Tatsuoka et al. 1996)

2.4.1 Physical model studies

Dynamic behavior of reinforced soil retaining structures by shaking table tests has been the subject of several researchers for the past three decades (Richardson and Lee 1975; Koga et al. 1988; Sakaguchi et al. 1992; Murata et al. 1994; Telekes et al. 1994; Palmeira and Gomes 1996; Matsuo et al. 1998; Perez 1999; Watanabe et al. 2003; Perez and Holtz 2004; Lo Grasso et al. 2005; El-Emam and Bathurst 2004, 2005 and 2007; Ling et al. 2005a; Krishna and Latha 2007; Sabermahani et al. 2009 etc.).

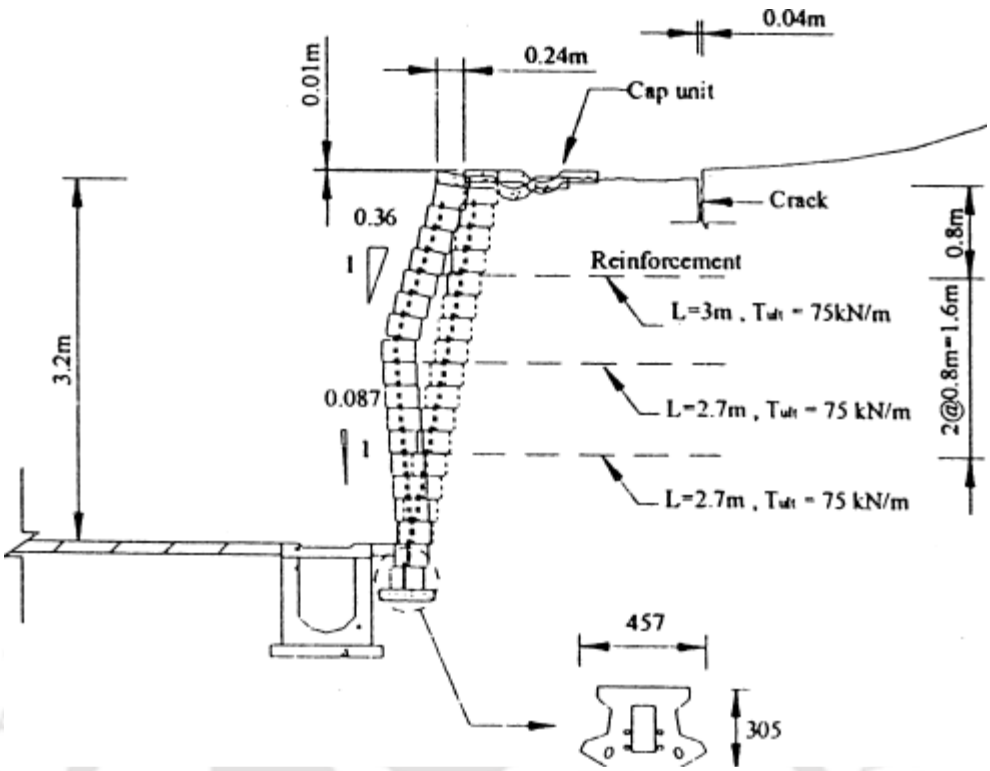

Fig. 2.4 Large deformation in geosynthetic reinforced modular block wall during Chi-Chi (Taiwan) Earthquake (after Huang, 2000)

Richardson and Lee (1975) conducted small scale shaking table tests on reinforced soil retaining walls with aluminum sheets and aluminum foils as reinforcement. They had observed that the reinforced soil walls failed either due to tie break of reinforcement or pull out of reinforcement. It was recommended that reinforced earth wall should be designed for a lower Factors of safety with respect to pull out than for tie breaking. Richardson et al. (1977) performed seismic testing on full-scale reinforced soil walls by generating low strain dynamic loads using vibrator and high strain dynamic loads using blasting.

Nakanishi and Sakaguchi (1990), Sakaguchi et al. (1992) and Sakaguchi (1996) carried out shaking table tests on reinforced wall models of height 1.5 m. Influences of various parameters, such as density of backfill, reinforcement strength and length on seismic behavior of reinforced soil walls were observed. The models

were excited using sinusoidal loading with acceleration upto 0.7g at 4 Hz frequency. It was observed that the reinforced zone acted as a monolithic body with no evidence of yield surface, propagating across the reinforcement layers, even after the developments of large wall displacements.

Murata et al. (1994) reported the results of shaking table tests carried out on reinforced embankment model with a crest width of 3.45 m contained by two 2.5 m high walls constructed with gabion baskets and outer continuous concrete panel. The model was subjected to both harmonic and actual earthquake records. The models subjected to harmonic excitation generate larger deformations than the actual record. The effects of facing stiffness on response of walls subjected to earthquake load were also being investigated.

Telekes et al. (1994) summarized the results of shaking table tests on reinforced embankment models and presented the effects of scale factor, slope angle and reinforcements. The results of shaking table tests on models of different scales (1/6 and 1/9) were compared and observed the response to acceleration and eigen frequency.

Sakaguchi et al. (1994) and Sakaguchi (1996) carried out centrifuge tests of 150 mm high reinforced soil wall using 30g acceleration to represent 4.5 m high wall. The tests were conducted for wall models with three types of geotextile reinforcement and light weight facing blocks. It is observed, that denser the sand in model embankment, smaller the displacement of facing.

Koseki et al. (1998) performed series of shaking table tests on relatively small scale models of GRS retaining walls with full height rigid facing and conventional type retaining walls (gravity, leaning and cantilever types). Tilt table tests were also conducted on the model walls. Seismic stability of these different types of walls was

evaluated by both the test methods and compared with the values predicted by the conventional pseudo-static approach. It was observed that the major failure mode was overturning with tilting of the wall face, which may have been triggered by a bearing capacity failure in the subsoil below the wall facing.

Matsuo et al. (1998) conducted shaking table tests on GRS retaining wall models with variation in geogrid length, wall height, wall facing type, wall slope and input acceleration waveform to observe the behavior and reinforcement mechanisms. The test results are compared with the results of pseudo-static seismic stability analysis and it was showed that current design method provides a margin of safety against the failure of reinforced soil walls. Ramakrishna et al. (1998) presented the results of model tests of geotextile wrap-faced (Fig. 2.5) and segmental retaining walls of 0.95 m wide, 2.05 m long and 0.81 m high subjected to horizontal base acceleration. The lateral movements of both walls were monitored. The wrap-faced wall moved laterally at acceleration of 0.25g and segmental retaining wall at acceleration of 0.45g. An analytical method was suggested to calculate the critical acceleration (i.e the acceleration before lateral movement is initiated) of the model.

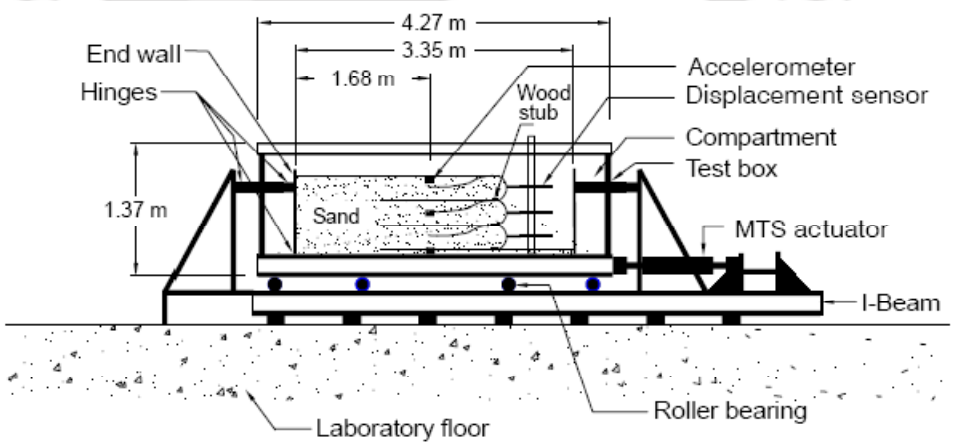

Fig. 2.5 Test setup and cross section of model wall considered by Ramakrishna et al. (1998)

Tatsuoka (2002) described the staged construction procedure of GRS retaining walls with a full-height rigid facing cast-in-place. The dynamic performances of wall models from shaking table tests were also reported. Koseki et al. (2006 and 2007) summarized several aspects of the seismic stability of geosynthetic reinforced soil structures referring to these test results.

Ling (2003) reviewed several shaking table tests conducted on reinforced soil retaining walls and observed the contribution of wall facing to the better performance of walls in terms of deformation and acceleration response. The requirement of additional test results for the purpose of validating numerical procedures and centrifuge models were also emphasized.

Watanabe et al. (2003) conducted 1-g model shaking test on relatively small scale models of six different types of retaining walls resting on level ground (Fig. 2.6). The wall models were about 500 mm high and the subsoil and backfill constituted very dense dry sand layers. It was reported that the reinforced soil retaining walls showed more ductile behavior than conventional type of retaining walls at high seismic loads. It was also observed that the extension of several upper reinforcements effectively improve the seismic stability of reinforced soil-walls.

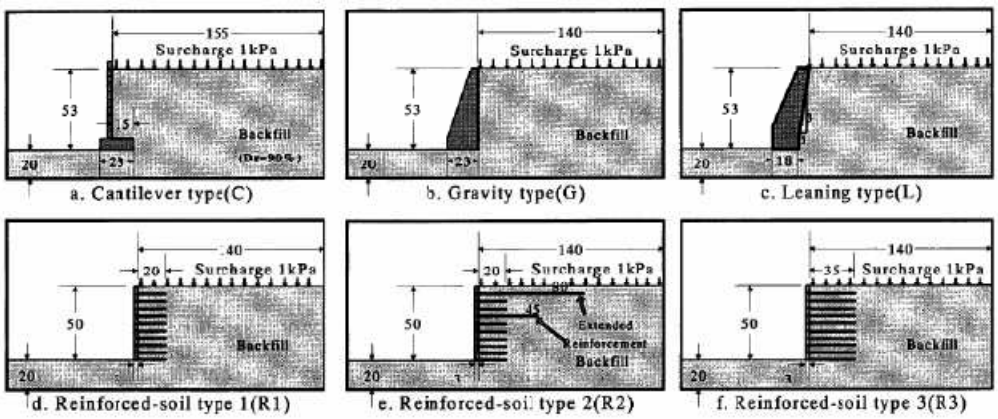

Fig. 2.6 Different types of retaining wall model walls on level ground (after Watanabe et al. 2003)

El-Emam and Bathurst (2004, 2005 and 2007) conducted a series of shaking table tests on instrumented, reduced scale reinforced soil wall models constructed with different toe boundary conditions, facing panel configuration and reinforcement layout (Fig. 2.7 and Fig. 2.8). The effects of various parameters on seismic behavior of reinforced soil walls were studied. The toe boundary condition and facing pane configuration were found to have significant effect on model response. It was also observed that magnitude and distribution of connection loads significantly affected by the reinforcement length, vertical spacing and stiffness of reinforcement.

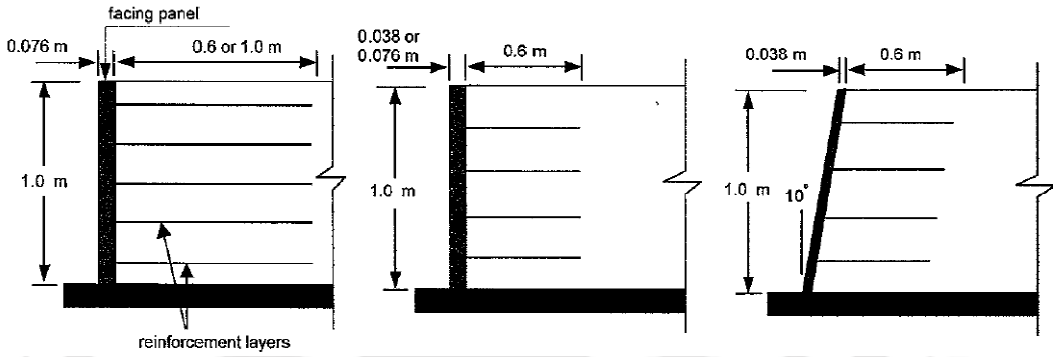

Fig. 2.7 Reinforced wall model configuration (after El-Emam and Bathurst 2004)

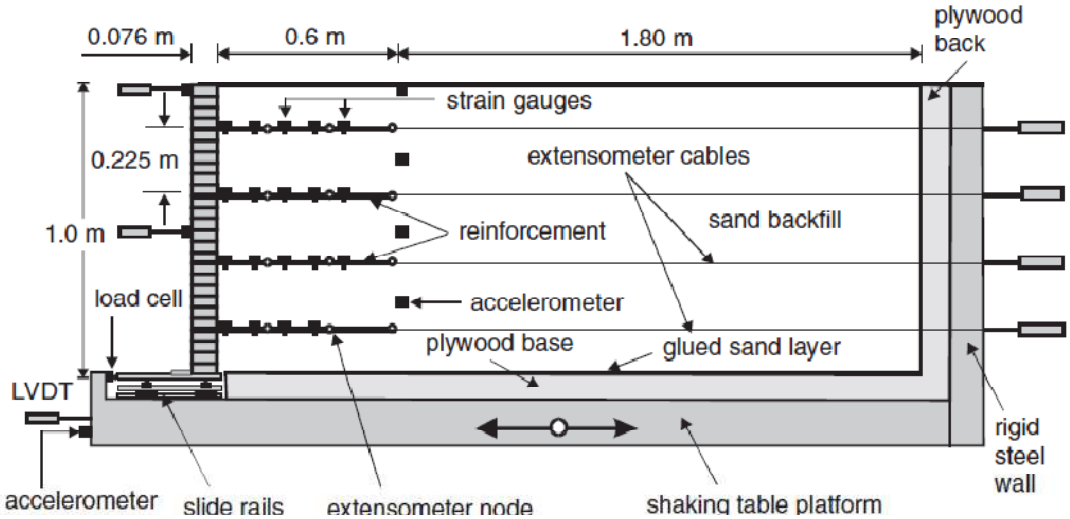

Fig. 2.8 Model configuration and instrumentation adopted for reduced scale RS walls (after El-Emam and Bathurst 2005)

Ling et al. (2004) conducted model tests in centrifuge to study the dynamic behavior of GRS walls. The wall facing deformations, strains in the geogrid reinforcement layers, the lateral earth pressures acting on the facing block and vertical stresses on foundation were reported. Dynamic finite element simulations were adopted to study the same. The experimental and numerical results were compared.

Lo Grasso et al. (2005) conducted shaking table tests to observe the performance of reinforced soil slopes. Typical geometry of the reinforced slope before and after the test is shown in Fig. 2.9. The effect of surcharge on altering the shape of failure surface mechanism was reported. An approximately circular surface failure mechanism for slope with surcharge and two-wedge failure mechanism for slope without surcharge is observed.

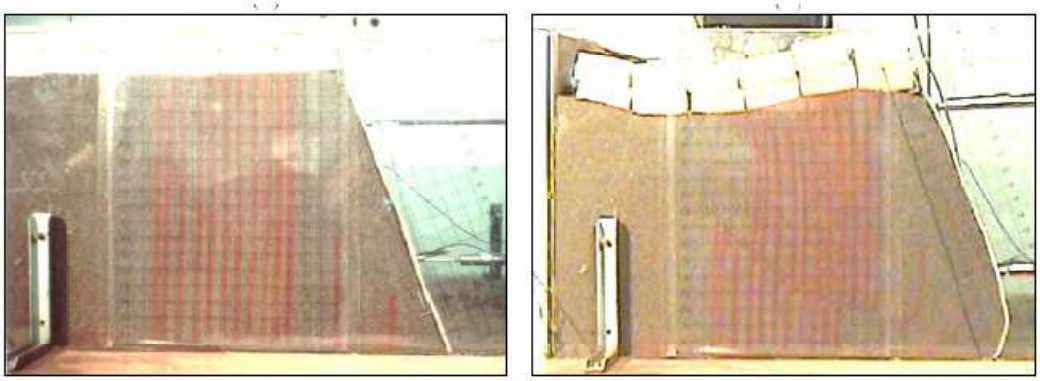

(a) Before test (b) After test

Fig. 2.9 Test slope before and after shaking test (after Lo Grasso et al. 2005)

Ling et al. (2005a) conducted shaking table tests on three large scale 2.8 m high modular block geosynthetic reinforced soil walls (Fig. 2.10) that were subjected to simulated Kobe earthquake motion. It was demonstrated that the seismic performance of the wall could be increased by increasing the length of the top reinforcement, reducing vertical spacing and grouting the top blocks to ensure the firm connection to the reinforcement. A large deformation and surface cracks were

reported in the unreinforced zone and behind the facing of reinforced wall after seismic shaking as shown in Fig. 2.11.

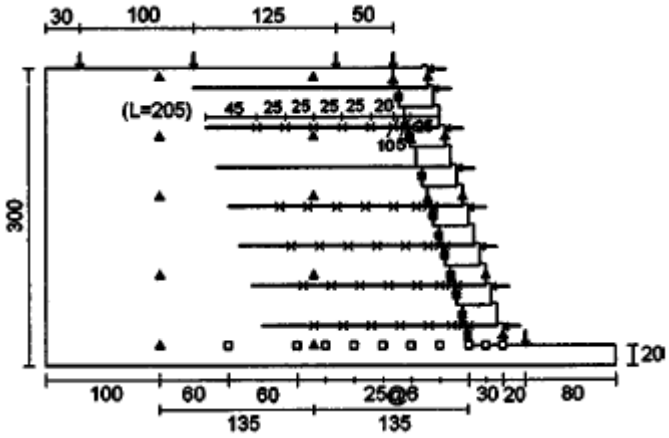

Fig. 2.10 Typical wall model configuration adopted by Ling et al. (2005a)

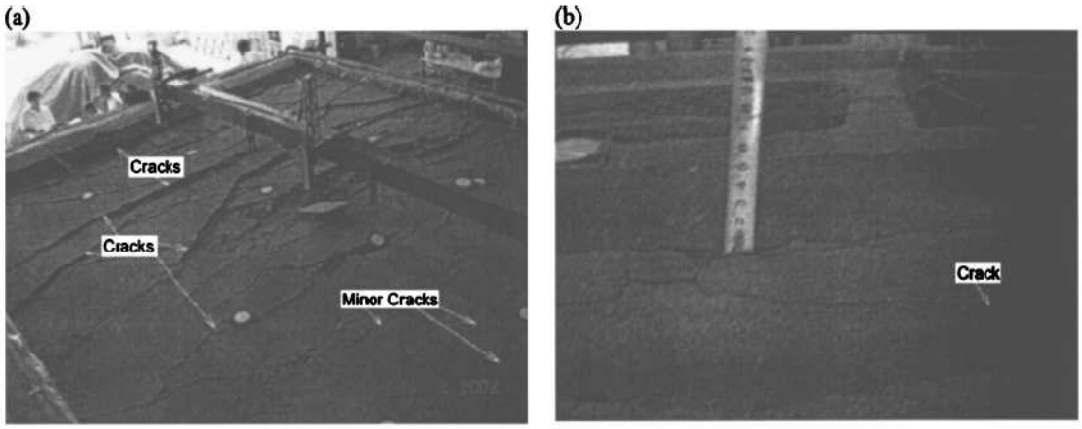

Fig. 2.11 Visual observation of deformation (a) surface cracking behind reinforced zone (b) settlement behind block facing (after Ling et al. 2005a)

Nova-Roessig and Sitar (2006) studied the dynamic behavior of soil slopes reinforced with geosynthetics and metal grids using centrifuge tests and observed the failure mechanism and deformations related to backfill density, reinforcement stiffness and spacing and slope inclination. No distinct failure surfaces other than some small horizontal displacements and vertical settlements were reported.

Krishna and Latha (2007, 2009) and Latha and Krishna (2008) reported shaking table tests on wrap-faced and rigid-faced reinforced soil walls (Fig. 2.12). Dynamic excitation parameters, surcharge pressure and number of reinforcing layers,

types of reinforcement and backfill relative density were varied in different model tests. It was observed that the response of warp-faced walls were significantly affected by the base acceleration levels, frequency of shaking, quantity and types of reinforcement, backfill relative density and magnitude of surcharge pressure on the crest. The effects of these different parameters on acceleration response at different elevations of the retaining wall, horizontal soil pressures and face deformations were also studied.

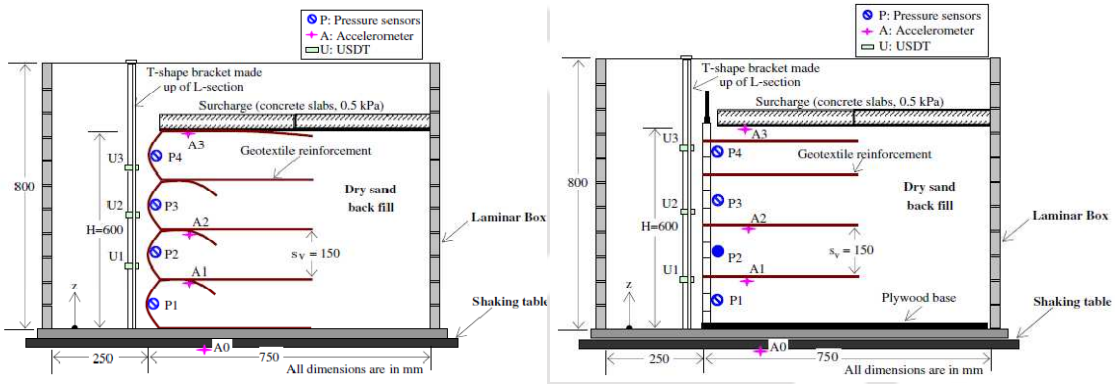

(a) Wrap-faced wall (b) Rigid-faced wall

Fig. 2.12 Schematic diagrams of typical test wall configurations and instrumentation adopted by Latha and Krishna (2008)

Sabermahani et al. (2009) conducted a series of 1-g shaking table tests on 1 m high reinforced-soil wall models. The physical models were subjected to sinusoidal input motions at frequencies of 2, 5, 8 and 10 Hz. The effects of parameters such as soil density, reinforcement length, spacing and stiffness on the seismic response of the model walls were studied. The deformation modes of free sliding toe boundary and wrap-around wall facing were studied.

Huang (2013) conducted shaking table tests to investigate the vertical acceleration response of geosynthetic-reinforced slopes subjected to horizontal input ground acceleration. It was observed that small vertical acceleration at top associated

with small displacement while large vertical acceleration at top associated with large displacements.

2.4.2 Analytical studies

The analytical studies were conducted by different researchers to analyze the reinforced soil retaining walls and to establish some design curves. Analytical studies can be divided into two categories: (i) the strength based study, in which load acting on reinforced soil wall is determined by pseudo-static and pseudo-dynamic methods; (ii) the performance based study, in which the displacement of the wall is determined. Some of the important analytical studies related to dynamic behavior of the structures are discussed below.

Bathurst and Cai (1995) conducted seismic stability analyses of geosynthetic-reinforced segmental retaining walls (modular block walls). Stability analyses were developed within the framework of a pseudo-static approach that gives factors of safety against collapse mechanisms or rupture of component materials. The Mononobe-Okabe (1929) method was used to estimate dynamic earth pressures. Parametric analyses of forces and factors of safety related to external, internal and facing failure modes for walls constructed on competent foundations were presented. Fig. 2.13 and Fig. 2.14 show the calculation details of dynamic earth pressure and reinforcement loads, respectively, using the pseudo-static method. Cai and Bathurst (1996) described the application of conventional displacement methods to estimate seismic induced permanent displacements of geosynthetic reinforced segmental retaining walls constructed on firm foundations. Permanent displacements associated with three sliding mechanisms were investigated: (1) external sliding along the base of the total structure, (2) internal sliding along a reinforcement layer and through the facing column and (3) block interface shear between facing column units. A pseudo-

static method based on the Mononobe-Okabe(1929) earth pressure theory was used to determine the values of the critical acceleration associated with each potential failure mechanism. Newmark's sliding block displacement method and a number of empirical methods were used to estimate the permanent displacements of segmental retaining walls.

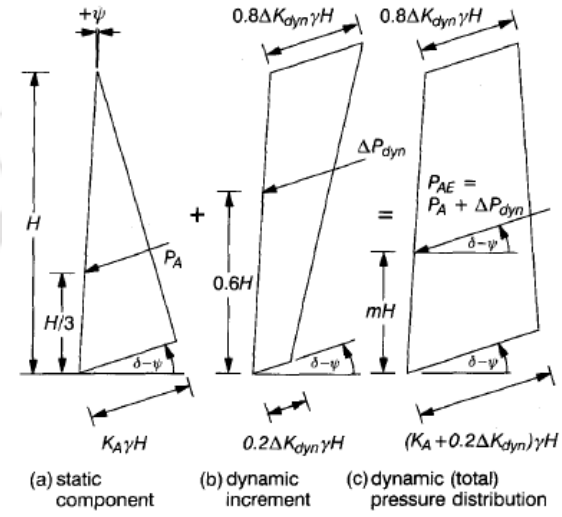

Fig. 2.13 Calculation of dynamic earth pressure under seismic loading (after Bathurst and Cai, 1995)

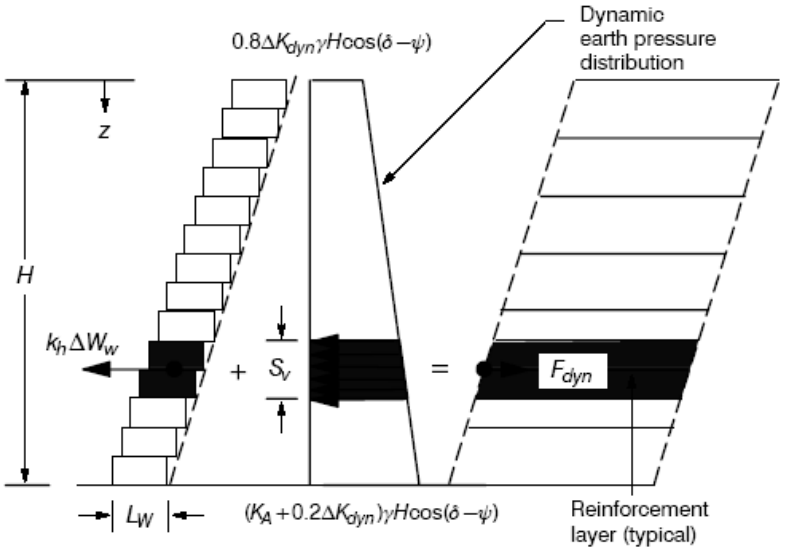

Fig. 2.14 Calculation of tensile load in a reinforcement layer due to dynamic earth pressure and wall inertia (after Bathurst and Cai, 1995)

Ling et al. (1997) proposed seismic design procedures for geosynthetic-reinforced soil structures. The procedures were based on a pseudo-static limit

equilibrium analysis, which considers horizontal acceleration and incorporates a permanent displacement limit. Internal and external stability analyses in the form of tieback analysis, compound stability analysis and direct sliding analysis were conducted to determine the required strength and length of geosynthetic.

Ismeik and Guler (1998) analyzed the effect of wall facing thickness on stability of full height concrete facing by using two-wedge failure mechanism. An analytical method had developed to correlate the effect of facing thickness with the amount of geosynthetic reinforcement required using limit equilibrium method.

Ling et al. (2001) studied the performance of several modular-block reinforced soil retaining walls and reinforced slopes during Chi Chi earthquake of Taiwan in 1999. They had studied six numbers of reinforced walls and emphasized on the proper seismic design of the reinforced soil wall. Ling (2001) discussed on application of sliding block theory to different geotechnical structures. The reinforced soil was divided into two zones (Fig. 2.15). In this study a simplified procedure was used with vertical acceleration to calculate yield acceleration and permanent displacement.

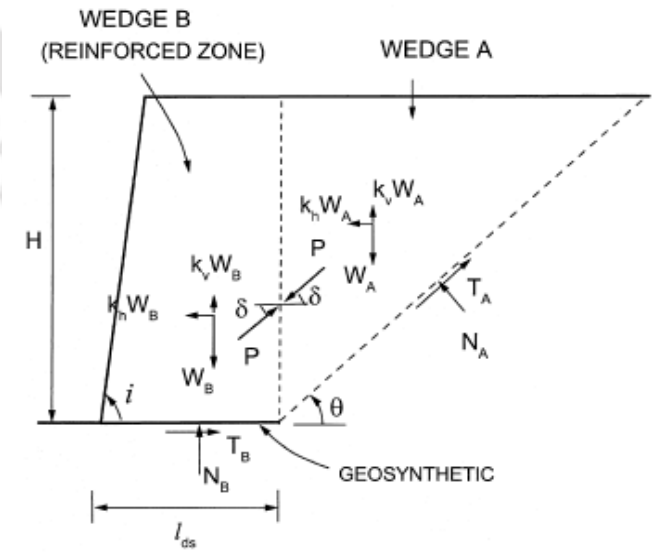

Fig. 2.15 Direct sliding of reinforced soil retaining wall (after Ling, 2001)

Huang et al. (2003) investigated four geosynthetic-reinforced soil modular block (GRS-MB) retaining walls that behaved differently during the 1999 Taiwan Chi-Chi earthquake by field surveying and soil testing. Pseudo-static analyses based on the two-wedge failure mechanism with contribution of facing and reinforcement facing connection strength was used to investigate the seismic stability of such GRS-MB walls. Newmark's sliding block theory together with a 'displacement diagram' was used to evaluate the seismic displacements of the investigated walls.

Ling and Leschinsky (2005) studied several modular-block reinforced-soil retaining walls, which were failed during 1994 Northbridge earthquake and 1999 Chi-Chi earthquake. The results of analysis indicated that these walls had adequate internal stability under estimated site acceleration. But reinforcement length was inadequate to resist compound modes of failure where the potential failure surface extends beyond the reinforced zone. It was also observed that, the external stability was most critical in the presence of horizontal and vertical accelerations.

Huang and Wang (2005) presented a pseudo-static based approach for evaluating the mechanical effects of facing components on the seismic displacement of reinforced soil walls backfilled with cohesionless soils. A multi-wedge analysis method (Fig. 2.16) over the conventional two-wedge method was proposed for seismic stability of reinforced soil wall. It was also observed that structural facing component and connection strength between facing and reinforcement significantly increase the seismic stability.

Nimbalkar et al. (2006) determined the internal stability of reinforced soil wall under earthquake condition by pseudo-dynamic method. Pseudo-dynamic method adopted in the analysis considered the effect of phase difference in both the shear and primary wave traveling through the backfill due to seismic excitation. The horizontal

slice method was used for determining internal stability or for tieback analysis of the reinforced soil. Choudhury et al. (2007) presented external stability aspects of reinforced soil retaining walls.

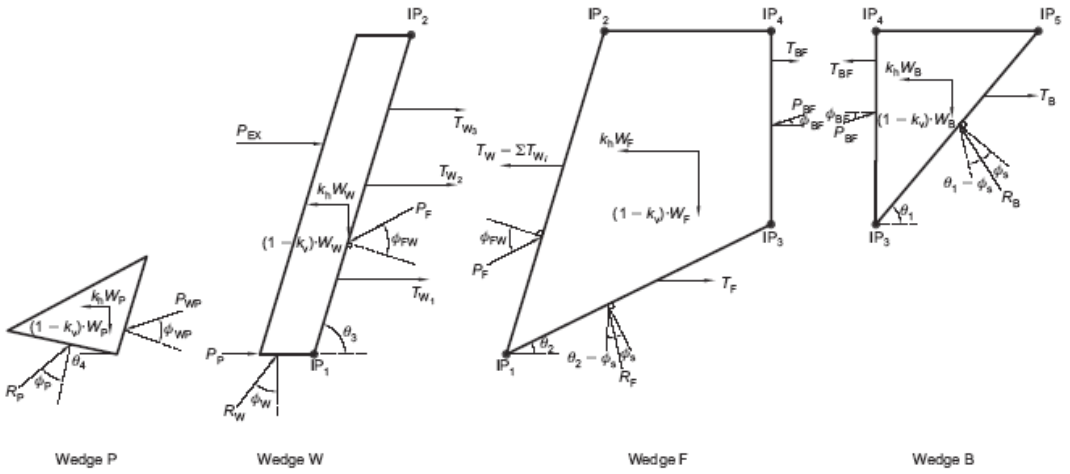

Fig. 2.16 Failure mechanism and force equilibrium in multi-wedge method (after Huang and Wang, 2005)

Huang and Wu (2006 and 2007) calculated critical seismic coefficient (k_{hcr}) and seismic displacement of some idealized geosynthetic-reinforced walls with full-height rigid panel facing (GRS-FHR walls) using a pseudo-static-based multi-wedge method in association with Newmark's sliding block theory. Empirical equations were developed for the values of critical seismic coefficient (k_{hcr}) as functions of internal friction angle (δ_s), the ratio between reinforcement length (L) and wall height (H_t) and other factors.

Nouri et al. (2008) studied the effects of horizontal and vertical pseudo- static forces on reinforced soil structures and evaluated the seismic stability of reinforced soil slopes and walls using horizontal slice method. It had been observed that the effect of horizontal seismic acceleration on the response of reinforced slopes and walls depends mainly on the geotechnical strength parameters. The effect of vertical

seismic acceleration on the performance of reinforced slopes was not significant for low values of horizontal seismic acceleration. But ignoring the effect of the amplification phenomenon could result in an underestimated design.

Reddy et al. (2008) analyzed pseudo-static seismic stability of reinforced soil wall considering displacements of the sliding mass obliquely to the alignment of reinforcement layers causing non-axial pull (Fig. 2.17). The transverse component of oblique pull generates additional stress and consequently larger pullout forces. The analysis for new Factors of safety had been carried out considering the additional stresses due to oblique pull.

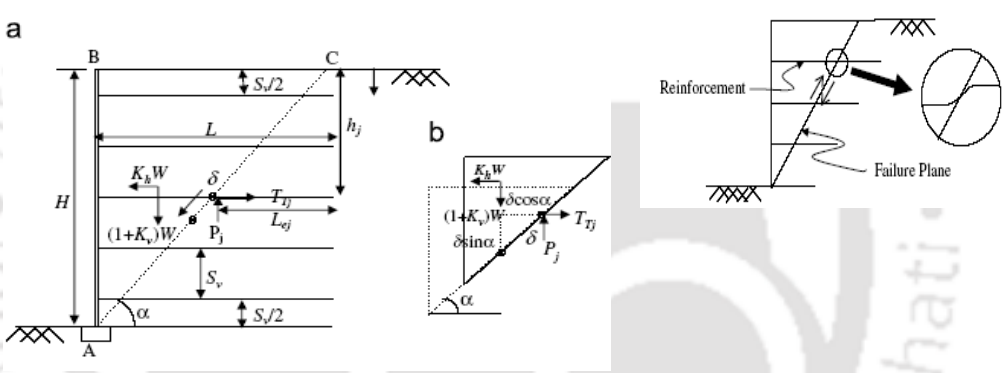

Fig. 2.17 Reinforced wall with kinematics of deformation of the reinforcement (after Reddy et al., 2008)

Shekarian et al. (2008) developed a new analytical method to determine the extension force of reinforcements and the distribution of reinforced mass in the determination of active earth pressure on reinforced soil walls. The application of this approach suggested a pseudo-static method that compared with the results of MSEW software.

Ahmed and Choudhury (2008, 2012) and Choudhury and Ahmed (2009) developed a design methodology for waterfront reinforced soil retaining wall by considering both the hydrodynamic pressure and seismic forces acting simultaneously on the wall.

Huang et al. (2009) developed a seismic displacement criterion for conventional soil retaining walls based on the observations of a series of shaking table tests and seismic displacement analysis using Newmark's sliding block theory taking into account the internal friction angle mobilization along the potential failure line in the backfill.

Basha and Babu (2009 and 2011) presented a method of evaluation of external and internal stability of reinforced soil walls subjected to earthquakes by pseudo-dynamic approach. The seismic reliability of the wall was evaluated by considering the different possible failure mechanism such as sliding along base, overturning about toe, bearing capacity and eccentricity of the resultant forces. Basha and Babu (2010) presented reliability based optimum design methods for assessing the external stability of reinforced soil walls.

Huang and Chen (2012) modified limit-equilibrium based internal and external stability analyses considering toe scouring. It was observed that a low reinforcement-facing connection result in full mobilization of reinforcement force in lower most layer of reinforcement and accelerated failure process. The wall with high connection strength collapse was due to bearing capacity failure of toe. A new Factors of safety of internal and external stability considering toe failure was developed.

Mojallal et al. (2012) used upper-bound limit equilibrium approach and Newmark's sliding block theory to develop a group of charts to estimate the coefficient of yield acceleration and permanent sliding displacements of full-height rigid concrete faced reinforced wall. The effect of parameters such as vertical spacing of reinforcement, ratio of width to height of spacing, ratio of reinforcement length to height of facing and inter friction angle of soil on magnitude of permanent displacements on coefficient of yield acceleration were also being studied.

2.4.3 Numerical model studies

Numerical simulation is one of the useful techniques to study the behavior of the retaining wall structures. The analytical approaches are based on some assumptions and cannot represent the real field effects. On the other way, the experimental approaches are costly and time consuming and are associated with the problems related to repetition and scaling effects. A properly calibrated numerical model can be used to study the real field problem that facilitates extensive parametric analyses. The numerical approaches can be divided into two major categories: finite element method and finite difference method. In this section of literature review, the studies related to the seismic behavior of reinforced soil retaining wall based on finite element and finite difference methods have been discussed. A summary of numerical studies on reinforced soil walls, showing salient features in terms of models and observations, is shown in Table 2.2.

Yogendrakumar et al. (1992) reviewed two methods for the dynamic response analysis of reinforced soil retaining wall. The first method was an iterative equivalent linear elastic approach and the second was an incremental elastic approach. The response of walls was compared with the tests conducted by Richardson et al. (1977). The results were in good agreement for actual and model response using blast loading.

Cai and Bathurst (1995) presented the results of 2D finite element analysis of the dynamic response of GRS retaining walls, that were constructed with dry-stacked modular concrete blocks (Fig. 2.18). In the finite element model, the cyclic shear behavior of the backfill soil was described by a hysteretic stress-strain relationship. The reinforcement material was modeled using hysteretic model which takes into account the measured response of cyclic load-extension tests performed on unconfined geogrid specimen in the laboratory. Interface shear between wall

Table 2.2 Summary of numerical studies seismic behavior of RS retaining structures.

Reference	Method	Code	Facing model	Reinforcing model	Backfill model (element)	Interface model		Observations
						soil/ reinforcement	soil/wall	
Yogendrakumar et al.(1992)	FEM	QUAD4B & TARA-3	Not used	One dimensional beam	Hysteretic model (quadrilateral element)	No slip model	Not mentioned	Good agreement between field test and simulated result
Cai and Bathurst (1995)	FEM	Modified TARA-3	Linear elastic (Quadrilateral element)	Hysteretic unload-reload model (tension only reinforcing element)	Hysteretic model (4 noded isoparametric element)	Slip element obey Mohr-Coulomb criterion	Not mentioned	Effect of dynamic loading on wall displacement, interface shear force between facing units, tensile force in reinforcement, acceleration response over height of wall
Bathurst and Hatami (1998)	FDM	FLAC 2D	Linear elastic (solid element)	Elastic-plastic (2 nodded Cable element)	Elastic-plastic material with Mohr-Coulomb failure criterion and non associated flow rule	Grout material with negligible thickness	Thin soil column with no slip boundary with wall. with Mohr-Coulomb failure criterion	Variation of seismic response with toe condition, effect of damping ratio, distance and type of far end boundary.
Hatami and Bathurst (2000) El-Emam et al. (2001), El-Emam et al. (2004)	FDM	FLAC 2D	Linear elastic (solid element)	Elastic-plastic (2 nodded Cable element)	Elastic-plastic material with Mohr-Coulomb failure criterion and non associated flow rule	Grout material with negligible thickness	Not given	Influence of reinforcement stiffness, reinforcement length or toe restraint condition on fundamental frequency
Helwany et al. (2001) and Helwany and McCallen(2001)	FEM	DYNA 3D	Linear elastic (Solid hexahedron element)	Linear elastic (Shell element)	Rams-Osgood model (Solid hexahedron element)	Sliding interface	Sliding interface	Numerical results consistent with laboratory results
Bruke et al. (2004)	FEM	DIANA-SWANDY NE II	Linear elastic (8 & 6 noded element)	1D bounding surface (Bar element)	Pastor-Zeinkiewicz III (8 & 6 node element)	Slip element	Slip element	Wall facing deformation, crest settlement and acceleration
Ling and Leschinsky (2003)	FEM	M-CANDE	Linear elastic	1D nonlinear eleastic model	Mohr-Coulomb with hyperbolic soil modulus model	Sliding interface follow stiffness method	Sliding interface follow stiffness method	Influence of reinforcement length, spacing, stiffness, backfill and foundation soil properties, block interaction and connection strength.
Ling et al.(2004)	FEM	Modified DIANA-SWANDY NE II	Linear elastic (8-node quadrilateral and 6-node triangular element)	1D bounding surface model (3-node 1D element)	Generalized plasticity model (8-node quadrilateral and 6-node triangular element)	Elastic perfectly plastic obey Coulomb failure criterion	Elastic perfectly plastic obey Coulomb failure criterion	Wall facing deformation, crest settlement, lateral earth pressure and tensile force in reinforcement layer and acceleration amplification.

…contd

Fakharian and Attar (2007)	FDM	FLAC 2D	Linear Elastic element	Elastic-plastic (2 nodded Cable element)	Mohr-Coulomb with hyperbolic stress-strain model for static case and hysteretic model for dynamic case	Grout material with zero thickness	Slip element	Comparison between predicted result from numerical model and measured physical result from instrumented prototype
Lee et al.(2010)	FEM	LS-DYNA	Linear elastic element	Plastic-Kinematic (4-node shell element)	Geologic cap model (8-node solid element)	Contact interface capability of LS-DYNA	Contact interface capability of LS-DYNA	Wall displacement, backfill settlement, lateral earth pressure, bearing pressure, reinforcement tensile load, maximum acceleration in reinforced soil zone, maximum acceleration in retained zone
Liu (2009)	FEM	Modified DIANA-SWANDYNE II	Linear elastic element	Elastoplastic-visco elastic bounding surface model	Generalised plasticity model for sand	Reinforcement and soil is perfectly bounded	Thin-layer slip element based on Mohr-Coulomb failure criterion	Effects of various wall parameters, earthquake excitations, behavior of geosynthetics to earthquake at end of construction and 10years after construction.
Ling et al.(2010)	FEM	DIANA-SWANDYNE II	Linear elastic (8 &3noded element)	3 noded one dimensional bar element based on bounding surface concept	Generalized plasticity model (8-node quadrilateral and 3-node triangular element)	Thin layer interface having elastic perfectly plastic	Thin layer interface having elastic perfectly plastic	Time response of horizontal and vertical accelerations, wall deformations, tensile force in geogrid
Liu et al. (2011)	FEM	ABAQUS 6.4	Linear elastic	1D bar element following elastoplastic viscoplastic bounding surface model	Drucker-Prager Creep model modified with nonlinear and cyclic hysteric behaviour	Thin-layer elements follow Mohr-Coulomb failure criterion	Thin-layer elements follow Mohr-Coulomb failure criterion	Reinforced soil wall with marginal backfill exhibits two wedge deformation mode, little influence of creep rates of soil and reinforcement on reinforcement load, changes in two wedge failure mode with long reinforcement
Liu and Ling (2011)	FEM	Modified DIANA-SWANDYNE II	Wrap-faced wall so no facing element	Bounding surfaced model (3 noded bar element)	Generalized plasticity model	Thin layer of slip element following Mohr-coulomb failure criterion	Wrap-faced wall so no facing element	Influence of strain softening of backfill soils on deformation and reinforcement load
Zarnani et al. (2011)	FDM	FLAC 2D	2 noded 1-D beam element	Elastic-plastic (2 nodded Cable element)	Elastic-plastic material with Mohr-Coulomb failure criterion	Reinforcement and soil is perfectly bounded	Thin soil column following Mohr-Coulomb criterion	Simple Mohr-Coulomb soil model can give satisfactory result, summarizes lessons for seismic design and performance of reinforced soil walls
Krishna and Latha (2012)	FDM	FLAC 2D	Wrap-faced wall so no facing element	2 dimensional beam element	Mohr-Coulomb with hyperbolic soil modulus model	Linear spring slider system following Mohr-Coulomb failure criterion	Wrap-faced wall so no facing element	Validated with experimental results and sensitivity analysis to check influence of backfill friction angle, dilation angle, stiffness properties geotextile

FEM – Finite element method
FDM – Finite difference method

components were simulated using slip element. The relative displacement, interface shear between soil and reinforcement, tensile force on reinforcement during dynamic loading were observed.

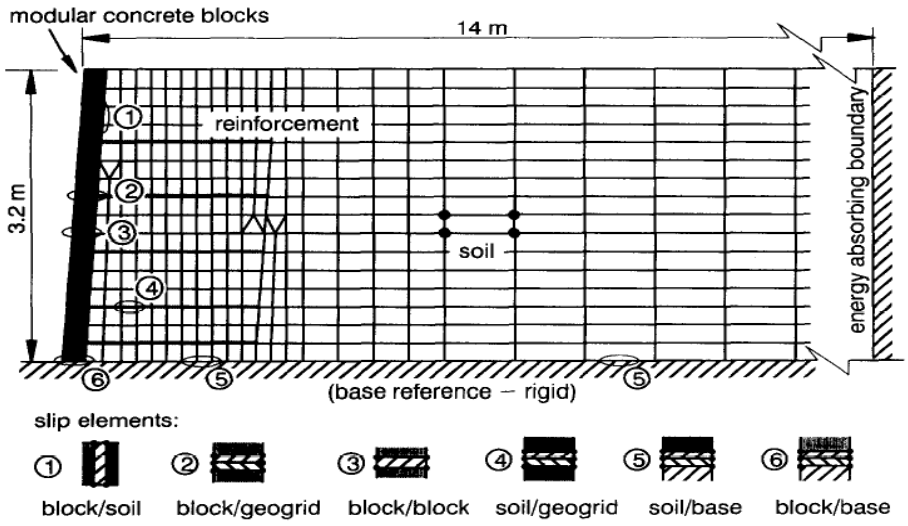

Fig. 2.18 Finite element mesh for simulation of segmental retaining wall (after Cai and Bathurst, 1995)

Bathurst and Hatami (1998) conducted numerical model studies to investigate the influence of reinforcement stiffness, reinforcement length, and base boundary condition on seismic response of an idealized 6 m high geosynthetic-reinforced soil retaining wall constructed with a very stiff continuous facing panel. Numerical results illustrated that the seismic response of the wall was very different, when the wall and soil is allowed to slide freely and when the wall is constrained to rotate only about the toe (Fig. 2.19). Parametric analyses were also carried out to investigate the quantitative influence of the damping ratio value and the effects of distance and type of far-end truncated boundary in numerical simulations. The effects of parameters like reinforcement stiffness, reinforcement length and base condition to the displacement of walls were observed as depicted in Fig. 2.20 .

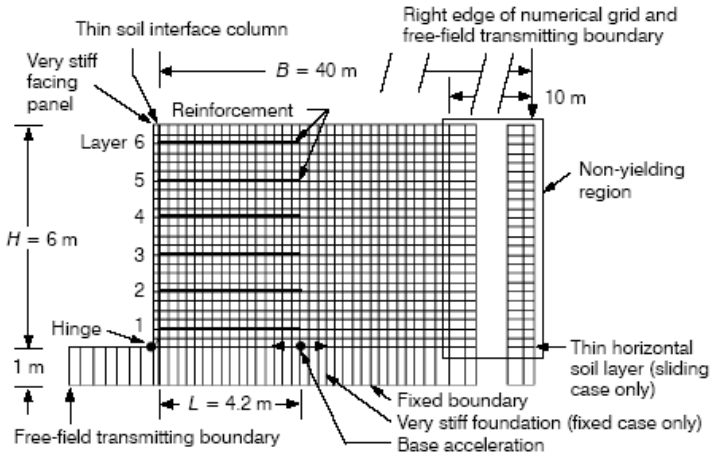

Fig. 2.19 Finite difference mesh (using FLAC) of geosynthetic reinforced soil wall (after Bathurst and Hatami, 1998)

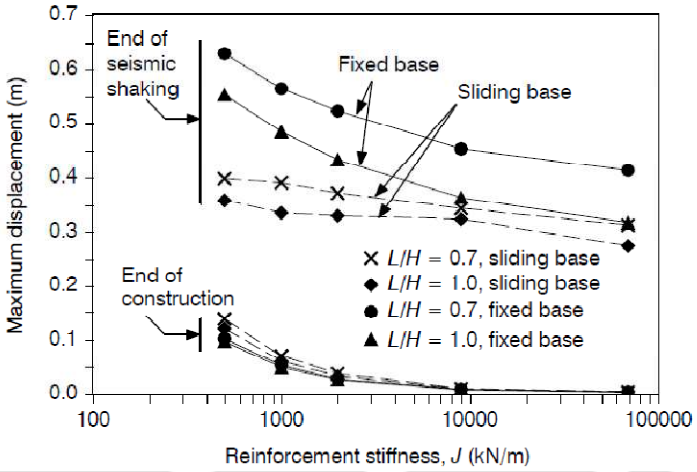

Fig. 2.20 Influence of reinforcement stiffness, reinforcement length and base condition on maximum wall displacement (after Bathurst and Hatami, 1998)

Hatami and Bathurst (2000) investigated the influence of a number of structural design parameters on the fundamental frequency of reinforced soil retaining wall models. The numerical study showed that the fundamental frequency of reinforced-soil wall models with sufficiently wide backfill subjected to moderately strong vibrations could be estimated with reasonable accuracy from available formulae based on linear elastic wave. Numerical analyses showed no significant influence of the reinforcement stiffness, reinforcement length or toe restraint condition, strength of granular backfill and its friction angle on the fundamental

frequency of wall models. However, the resonance frequencies of wall models were dependent on the ground motion intensity and to some extent, on the width to height ratio of the backfill (Fig. 2.21).

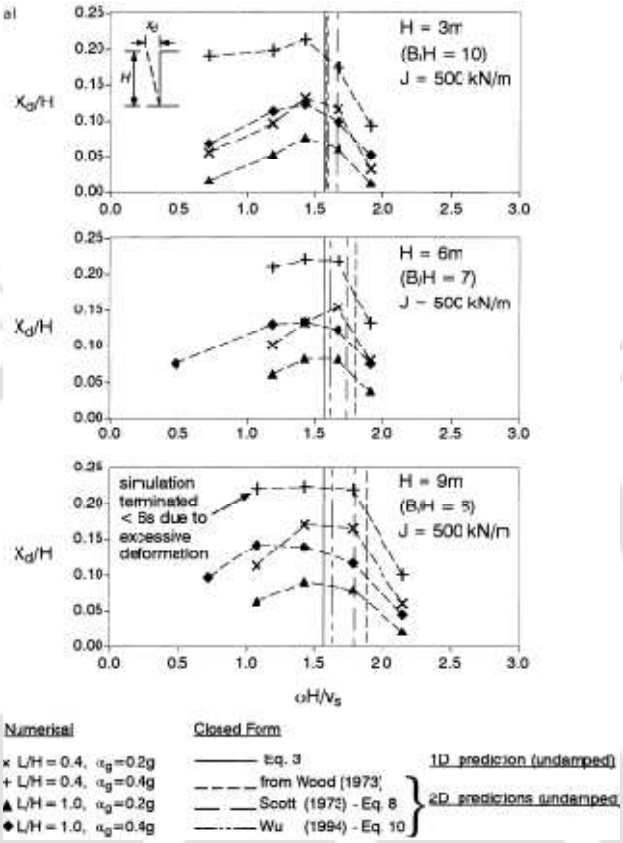

Fig. 2.21 Normalized maximum lateral displacement of wall crest with normalized frequency (after Hatami and Bathurst, 2000)

Helwany et al. (2001) studied the dynamic behavior of segmental retaining walls subjected to earthquake loading using shaking table tests. The same models were simulated using finite element analysis based computer programme DYNA3D. Conceptual diagram of the numerical model developed is shown in Fig. 2.22. The study showed that the results obtained from DYNA3D were consistent with observed results from shaking table tests on segmental walls. Helwany and McCallen (2001) showed that the segmental facings remained intact throughout the earthquake

simulation, with limited relative deformations and rotations between the concrete blocks after dynamic excitation.

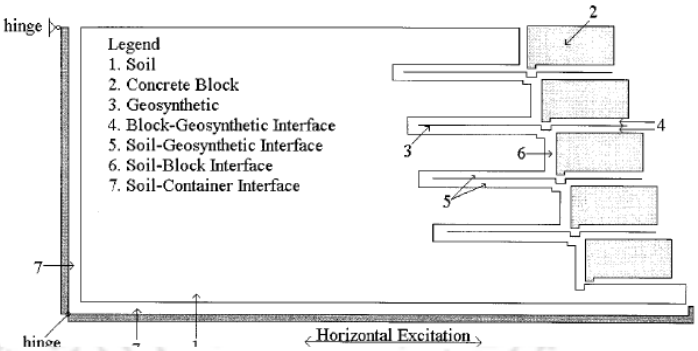

Fig. 2.22 Details of finite element mesh of segmental reinforced wall (after Helwany et al., 2001)

Ling et al. (2004) implemented generalized plasticity soil model and bounding surface geosynthetic model in finite element procedure to simulate the geosynthetic-reinforced soil retaining wall shaking tests conducted in centrifuge. The results of tests, in form of wall facing deformations, strains in geogrid reinforcement layers, lateral pressure acting at facing block and vertical stresses on foundations, for both static and dynamic tests were compared. Ling et al. (2005b) conducted a series of parametric studies on the behavior of reinforced soil wall subject to earthquake loading, using a numerical model developed (Fig. 2.23) in finite element frame work. The effects of soil properties, earthquake motion and reinforcement layouts were studied under earthquake loading.

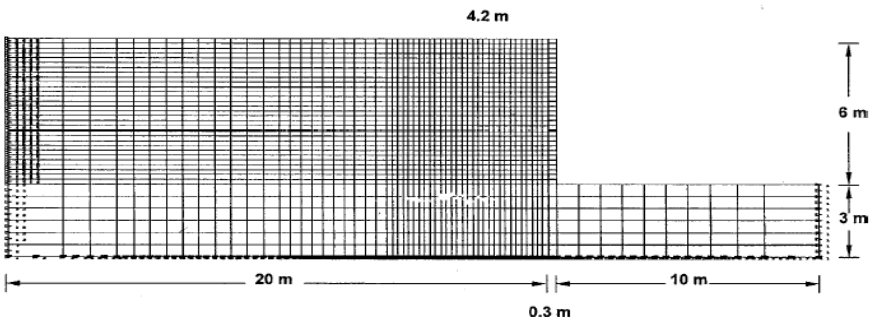

Fig. 2.23 Finite element mesh adopted by Ling et al. (2005b)

Liu (2009) calibrated a finite element model to investigate reinforcement loads of GRS walls subjected to seismic loading during service life. It was observed that the reinforcement loads during earthquakes after 10 years of construction are similar to those if the earthquakes occur after end of construction (Fig. 2.24). It was observed that under same seismic loading, little variation in reinforcement loads for GRS walls with various backfill peak strengths.

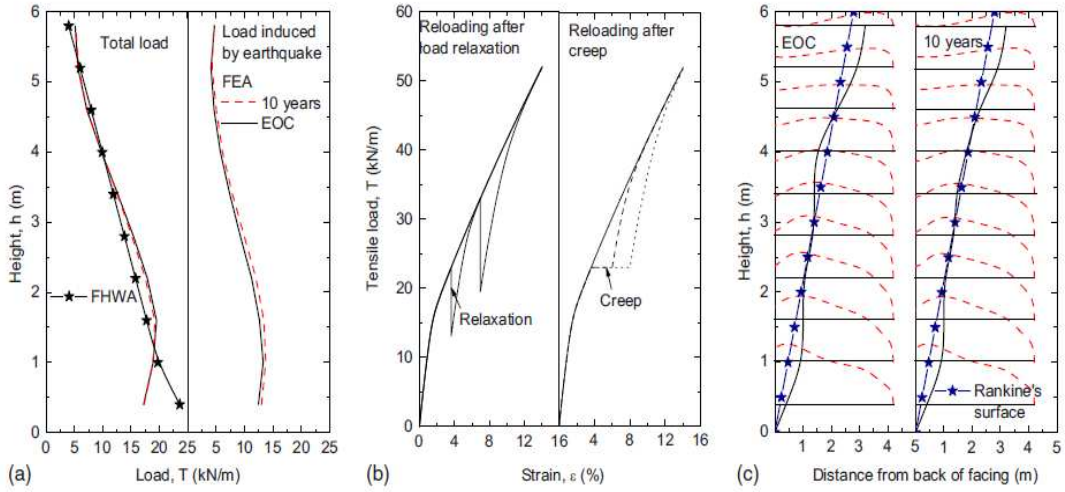

Fig. 2.24 Reinforcement loads of GRS walls subject to seismic loading at end of construction (EOC) and 10 years afterward (after Liu 2009)

Lee et al. (2010) conducted numerical model studies to simulate full-scale shaking table tests on GRS walls subjected to both horizontal and vertical accelerations (Fig. 2.25). The backfill soil was simulated with a geologic cap model.

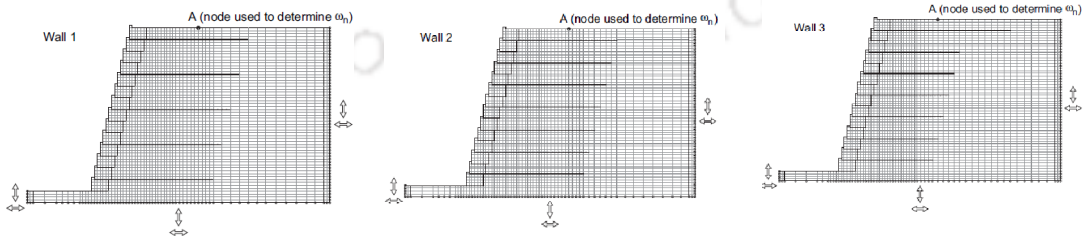

Fig. 2.25 Finite element mesh used for numerical simulation of three wall models (after Lee et al. 2010)

The responses of numerical model in the form of wall displacements, backfill settlements, and lateral earth pressures, bearing pressures, reinforcement tensile load and absolute maximum acceleration in reinforced and retained zone were compared with shake table test results (Fig. 2.26).

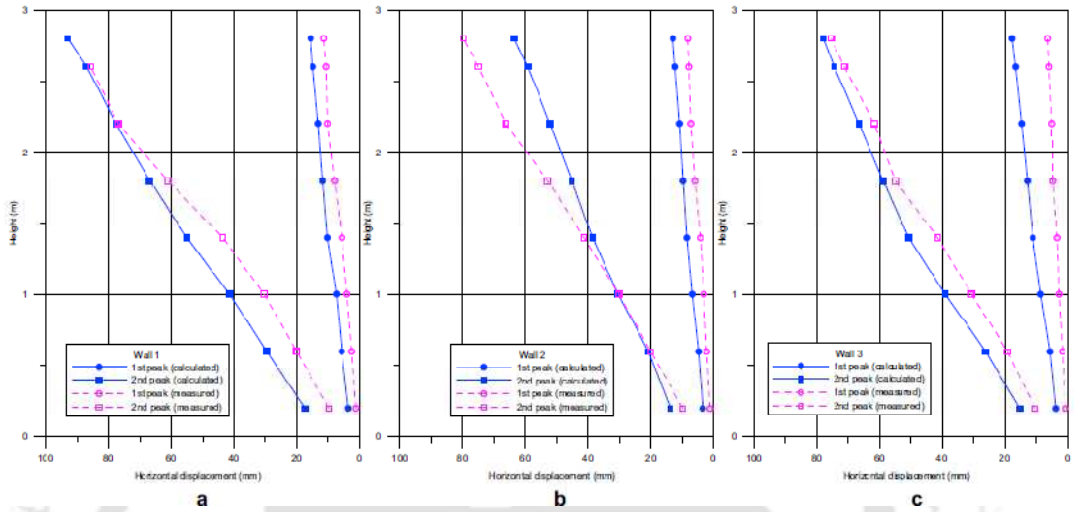

Fig. 2.26 Wall face peak horizontal displacement comparison (after Lee et al. 2010)

Ling et al. (2010) reported shaking table tests on full-scale reinforced soil retaining walls subjected to earthquake loading. The models were subjected to horizontal acceleration alone and both horizontal and vertical accelerations. The numerical simulations of models were conducted using finite element method. The soil was modeled using generalized plasticity model and geosynthetics were modeled using bounding surface model. The results obtained from the numerical simulations were compared with experimental results and found to be reasonably compared.

Liu et al. (2011) developed a finite element model of GRS walls with marginal backfill subjected to seismic loading during their service life. The study highlighted a distinctive two-wedge deformation mode under strong seismic loading (Fig. 2.27). It was also observed that creep rates of soil and reinforcement had small influence on reinforcement load and deformation mode, but reinforcement stiffness played a major role and could be restricted with sufficiently long reinforcement (Fig. 2.28).

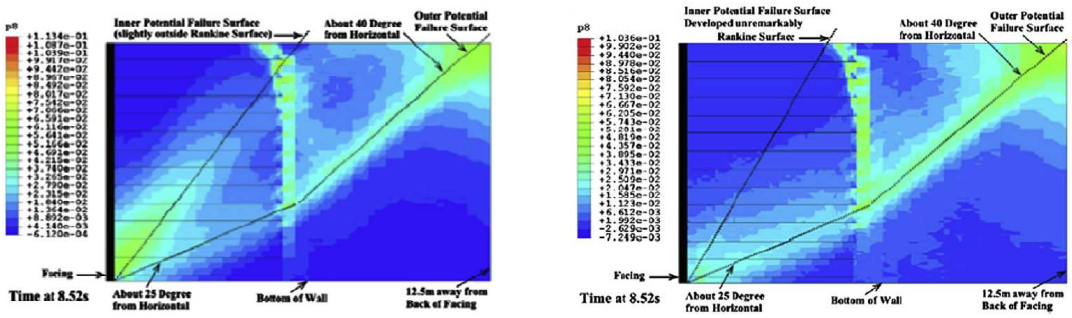

Fig. 2.27 Plastic shear strains within soil for at peak acceleration and at end of shaking (after Liu et al. 2011)

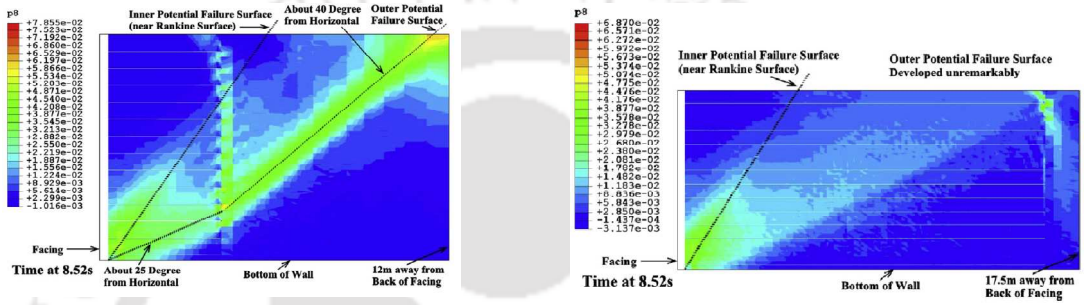

Fig. 2.28 Plastic shear strain within soil for reinforcement length (L) 0.5H and L=1.0H (after Liu et al. 2011)

Zarnani et al. (2011) simulated dynamic response of shaking table tests on reduced scale reinforced soil wall models. The physical and numerical models were subjected to stepped amplitude of sinusoidal base acceleration. The soil was simulated as cohesionless material with linear elastic-plastic response of Mohr-Coulomb failure criterion. The comparison of results with physical model tests showed that a simple elastic-plastic model was sufficient, to predict wall deformation, footing and reinforcement loads provided, the values of shear and bulk modulus are selected accurately with reasonable accuracy.

Krishna and Latha (2012) developed numerical models using FLAC to simulate shaking table tests of reduced-scale wrap-faced reinforced soil wall subjected to uniaxial shaking (Fig. 2.29). Sensitivity analyses were carried out on validated numerical model to observe the effect of friction angle, dilation angle, stiffness and

tensile strength of reinforcement and stiffness of interface between soil and reinforcement. The results showed that friction and dilation angle of backfill material and stiffness properties of geotextile-soil interface were most affecting parameters of model response.

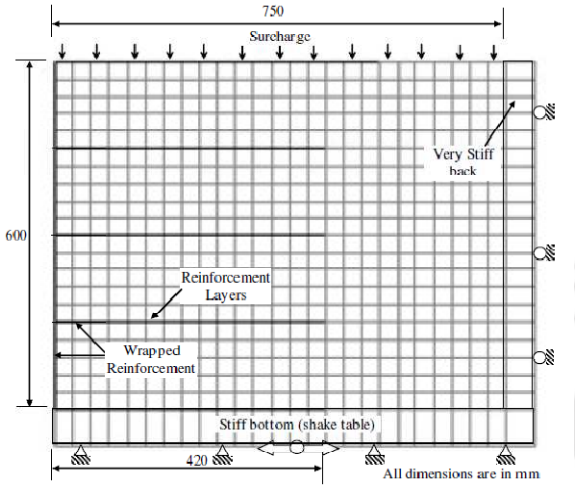

Fig. 2.29 Numerical grid considered for reinforced soil retaining wall model (after Krishna and Latha 2012)

Liu and Ling (2012) studied a calibrated finite element model of wrap-faced reinforced soil wall to investigate the influence of strain softening of backfill soils on deformation of backfill and reinforcement load (Fig. 2.30). The numerical models were developed with three different types of backfill soils (dense Toyoura sand, medium dense Japanese silty sand and loose Fuji river sand) subjected to accelerations in the range of 0.1g to 0.6g. It was observed from the study that permanent deformation of GRS wall attributed to compaction of backfill, smeared deformation soil; shear deformation of along slip surface and free field displacement of retained earth (Fig. 2.31). Three distinct modes of deformation of seismic loading were observed: the relative compaction between reinforced soil zone and retained earth, shear deformation of whole wall and sliding deformation along slip surface.

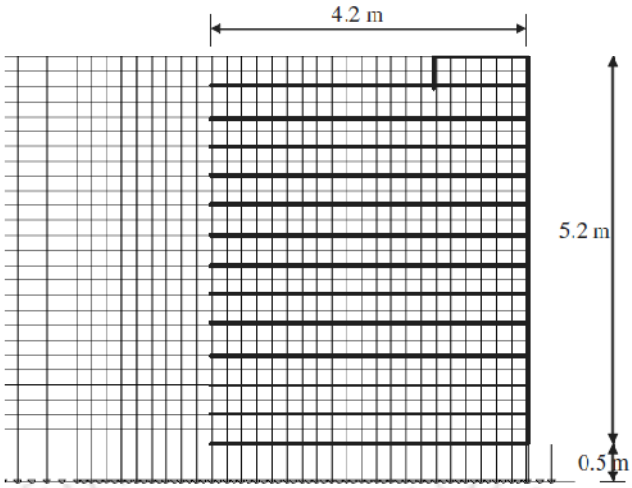

Fig. 2.30 Finite element mesh of wrap-faced wall (after Liu and Ling 2012)

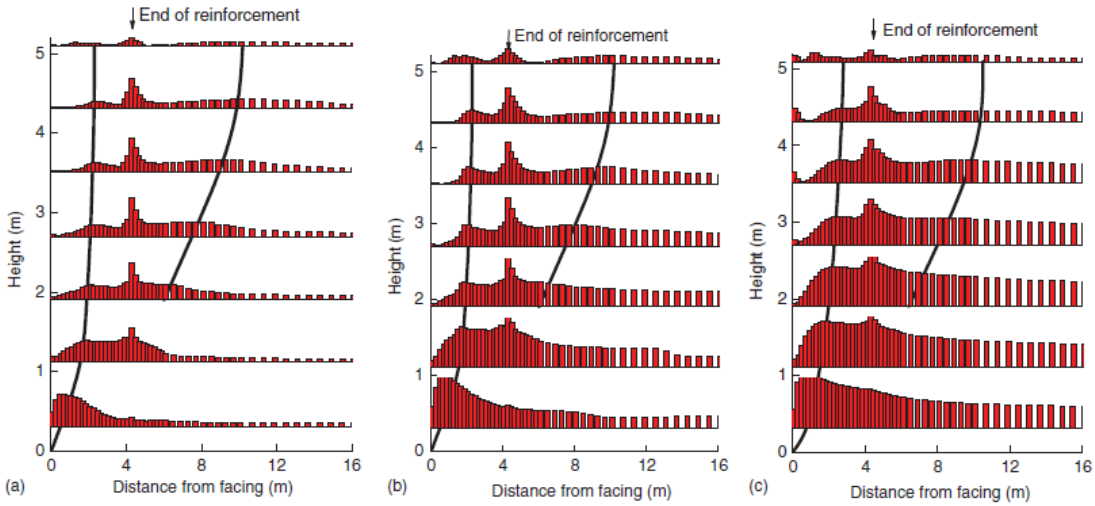

Fig. 2.31 Octahedral shear strain in reinforced soil walls with different types of sands as backfill (after Liu and Ling, 2012)

Lee and Chang (2012) used a validated finite element model to conduct parametric study of GRS walls subjected to multidimensional ground motion shaking. The parameters evaluated from the study were: wall height, wall batter angle, soil friction angle, reinforcement spacing and reinforcement stiffness. Multivariate regression equations were developed using FEM results of various seismic performances based on design parameters of GRS walls.

Liu et al. (2014) investigated similarities and differences of seismic performances between single and multi-tiered reinforced soil walls using validated finite element model. It was observed that resonant frequency of multi-tiered reinforced soil wall increases with increase in tier-offset. It was also observed that reduction of facing displacement, reinforcement load and their distribution with height, in multi-tiered reinforced soil walls compared to that of single vertical reinforced soil walls.

2.5 CRITICAL APPRAISAL

The literature related to the static and dynamic behavior of reinforced soil retaining walls was reviewed. The physical model studies include shaking table tests, mostly on small scale models (Sakaguchi et al. 1992; Koseki et al. 1998; Ramakrishna et al. 1998; Watanabe et al. 2003; El-Emam and Bathurst 2004; Krishna and Latha 2007 etc.); and a few large scale models (Murata et al. 1994; Ling et al. 2005a etc.) as well as centrifuge models (Sakaguchi et al. 1994; Ling et al. 2004; Nova-Roessig and Sitar 2006 etc.). The numerical model studies include the simulations of GRS wall models using finite element method (Cai and Bathurst 1995; Helwany et al. 2001; Ling et al. 2004; Liu et al. 2011 etc.) and/or finite difference (Bathurst and Hatami 1998; El-Emam et al. 2004; Fakharian and Attar 2007; Krishna and Latha 2012 etc.) approach. The analytical studies based on pseudo-static (Bathurst and Cai 1995; Ling et al. 1997; Huang et al. 2003; Nouri et al. 2008 etc.), pseudo-dynamic (Nimbalkar et al. 2006; Ahmed and Choudhury 2008; Basha and Babu 2009 etc.) and displacement analysis (Ling 2001) and some design curves are suggested considering different parameters. The review of literature brings out the following important points:

- Most of the physical and numerical studies targeted to observe the effect of different aspects such as reinforcement parameters, facing parameters and soil parameters on seismic performance of wall.
- The model studies are focused on analyzing the response in terms of wall displacements, lateral pressure, acceleration amplification and reinforcement load/strain against variations in different reinforcement parameters like stiffness, spacing, length etc. and seismic excitation parameters. Very few studies are available on the strain behavior of the backfill soil and corresponding reinforcement strains and deformation zones formed at backfill of reinforced soil wall.
- Formation of deformation zones in the model studies was not discussed in detail. But this aspect was given importance in the analysis of GRS wall failure case studies during earthquakes.
- Facing contribution in the stability of the walls is not being considered in the design aspects. However, few researchers highlighted the importance of this parameters on the structure behaviour.
- Further, most of the studies were considered idealized seismic excitations in the form simple sinusoidal dynamic shaking at fixed frequency levels. Limited studies are reported in exploring the effect of actual earthquake ground motions on the performance of structure.

2.6 OBJECTIVES AND DETAILED SCOPE OF WORK

Objective of the study is to investigate the dynamic response of reinforced soil retaining walls (RSRW) with more emphasis on strain variations in soil and reinforcement members. To analyze formation of deformation zones in RSRW of

different facing. Evaluating the effect of different earthquake ground motions which are rich in frequency content on behavior of reinforced soil walls is another goal of the project.

To achieve the above objectives, through numerical simulations, the following scope is formalized.

- To verify different modeling options for components of reinforced soil retaining walls – backfill soil, reinforcements, and interface between soil and reinforcement and reinforcement and facing.
- Development of numerical models of two types of reinforced soil retaining walls: Wrap-faced and rigid-faced reinforced soil wall models representing fully flexible and rigid wall systems.
- Validation of numerical models with physical model results available in literature and to extend the models to full scale models.
- To conduct parametric studies to observe the influence of parameters like reinforcement length, reinforcement stiffness, number of reinforcing layers and backfill soil parameters on response such as horizontal displacement, vertical displacement, acceleration amplification and horizontal pressure.
- Analysis of strain behavior of reinforced soil retaining walls in terms of octahedral shear strains developed in backfill soil and axial strains developed in reinforcement.
- Comparison of strains with the horizontal and vertical displacements along the length of wall to observe the probable location of deformation zones in backfill soil.
- Analyzing the responses of wall models subjected to real earthquake excitations to observe the effect of frequency content on response.

2.7 SUMMARY

This chapter presented the review of the literature related to the design and analyses of reinforced soil retaining walls subjected to seismic excitation. Design considerations for the reinforced soil retaining walls are discussed briefly. Review of the studies on seismic analyses of GRS walls was presented in three parts: physical model studies, analytical studies and numerical model studies. Critical Appraisal of the literature and needs for further understanding of the seismic behavior of GRS walls followed by detailed scope of the present study were presented.

Chapter 3. DESCRIPTION OF NUMERICAL PROGRAMME AND MODEL PROPERTIES

3.1 INTRODUCTION

Numerical modeling techniques are powerful tools that have been used to study the behavior of various structures under variety of loading conditions. Numerical models are particularly advantageous in situations where the prototype structures are too big to be tested in laboratory. Even if they can be tested using small scale models, it is difficult to analyze various behavioral aspects owing to the limitation associated with the instrumentation and tediousness in repeating the laboratory tests for variety of parametric variations. Numerical studies on GRS walls have been started in early nineties and becoming more popular due to advent of increasing computational facilities. The response of numerical model depends on the selection of constitutive relations for different materials involved in the model and their parameters. The reinforced soil retaining wall comprises of soil, reinforcement and facing elements. These materials are dissimilar and proper interface behavior between them shall also be considered for proper simulation and analyses. In the present research program, FLAC^{3D} (Fast Lagrangian Analysis of Continua 3D, (Itasca, 2008, Ver. 3.1) is being adopted for numerical modeling of the dynamic behavior of GRS walls. Brief description of the numerical programme, and implementation of constitutive models and their properties are presented in this chapter.

3.2 OVERVIEW OF FLAC^{3D}

FLAC^{3D} is a commercial geotechnical finite difference programme that is being applied to analyze wide range of geomechanics applications. It uses an explicit

Lagrangian calculation scheme and mixed discretization zoning techniques, for accurate modeling of plastic collapse and plastic flow behavior of materials in addition to elastic behavior. The non-linearity in stress/strain laws can be solved in same computer time as linear laws in explicit scheme, but implicit solution take significantly longer time to solve non-linear problem (Itasca 2008). The model response will be derived from the mathematical model of material and its numerical implementation. The mathematical models are derived from rate of strain, laws of motion and constitutive equations defining the idealized material. In numerical implementation, laws of motion for the continuum are transformed into discrete forms by finite difference approach. The resulting system of ordinary differential equations is then solved numerically using an explicit finite difference scheme.

In FLAC^{3D}, material zones are represented by polyhedral elements within a three-dimensional grid. The model solving involves large number of calculation steps. For every time step new strain rates are calculated from nodal velocities. The new stresses are calculated from strain rates and stresses at previous time using constitutive equations. The equations of motion are invoked to derive new model velocities and displacements from stresses (Itasca 2008). The calculation sequence of FLAC^{3D} is illustrated in Fig. 3.1. The maximum unbalanced force in the model is monitored to confirm the convergence of solution scheme. This unbalanced force will either approach zero, indicating system is approaching equilibrium state, or approach a constant non-zero value, indicating plastic flow of material. The model is assumed to be in equilibrium when the maximum unbalanced force ratio falls below 1×10^{-5} (Itasca 2008). Unbalanced force ratio is the ratio between the magnitude of maximum unbalanced force and the magnitude of the average applied mechanical force within the mesh.

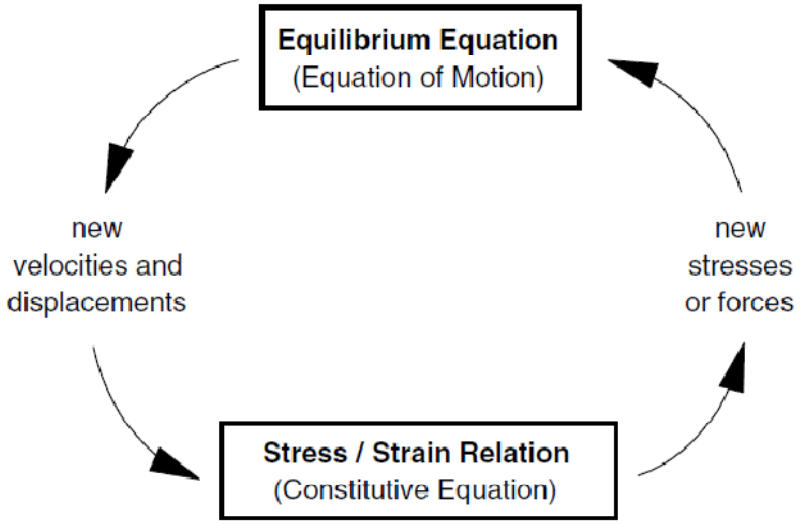

Fig. 3.1 Basic calculation sequence in FLAC^{3D} (Itasca 2008)

3.2.1 FISH programming

FISH programming language is one of the most useful features in FLAC^{3D} that can be used to implement user defined constitutive models and to perform programming techniques. Defining FLAC^{3D} model variables, operating conditional statements, and loops for repetitive tasks are included in FISH. These help to carry out user defined mathematical operations, define new variables and functions, extract stresses, strains and displacements from analysis and also to set zone properties directly from functions. The users can define their own constitutive model by programming in FISH and can be implemented in FLAC^{3D}.

The constitutive behavior of geologic materials is represented by their material models. FLAC^{3D} has twelve built in material models to represent different geologic materials. Three of the material models are in elastic model group and eight are of plastic model group. The other is the null model which can be used to represent a void or excavated material. Beside these built in constitutive models, the user can implement own constitutive model using the FISH programming language.

3.2.2 Structural elements

Structural members (beam, pile, plate etc.) or reinforcements, to support and stabilize rock or soil mass, are important aspects of geotechnical analysis and design. The structural members and their interaction with rock or soil mass can be modeled in FLAC^{3D} by built in structural elements. FLAC^{3D} has six forms of structural members: beam element, cable element, pile element, shell element, geogrid element, and liner element. The beam, cable and pile elements are one dimensional elements and shell, geogrid and liner elements are two dimensional elements.

The structural element can either be independent or coupled to the grid representing the solid continuum. Mutual interaction between the structural elements is through nodes. Structural nodes interact with grids through links. The link supports three attachment conditions – (i) free when velocity of source node is unrelated to velocity of target entity, (ii) rigid when source node is slaved and velocity of source node remain equal to velocity of target entity (iii) deformable when source node and target entity is connected by a spring and spring stiffness is average stiffness per unit area associated with link (Itasca 2008).

3.2.3 Dynamic modeling in FLAC^{3D}

The dynamic analysis is based on solving the equations of motions using lumped grid point masses derived from the density of surrounding zones. This formulation can be coupled to the structural element model, thus permitting analysis of soil-structure interaction brought about by ground shaking (Itasca 2008).

The dynamic analysis for FLAC^{3D} model is based on three aspects. These are: (1) dynamic loading and boundary condition (2) mechanical damping and (3) wave transmission through the model.

In FLAC^{3D}, a region of material subjected to external and/or internal dynamic loading can be modeled by applying a dynamic input boundary condition at either the model boundary or at internal grid points. One of the following ways may be adopted to apply dynamic input in FLAC^{3D} model: (1) acceleration histories; (2) velocity histories; (3) stress (pressure) history and (4) force history (Itasca 2008).

In static analysis, fixed or elastic boundaries can be realistically placed at some distance from the region of interest. But in dynamic analysis, such boundary condition cause reflection of outward propagating waves into the model and do not allow necessary energy radiation. Of course, use of larger model minimizes the problem, since material damping will absorb most of the energy in waves reflected from distance boundaries. However, this leads to larger computational burden. Alternatively, FLAC^{3D} enables two types of dynamic boundary conditions: the quiet (viscous) or free-field boundary conditions to reduce the wave reflections at model boundaries.

Material damping in numerical simulation should be able to reproduce the magnitude of energy losses in the natural system subjected to dynamic loading. Four different forms of built-in damping options available in FLAC^{3D} are: Rayleigh damping, local damping, artificial viscosity and hysteretic damping. Rayleigh damping is commonly used to provide damping that is approximately frequency-independent over a restricted range of frequencies. Local damping operates on overall conservation of mass. Mass is added when velocity changes sign and subtracted when it passes a maximum or minimum point. The amount of energy added or removed is proportional to the maximum transient strain energy and hence independent of rate and frequency. A third form of damping, artificial viscosity used for analysis with sharp dynamic fronts, is also available in FLAC^{3D}. Hysteretic damping is a fully non-

linear method capable of implementing modulus degradation with changes in cyclic strain. However, if a constitutive model that contains an adequate representation of the hysteresis, that occurs in real material, then no additional damping is necessary (Itasca 2008).

Numerical distortion of propagating wave in dynamic analysis is a function of modeling conditions. The size of grids should be selected in such a way that, the mesh size of the model shall be approximately smaller than one-tenth to one-eighth of the wavelength associated with highest frequency component of the input wave for accurate transmission of wave through the model (Kuhlemeyer and Lysmer 1973). The speed of *p*-wave and *s*-wave propagation through medium can be calculated using following relationship:

$$C_p = \sqrt{\frac{K+4G/3}{\rho}} \quad 3.1$$

$$C_s = \sqrt{G/\rho} \quad 3.2$$

Where C_p =speed of p-wave propagation through medium; C_s = speed of s-wave propagation through medium; K =Bulk modulus of medium; G = Shear modulus of medium; ρ = mass density of medium

The maximum frequency that can be modeled accurately for vertically propagating waves is (Kuhlemeyer and Lysmer 1973):

$$f = \frac{C_s}{\lambda} = \frac{C_s}{10\Delta l} \quad 3.3$$

where f = frequency of vertically propagating waves; λ = wave length associated with highest frequency component; Δl = largest zone dimension in model (considering $\Delta l = \lambda/10$).

3.3 MATERIAL MODELS FOR NUMERICAL SIMULATION

Modeling the reinforced soil retaining walls comprises of backfill soil, facing and reinforcement elements and interface elements between dissimilar materials. Various components of numerical models of wrap and rigid-faced reinforced soil retaining walls and their model parameters are discussed in the following sections.

3.3.1 Backfill soil

Static and dynamic behavior of any soil in numerical analyses is governed by the choice of appropriate constitutive model. Different researchers simulated the behavior of backfill soils with different constitutive models. For example, Mohr-Coulomb shear criteria, modified generalized plasticity model, geologic cap model, and time dependent generalized plasticity model, as listed in Table 2.2. The numerical model studies by Huang et al. (2009) and Zarnani and Bathurst (2011) showed that numerical models of reinforced soil walls, with simpler constitutive model are adequate to predict the static behavior and its hysteretic behavior during cyclic loading.

In present study, the static behavior of soil is simulated with elasto-plastic Mohr Coulomb material, coded with stress dependent hyperbolic soil modulus proposed by Duncan et al. (1980). Dynamic behavior is simulated as non-linear and hysteretic constitutive relation that follows the Masing rule (Masing 1926). The numerical implementation of the constitutive model using FISH programming is presented in the following sub-sections.

Backfill Material Properties from Physical Tests

The backfill material used for physical model of GRS wall, as described by Krishna (2008), is considered for the development of reinforced soil wall. The soil,

used in the shaking table tests, had maximum dry weight of 17.66 kN/m^3 at the densest state and minimum dry unit weight of 14.03 kN/m^3 at the loosest state. The angle of internal friction obtained from triaxial tests on sand at relative density of 63% was reported as 43° (Krishna 2008).

Constitutive Model for Backfill Soil

In numerical models of GRS walls, the backfill soil is simulated in layer by layer as illustrated in physical model tests (Krishna and Latha 2007, 2009 and Latha and Krishna 2008). As the model is simulated in layers, confining pressure on each zone changes with change in height of fill and hence the modulus. Hence the modulus during construction is modelled as stress dependent deformation modulus (E_t), that change as the height of the soil changes. Hence, the backfill soil is modeled as elasto-plastic Mohr Coulomb material coded with hyperbolic soil modulus. The hyperbolic stress dependent soil modulus is expressed as Eq. 3.4 (Duncan *et. al.* 1980).

$$E_t = \left[1 - \frac{R_f(1-\sin\phi)(\sigma_1-\sigma_3)}{2(c.\cos\phi+\sigma_3\sin\phi)}\right]^2 K_n.P_a\left(\frac{\sigma_3}{P_a}\right)^n \qquad 3.4$$

where K_n is the modulus number; n is the modulus exponent; c is the cohesion; σ_1 and σ_3 are the major and minor effective confining stress respectively; ϕ is the angle of internal friction; R_f is the failure ratio; p_a is atmospheric pressure. Krishna (2008) determined the hyperbolic soil parameters as mentioned by Duncan et al. (1980), from laboratory triaxial test data. The hyperbolic model parameters K_n, n and average R_f obtained by Krishna (2008) for backfill sand at 63% relative density were 831, 0.678 and 0.93, respectively.

As FLAC^{3D} do not have built in hyperbolic model, the model is incorporated by FISH subroutines (Itasca 2008). The principal stresses (σ_1 and σ_3) are extracted by FISH

variables from each element of the model after every 10 steps and stress dependent modulus (E_t) is calculated. The modulus is then updated using zone variables in FISH programme.

Numerical Triaxial Tests

Numerical triaxial tests are performed to verify the implementation of hyperbolic soil model parameters in backfill soil. A cylindrical grid of diameter 38 mm and length 76 mm is considered for simulation of numerical triaxial test. The numerical model considered for triaxial test sample is shown in Fig. 3.2

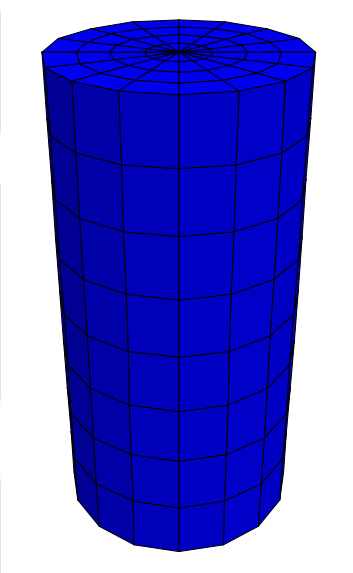

Fig. 3.2 Numerical model of triaxial test sample (dia 38 mm & height 76 mm)

The soil is simulated as elasto-plastic Mohr Coulomb material coded with hyperbolic soil modulus proposed by Duncan et al.(1980). The angle of internal friction and other hyperbolic model parameters as mentioned in Krishna (2008) are considered in numerical simulation. The all around confining pressures of 10 kPa, 50 kPa, 100 kPa and 150 kPa are applied to the model. The results obtained are compared with physical triaxial test results (Krishna 2008) and are shown in Fig. 3.3. Comparison of the results between numerical and physical triaxial tests, at different

confining pressures, indicates that the deviator stresses in numerical simulations are reasonably comparable to that of physical tests. This validates the hyperbolic model parameters obtained from physical model tests and also its proper implementation in numerical modeling.

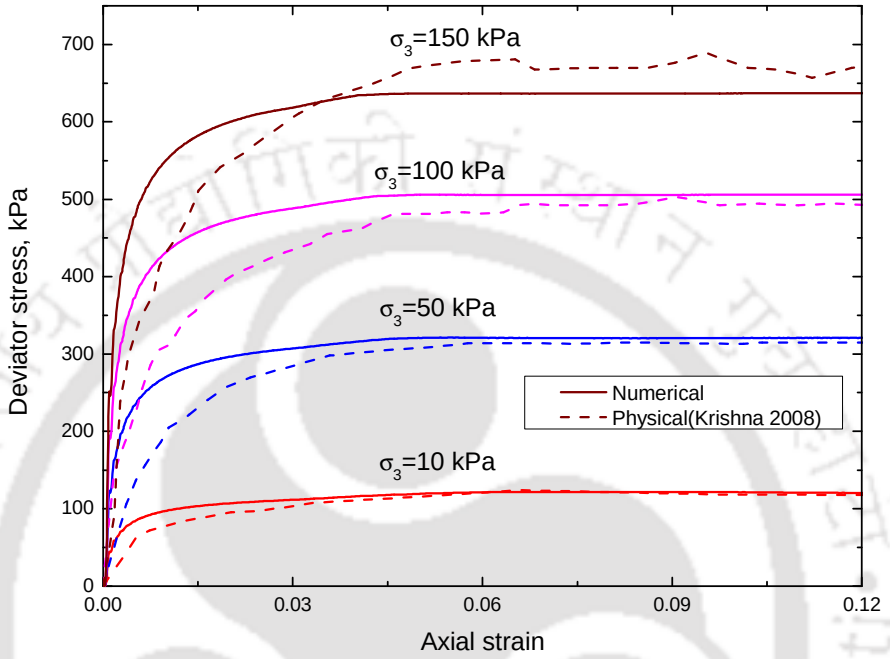

Fig. 3.3 Comparison of results between numerical and physical triaxial tests at different confining pressure

Fig. 3.4 shows variation of stress ratio with respect to the octahedral shear strain (γ_{oct}) obtained from numerical triaxial tests at different confining pressures. The variation of stress ratio with respect to octahedral shear strain is divided into three zones. They are: (I) Elastic zone - the stress and strain variation is linear and and elastic (II) Non-linear zone – stress and strain interdependency is non-linear and (III) Plastic zone - the stress increase is not significant compared to the strain increment indicating plastic deformation. From the figure it is seen that the elastic zone is extended upto octahedral shear strain of 0.3%, non-linear zone lies within 0.3% - 2.0% strain levels (γ_{oct}) and plastic zone exist beyond 2.0% strain (γ_{oct}).

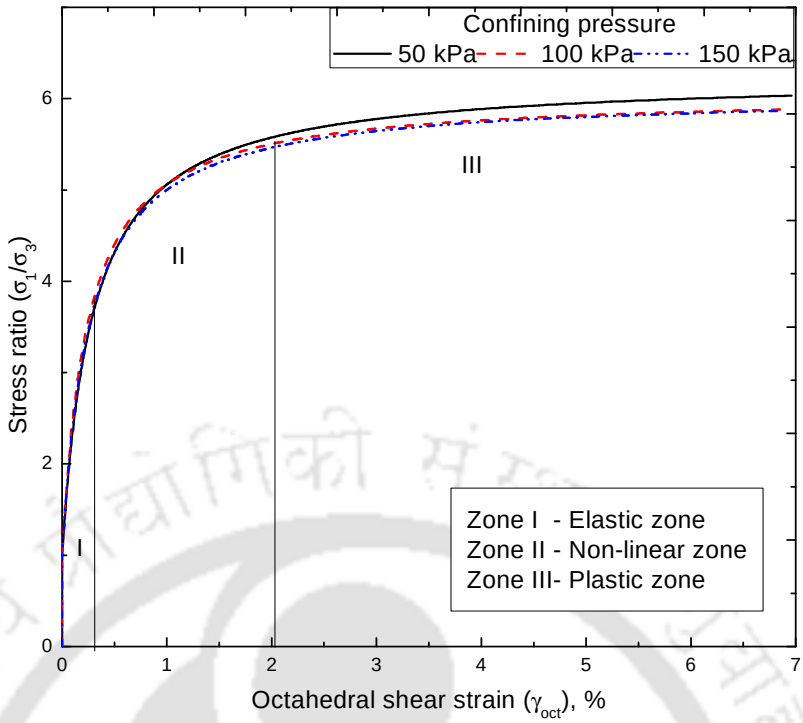

Fig. 3.4 Behavior of soil in numerical triaxial compression

Constitutive Model for Soil during Cyclic Loading

In the numerical model, subjected to seismic excitation, use of constant shear modulus during cyclic loading is not appropriate due to cyclic/hysteresis nature of soil. Massing model (Masing 1926) is the simple cyclic model which can incorporate cyclic as well as hysteric behavior of soil. In Massing rule, a skeleton curve is used to express hysteresis loop in unloading and reloading process. A proper hysteresis loop can be simulated efficiently with skeleton curve in Massing rule. The shear behavior of granular soils under cyclic loading is modeled using non-linear and hysteretic constitutive relation according to Massing rule (Masing 1926). Cai and Bathurst (1995); Fakharian and Attar (2007) and Liu et al. (2011) were also adopted the Masing rule for two dimensional numerical simulations of GRS Walls. Schematic representation of shear stress and shear strain relation during unloading and reloading cycles, according to Masing rule, is shown in Fig. 3.5. Here, octahedral shear stress τ_{oct} and octahedral shear strain γ_{oct} are used to represent stress and strain conditions in

three dimensional states. The octahedral stress and strain states are calculated from six stresses and strains acting on each element. The octahedral stress invariants, namely octahedral normal stress, σ_{oct} and octahedral shear stress, τ_{oct}, are stress parameters independent of the choice of reference axis and adopted to analyze the stress variation (Chen and Mizuno, 1990).

$$\sigma_{oct} = \frac{1}{3}(\sigma_1 + \sigma_2 + \sigma_3) \quad 3.5$$

$$\tau_{oct} = \frac{1}{3}[(\sigma_1 - \sigma_2)^2 + (\sigma_2 - \sigma_3)^2 + (\sigma_3 - \sigma_1)^2]^{1/2} \quad 3.6$$

where σ_1,σ_2 and σ_3 are the principal stresses on an element. Similarly the octahedral strain invariants are strain parameters independent of the choice of reference axis (Chen and Mizuno, 1990) and are expressed as

$$\gamma_{oct} = \frac{2}{3}[(\epsilon_{xx} - \epsilon_{yy})^2 + (\epsilon_{yy} - \epsilon_{zz})^2 + (\epsilon_{zz} - \epsilon_{xx})^2 + 6(\epsilon_{xy}{}^2 + \epsilon_{yz}{}^2 + \epsilon_{zx}{}^2)]^{1/2} \quad 3.7$$

Where ε_{xx}, ε_{yy}, ε_{zz}, ε_{xy}, ε_{yz} and ε_{zx} are strain parameters acting on each element in three dimensional state.

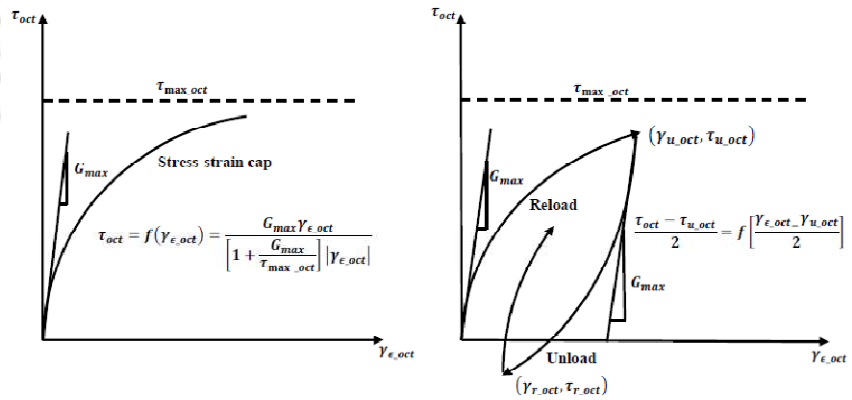

Fig. 3.5 Non-linear hysteretic stress-strain model of granular soil: (a) stress-strain cap; (b) unload-reload cycle (modified after Cai and Bathurst 1995)

In the Masing model, the shear modulus is determined on the basis of stress and strain states that may vary during cyclic loading condition. The tangent shear modulus during the first cycle is expressed as

$$G_t = \frac{G_{max}}{\left[1+\left(G_{max}/\tau_{\max\_oct}\right)|\gamma_{\epsilon\_oct}|\right]^2} \quad 3.8$$

where G_{max} is the initial shear modulus, τ_{max_oct} is the maximum octahedral shear stress which is related to shear parameters of soil through cohesion c and internal angle of friction ϕ, and γ_{ϵ_oct} is the octahedral shear strain. The initial shear modulus G_{max} is extracted from each soil element by FISH variables before the application of dynamic excitation. The tangent modulus during unloading/reloading cycle is

$$G_t = \frac{G_{max}}{\left[1+\left(G_{max}/2\tau_{max\_oct}\right)|\Delta\gamma_{oct}|\right]^2} \quad 3.9$$

where $\Delta\gamma_{oct}$ represents the difference in octahedral shear strain during unloading/reloading cycle. In unloading case as it equals to $(\gamma_{\epsilon\_oct} - \gamma_{u\_oct})$ and in reloading case it is $(\gamma_{\epsilon\_oct} - \gamma_{r\_oct})$. γ_{ϵ_oct} is the octahedral shear strain at present state and γ_{u_oct} and γ_{r_oct} are octahedral shear strains at starting points of unloading and reloading, respectively, for that cycle.

The tangent bulk modulus B_t is expressed in the following form:

$$B_t = K_b \times p_a \times \left(\frac{\sigma_m}{p_a}\right)^n \quad 3.10$$

where K_b is the bulk modulus constant and n is the bulk modulus exponent.

3.3.2 Geosynthetic reinforcement

Geosynthetic reinforcement members are planner products manufactured from polymeric materials. The main function of reinforcement member within the soil is to reinforce the backfill soil by developing tensile force in it. The reinforcements are simulated as structural elements in numerical simulations of reinforced soil wall.

Different researchers adopted different methods to model the reinforcement members as mentioned in Table 2.2. They are modeled as 1D beam element (Yogendrakumar et al.1992; Bruke et al. 2004; Ling et al. 2010; Liu et al. 2011; Liu and Ling 2011; Krishna and Latha 2012), cable element (Bathurst and Hatami 1998; Hatami and Bathurst 2000; El-Emam et al. 2001; El-Emam et al. 2004; Fakharian and Attar 2007; Zarnani et al. 2011) and shell element (Helwany et al. 2001; Helwany and McCallen 2001; Lee et al. 2010). The constitutive models applied to simulate non-linear hysteretic behavior of reinforcements are: nonlinear equation developed from load-strain-time test data (Karpurapu and Bathurst 1995), hysteretic unload-reload model of soil materials for polymeric reinforcement materials (Cai and Bathurst 1995) and cyclic behavior of high density uniaxial geogrid using bounding surface model (Ling et al. 2004; Ling et al. 2010; Liu 2009 and Liu et al. 2011).

In this present study, the geosynthetic reinforcement is modeled using the geogrid structural element available in FLAC^{3D}. The geogrid elements are three nodded shell elements used to model flexible membrane that resist as membrane but do not resist any bending loading.

The shell elements are similar to 3-noded triangular shell type elements available in finite element methods. Five types of 3-noded triangular elements available for shell-type are: 2 plane-stress elements, 1 plate-bending element and 2 shell elements. The plane-stress elements model the membrane action only, the plate-bending elements simulate the bending action only and shell elements are superpose the membrane and bending actions. In membrane action, a flat plate subjected to plane-stress conditions (loaded only in its own plane). In bending action, a flat plate subjected to external loads which do not have any component parallel to its own plane. It supports the transverse load by bending.

The geogrid element behaves as isotropic linear elastic material with no failure limit. The studies of failure of reinforced soil walls (Ling et al. 2001; Pamuk et al. 2004 and Ling and Leschinsky 2005) revealed that the failure of reinforced soil wall is due to subsidence of facing system and backfill soil. The reinforcement failures are rarely observed. So geogrid element without any failure limit can be used in numerical simulations. The effective confining stress and total shear stress developed on geogrid are balanced by the membrane stress developed within the geogrid itself (Itasca 2008). The geogrid element embedded in FLAC^{3D} is schematically represented as shown in Fig. 3.6. The stresses consisting of effective confining pressure σ_m on a geogrid node and total shear stress τ acting on tributary area of geogrid nodes are balanced by membrane stress N developed within geogrid.

The required input parameters for geogrid element, in FLAC^{3D}, are: (1) elastic modulus (2) Poisson's ratio (3) thickness of geogrid. The hysteretic behavior of geosynthetics material is not considered in simulation because the hysteretic behavior of soil is predominant one. This approach is also adopted by several researchers (Yogendrakumar et al. 1992; Bathurst and Hatami 1998; Hatami and Bathurst, 2000; El-Emam and Bathurst 2004; Helwany et al. 2001; Helwany and McCallen 2001; Fakharian and Attar 2007 and Krishna and Latha 2012).

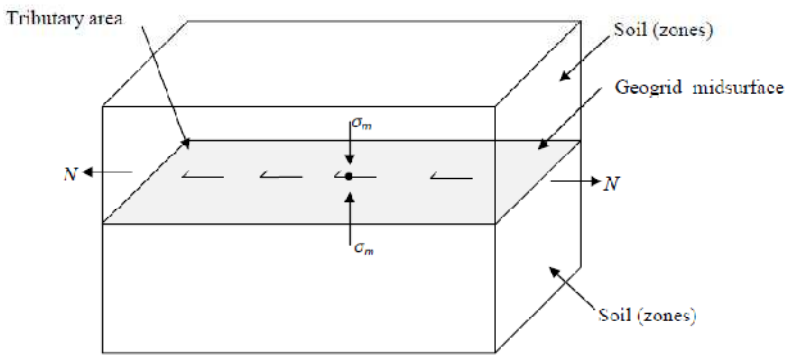

Fig. 3.6 Stresses acting on geogrid surrounding a node (Itasca 2008)

3.3.3 Facing elements

The facing elements are, generally, simulated as linear elastic material model (Cai and Bathurst 1995; Helwany et al. 2001; Ling et al. 2004; Fakharian and Attar 2007; Lee et al. 2010). In the present study two different types of facing elements are used. The facing of wrap-faced walls are simulated by geogrid structural element. The facing of rigid-faced walls are simulated as elastic material. The properties required for the elastic material model are mass density, shear modulus and bulk modulus.

3.3.4 Interface elements

An interface element enables proper interaction between dissimilar materials. Karpurapu and Bathurst (1995) modeled the interface between reinforcement layer and soil as a zero thickness element. The shear strength and stiffness behavior between the soil and reinforcement are modeled as stick-slip formulation following Mohr Coulomb failure criterion by Cai and Bathurst 1995; Ling et al. 2004; and Liu et al.2011. Few researchers considered the interface as grout material with negligible or zero thickness (Hatami and Bathurst 2000; El-Emam et al. 2004; Fakharian and Attar 2007). Liu (2009) and Zarnani et al. (2011) considered the soil and reinforcement perfectly bounded.

In the present study two different interfaces are considered: interface between backfill soil and facing; and interface between soil and reinforcement. The interface between the backfill soil and reinforcement at facing for wrap-faced walls are kept same as that of interface between the soil and reinforcement.

The interface between backfill soil and rigid wall controls the relative movement between them. The relative interface movement is controlled by interface normal stiffness (k_n) and shear stiffness (k_s). A recommended thumb rule is that k_s and

k_n be set to ten times the equivalent stiffness of the stiffest neighboring zone (Itasca 2008). The maximum stiffness value is given by Itasca (2008) as

$$k_n = k_s = 10 \times max\left[\frac{K+\frac{4}{3}G}{(\Delta z)_{min}}\right] \qquad 3.11$$

Where the parameters $(\Delta z)_{min}$ is the smallest dimensions in normal direction, K and G are bulk modulus and shear modulus of continuum zone adjacent to the interface, respectively. This approach gives the preliminary values of the interface stiffness components, and these can be adjusted to avoid intrusion to adjacent zone and to prevent excessive computation time.

The interface behavior of geogrid is represented numerically at each geogrid node by a rigid attachment in normal direction and spring-slider in the tangent plane to the geogrid surface. The orientation of the spring-slider changes in response to the shear displacement between geogrid and neighboring soil elements. The shear behavior of the geogrid-soil interface is cohesive and frictional in nature and is controlled by effective confining stress σ_m and coupling spring properties: (i) stiffness per unit area k; (ii) cohesive strength c; (iii) friction angle ϕ. The effective confining stress, σ_m, acts perpendicular to the geogrid surface and computed at each geogrid node (Itasca 2008).

3.4 SOIL-REINFORCEMENT INTERACTION

The soil-reinforcement interaction is one of the major influencing parameters governing the performance of reinforced soil retaining wall. In a GRS retaining wall, the wall (facing) movement mobilizes interface shear stress between soil and reinforcement. Further, this leads to tensile stress mobilization within the reinforcement (geosynthetic), which supports the facing system to keep the structure

stable. Thus pullout mechanism takes place which depends on confining stress and degree of movement. In general, soil-reinforcement interaction behavior/parameters can be determined experimentally by either direct shear tests or pullout tests (ASTM D 6706-01(2007)). Therefore interaction parameters obtained from pullout tests are used in design of reinforced structures (BS 8006, 1995).

In the numerical model, the input parameters for modeling the soil-reinforcement interaction are interface friction and interface stiffness. Properties of the soil element and reinforcement elements, required for development of numerical model can be determined from laboratory tests. The laboratory pullout tests can give the interface friction value between soil and reinforcement, and also provide an estimate of interface stiffness. However, the interface parameters shall be verified by trials in numerical simulations of pullout tests. In this regard, laboratory pullout tests were performed to observe pullout behavior of soil reinforcement system. Further the pullout tests have been numerically simulated to obtain reliable interaction parameters and to verify the implementation of soil-geosynthetic interaction behavior.

3.4.1 Laboratory pullout tests

Laboratory pullout tests were conducted on sand-geotextile system to observe the pullout behavior (Prashant et al. 2011). In pullout test, the geosynthetic, confined in the neighboring soil, is pulled out at constant rate. The geosynthetic is strained by offering shear stress on both the faces.

Materials

Locally available river sand was used in the pullout tests. Particle size distribution (ASTM D 6913-04) and physical characteristics are shown in Fig. 3.7. and Table 3.1, respectively.

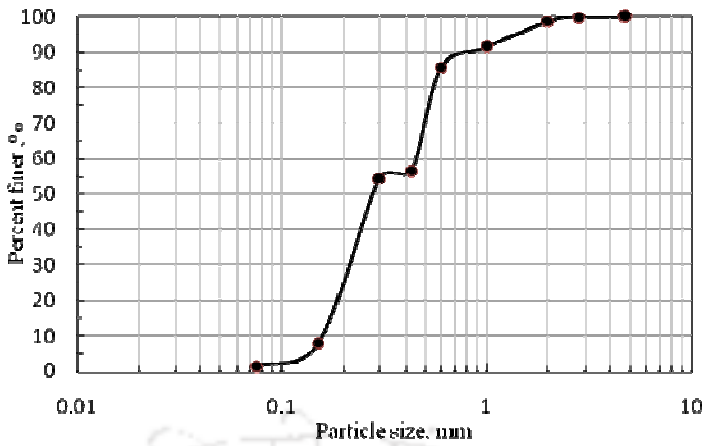

Fig. 3.7 Grain size distribution of sand used in the study

Table 3.1 Soil Physical Characteristics

D_{60} (mm)	D_{30} (mm)	D_{10} (mm)	C_u	C_c	γ_{min} (kN/m^3)	γ_{max} (kN/m^3)	Classification (USCS)
0.45	0.22	0.16	2.81	0.67	14.02	16.58	SP

Shear strength parameter (friction angle) of the sand was determined from triaxial tests (as per IS: 2720 (Part-II)) on 38 mm diameter and 76 mm height samples. Triaxial test samples were prepared at 70% relative density and tested at confining pressures 100, 200 and 400 kPa. Test results are shown in Fig. 3.8 The angle of internal friction angle (ø) was determined as 39°. From this test data, hyperbolic model parameters (Duncan et al. 1980) of the soil were evaluated as described in Appendix A and listed in Table 3.2. A numerical model of cylindrical soil sample was simulated (as explained in section 3.3.1) and solved to verify the hyperbolic soil parameters. The results obtained from numerical simulation of triaxial tests are compared with the physical triaxial test results, as shown in Fig. 3.8. It is observed from the figure that, the deviator stresses in numerical simulations are matching reasonably well to that of physical test results. This validates the hyperbolic model parameters obtained from physical model tests and also its proper implementation in numerical modeling.

A woven geotextile was considered for pullout tests. Tensile properties of the geotextile were determined as per ASTM D 4595. The load elongation behavior of woven geotextile is shown in Fig. 3.9. The tensile strength of geotextile is 38.17 kN/m and its elongation at break is 38.5%. Mass per unit area, of the same was determined as 244 g/m^2 according to ASTM D5261.

Table 3.2 Hyperbolic model parameters obtained from triaxial test

Soil properties for Mohr Coulomb model with hyperbolic soil parameters	
Mass density, kg/m^3	1570
Friction angle	39°
Dilation angle	15°
Cohesion, kPa	0.0
Atmospheric pressure, kPa	101.3
Modulus number, K_n	534.6
Modulus exponent, n	0.42
Failure ratio, R_f	0.753

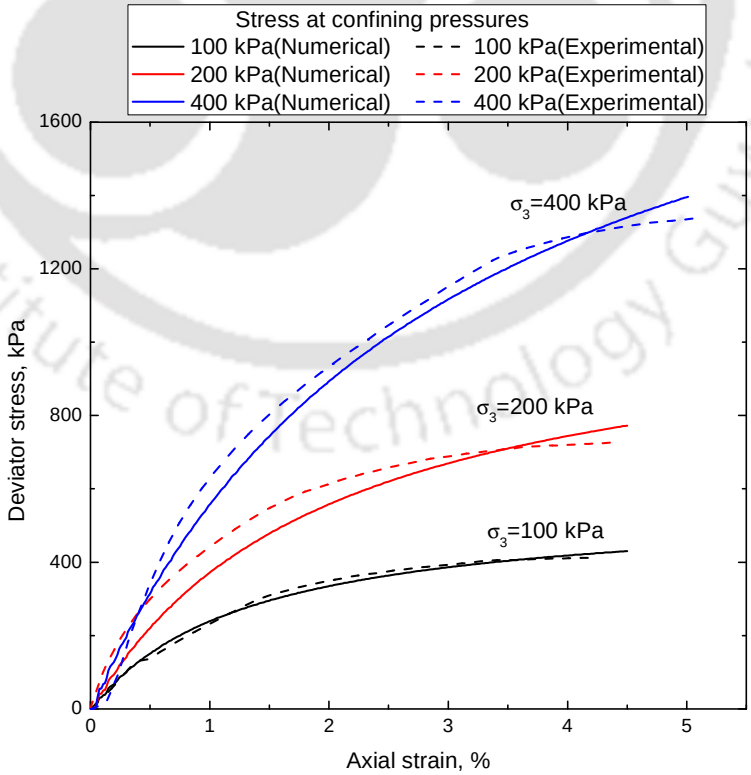

Fig. 3.8 Comparison numerical and physical triaxial test results on sand at different confining pressures

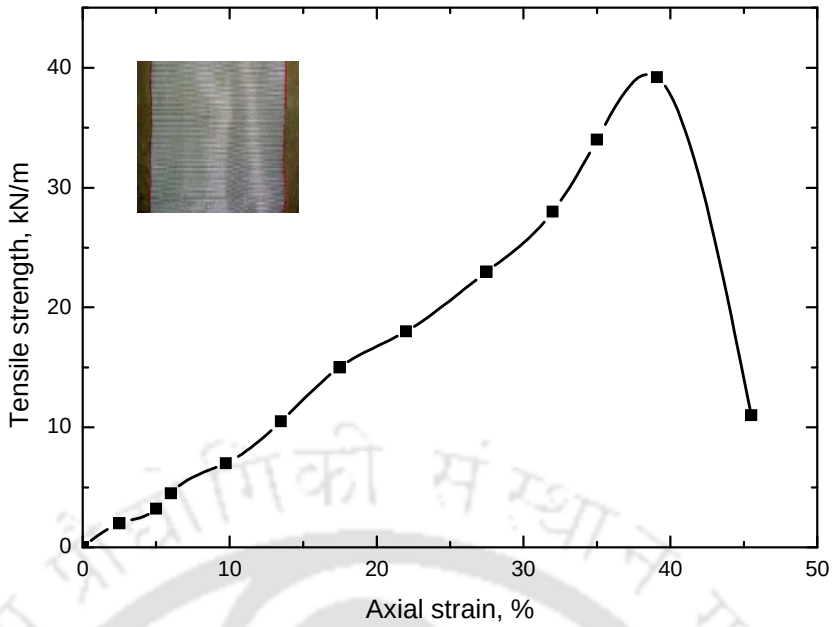

Fig. 3.9 Load elongation response of woven geotextile

Test apparatus and Instrumentation

Large size direct test apparatus that was modified for conducting pullout tests was used. Pullout test setup and associated instrumentation are shown in Fig. 3.10. The inner dimensions of the pullout box are 400 mm long, 393 mm wide and 230 mm height. A 12 mm thick horizontal slot was provided in the front face of the box to allow the pullout of reinforcement in soil. Sand was placed in the test box using dry pluviation technique. An elevated sand hopper was used to facilitate sand placement for achieving desired relative density. The woven geotextile of size 300 mm ×150 mm was placed at a depth of 115 mm from the top of box. The sample was clamped to the load cell as shown in Fig. 3.10. Normal stress was applied over the rigid plate resting on the sample by means of mechanical lever arm load system. The clamped geosynthetic was pulled out under controlled displacement rate. The corresponding displacement of geosynthetic was measured by placing LVDT at the geosynthetic clamper. All tests were conducted at relative density (RD) of 70% and displacement rate of 4.567 mm/min.

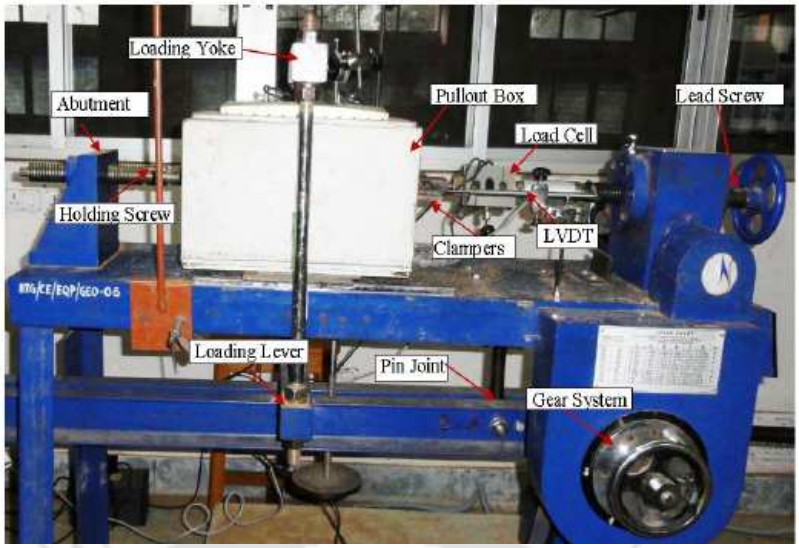

Fig. 3.10 Pullout box along with instrumentation

Test results

The pullout resistance-displacement behavior of sand-geotextile at different normal stresses (20, 33 and 67 kPa) is shown in Fig. 3.11. It is found that increase in normal stress results in significant increase in pullout resistance of geotextile. The interfacial friction angle (δ) is calculated as 31.9°. This interface friction angle corresponds to a friction ratio ($tan\delta/tan\phi$) of 0.77. The stiffness (K_s) values calculated at 2% and 5% strain for different confining pressures and found to be within a range of 2×10^4 - 5×10^4 kN/m^2/m.

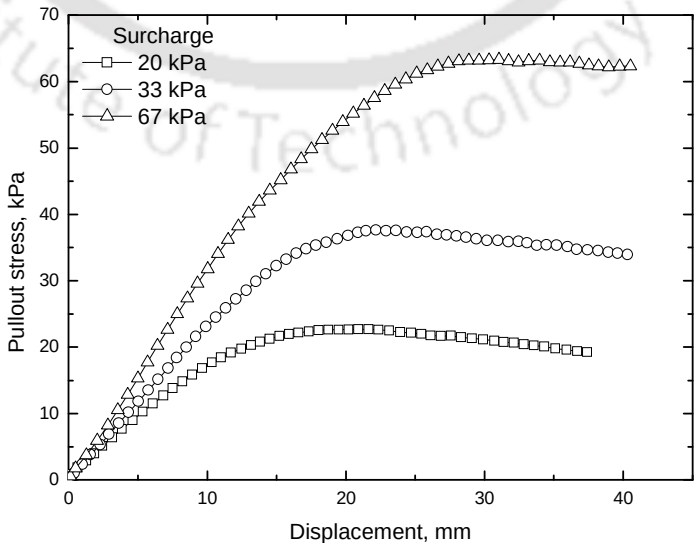

Fig. 3.11 Pullout response of composite geotextile at different confining pressure

3.4.2 Numerical simulation of pullout tests

The laboratory pullout tests are simulated using FLAC^{3D}. The materials required for numerical modeling of pullout tests are of three types: (i) soil, (ii) reinforcement and (iii) interfaces. The soil is modeled as elasto-plastic Mohr-Coulomb material model coded with hyperbolic soil modulus as described in section 3.3.1. The geotextile reinforcement is modeled using the geogrid structural element available in FLAC^{3D} (Section 3.3.2). The soil-geosynthetic interaction behavior is represented numerically at each geogrid node by a rigid attachment in normal direction and spring-slider in the tangent plane to the geogrid surface described in section 3.3.2. The model parameters adopted for the numerical simulation of pullout tests are presented in Table 3.3. The interfaces friction angle between the soils and geosynthetic are determined based on interface friction angle, $\delta = tan^{-1}\left(\frac{2}{3}tan\phi\right)$ (Liu and Ling 2012).

Model development

The soil elements are modeled using eight nodded brick elements. The dimensions for soil material are 400 mm x 400 mm x 230 mm. The whole grid is divided into cubical brick elements of size 25 mm each. The reinforcement material used for pullout tests is 150 mm wide, 300 mm long and 3 mm thick. The reinforcement is placed at a depth of 115 mm from the top of soil element. The boundary conditions applied to the model represent the actual boundary of the physical model tests. The numerical simulation of pullout test is shown in Fig. 3.12. The bottom boundaries are completely fixed in vertical direction. The lateral boundaries are fixed in their respective directions. The model is brought to equilibrium after placing the reinforcement. The confining pressure of 20 kPa, 33 kPa

and 67 kPa is applied at the top of soil element. The model is again brought to equilibrium after applying surcharge. The pullout tests are performed by applying a constant horizontal velocity to the reinforcement nodes along the box front. The pullout force is calculated as cumulative unbalanced forces in the reinforcement acting at the grid nodes on pullout face. The pullout stresses are obtained by dividing the pullout force by the embedded area of the reinforcement. The pullout displacements are monitored by the grid point displacement in the pullout face.

Table 3.3 Material properties used in numerical model for pullout tests

Soil properties for Mohr model with hyperbolic soil parameters	
Mass density, kg/m^3	1570
Friction angle	39°
Dilation angle	15°
Cohesion, kPa	0.0
Atmospheric pressure kPa	101.3
Modulus number, K_n	534.6
Modulus exponent, n	0.42
Failure ratio, R_f	0.739
Reinforcement (Geotextile) properties	
Mass density, g/m^2	244
Thickness, m	0.003
Stiffness, kN/m	171.43
Reinforcement (Composite Geotextile) interface properties	
Coupling spring cohesion, kPa	0.0
Coupling spring friction,	28.5°

Numerical model results for pullout tests

Pullout responses obtained from the numerical simulations are presented in terms of pullout stress versus displacement (pull). The interface stiffness between soil and reinforcement is one of the major factors affecting the pullout behavior of

reinforcement in numerical modeling. Sensitivity of the numerical model is verified with varying interface stiffness of 1×10^3, 1×10^4, 1×10^6, 1×10^7, 1×10^8 and 1×10^9 kN/m^2/m. The pullout stresses versus displacements are presented in Fig. 3.13. The maximum pullout stress obtained from numerical model with a surcharge of 20 kPa is 20.99 kPa at interface stiffness of 1×10^3 kN/m^2/m and do not show any peak upto displacement of 40 mm. The maximum pullout stresses for numerical model at surcharge of 20 kPa is 21.03 kPa , 21.23 kPa and 22.69 kPa at displacements of 21.28 mm, 19.60 mm and 20.65 mm for interface stiffness of 1×10^4 , 1×10^6 and 1×10^7 kN/m^2/m, respectively.

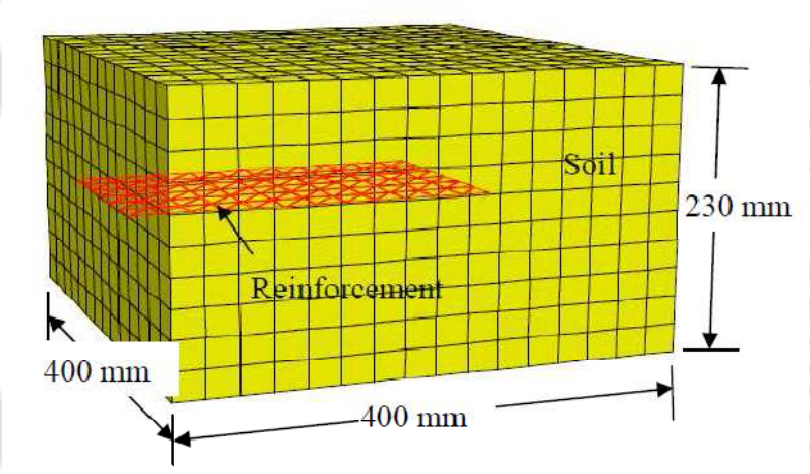

Fig. 3.12 Mesh for numerical model of pullout stress

The pullout stresses increase to more than 30 kPa at for interface stiffness of $1x10^8$ and 1×10^9 kN/m^2/m. So the pullout stresses obtained from the numerical model are comparable with experimental result (22.71 kPa at a displacement of 21.65 mm) at interface stiffness of 1×10^7 kN/m^2/m. It is also seen that the pullout stresses are for interface stiffness of 1×10^4 and 1×10^6 kN/m^2/m are fall within 10% of the experimental results. Similarly the pullout stresses, obtained from numerical model, at surcharges of 33 kPa and 67 kPa are comparable with that of experimental results at interface stiffness of 1×10^4 , 1×10^6 and $1x10^7$ kN/m^2/m. So the interface stiffness within a range of 10^4 to 10^7 does not have much variation in maximum pullout stress

variation. It is also observed from Fig. 3.13 that the pullout stresses increases with the increase in surcharge. The results obtained from numerical model are reasonably comparable with that of experimental results. The interfaces of geogrid structural elements used for simulation of reinforcement in pullout tests also responds to the surcharge.

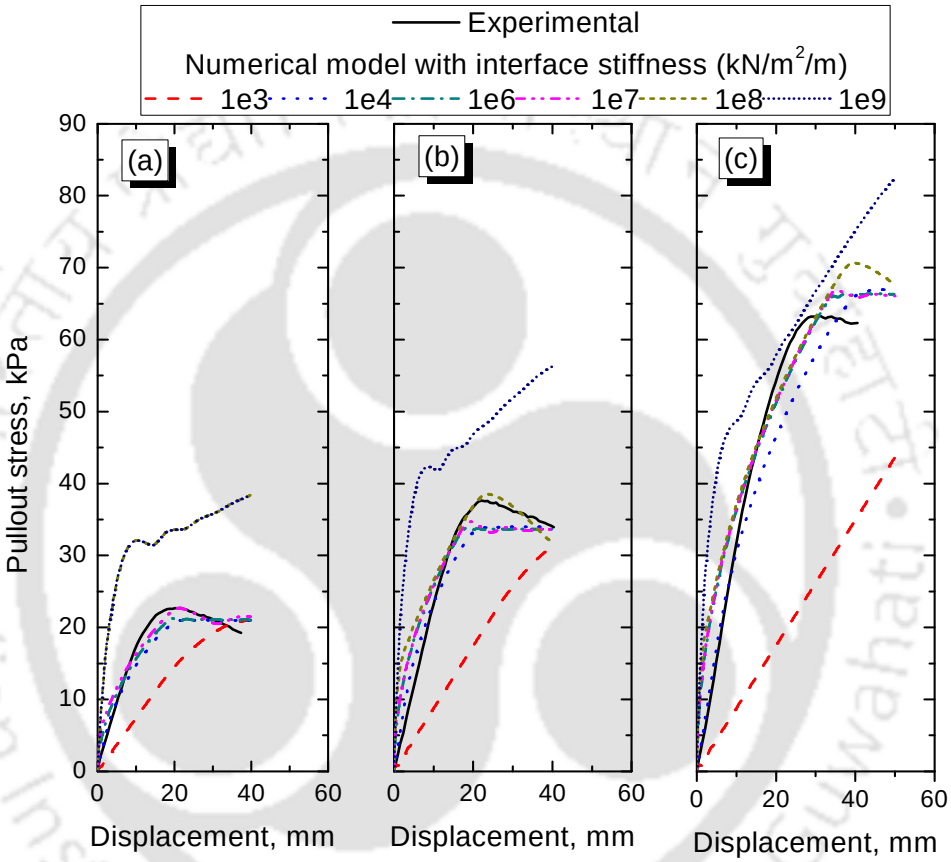

Fig. 3.13 Pullout stress versus displacement for surcharge of (a) 20 kPa (b) 33 kPa and (c) 67 kPa for numerical result with different interface parameter and experimental result

Sensitivity of the numerical model in simulating the pullout response is studied for different friction angle values. Internal friction angle values of 30°, 33°, 36°, 39°, 42° and 45° are considered for soil. The interface stiffness of 1×10^7 kN/m^2/m considered as soil geosynthetic interface. The pullout stresses with variation of friction angles are shown in Fig. 3.14. The pullout stresses increase with increase in angle of internal friction of soil for all surcharges. The numerical model is able to

simulate the effects of friction angle on pullout stress. The maximum pullout stresses for friction angles of 36°, 39° and 42° are 20.56 kPa, 22.69 kPa and 24.97 kPa at surcharge of 20 kPa; 35.22 kPa, 38.54 kPa and 42.22 kPa at surcharge 33 kPa and 59.78 kPa, 66.35 kPa and 73.30 kPa at surcharge of 67 kPa. The pullout stresses increased at a rate of 10% for variation of 3° of friction angle.

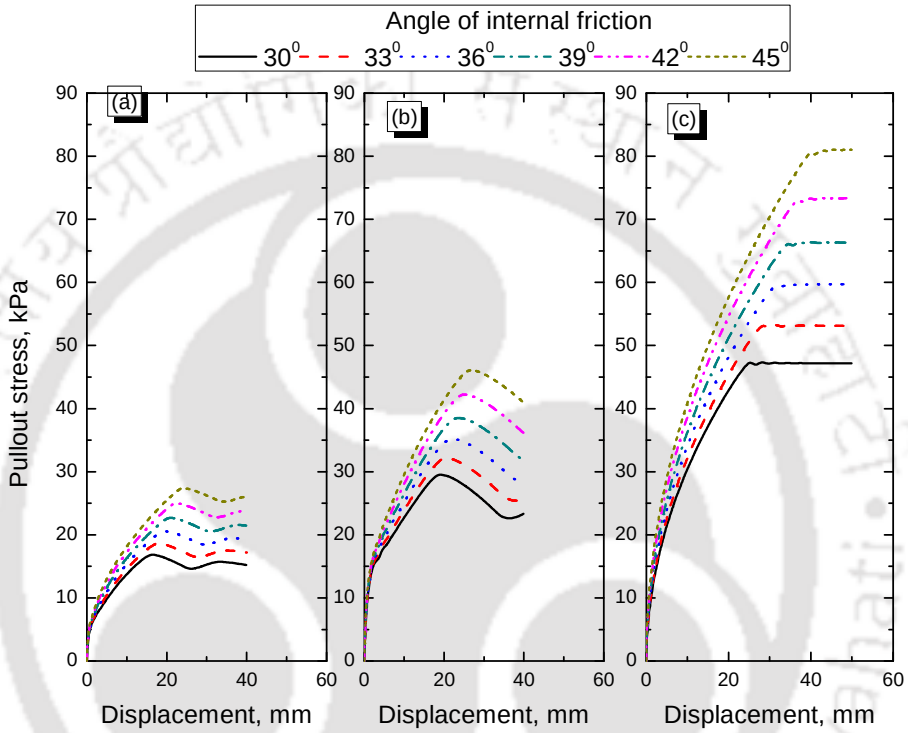

Fig. 3.14 Pullout stress versus displacement for surcharge of (a) 20 kPa (b) 33 kPa and (c) 67 kPa for numerical simulation with different angle of internal friction of soil

3.3 SUMMARY

This chapter presented description of numerical program and model parameters required for development of numerical models of GRS retaining walls. Implementation of numerical scheme in simulating the model response is briefly presented. Various soil constitutive models, structural elements available in FLAC^{3D} and implementation of dynamic loading simulation along with FLAC's FISH programming utility are briefly discussed. Various components of numerical models

of wrap and rigid-faced reinforced soil retaining wall and their model parameters are presented.

Laboratory triaxial tests are conducted on cohesionless soil at different confining pressures and its hyperbolic model parameters were evaluated and numerical simulation of triaxial tests conducted to validate soil behavior. The implementation of non-linear and hysteretic constitutive during dynamic loading is discussed. The interaction behavior of soil-geosynthetic system has been determined through laboratory pullout tests and numerical simulation of the same is performed to verify geogrid structural element and its interaction with soil in FLAC^{3D}. The interface stiffness values within a range of 10^4 to 10^7 kN/m^2/m are in close agreement with the pullout test results with 10% variation. The geogrid structural elements used for simulation of reinforcement in pullout test responds to the change in angle of internal friction of soil and confining stress.

Chapter 4. STUDIES ON WRAP-FACED WALLS

4.1 INTRODUCTION

Reinforced soil retaining walls are constructed with different facing systems. The wall facing system may be: wrap-facing, full height rigid-facing, segmental block facing and modular block facing. The wrap-faced reinforced soil walls are with flexible facing. The wrap-faced reinforced soil retaining walls are constructed by folding an extended reinforcing element (geotextile or geogrid) through 180°, to form the face and anchoring it back into the fill or to another element at higher elevation (Koerner, 1999). The reinforcements are wrapped around each layer of individual lifts. External formwork will be provided during the placement and compaction of fill. After removal of temporary formwork, free movements of facing will form the wrapped face in semi-circular shape (BS 8006:1995). The wrap-faced walls are generally preferred for temporary applications compared to other facing system walls. In this chapter, the studies on wrap-faced reinforced soil retaining walls are discussed. Development and validation of the numerical model, parametric studies are presented. Results are presented in the form of variations of horizontal displacements and vertical settlements (referred as vertical displacements), octahedral shear strains in soil along length of the wall, and discussed.

4.2 DEVELOPEMENT OF NUMERICAL MODELS

Numerical models are developed using finite difference programme FLAC^{3D} to simulate the shaking table studies on wrap-faced retaining walls reported in the literature.

4.2.1 Target physical model

Physical model tests on wrap-faced reinforced soil wall models reported by Krishna and Latha (2007) and Latha and Krishna (2008) are considered for development of the numerical model. The target physical models, tested on the shaking table, were of size 750 mm × 500 mm in plan area and 600 mm (H) deep. The models were constructed in flexible laminar container using four layers of geotextile reinforcement of length (L_{rein}) 420 mm (i.e., 0.7H). The models were constructed in equal lifts of sand filling by pluviation method and geotextile reinforcement layers were wrapped around to form the facing (by folding the geotextile through 180º to form face and anchoring it to backfill) using facing formwork. The backfill material used in the model tests was poorly graded sand having unit weight of about 16.2 kN/m^3 and friction angle of 43°. A 1mm thick woven geotextile having mass per unit area of 230 g/m^2 and breaking strength of about 55.5 kN/m was used in the tests. A nominal surcharge of 0.5 kPa was applied after completion of all lifts of the wrap-faced wall, and then the facing formwork was removed in sequence from top to bottom. After removing the supports, model wall was subjected to 20 cycles of sinusoidal motion at different base excitations. Results obtained through various instrumentations were discussed in terms of facing horizontal deformations, and acceleration amplification values. The details of the test configuration and location of various instrumentations (Krishna and Latha 2007) are shown in Fig. 4.1. Typical response of model, tested for 20 cycles of 0.1g acceleration at 1 Hz frequency, in terms of horizontal displacements and accelerations at different elevations are shown in Fig. 4.2 and Fig. 4.3, respectively.

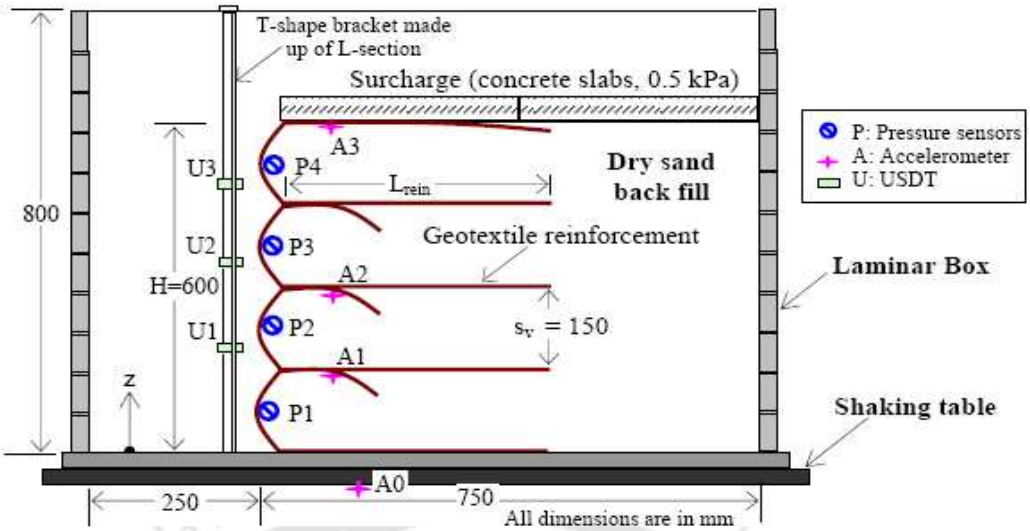

Fig. 4.1 Physical model configuration of wrap-faced wall (after Krishna and Latha, 2007)

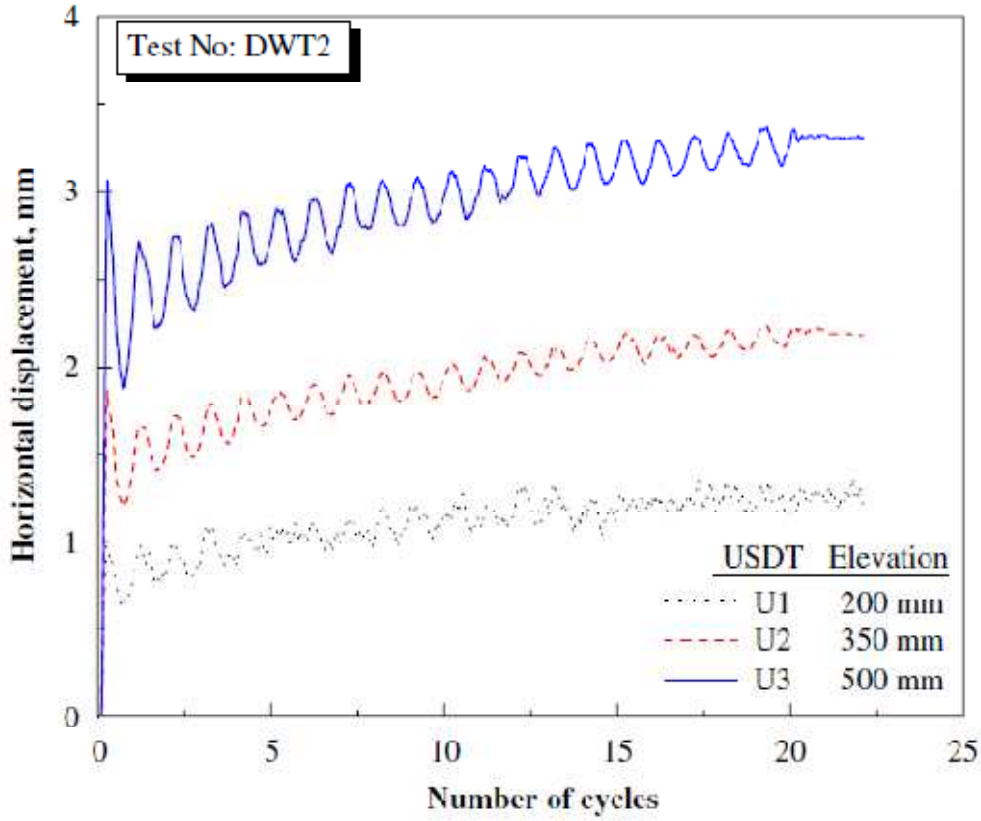

Fig. 4.2 Typical variation of horizontal displacements with time in physical model test (after Latha and Krishna, 2008)

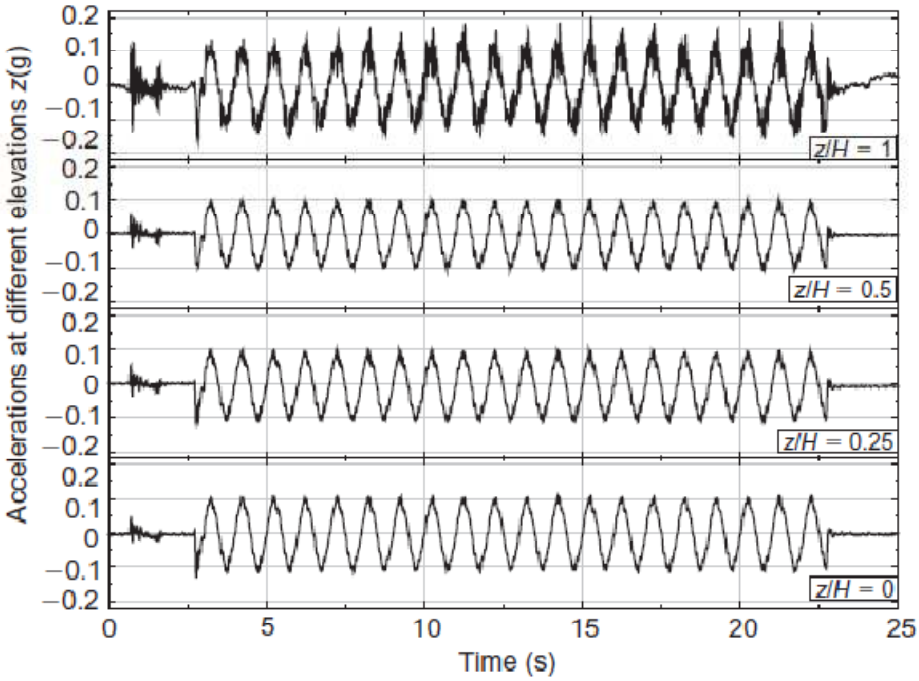

Fig. 4.3 Accelerations at different elevations from the physical model test (after Krishna and Latha 2008)

4.2.2 Development of numerical grid

Numerical model of wrap-faced wall has been generated in FLAC^{3D} by following method of construction in physical tests. A rigid foundation is first generated to represent the shaking table. The wrap-faced walls are constructed in a sequence of layers of equal thickness. Each layer is wrapped around with structural elements that represent the geotextile reinforcement members.

A rigid foundation zone of 800mm long and 50 mm thick is considered at the base of the wall as the shaking table. A grid of 600 mm height and 750 mm long is generated to represent the backfill of the wrap-faced wall. The lateral dimension of 100 mm is considered to observe the model response. Though the dimension of the physical model is 500 mm, 100 mm lateral dimension is considered to increase the speed of model solving. The model is generated in same sequence as that of physical model. Fig. 4.4 shows the steps followed in developing the wrap-faced wall numerical model with four layers of reinforcement.

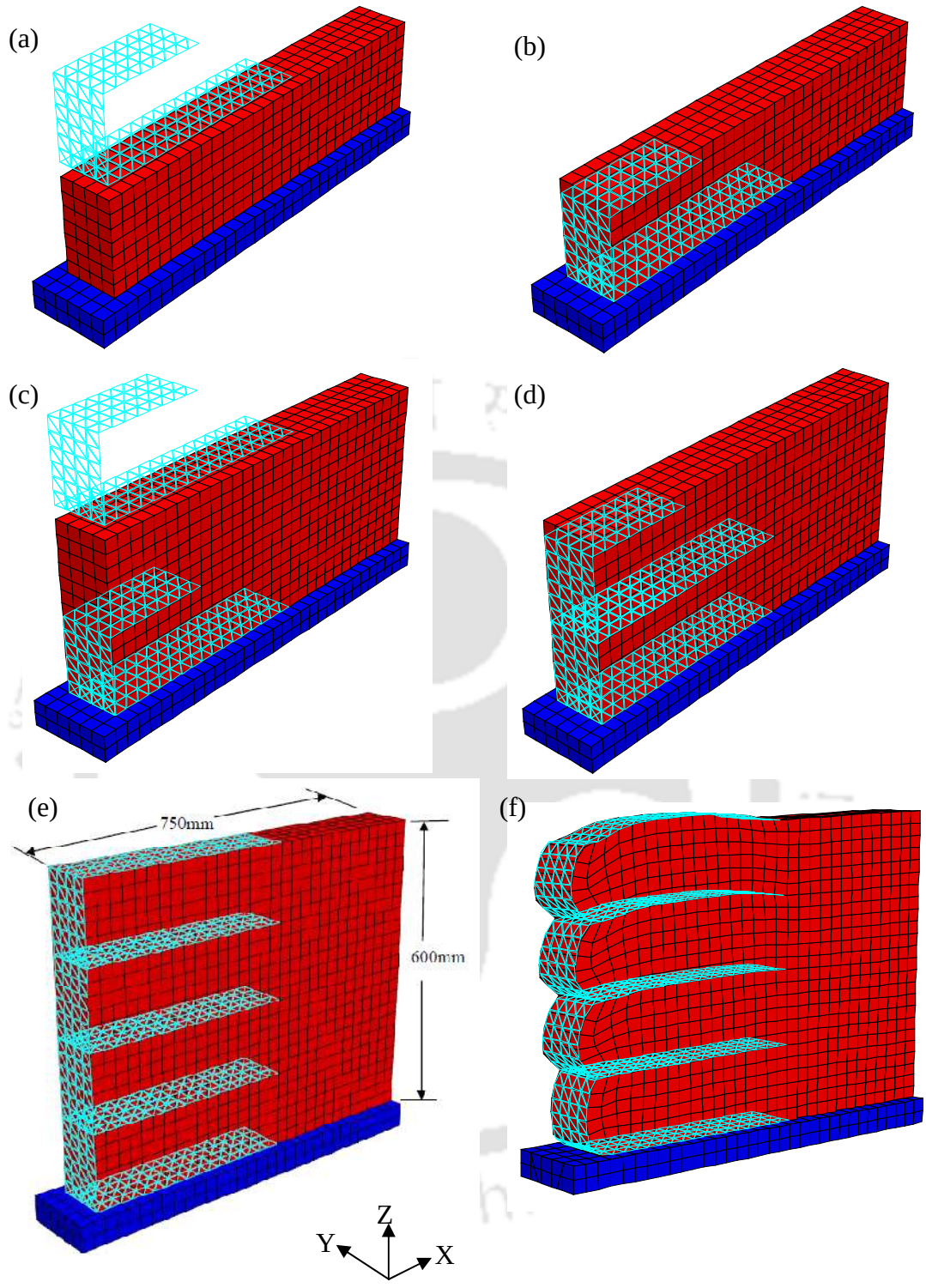

Fig. 4.4 Development of numerical grid of wrap-faced wall

The material properties for backfill soil and reinforcement are assigned based on their respective constitutive models as discussed in Chapter 3. In the numerical

models developed for validation, the length of reinforcement (L_{rein}) is considered as 420 mm, which corresponds to the L_{rein}/H ratio of 0.7 (Krishna and Latha 2007). Before placing the first layer of backfill, the foundation zone is generated and brought to static equilibrium. The first layer of backfill soil is generated on foundation. The reinforcement in wrapped form is simulated separately, and moved down, to be placed as wrap around the first layer of backfill soil (Fig. 4.4a and Fig. 4.4b). The first layer is then solved for static equilibrium, keeping the facing deformations restricted in x-direction to simulate the temporary formwork. The second layer is generated over the first layer in a similar way as shown in Fig. 4.4c and Fig. 4.4d. The model is generated in similar equal lifts with reinforcement wrapped around to form the facing for each lift. The model is solved for static equilibrium after generation of all the lifts up to the total height (H) of the wall. A surcharge pressure of 0.5 kPa is applied at the top, and model is solved to static equilibrium (Fig. 4.4e). The supports are then removed in sequence from top to bottom (layer wise). After support removal of each layer, the model is solved for static equilibrium. Fig. 4.4f shows the numerical model generated, to simulate the wrap-faced wall, after the support removal.

The backfill soil is modeled as elasto-plastic Mohr Coulomb material coded with hyperbolic soil modulus proposed by Duncan et al. (1980) (Section 3.3.1). The cohesionless soil as described by Krishna and Latha (2007) is considered for the present analysis. But a small cohesion of 0.1 kPa has been adopted to prevent computational instability. Similar small value of apparent cohesion was also adopted by Hatami and Bathurst (2005) for numerical simulation of reinforced soil walls. The hyperbolic model is incorporated, by FISH subroutines (Itasca 2008), to update the soil modulus according to their stress condition. The shear behavior of granular soils under cyclic loading is modeled using non-linear, hysteretic constitutive relation that

follows the Massing rule (Section 3.3.1), during unloading and reloading cycles of dynamic excitation. The constitutive model for soil is able to implement the damping of soil through the cyclic hysteresis. However, a minimum values of local damping of 5% is adopted for considering damping at low strain levels (Ling et al. 2005a, Lee et al. 2011). The geotextile reinforcement members are modeled using the geogrid structural element available in FLAC^{3D} as explained in Section 3.3.2. The interface between the soil and reinforcement is modeled as linear spring-slider system (Section 3.3.4).

Boundary conditions

The boundary conditions applied to the model represent the actual boundary of the physical model tests (Krishna and Latha, 2007). The bottom boundary is completely fixed in vertical direction to represent the rigid boundary between the model wall and the shaking table. The far end boundary elements are fixed in *x* direction to represent the container boundary. The boundary of model opposite to the reinforced wall facing is considered as far end boundary. During the construction, the model facing is fixed in horizontal (*x*) direction to represent the temporary support. The lateral boundaries are fixed in *y* direction to represent the lateral boundaries at the side of the physical model. After all the layers are constructed and the model has been brought to equilibrium, the facing boundaries are released stage by stage, representing the stage wise removal of temporary support. The boundary conditions after support removal are shown in Fig. 4.5.

During dynamic loading, free field boundary is applied at far end. The free field boundary conditions are applied to the lateral boundary grid points, automatically. As the free field boundary should not be applied in the front face, the base of wall (foundation) is made longer and wider than backfill and free field

boundary applied. Fig. 4.6 shows the model with free field boundary condition for dynamic loading.

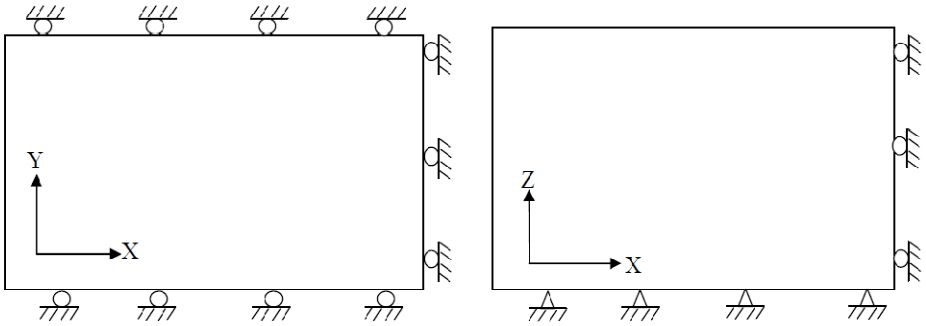

Fig. 4.5 Boundary conditions of the model in X-Y plane and Z-X plane

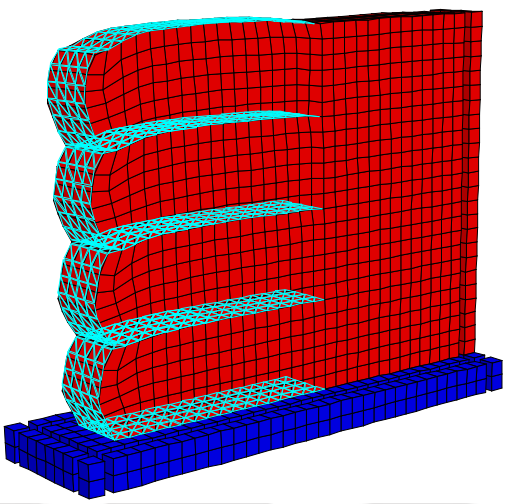

Fig. 4.6 Model wall with free field boundary condition before dynamic loading`

4.2.3 Selection of grid size

Sensitivity analysis is conducted to verify the effect of grid size on model behavior. Four different grid sizes, 7.5, 12.5, 25 and 50 mm are considered for the purpose. Horizontal pressures and deformations at the wall facing after support removal are determined and presented in Fig. 4.7. Maximum horizontal displacement of about 58 mm is observed for model with 50 mm size grid while it is about 50 mm with ± 2 % variation for other grid sizes. Horizontal pressure variations are observed

to be not so sensitive for the range of grid sizes considered. From these observations a grid size of 25mm is considered for numerical simulation of laboratory models.

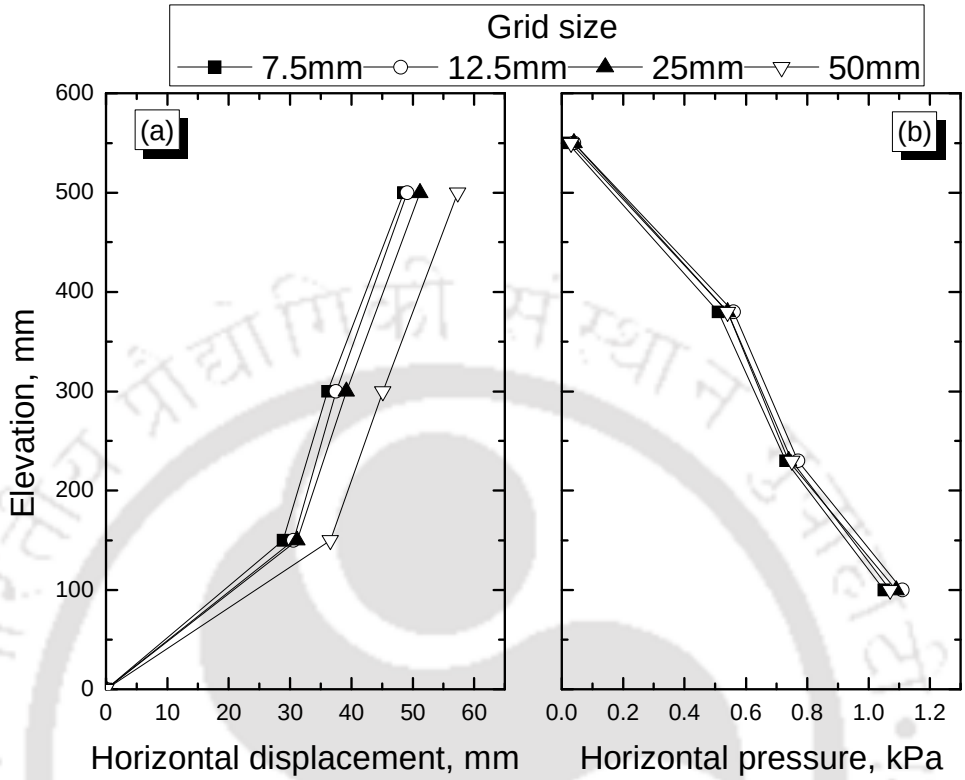

Fig. 4.7 Sensitivity of grid size on model response

The dynamic behavior of model depends upon size of grid which is governed by the accurate transmission of waves through the model. The maximum frequency that can be propagated accurately in a model of zone size 25 mm, having density of 1600 kg/m^3 and average shear modulus of 115 kPa, is calculated (as per Eqs. 3.2 and 3.3) as 34 Hz. As most of the seismic wave energy is concentrated within 15-20 Hz frequency, selection of 25 mm grid size is confirmed.

4.2.4 Sensitivity analysis

Sensitivity analyses were performed to verify the response of numerical model with variation of different model parameters. The model parameters considered for the numerical simulations and their values are listed in Table 4.1.

Table 4.1 Material properties used in numerical simulation for sensitivity analysis

Soil properties (* indicates the reference case)	
Mass density, kg/m^3	**1630**
Elastic modulus, kPa	**1×10^4**
Poisson's ratio	**0.3**
Friction angles, degree	30,**45***,52
Dilation angle, degree	5,**10***,15
Cohesion, kPa	**0.1**
Hyperbolic properties for Duncan's model	
Atmospheric pressure kPa	**101.3**
Modulus number, K_n	**831**
Modulus exponent, n	**0.678**
Failure ratio, R_f	**0.9**
Reinforcement (Geotextile) properties	
Mass density, g/m^2	**230**
Thickness, m	**0.001**
Stiffness, kN/m	100,**150***,200
Reinforcement (Geotextile) interface properties	
Coupling spring cohesion, kPa	**0.1**
Coupling spring friction, Degree	**28**
Coupling spring stiffness, kPa	1×10^5,**1×10^6***,1×10^7

The dynamic model studies are conducted for sinusoidal dynamic excitation at 0.2g base input acceleration (a). The models are subjected to 20 cycles of sinusoidal shaking at different frequency (f) 3Hz, and 5Hz. Fig. 4.8 shows the acceleration, velocity and displacement components of a typical sinusoidal excitation with a = 0.2g; f = 3 Hz. The dynamic excitation is applied at the stiff bottom, in the form of velocity in horizontal direction (uniaxial shaking).

During dynamic excitation, facing horizontal displacement histories at elevations of 200, 350 and 500 mm and incremental pressures acting on facing at

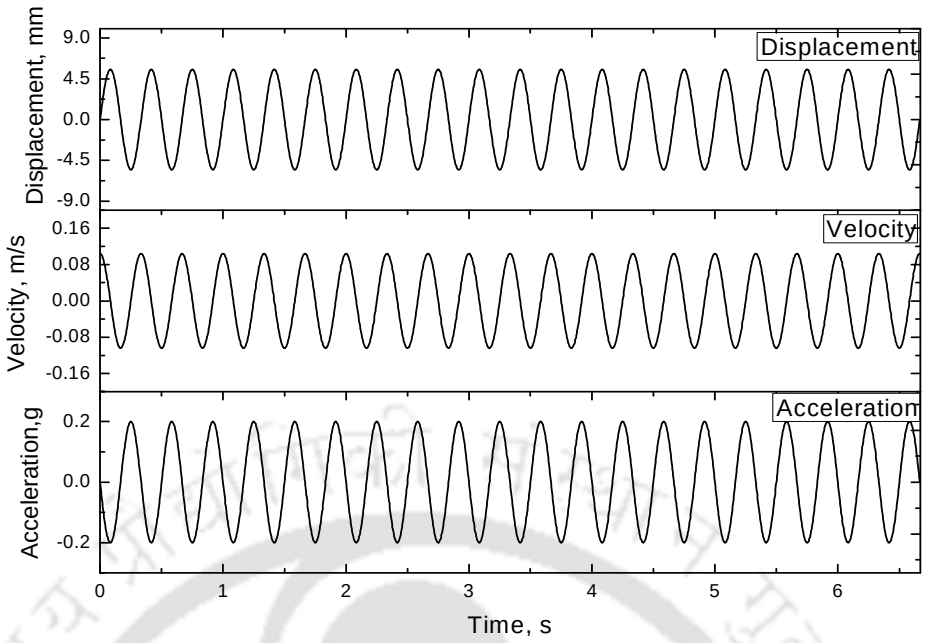

Fig. 4.8 Typical sinusoidal dynamic excitation components (a = 0.2g; f = 3 Hz)

elevations 100, 230, 380 and 500 mm are recorded. The incremental pressure is the measured increase in lateral pressure during dynamic excitation. Acceleration histories at a distance of 50 mm from the facing and at elevations 150, 300 and 600 mm are recorded.

Typical variations of displacements and accelerations with the number of cycles of dynamic loading (a = 0.2g and f = 3 Hz), at different elevations of wrap-faced wall are shown in Fig. 4.9 and Fig. 4.10, respectively. The horizontal displacements increase nonlinearly with increase in the number of cycles. Larger horizontal displacements are observed (Fig. 4.9) at higher elevations. It can be observed, from Fig. 4.10, that the accelerations are amplified at higher elevations. Displacements and acceleration histories obtained from the numerical model are similar to that of physical model tests reported by Krishna and Latha (2007).

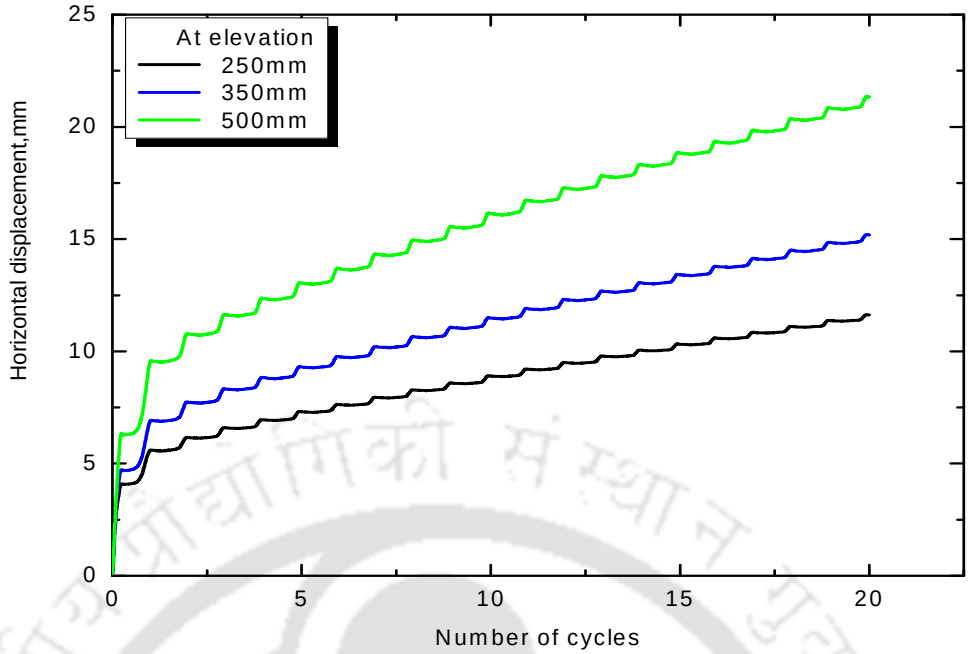

Fig. 4.9 Typical displacement histories at different elevation for acceleration 0.2g and frequency 3Hz

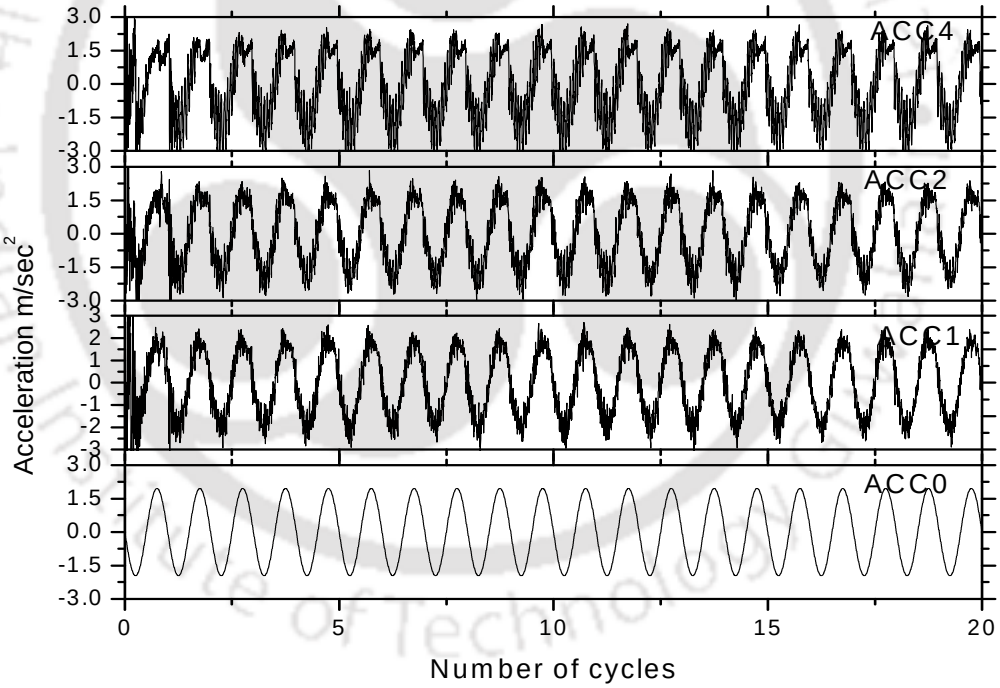

Fig. 4.10 Typical acceleration histories obtained in numerical simulation

The acceleration amplifications at different elevations of wall are quantified as *root mean square acceleration* (RMSA) amplification factor. The RMSA amplification factor is the ratio of RMSA value at any elevation to the RMSA value at the base. The RMSA value can be calculated according to Eq. 4.1 (Kramer, 1996).

$$RMSA = \left[\frac{1}{t_d}\int_0^{t_d} a(t)^2\, dt\right]^{1/2} \quad 4.1$$

where *a(t)* is acceleration at time 't', t_d is the duration of the acceleration record and *dt* is time interval of the acceleration record.

The sensitivity of numerical model to different material properties like backfill friction angle, backfill dilation angle, stiffness of reinforcement material and stiffness properties of soil-reinforcement interface are shown in Fig. 4.11, Fig. 4.12, Fig. 4.13 and Fig. 4.14, respectively.

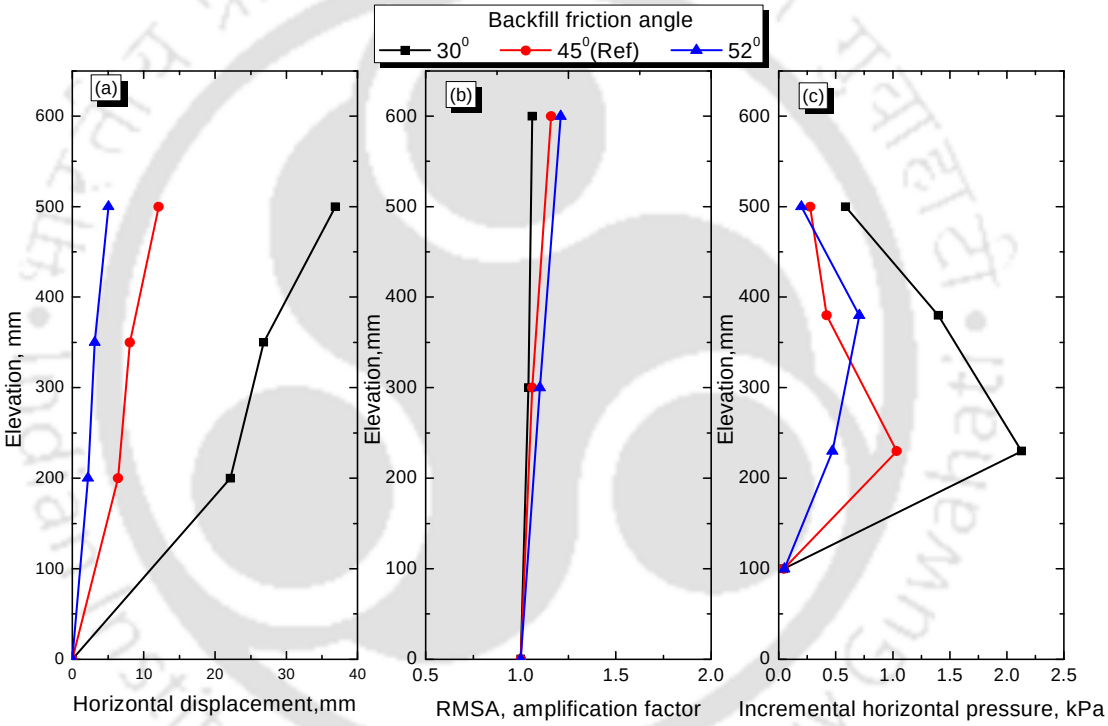

Fig. 4.11 Sensitivity of numerical model with respect to backfill friction angle: a) Displacement profiles; b) Acceleration amplification factor; c) Incremental pressure

The horizontal displacements and incremental horizontal pressures are obtained at different elevation at 25 mm from the facing. The RMSA amplification factors are calculated (Equation 4.1) from the acceleration records at different elevations. From the figures, it is observed that the model is sensitive to different material properties and efficient in capturing the behavior of model wall under seismic excitation. The backfill soil friction and dilation angle and stiffness of

reinforcing material are the most influencing parameters on model response in terms of displacements, acceleration amplifications and incremental pressures.

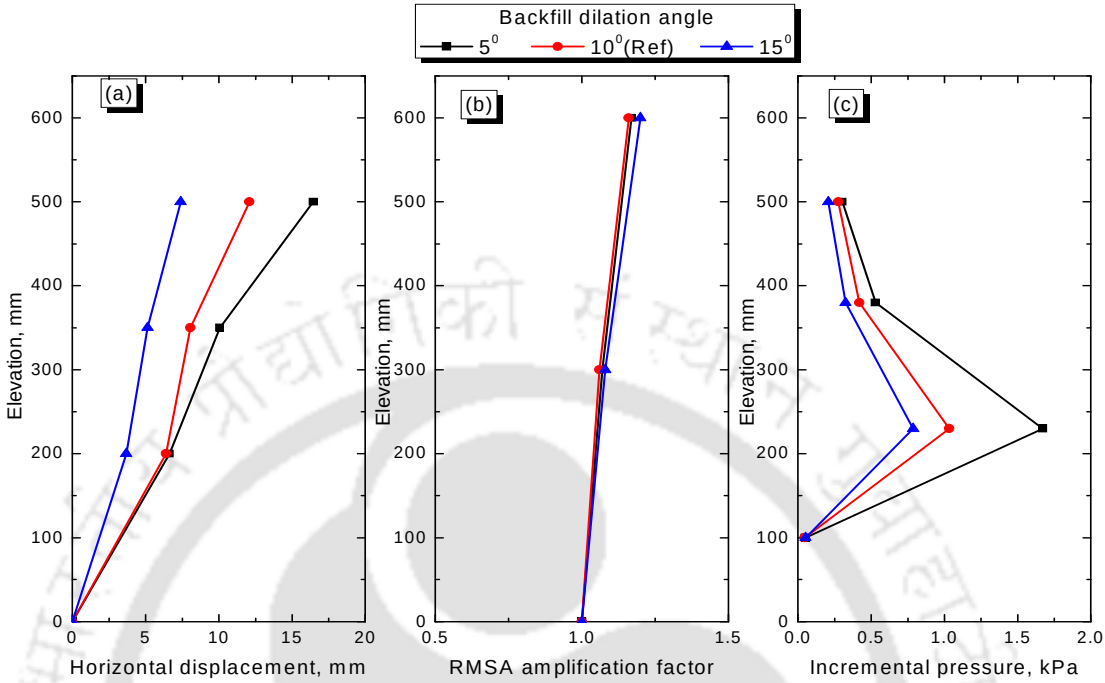

Fig. 4.12 Sensitivity of numerical model with respect to backfill dilation angle: a) Displacement profiles b) Acceleration amplification c) Incremental pressure

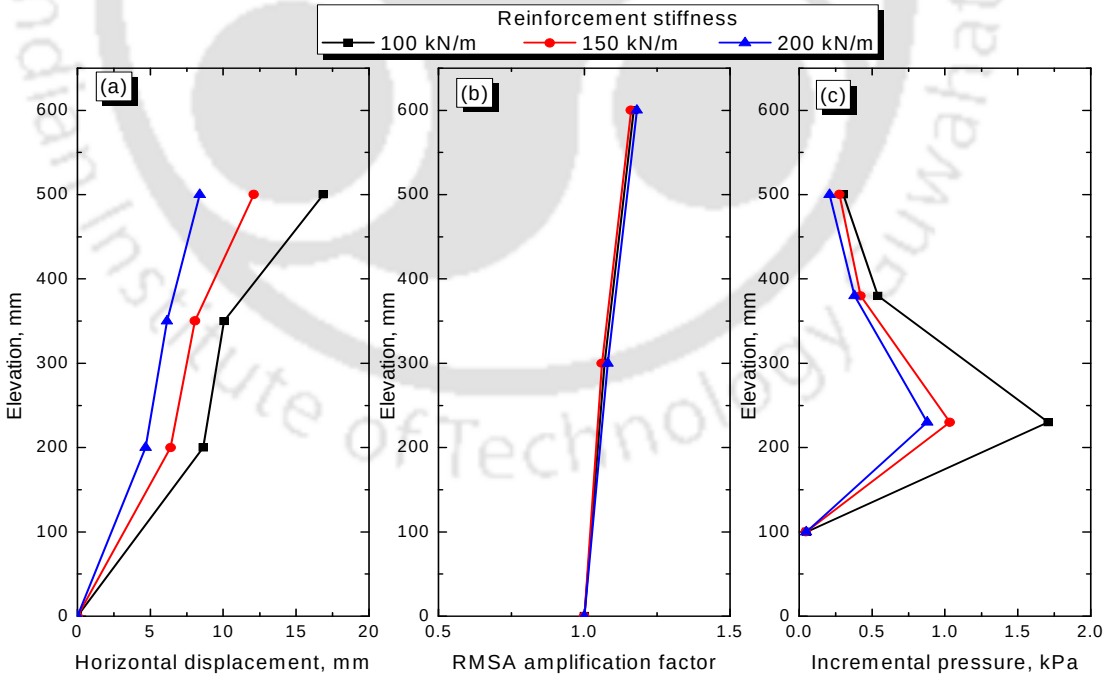

Fig. 4.13 Sensitivity of numerical model with respect to reinforcement stiffness: a) Displacement profiles b) Acceleration amplification c) Horizontal pressure

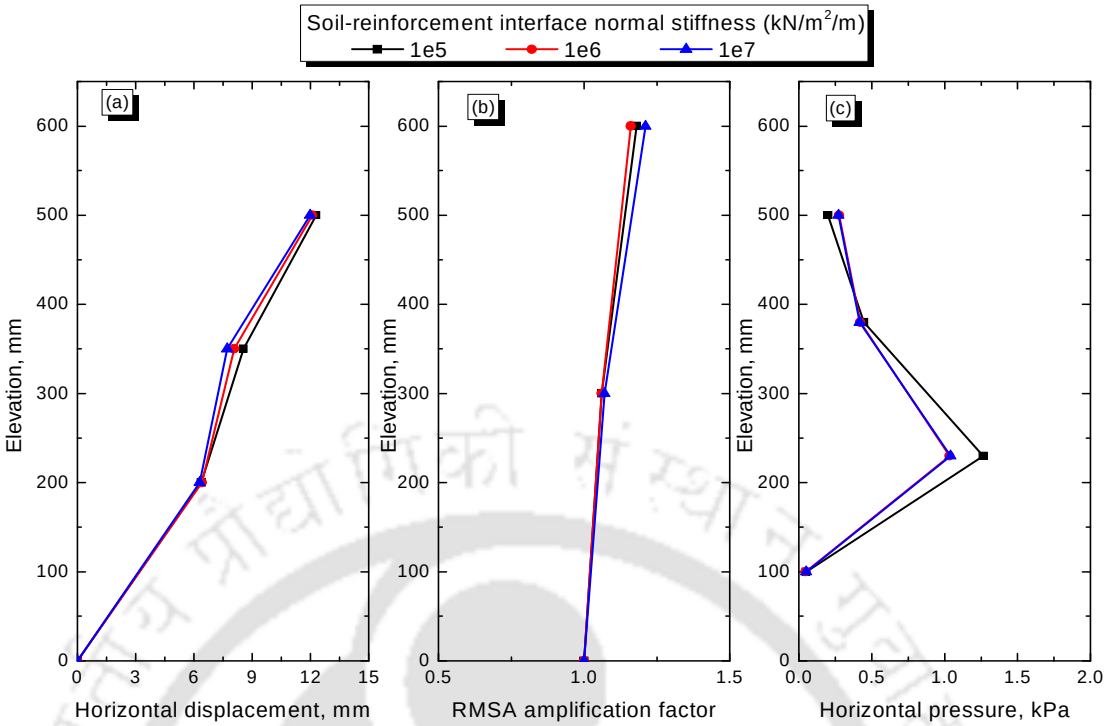

Fig. 4.14 Sensitivity of numerical model with respect to soil-reinforcement interface stiffness: a) Displacement profiles b) Acceleration amplification c) Horizontal pressure

The influence of stiffness of soil-reinforcement interface is not so prominent for the range of values considered (as discussed in Chapter 3). It has been established from this analysis that numerical model is sensitive to different material properties. The following section presents validation of the numerical model by comparing the results from the physical model tests.

4.2.5 Validation of numerical model

The numerical model developed to simulate the shaking table tests of wrap-faced wall is validated by comparing with the results of physical model tests as reported by Krishna and Latha (2007). The material properties considered in the numerical model for validation purpose are mentioned in bold font in Table 4.1.

Comparisons of the results obtained from the physical tests and the corresponding numerical model, with four layers of reinforcements tested for 20 cycles of excitation of 0.2g acceleration at 3Hz and 5Hz frequencies, are shown in Fig.

4.15. The maximum horizontal displacements at an elevation of 500 mm are 26.79 mm from the numerical model and 30.08 mm from physical model for 3Hz frequency excitation, while the corresponding values are 16.90 mm and 16.21 mm for 5Hz frequency excitation. The acceleration amplification at an elevation of 600 mm is 1.57 for numerical model and 1.71 for the physical model for 3Hz frequency excitation. For 5Hz frequency excitation, the values are 1.61 and 1.78 for numerical and physical models, respectively. The comparison of results from physical and numerical models and their percentage differences are tabulated in Table 4.2. The variation of horizontal displacements and RMSA amplification factors between physical and numerical models are within 10% for model subjected to 3 Hz and 5 Hz frequency.

Table 4.2 Comparison of results from physical and numerical model

Frequency	Horizontal displacement (mm)			RMSA amplification factors		
	Physical	Numerical	% difference	Physical	Numerical	% difference
3 Hz	30.08	26.79	10.9%	1.71	1.57	8.18%
5 Hz	16.21	16.90	4.25%	1.78	1.61	9.55%

The pressures observed in physical tests were reported (Krishna and Latha 2007) to be inconsistent due to the limitations of the pressure sensors' sensing range (0-100 kPa) and the low level pressures encountered in the model tests (order of about < 5 kPa). So discrepancies in the incremental pressures are observed between experimental and simulated results. The variations of horizontal displacements, RMSA amplification factors and incremental pressures for physical and numerical model with 3, 4 and 6 numbers of reinforcing layers are shown in Fig. 4.16. The figure shows similar behavior of decreasing horizontal displacements with increase in reinforcing layers for both physical and numerical simulations. The maximum horizontal displacements for model with 3, 4 and 6 numbers of reinforcing layers at

elevation of 500 mm are 38.98 mm, 26.79 mm and 10.27 mm for numerical models and 47.19 mm, 30.08 mm and 10.91 mm for physical models, respectively. The RMSA amplification factors are not affected by variation in the number of reinforcement layers. The comparative results presented in Fig. 4.15 and Fig. 4.16 show the ability of numerical model to capture the behavior of physical model with reasonable accuracy.

4.2.6 Dynamic response of wrap-faced walls: displacements and strains

The response of wrap-faced wall with four layers of reinforcement (L_{rein}/H = 0.7) subjected to dynamic excitation of 0.2g acceleration at 3Hz frequency is being presented. Horizontal and vertical displacements are determined along the length of backfill at different elevations and are shown in Fig. 4.17. The maximum horizontal displacements are 14.20, 9.65, and 6.35 mm, near wall facing, at elevations 525, 375 and 225 mm elevations, respectively. The horizontal displacements (u) decrease moderately within the reinforced zone and decrease sharply after the end of reinforcement. The vertical displacements (v) are high near the facing and gradually decrease to zero at a distance of 0.2 m from facing (within reinforced zone). The values (v) again increase near the end of reinforcement to 5.09, 3.22 and 1.56 mm at 525, 375 and 225 elevations, respectively. The variations of octahedral shear strain increments ($\Delta\gamma_{oct}$), developed at end of dynamic excitation, along the length of backfill are studied at middle of two reinforcing layers (Fig. 4.18a) and at reinforcement level (Fig. 4.18b). The $\Delta\gamma_{oct}$ is the measured increase in octahedral shear strain (γ_{oct}) during dynamic excitation. By comparing both Fig. 4.18(a) and Fig. 4.18(b), it is observed that the $\Delta\gamma_{oct}$ are maximum near the end of reinforcement zone.

This increase in octahedral shear strains near end of reinforcement is due to higher vertical settlements at the location. Nearly constant horizontal displacements

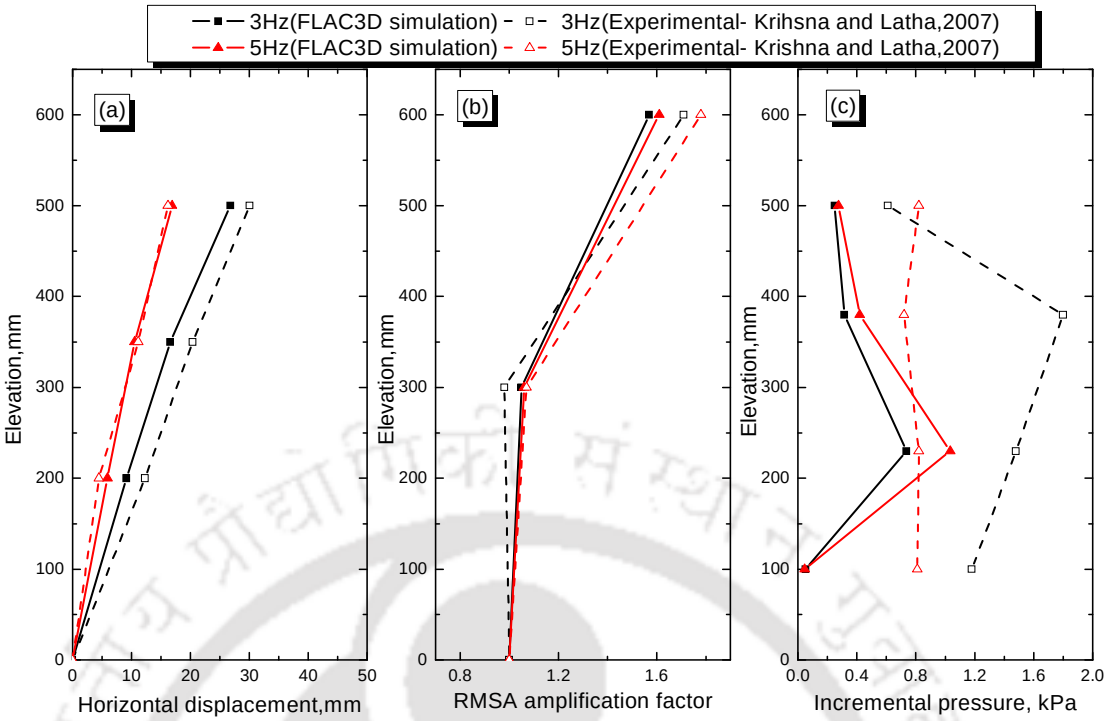

Fig. 4.15 Comparison of results of numerical and physical model tests (a = 0.2g, L_{rein}/H =0.7, N_L =4) (a) horizontal displacement, (b) RMSA amplification factor and (c) incremental pressure

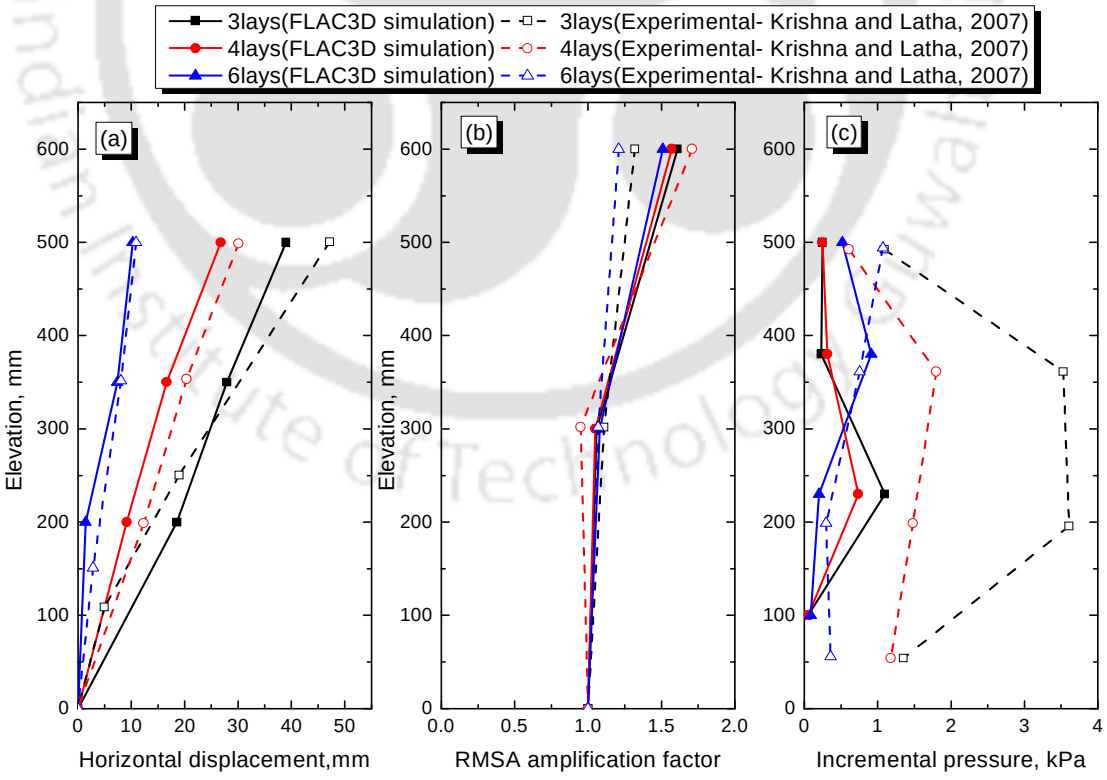

Fig. 4.16 Comparison of results of numerical and physical model tests for different number of reinforcement layers (a = 0.2g, f = 3 Hz and L_{rein}/H=0.7)

within reinforced backfill zones, and higher vertical settlements and octahedral shear strains near the end of reinforcement zones show that the reinforced zone is acting as monolithic section. This also confirms the formation deformation zones at the end of reinforcement zone. The formation of deformation zone is not properly defined in laboratory model test reported in literature (Krishna and Latha, 2007).

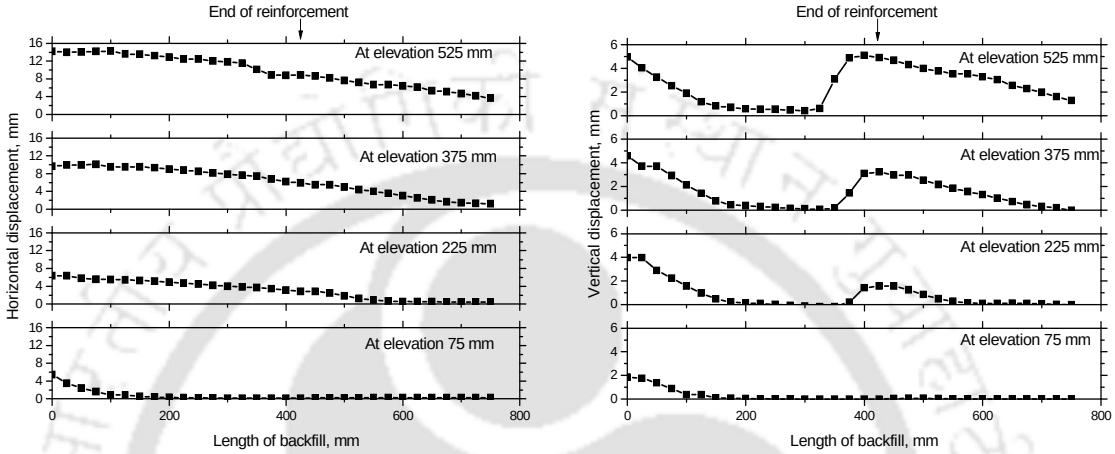

Fig. 4.17 (a)Horizontal displacement and (b) vertical displacements along length of backfill after 20 cycles (a =0.2g, f =5Hz, L_{rein}/H=0.7, N_L=4)

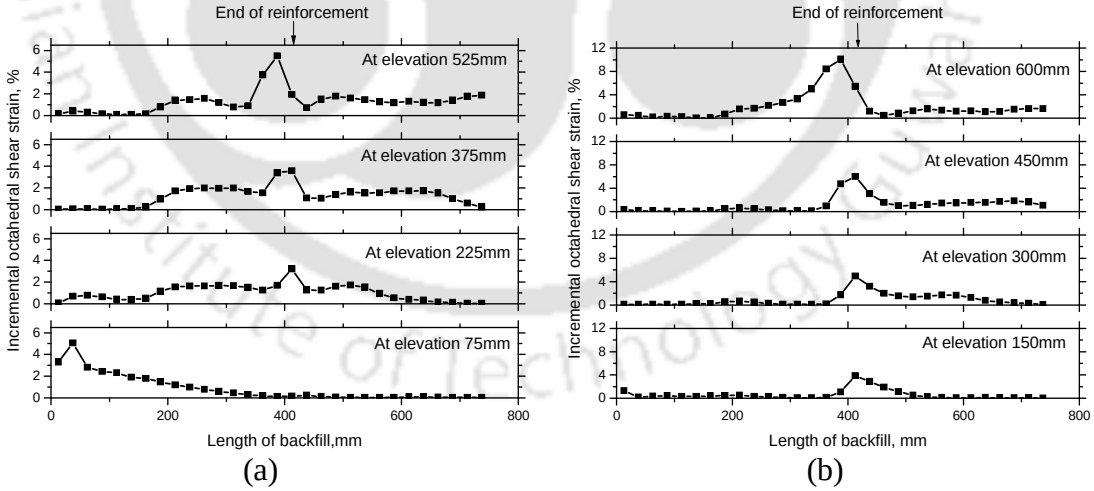

Fig. 4.18 Variation of $\Delta\gamma_{oct}$ in soil along length of backfill (a) between two reinforcement layers (b) at reinforcement level (a =0.2g, f =5Hz, L_{rein}/H=0.7, N_L=4)

4.3 SEISMIC BEHAVIOR OF FULL SCALE MODEL

Using the validated numerical model, a full scale wrap-faced model of size 6 m high, 18 m long and 1 m wide with 6 numbers of reinforcing layers is developed for

analysis of its seismic behavior. The model parameters considered for full scale model are kept same as that of laboratory model. The length of reinforcement (L_{rein}) is considered as 4.2 m, which corresponds to the L_{rein}/H ratio of 0.7 (FHWA 2001). The procedure described in development of laboratory scale numerical model (section 4.2.2) is followed for the full scale model. The numerical model considered for full scale wrap-faced wall and model after support removal is shown in Fig. 4.19.

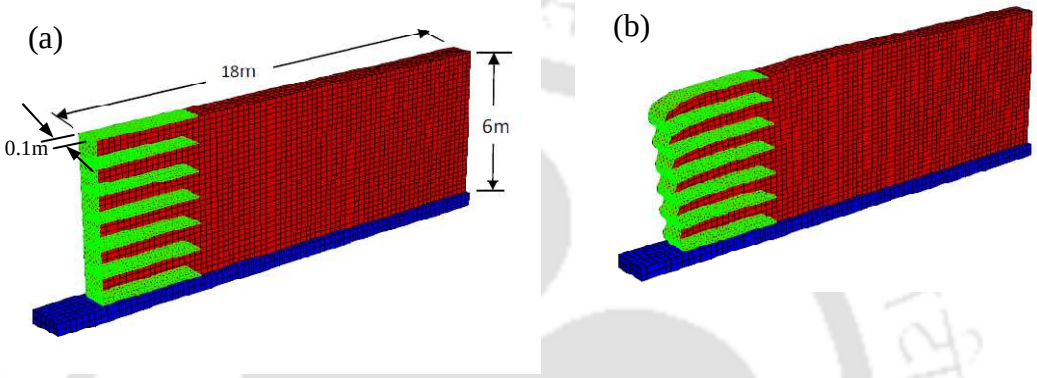

Fig. 4.19 Numerical grid for full scale wrap-faced wall (a) before support removal (b) after support removal

4.3.1 Response of full scale wall after dynamic excitation

The behavior of full scale wrap-faced wall models are studied under dynamic excitation in terms of horizontal and vertical displacements, RMSA amplification factors, horizontal pressures and probable deformation zones formed during dynamic excitation. Sinusoidal dynamic excitation of 0.2g acceleration at 5 Hz frequency, for 20 cycles has been considered. Variations of horizontal and vertical displacements, RMSA amplification factors and horizontal pressures at wall facing, end of reinforcement and unreinforced backfill (within retained backfill at a distance of 14 m from facing), after the dynamic excitation, are shown in Fig. 4.20. In general, the horizontal displacements are decreased with increase in the distance from the wall facing. The maximum horizontal displacements at an elevation of 5.5 m are 168.8 mm near the facing, 94.3 mm at end of reinforcement and 0.8 mm at deep backfill. The

vertical displacements at the corresponding locations are 61.9 mm, 104.5 mm and 0.5 mm, in the order. The horizontal and vertical displacements are negligible at deep backfill (at a distance of 14 m) from the wall facing and so will not have much effect on formation of deformation surfaces either within or outside the reinforced portion of the wall. The RMSA amplification factors are observed to be larger at higher elevation but did not show significant variation with distance from wall facing. Horizontal pressures at elevation of 0.5 m are 30.2 kPa near the facing; and 20.0 kPa near the end of reinforcement. The horizontal pressure at higher elevation is more near the facing and nearly equal at end of reinforcement and far field.

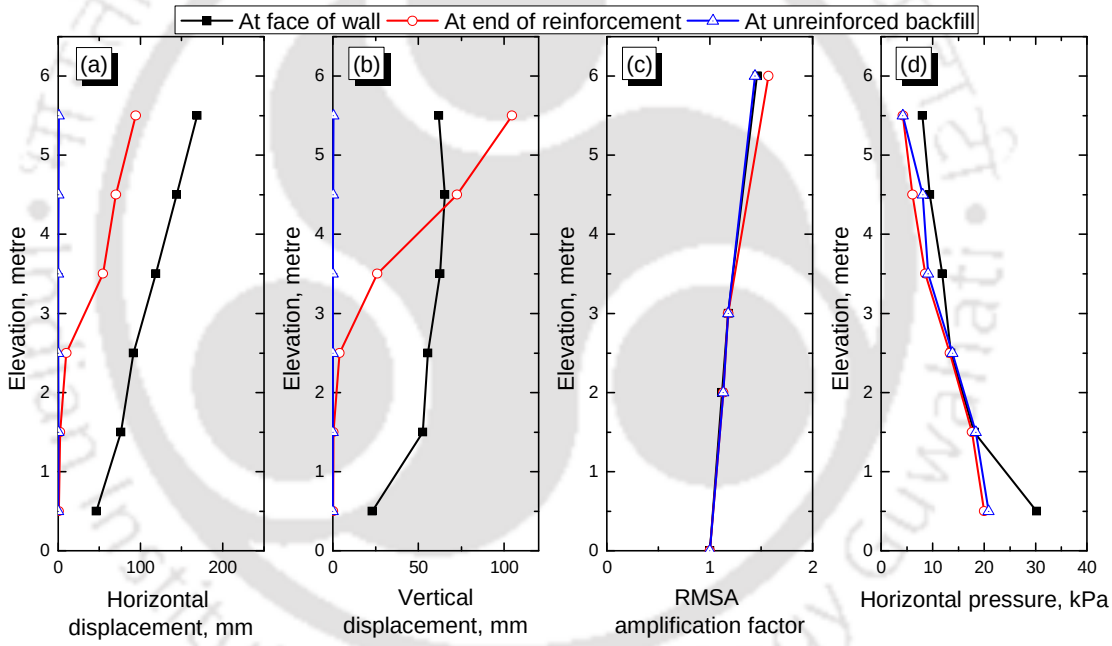

Fig. 4.20 Variation of (a) horizontal displacement (b) vertical displacement (c) RMSA amplification factor and (d) Horizontal pressure for wall subjected to dynamic excitation (a = 0.2g, f = 5Hz, N_L = 4 and L_{rein}/H = 0.7)

The formation of deformation zones within reinforced and unreinforced portion (retained backfill) zones can be determined by studying the shear strain variation within backfill soil (Bathurst and Hatami, 1998). The incremental octahedral shear strains ($\Delta\gamma_{oct}$), horizontal displacements (u) and vertical

displacements (v) along the length of backfill after the dynamic excitation (a = 0.2g and f = 5 Hz) are presented together in Fig. 4.21.

The horizontal displacement (u) of the soil element near the wall facing is 171.4 mm at an elevation of 5.5 m and remains almost constant up to 3.5 m from the wall facing. It is then decreases and become almost zero at 7 m from the facing. The vertical displacement (v) of soil element is 69.8 mm near wall facing at that elevation. So from the Fig. 4.21, it can be seen that the values of u within reinforced zone are at maximum, but they decrease gradually and become negligible after end of reinforcements at elevations of 5.5 m, 4.5 and 3.5 m. However, at the lower layers (i.e 2.5 m, 1.5 m and 0.5 m elevations) the horizontal movement of soil element decreases to zero within reinforced zone. The vertical displacements (v) are almost uniform within reinforced zone, up to a distance of 3.0 m from wall facing, at elevations of 5.5 m, 4.5 m and 3.5 m. The vertical displacement (v) increases suddenly near the end of reinforcement at the higher layers, at elevations of 5.5 m and 4.5 m. The vertical settlements are less (in the order of 40-50 mm) at lower layers (2.5 m and 1.5 m elevations), and decreases to zero within reinforced zone. The $\Delta\gamma_{oct}$ near the facing are negligible at elevations, higher than 3.5 m, but increase to about 3.0 % at a distance 2 m from the facing.

The strain values attain higher peak (about 8-9% at 4.5m and 5.5m elevations) near end of the reinforcement. At the lowest elevation (0.5 m), maximum shear strain increment (about 7%) can be seen near the facing. By comparing the $\Delta\gamma_{oct}$, u and v at different elevations, it can be seen that the deformation of a wrap-faced wall, subjected to dynamic excitation, consist of three different modes. Fig. 4.21 shows two

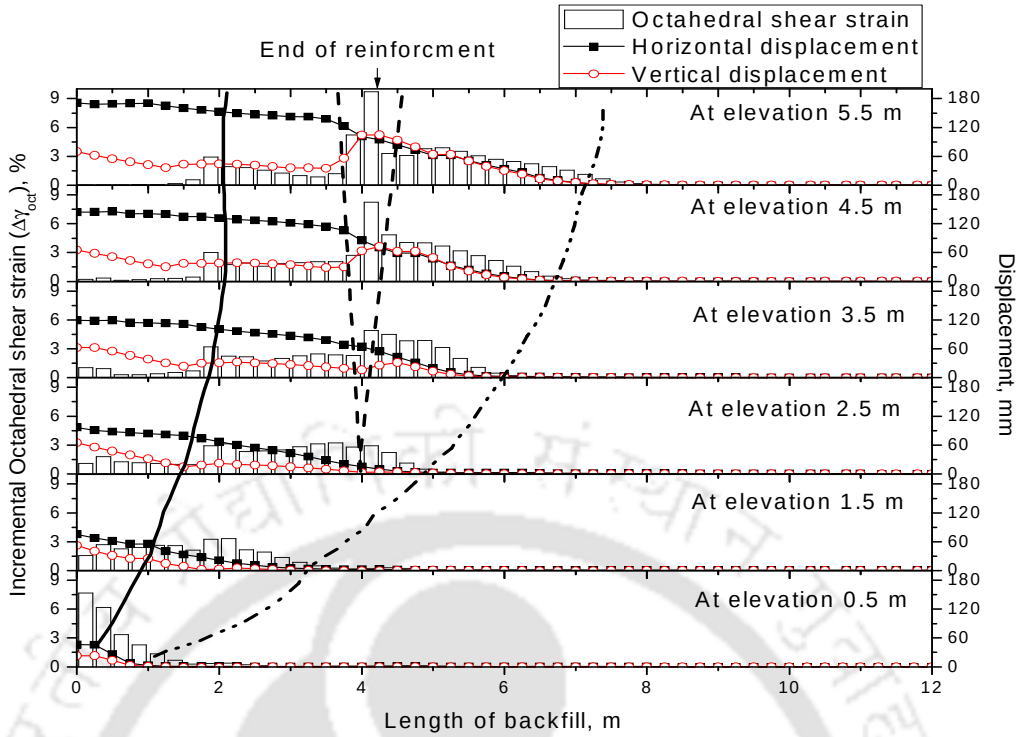

Fig. 4.21 Octahedral shear strain, horizontal displacement and vertical displacement along the length of backfill after 20 cycles of dynamic excitation (a =0.2g, f =5Hz, L_{rein}/H=0.7, N_L =6)

deformation zones; one shear deformation zone within the reinforced block (solid line) and the other shear deformation zone extending beyond reinforced block (dash-dotted line). Besides these two deformation zones a zone of relative compaction (dashed line) can be observed at the end of reinforcement which is due to higher vertical settlements and shear strains. Similar deformation zones were also reported in dynamic analysis of wrap-faced walls by Liu and Ling (2012) and in segmental facing walls by Liu et al. (2011). The horizontal displacements are attributed to the formation of a deformation surface within the reinforced zone. It can be seen from Fig. 4.21 that the vertical displacements near end of reinforcement are more only at an elevation 5.5 m, 4.5 m and 3.5 m and negligible at lower layers. Therefore the relative compaction zone developed near the end of reinforcement does not extend to the lower layers. The second deformation surface can be considered as indicative of the

backfill zone moving along with reinforced zone. A similar zone was considered to be the compound failure zone by Liu and Ling (2011). Variation of $\Delta\gamma_{oct}$ within the model is shown in contours form in Fig. 4.22. The figure also confirms the formation of the deformation zones. Further, the deformation zones determined are shown schematically in Fig. 4.23.

To observe the behavior of reinforcement strains, incremental values of reinforcement axial strains ($\Delta\varepsilon_{a\_rein}$), during dynamic excitation are calculated. An incremental value is the change in axial strain value during dynamic excitation. To compare $\Delta\varepsilon_{a\_rein}$ with the soil strains at the reinforcement location, Fig. 4.24 presents variations of $\Delta\gamma_{oct}$ in the soil at reinforcement level; and $\Delta\varepsilon_{a\_rein}$ in reinforcement layers, along length of the wall.

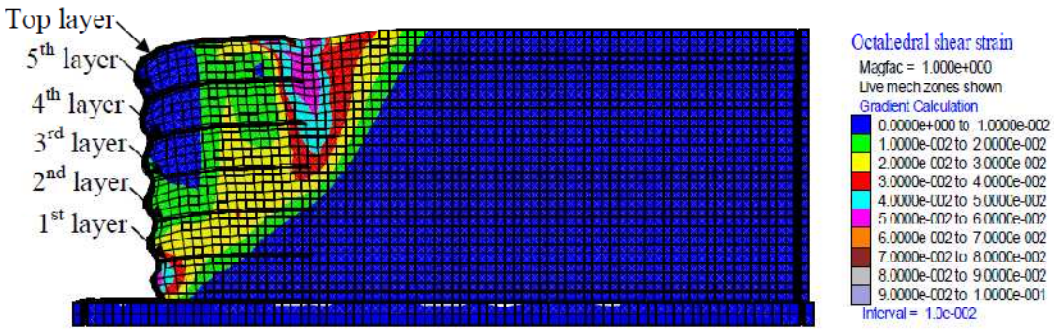

Fig. 4.22 Contour of octahedral shear strain after 20 cycles of dynamic excitation (a=0.2g, f=5Hz, L_{rein}/H=0.7, N_L=6)

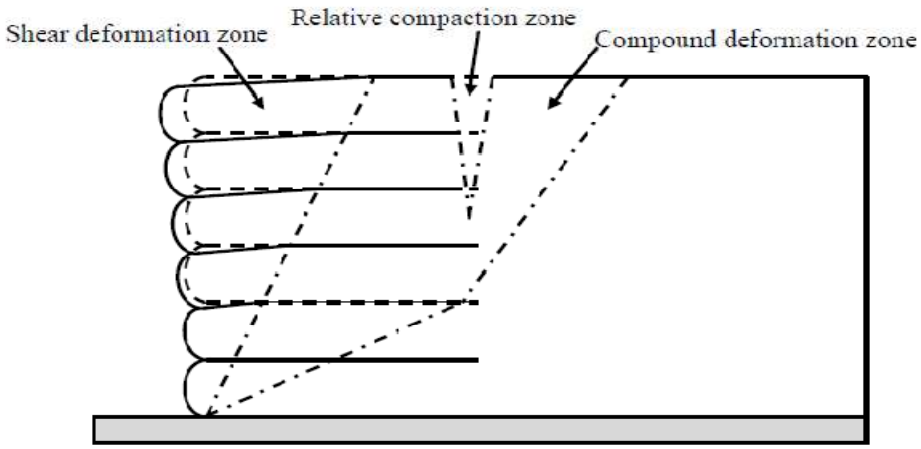

Fig. 4.23 Deformation zones of wrap-faced reinforced soil retaining wall after dynamic excitation

The $\Delta\gamma_{oct}$ reduce to negligible values at distance of 8.0 m from facing at 6.0 m elevation, denoting maximum mobilization of retained backfill beyond reinforced soil zone (also shown in Fig. 4.23). The octahedral shear strain reduces to negligible value at distance of 7.0 m and 6.0 m from facing at elevations 5.0 m and 4.0 m, respectively. The compound deformation zones extend to deeper retaind backfill at higher elevations. The $\Delta\gamma_{oct}$ reduces to negligible value within reinforced zone in lower layers. From the figure it is seen that $\Delta\varepsilon_{a\_rein}$ are less than 2% in the top three layers (top, 5th and 4th layer) of reinforcement. At these elevations, whole reinforcement length is located within the maximum strained zone of soil due to deeper extension of compound deformation zone into retained backfill, as a result insignificant strain increments are noticed within reinforcement. In the 1st layer of reinforcement, which is extended to the zone of negligible soil strain, i.e., beyond 2.0 m from the facing, the strain increment is 2.8% at a distance of 0.8 m from facing.

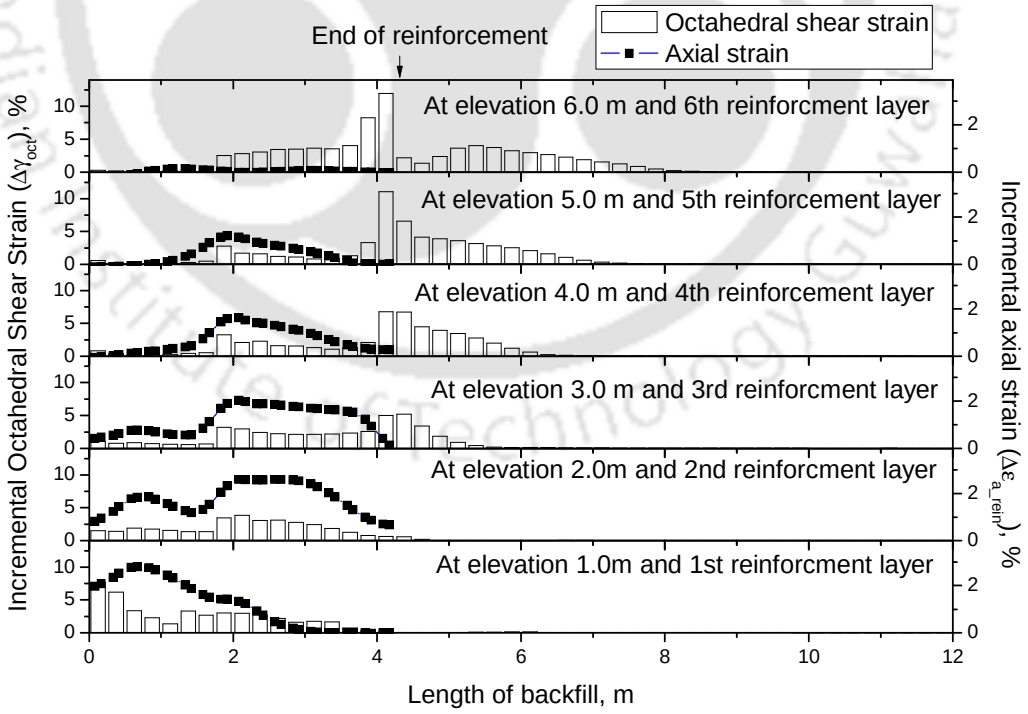

Fig. 4.24 Incremental Octahedral shear strain on soil element and incremental axial strain on reinforcement after 20 cycles of dynamic excitation (a = 0.2g, f = 5Hz, L_{rein}/H=0.7, N_L=6)

The friction developed in top reinforcement layer is only due to surcharge acting over it. This friction is insufficient to restrain the dynamic earth pressure. Moreover, the overburden pressure on reinforcement increases with increasing depth of reinforcement layers. So the friction developed on reinforcement at lower layers is more than that of top layers. From the above observations, it can be stated that during dynamic excitation, the reinforcement strain increments are affected by the extent compound deformation zone into backfill and friction developed on reinforcement due to overburden pressures. The mechanism, dependence of normal stress and shear stress (friction) can be seen schematically as explained in Fig. 4.25.

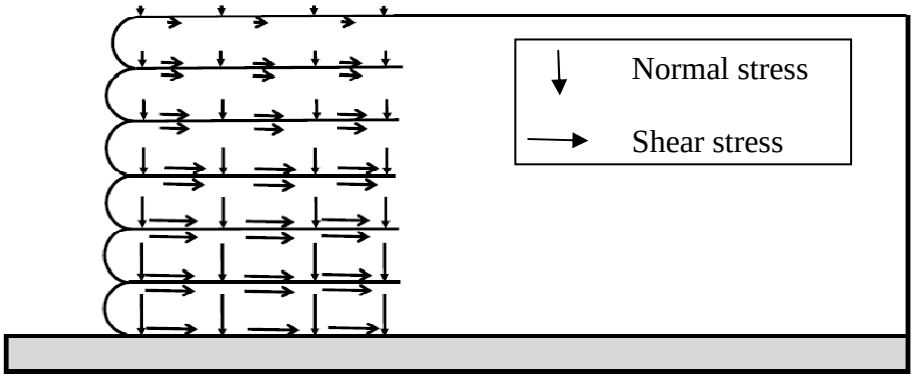

Fig. 4.25 Overburden pressure acting on reinforcement at different elevations

4.4 PARAMETRIC STUDIES

Parametric studies are conducted to analyze the $\Delta\gamma_{oct}$ of soil and $\Delta\varepsilon_{a\_rein}$, and the location of deformation zones during dynamic excitation. Reinforcement length, number of reinforcing layers and type of backfill (friction angle) are varied in different simulations. Sinusoidal dynamic excitation of 0.2g acceleration at 5 Hz frequency, for 20 cycles has been considered. The parameters varied for parametric studies are listed in Table 4.3. All other model parameters are kept same as discussed in earlier section.

Table 4.3 List of parameters considered for parametric studies

Soil properties	
Friction angles, degree	30, 38, 43
Reinforcement configuration	
Length of reinforcement	0.7*H*, 1.0*H*, 1.2*H*
No. of reinforcing layers	4, 6, 8

4.4.1 Effect of length of reinforcement

Three different reinforcement lengths (L_{rein}) of 0.7*H*, 1.0*H* and 1.2*H* (*H* is height of wall) are considered. The horizontal and vertical displacements, RMSA amplification factors and horizontal pressures are compared between wall models with different reinforcement lengths, as shown in Fig. 4.26. The horizontal and vertical displacements are maximum for wall with reinforcement length of *0.7H*. The horizontal displacements at facing, near top of the wall, are 168.8 mm and 94.3 mm for walls with reinforcement length 0.7*H* and 1.0*H*, respectively. About 44% reduction in horizontal displacement is observed for increase in reinforcement length from 0.7*H* to 1.0*H*. The vertical displacement is 104.5 mm near the end of reinforcement for wall with reinforcement length of 0.7*H*; but it is 61.8 mm near the facing.

The vertical displacement near the end of reinforcement is 48.7 mm for 1.0*H* reinforcement indicating about 53% reduction. Near the facing, 27% reduction in vertical displacement is seen for increase in L_{rein} from 0.7*H* to 1.0*H*. The reduction in vertical settlement is 68% near the end of reinforcement and 11% near facing for increase in reinforcement length from 1.0*H* to 1.2*H*. The RMSA amplification factor is almost similar for all three types of wall. Ling et al. (2005) also did not observed any significant variation in acceleration amplification with increase in length of reinforcement. The changes length of reinforcement do not have significant effect on

unit weight of reinforced soil. The horizontal pressures on wall are almost same for wall with 0.7*H*, 1.0*H* and 1.2*H* layers of reinforcement.

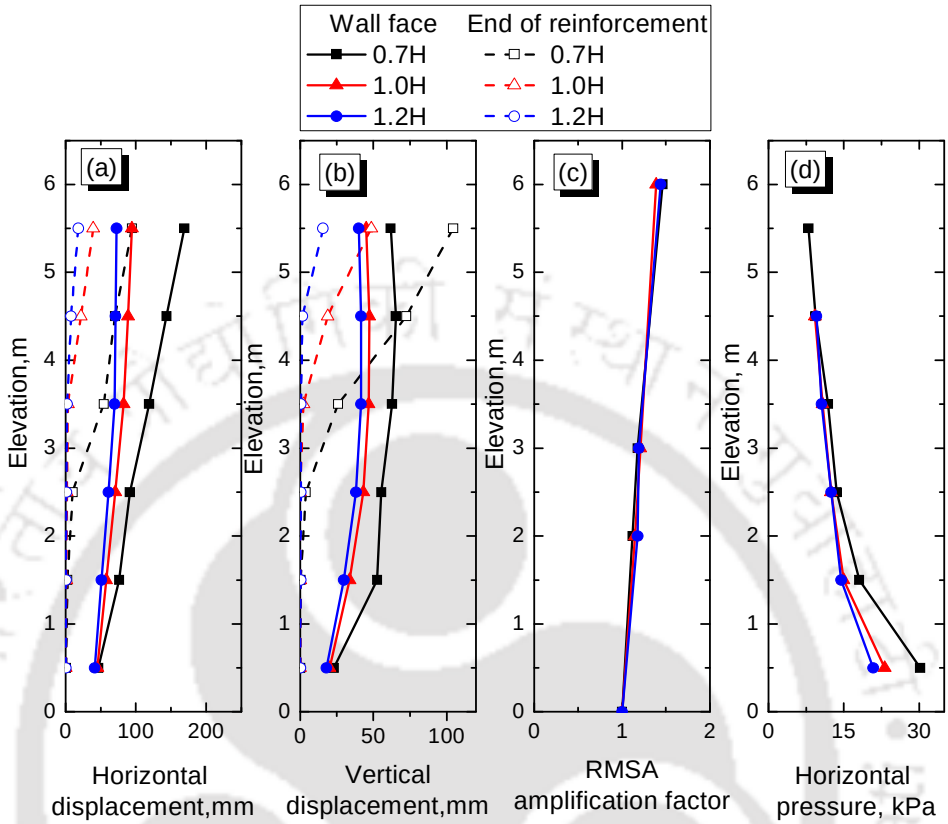

Fig. 4.26 Response of model wall with length of reinforcement lengths (0.7*H*, 1.0*H* and 1.2*H)* after dynamic excitation (a = 0.2g, f = 5Hz and N_L= 6)

Variation of $\Delta\gamma_{oct}$, u and v along the length of backfill, for a model wall with L_{rein} = 1.0*H*, at the end dynamic excitation are shown in Fig. 4.27. Overall, the trends in the displacements and strains are similar to the explanation provided on Fig. 4.21. However, maximum values of displacements, strains and their location are changed. It is observed from Fig. 4.27, that the horizontal displacement of soil elements near facing is 94.7 mm and decreases to zero at the end of reinforcement at an elevation of 5.5 m. At lower layers, i.e 2.5 m, 1.5 m and 0.5 m elevations, horizontal movements of soil elements decrease to zero within reinforced zone. The vertical displacement is 47.4 mm near the facing and reduces to 24.6 mm within reinforced zone and again increases to 49.4 mm at the end of reinforcement at an elevation 5.5 m. The vertical

displacement then reduces to zero at distance of 7.75 m from the facing at that elevation. The vertical settlements also decrease to zero within the reinforced zone at lower elevations. The maximum octahedral shear strain within the reinforced zone is 1.2% and increase to 4.7% near the end of reinforcement at elevation 5.5 m. The $\Delta\gamma_{oct}$ is 3.5% near the end of reinforcement at elevation 4.5 m. By comparing the $\Delta\gamma_{oct}$, u and v at different layers it can be concluded that warp faced wall with reinforcement length 1.0H subjected to dynamic excitation have only deformation zone formed due to shear deformation within the reinforced zone. The compaction zones at the end of reinforcements are developed but only in the top two layers. The compound deformation zones are developed at higher elevations and do not extend to lower elevations.

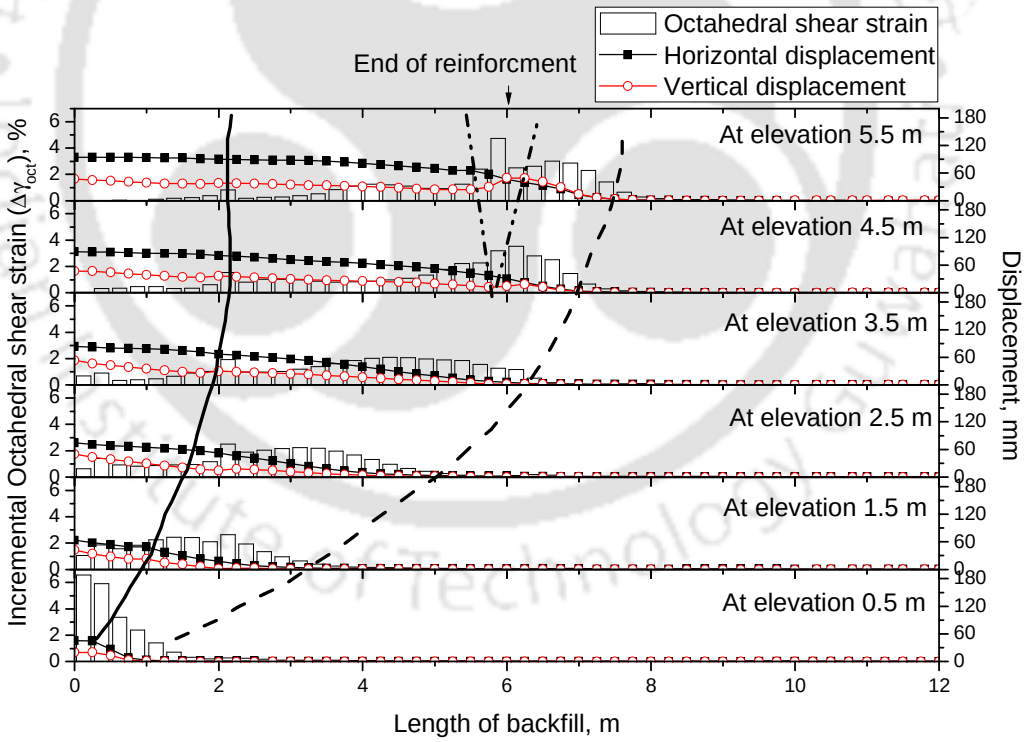

Fig. 4.27 Variation of $\Delta\gamma_{oct}$, u and v along the length of backfill after dynamic excitation for model wall with L_{rein}/H=1.0 (a=0.2g, f=5 Hz, N_L=6)

Fig. 4.28 shows the comparison of $\Delta\gamma_{oct}$ between reinforcement layers of backfill for different models (L_{rein} = 0.7H, 1.0H *and 1.2H)*. The maximum octahedral

shear strain is 9.7% near the end of reinforcement at elevation 5.5 m for wall with reinforcement length 0.7*H*. The $\Delta\gamma_{oct}$ near the wall facing is very small, at elevations 5.5 m, 4.5 m and 3.5 m, for all three walls. The $\Delta\gamma_{oct}$ variation shows three peaks – within reinforced zone, at the end of reinforcement and within retained backfill for wall with reinforcement length 0.7*H*. But for wall with reinforcement lengths 1.0*H* and 1.2*H*, the $\Delta\gamma_{oct}$ do not extend beyond end of reinforcement length except at elevation 5.5 m. So deformation zones are formed within backfill region but do not extend to the lower layers. The octahedral shear strains do not show any peak near the end of reinforcement for wall with reinforcement length 1.2*H*. So the zones of relative settlements do not form at the end of reinforcement. The deformation zone within reinforced backfill is the only prominent mode for wall with longer reinforcement. The formation of deformation zones in backfill soil for walls with reinforcement length 0.7*H* and 1.0*H* is as shown schematically in Fig. 4.29.

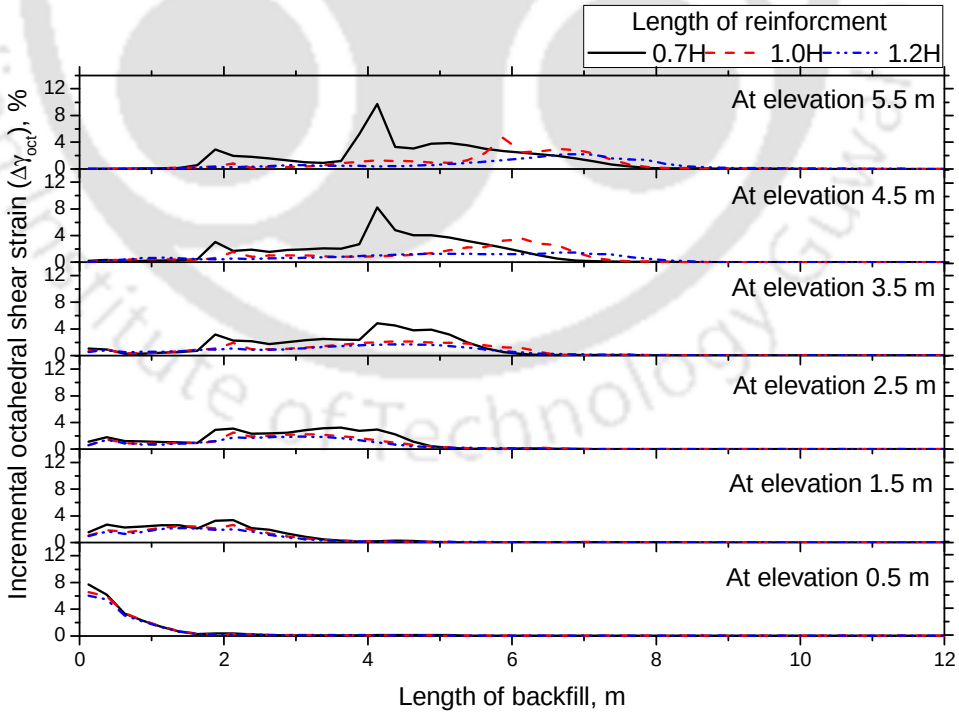

Fig. 4.28 Comparison of octahedral shear strain at backfill with reinforcement length 0.7*H*, 1.0*H* and 1.2*H* subjected to dynamic excitation (a = 0.2g, f = 5 Hz and N_L = 4)

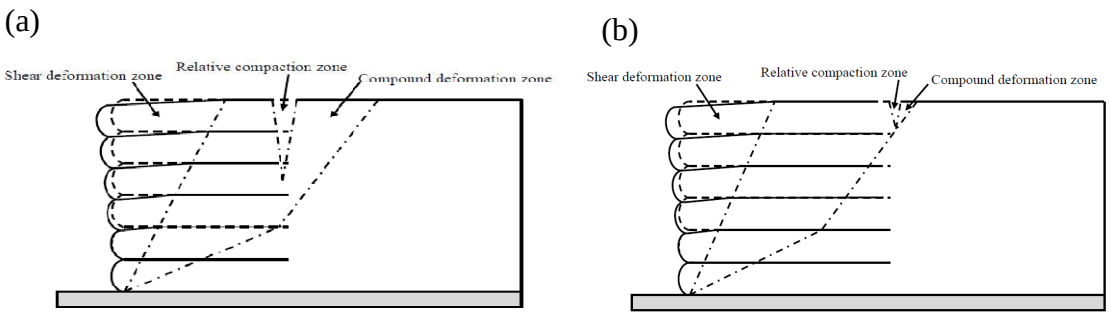

Fig. 4.29 Deformation zones of wrap-faced walls with (a) L_{rein}/H=0.7 (b) L_{rein}/H=1.0

The contours of octahedral shear strains in backfill soil with reinforcement length of 0.7*H*, 1.0*H* and 1.2H are shown in Fig. 4.30. The peak strain formed near the end of reinforcement is limited to near the surface of backfill soil for wall with longer reinforcement.

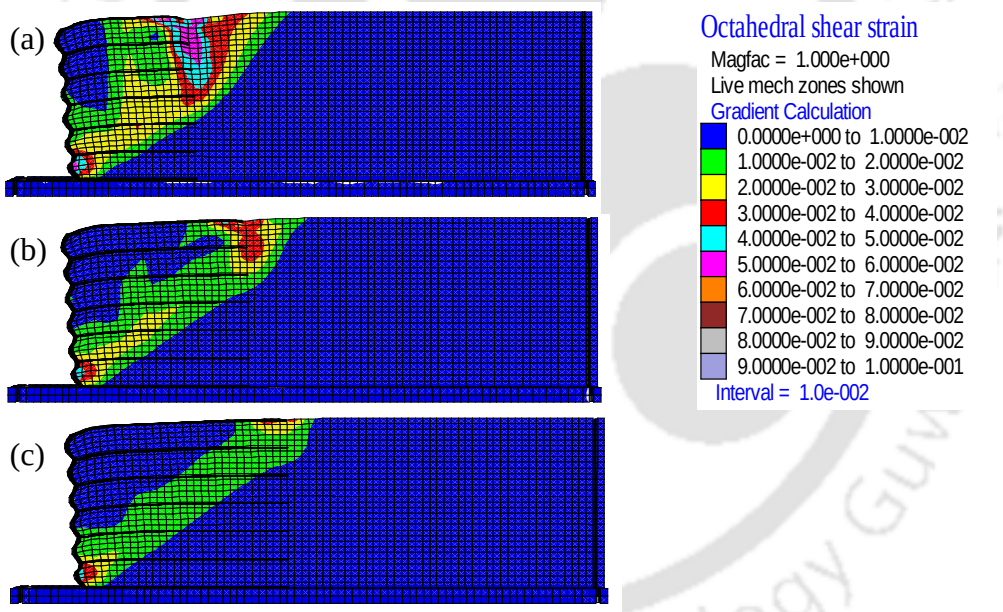

Fig. 4.30 Contours of octahedral shear strain after dynamic excitation (a = 0.2g, f =5Hz, N_L = 6) (a) L_{rein}=0.7H ; (b) L_{rein} = 1.0H and; (c) L_{rein} =1.2H

Variations of incremental reinforcement strains ($\Delta\varepsilon_{a\_rein}$) after dynamic excitation for model walls with different reinforcement lengths, at different elevations, are shown in Fig. 4.31. The maximum $\Delta\varepsilon_{a\_rein}$ at first layer of reinforcement (1.5 m elevation) are 2.8%, 2.5% and 2.3% for walls with reinforcement length of 0.7*H*, 1.0*H* and 1.2*H*, respectively. This indicates slightly higher reinforcement strain for model

wall with shortest length of reinforcement. With increase in elevation, it is seen that reinforcement strains for longer reinforcements are higher than that for shorter reinforcement lengths. The reinforcement strain increments are within range of 2.5% and 2.0% in second and third layer of reinforcement for wall with L_{rein} of *0.7H* and *1.2H*, while in fifth layer of reinforcement $\Delta\varepsilon_{a\_rein}$ are 1.2% and 1.4%, respectively. The $\Delta\varepsilon_{a\_rein}$ in top layers are minimum (< 0.5 %) for wall with different reinforcement lengths.

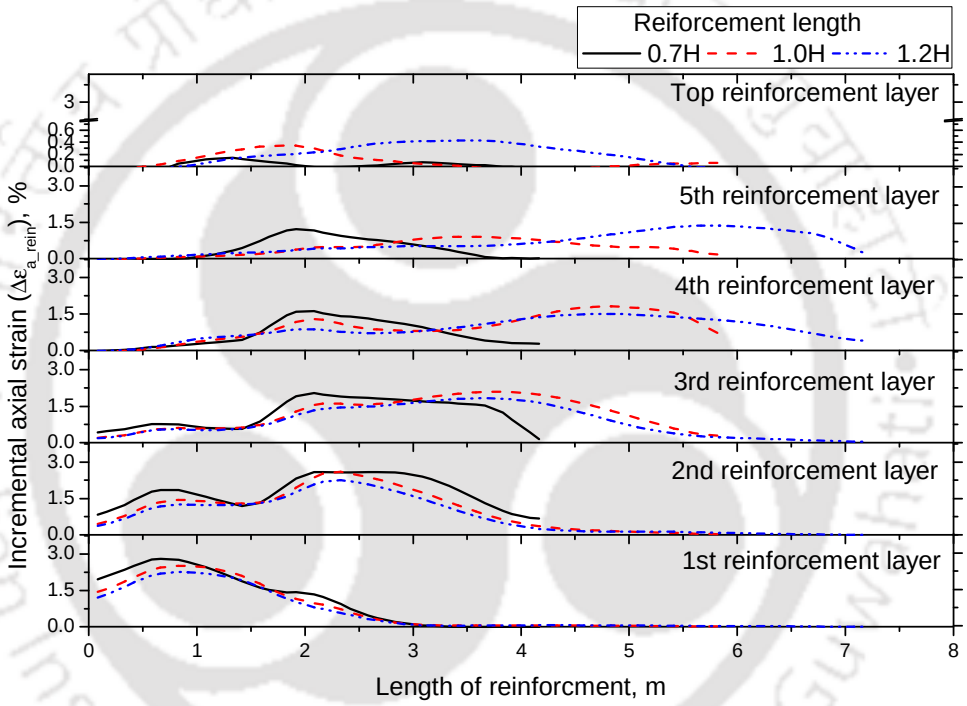

Fig. 4.31 Variation of $\Delta\varepsilon_{a\_rein}$ after dynamic excitation with L_{rein}/H=0.7, 1.0 and 1.2 (a = 0.2g, f = 5Hz, N_L = 6)

From comparison of the results it is observed that wall with the longest reinforcement length have least compound deformation zone and reinforcement strains are more at higher layers. At higher elevations the compound deformation zone is longer for wall with shorter L_{rein} causing more displacement of soil and reinforcement together, which result in lesser increments of reinforcement strain. For longer reinforcement model, smaller compound deformation zone, less displacements

and higher reinforcement strains are seen. The observations presented here can also be interpreted as, using longer reinforcement lengths at higher elevations (upto half the height of wall) and the remaining with shorter reinforcement lengths balances strain levels and lead to get the optimum benefit of reinforcement capacities.

4.4.2 Effect of number of reinforcing layers

Three different reinforcing layer configurations, 4, 6 and 8 layers were considered keeping the reinforcement length (L_{rein}) constant at 0.7H (Table 4.3). The displacements, RMSA amplification factors and horizontal pressures for models with different layer configurations are shown in Fig. 4.32. In general, it is observed that the displacements (u and v) are larger for lesser number of reinforcement layers. Both the displacements are increasing with elevation for all the three model walls with 4, 6 and 8 layers of reinforcement. The RMSA amplification factors didn't show significant variation for all three types of walls. The changes in number of reinforcing layers do not have significant effect on unit weight of reinforced soil. The acceleration amplification depends on density of soil. Ling et al. (2005) also did not observed any significant variation in acceleration amplification with decrease in vertical spacing of reinforcements. The horizontal pressures on wall are almost same for wall with 4, 6 and 8 layers of reinforcement.

Variations of incremental octahedral shear strains ($\Delta\gamma_{oct}$), horizontal (u) and vertical (v) displacements along the length of backfill for wall with 4 layers and 8 layers of reinforcement are presented in Fig. 4.33 and Fig. 4.34. The horizontal displacements (u) of soil near wall facing at an elevation of 5.25 m are 211 mm and 150 mm, for 4 and 8 layer configurations, respectively.

Maximum vertical displacements (v) at 5.25 m elevation and near end of reinforcement are about 130 mm and 90 mm respectively for 4 and 8 layers. Both,

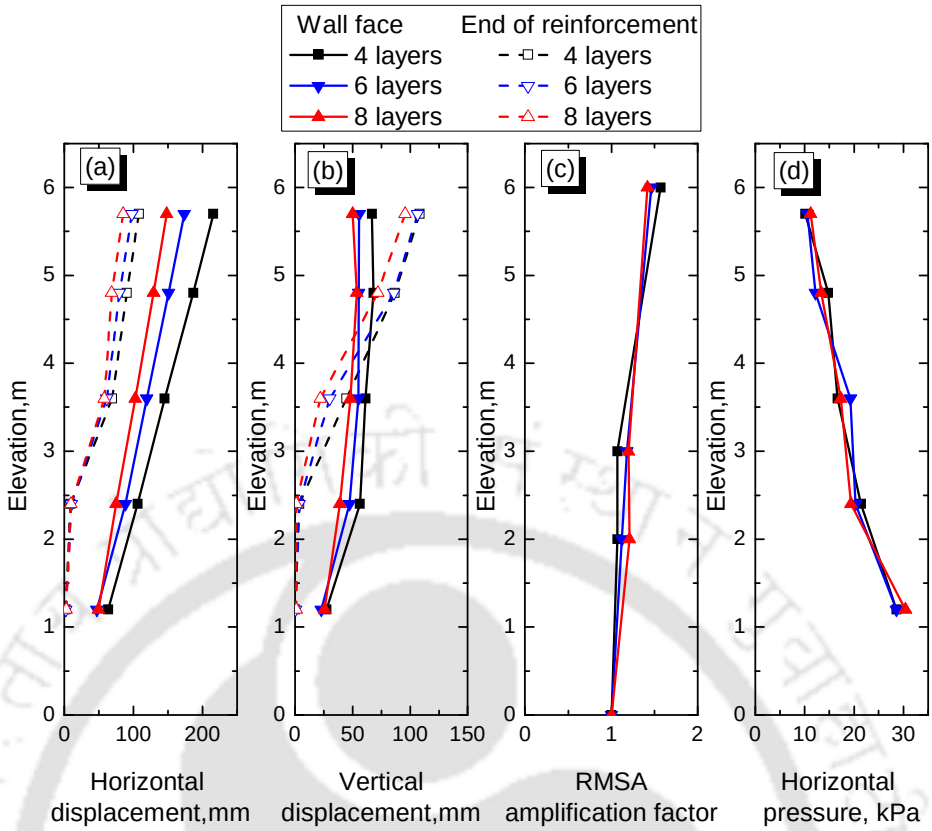

Fig. 4.32 Response of model walls with 4,6 and 8 layers of reinforcement subjected to dynamic excitation (a = 0.2g, f = 5Hz and L_{rein} = 0.7H)

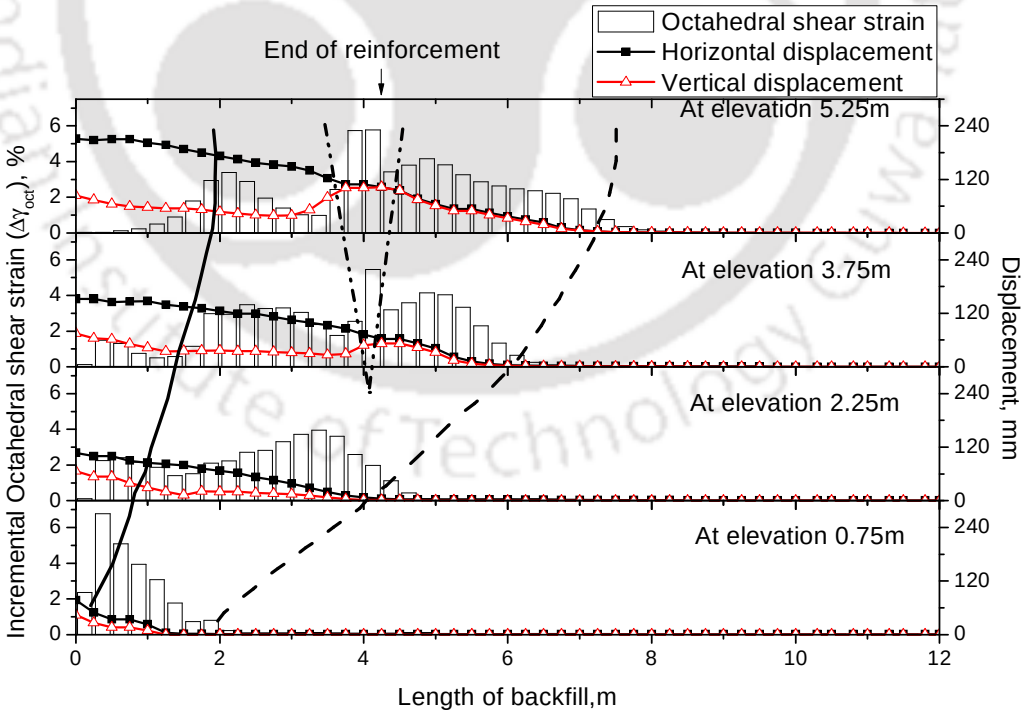

Fig. 4.33 Variation of $\Delta\gamma_{oct}$, u and v along the length of backfill after dynamic excitation for N_L=4 (a=0.2g, f=5 Hz, L_{rein}/H=0.7H)

Fig. 4.33 and Fig. 4.34, show that *u* of soil element near facing are maximum and they decrease gradually and become negligible after end of reinforcements, upto elevation of 2.25 m. But at the lower layers, i.e 2.25 m and 0.75 m, the horizontal movement of soil element decreases to zero within reinforced zone. $\Delta\gamma_{oct}$ reaches peaks within reinforced zone and near end of reinforcement. By comparing the $\Delta\gamma_{oct}$, *u* and *v* at different layers, it can be seen that shear deformation zone is formed within reinforced zone and zone of relative compaction is formed after end of reinforcement and compound deformation zone is formed and extended into deep retained backfill.

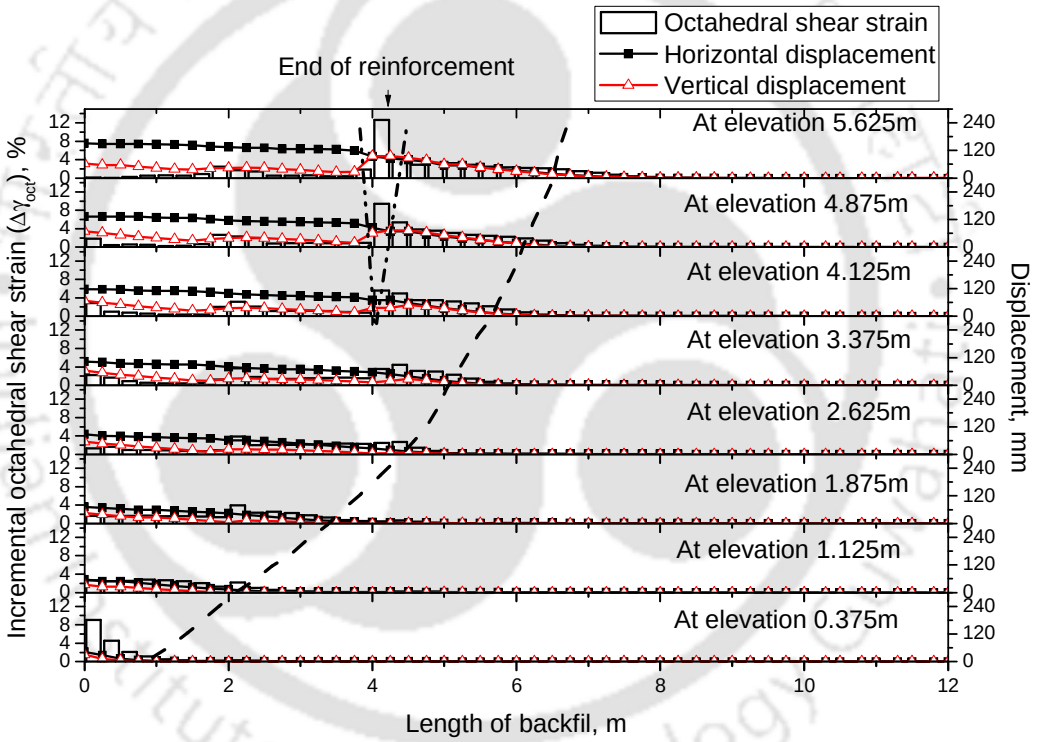

Fig. 4.34 Variation of $\Delta\gamma_{oct}$, *u* and *v* along the length of backfill after dynamic excitation for N_L=8 (a=0.2g, f=5 Hz, L_{rein}/H=0.7H)

Comparison of $\Delta\gamma_{oct}$, after dynamic excitation (a = 0.2g, f = 5Hz), for walls with different reinforcing layers is shown in Fig. 4.35. Incremental octahedral shear strains near the wall facing are very low in the order of less than 2.0% at higher elevations (5.7 m, 4.8 m and 3.6 m) for all three different reinforcement layer configurations. But the $\Delta\gamma_{oct}$ values increase gradually to higher values near end of the

reinforcement (4.2 m from facing). The octahedral shear strain of 3.5%, 1.6% and 0.5% at a distance of 3.0 m from facing are observed for wall with 4, 6 and 8 layers of reinforcements, respectively. The $\Delta\gamma_{oct}$ increases to 6.3%, 9.6% and 13.5% near the end of reinforcement for wall with 4, 6 and 8 layers of reinforcements, respectively. The contour of $\Delta\gamma_{oct}$ on backfill soil of wrap-faced wall with 4, 6 and 8 layers of reinforcement is shown in Fig. 4.36. The wall with lesser number of reinforcement subjected to shear deformation within reinforced zone and reinforced soil do not behave as single unit. While in case of wall with higher layers of reinforcement, less shear deformation within reinforced zone and more relative settlement at end of reinforcement indicate that reinforced soil is moving as single block.

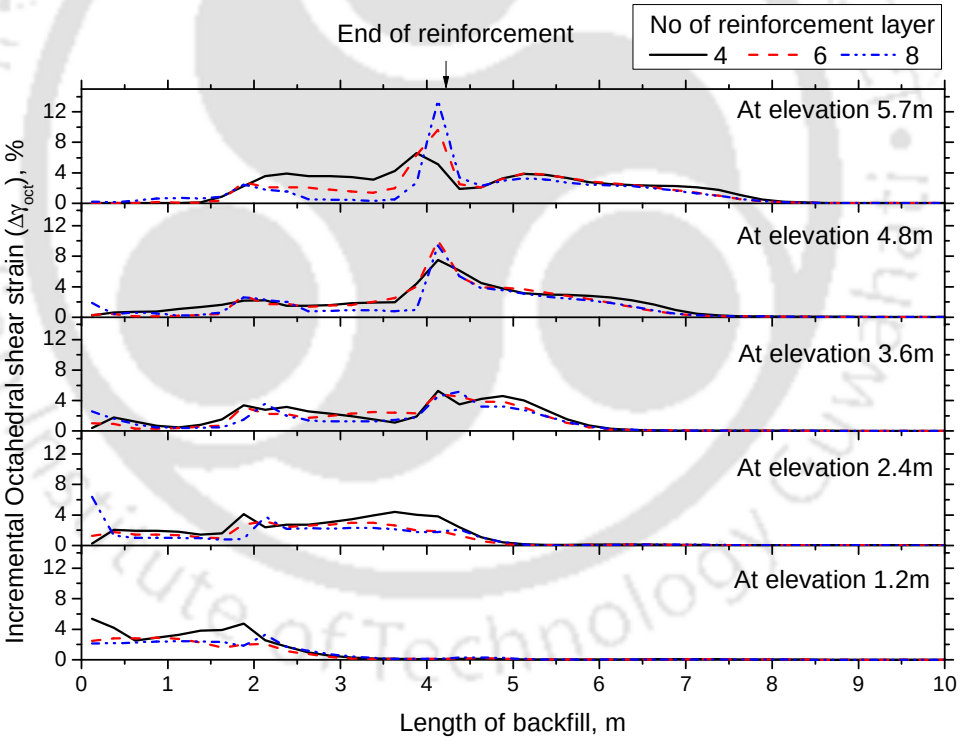

Fig. 4.35 Comparison of $\Delta\gamma_{oct}$ for walls with 4, 6 and 8 layers of reinforcement (a = 0.2g, f = 5Hz and L_{rein}/H = 0.7)

The variations in deformation zone in backfill soil of wrap-faced reinforced soil wall with reinforcement length 0.7H and 1.0H are shown with schematic diagram as shown in Fig. 4.37 schematically.

Variations of reinforcement axial strain increments ($\Delta\varepsilon_{a\_rein}$) after dynamic excitation for walls with 4, 6 and 8 layers of reinforcement are shown in Fig. 4.38. Figure shows that irrespective of layer configurations, all reinforcement layers attained local peak strain value at around 2 m distance from facing. However, their peak values are affected by layer configuration. The reinforcement strain increments at top layer are nearly 0.2% and 1.0% at 6 m elevation for wall with 4 and 8 layers of reinforcement, respectively. The average $\Delta\gamma_{oct}$ within the reinforced zone, decreases with increase in number of reinforcing layers and corresponding $\Delta\varepsilon_{a\_rein}$ increases. The increase in number of layers of reinforcement showed higher strains at higher elevations, indicating that reinforcement elements are effectively functioned by straining more and thus reducing the facing displacements.

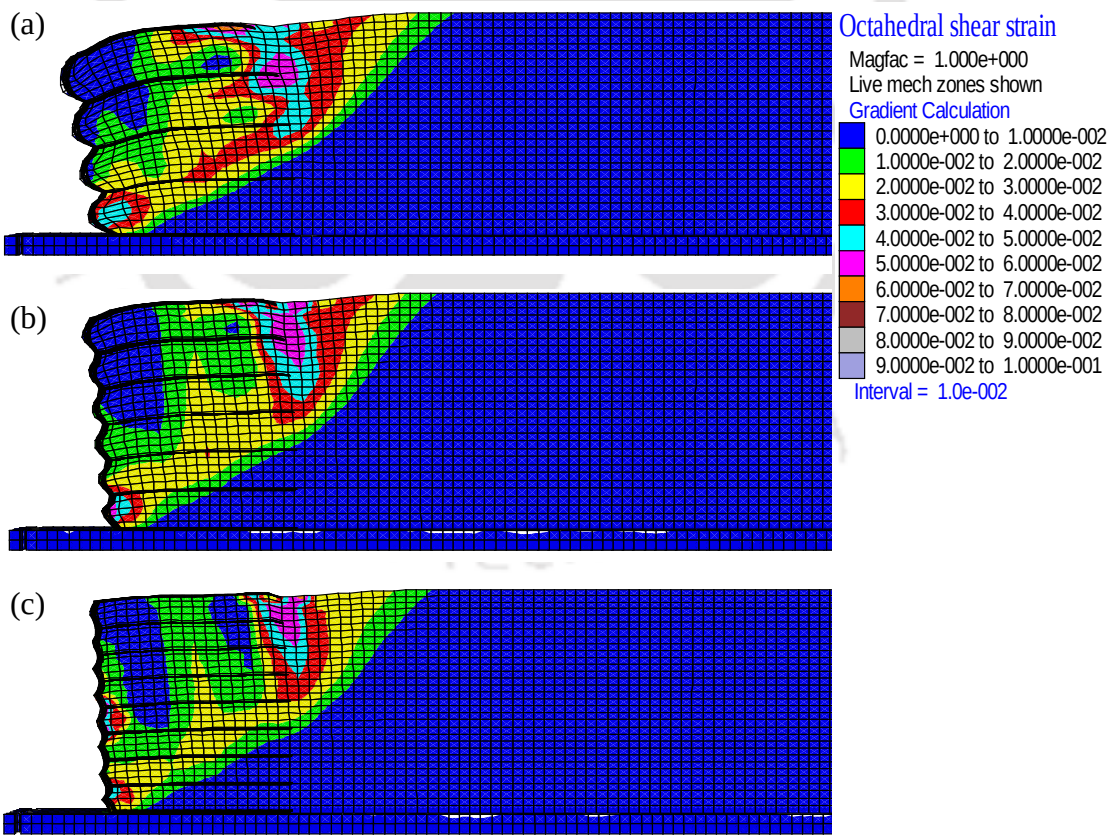

Fig. 4.36 Contour of octahedral shear strain after 20 cycles of dynamic excitation (a = 0.2g, f = 5Hz and L_{rein}/H = 0.7) with (a) N_L = 4 (b) N_L = 6 (c) N_L = 8

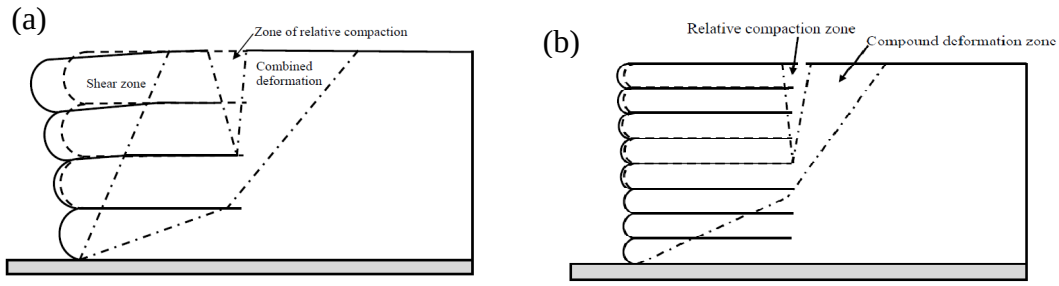

Fig. 4.37 Deformation zones of wrap-faced reinforced soil retaining wall after dynamic excitation with no. of reinforcing layer (a) 4 layers (b) 8 layers

4.4.3 Effect of backfill (angle of internal friction)

Different types of backfills, in terms of different friction angles, 30°, 38° and 43° are considered and the results are shown in Fig. 4.39. The figure depicts that horizontal displacements near facing; vertical displacement at end of horizontal displacements near facing; vertical displacement at end of reinforcement and horizontal pressures are influenced significantly by the backfill friction angle. The vertical displacement at 5.7 m elevation near end of reinforcement is 120.7 mm, 106.4 mm and 99.9 mm for wall with backfill friction angle 30°, 38° and 43° respectively. The horizontal and vertical displacements are maximum for wall with backfill friction angle of 30°; but they are comparable for 38° and 43° friction angle models. The RMSA amplification factor is almost similar for all three types of wall at lower elevation. However, walls with higher friction angles (38° and 43°) showed equal higher amplification at top. This behavior would be justified with reference to the low excitation level of 0.2g considered for this case. At this excitation level, the soils having friction angles more than 38° showed similar displacement and acceleration response. This may also due to the fact that unit weight of the soil was retained the same in all cases. The wall with backfill friction angle 30° is subjected to more

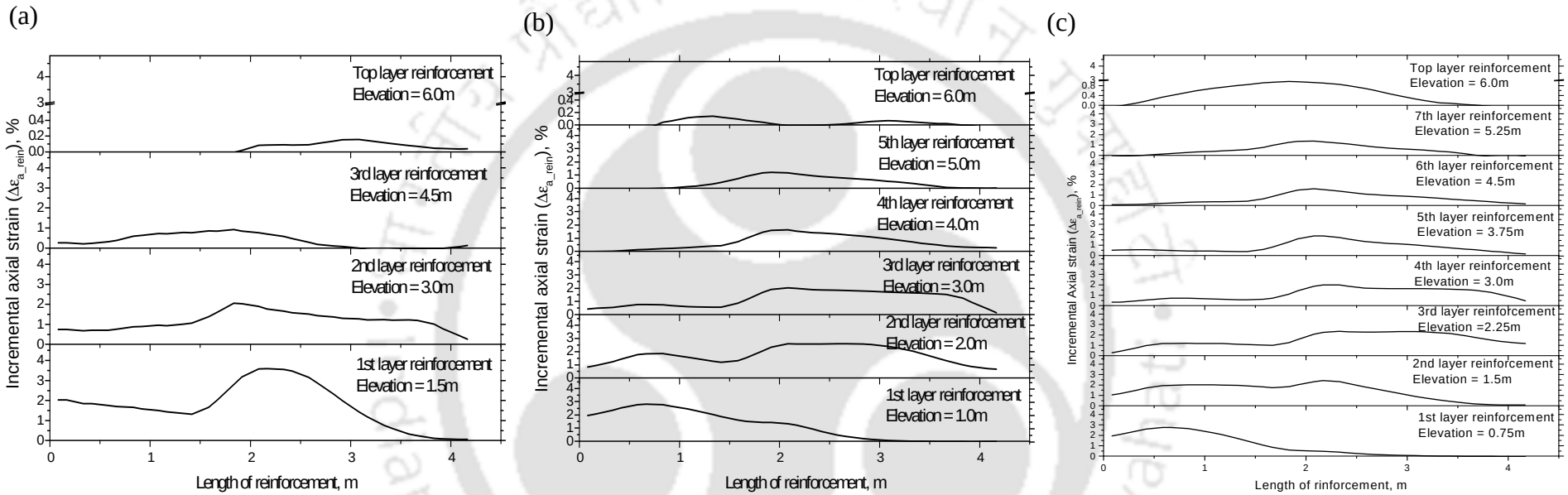

Fig. 4.38 Variation of $\Delta\varepsilon_{a\_rein}$ after dynamic excitation (a=0.2g, f=5Hz, L_{rein}/H=0.7) for walls with (a) N_L=4 (b) N_L=6 (c) N_L=8

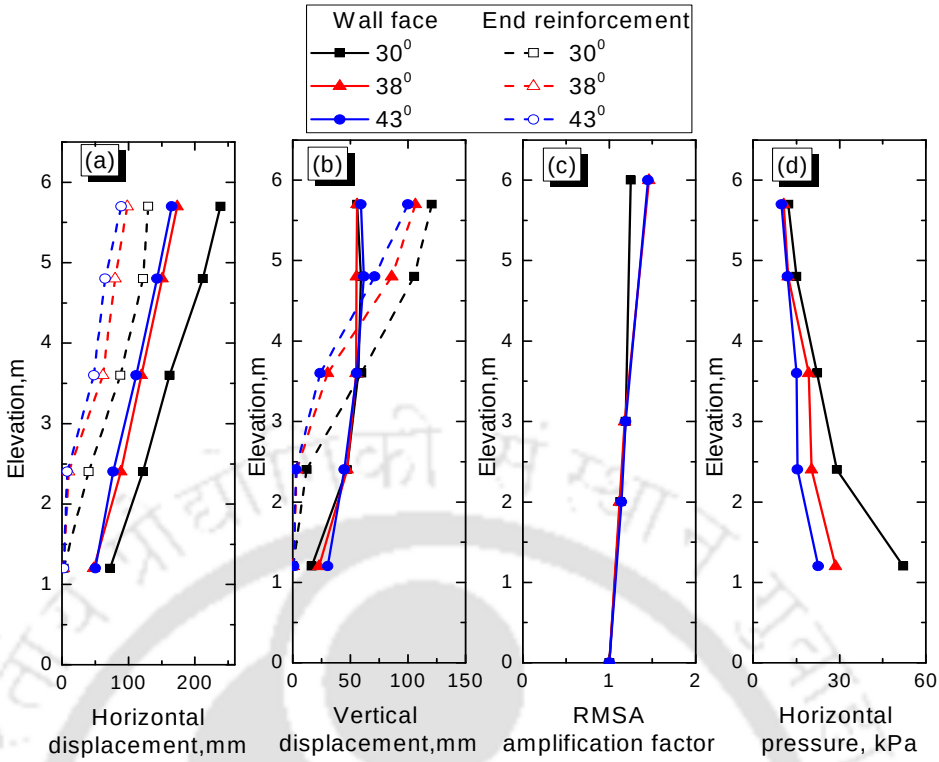

Fig. 4.39 Response of model walls with backfill friction angles 30°, 38° and 43° subjected to dynamic excitation (a = 0.2g, f = 5Hz, N_L = 6and L_{rein} = 0.7H)

horizontal pressure than that of wall with 38° and 43°, which following typical earth pressure theory.

Fig. 4.40 shows the comparison of $\Delta\gamma_{oct}$ at reinforcement levels in the backfill for three model walls, after the dynamic excitation. The length of compound deformation zones beyond the end of reinforcement is 4.8 m, 3.8 m and 3.3 m at elevation 5.5 m for walls with backfill friction angles of 30°, 38° and 43°, respectively. The extent of compound deformation zones gradually decrease with decrease in elevations of backfill. The compound deformation zone extends into deep for wall with backfill friction angle 30° (solid line in Fig. 4.40) causing more mobilization of retained backfill with reinforced backfill. The shear strain increments are more for wall with backfill friction angle of 30° at all elevations indicating more movement of soil.

The variation of $\Delta\varepsilon_{a\_rein}$ for the walls with different backfill soils is shown in Fig. 4.41. The $\Delta\varepsilon_{a\_rein}$ are more in the upper four reinforcement layers for wall with backfill friction angle of 43°. This is due to higher interface friction between soil and reinforcement and relatively smaller soil movement. However, in the bottom two layers, reinforcement length extended beyond the deformation zone within the reinforced zone, $\Delta\varepsilon_{a\_rein}$ are more in the model with backfill friction angle of 30°. This may be due to the fact that huge active movement (compound deformation zone) in the upper layers, forces the bottom layers to take more load (also reflected as higher horizontal pressures in Fig. 4.39).

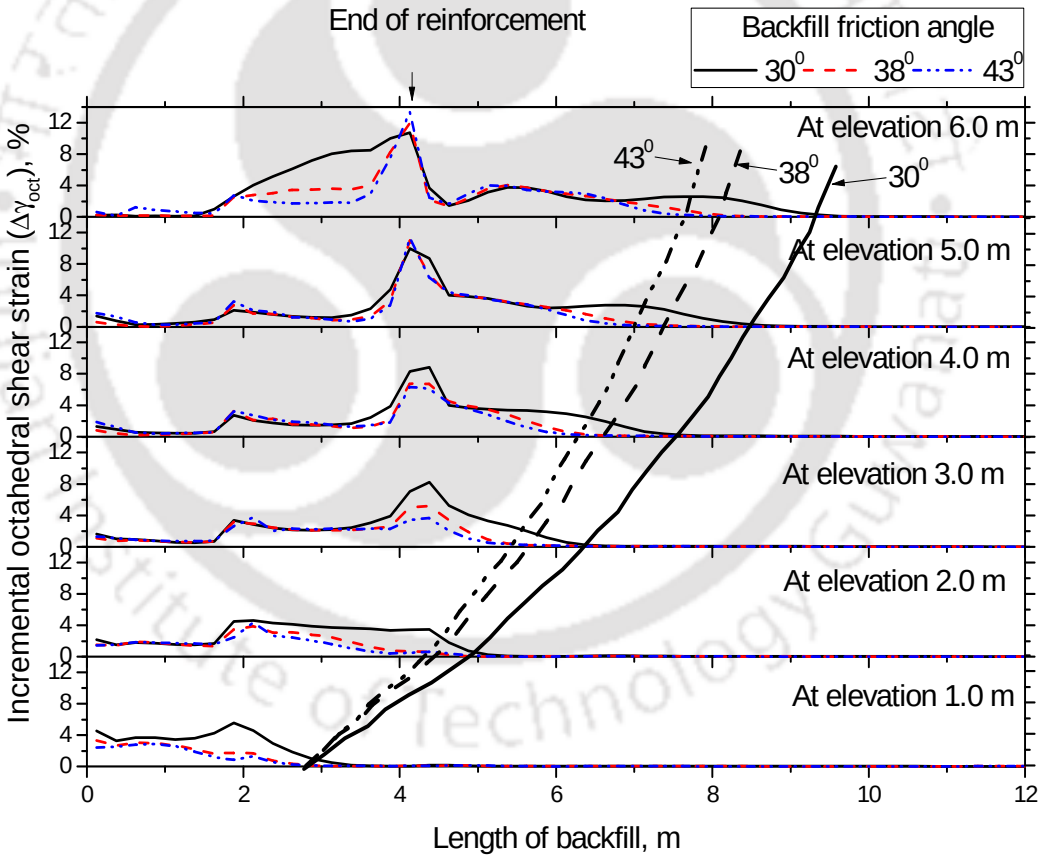

Fig. 4.40 Comparison of $\Delta\gamma_{oct}$ for walls with backfill friction angle 30°, 38° and 43° after dynamic excitation (a = 0.2g, f = 5Hz and L_{rein}/H = 0.7)

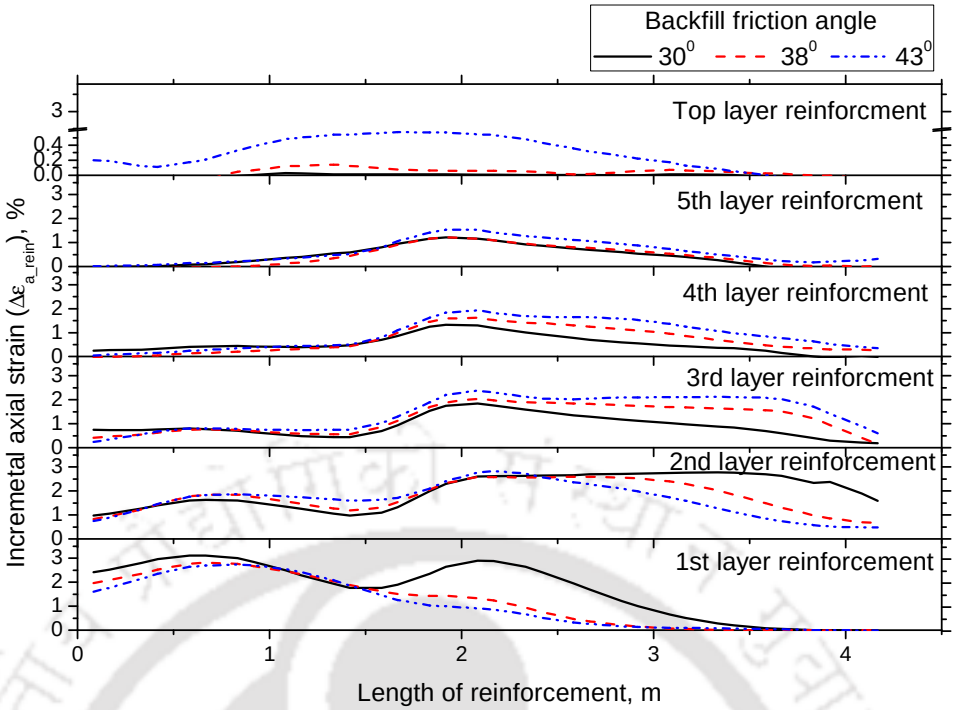

Fig. 4.41 Incremental axial strain in reinforcement after dynamic excitation (a=0.2g, f=5Hz, L_{rein}/H=0.7) with backfill friction angle 30°, 38° and 43°

4.4.4 Effect of reinforcement stiffness

Reinforcement stiffness values of 5.2 kN/m, 100 kN/m and 152 kN/m are considered for analyzing its effect on model (L_{rein}/H=0.7H, N_L=8) behavior. Results obtained for models with these different stiffness values are presented in Fig. 4.42 - Fig. 4.46. From Fig. 4.42 (a) and (b), it is observed that the horizontal and vertical displacements are influenced by the reinforcement stiffness, and showed maximum responses for lower stiffness values. The maximum horizontal displacements of wall facing are 242.4 mm, 171.4 mm and 146.3 mm for wall with reinforcement stiffness 5.2 kN/m, 100 kN/m and 152 kN/m, respectively. The vertical displacement at end of reinforcement is 130.2 mm, 103.4 mm and 92.8 mm for wall with reinforcement stiffness 5.2 kN/m, 100 kN/m and 152 kN/m respectively. The RMSA amplification factors and horizontal pressures does not show significant variations with different reinforcement stiffness values.

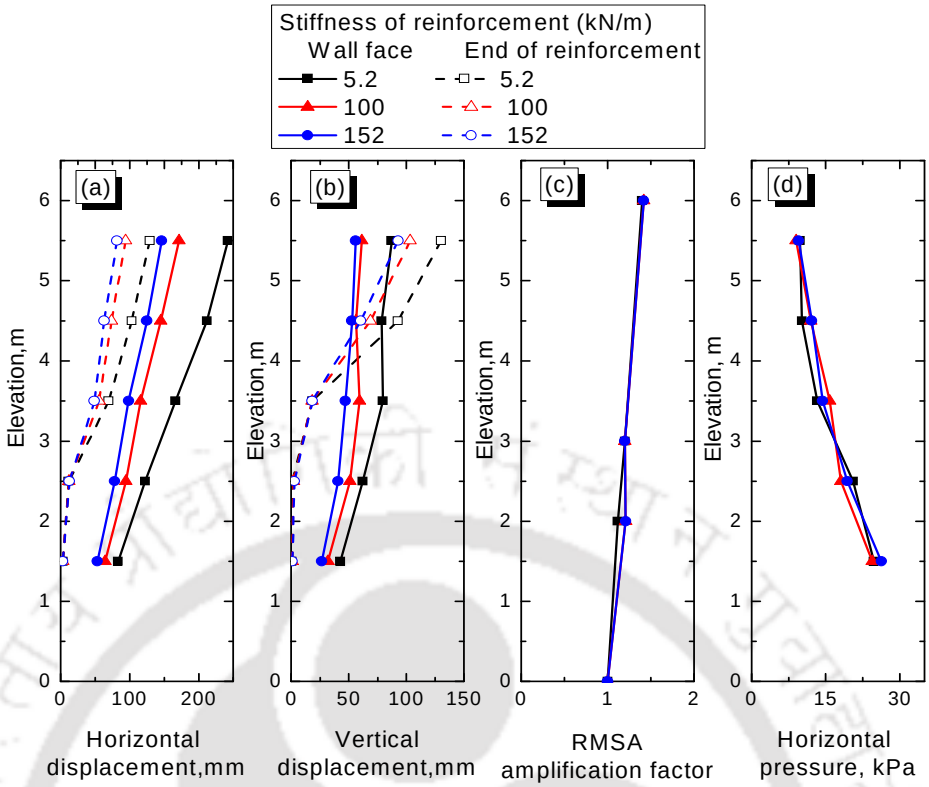

Fig. 4.42 Response of model walls with backfill different reinforcement stiffness subjected to dynamic excitation (a = 0.2g, f = 5Hz, N_L = 8 and L_{rein} = 0.7H)

Variations of horizontal and vertical displacements together with octahedral shear strains, along the length of backfill for models with reinforcement stiffness values of 5.2 kN/m and 152 kN/m are shown in Fig. 4.43 and Fig. 4.44, respectively. The average horizontal displacements within reinforced zone are 227 mm and 138 mm for wall with reinforcement stiffness 5.2 kN/m and 152 kN/m respectively. The maximum vertical displacement near end of reinforcement is 95.6 mm and 133.7 mm for wall with reinforcement stiffness 5.2 kN/m and 152 kN/m respectively. The $\Delta\gamma_{oct}$ increases to nearly 3% and 2.3% at a distance of 2 m from facing for wall with reinforcement stiffness 5.2 kN/m and 152 kN/m respectively. The $\Delta\gamma_{oct}$ is maximum (nearly 13%) near the end of reinforcement and gradually decreases to zero at distance of 8.0 from the facing for wall with both reinforcement stiffness. The formation of deformation zones are influenced by the stiffness of reinforcement.

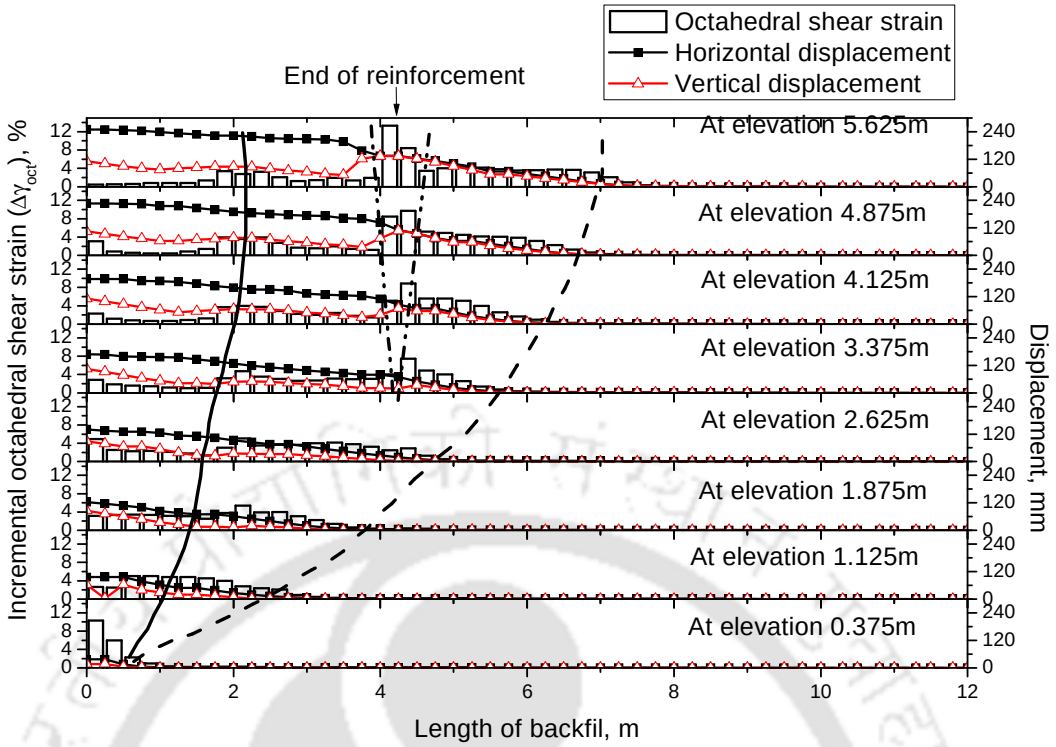

Fig. 4.43 Octahedral shear strain, horizontal and vertical displacement along the length of backfill with reinforcement stiffness 5.2 kN/m (a=0.2g, f=5 Hz, L_{rein}/H=0.7H, N_L=8)

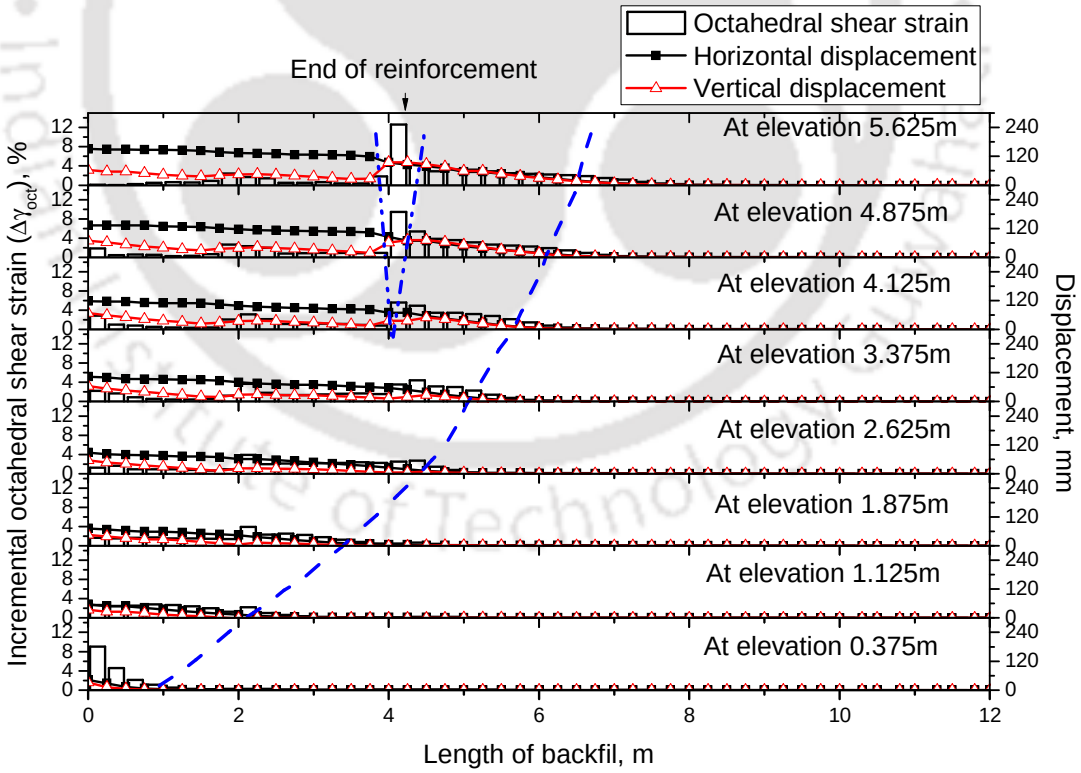

Fig. 4.44 Octahedral shear strain, horizontal and vertical displacement along the length of backfill with reinforcement stiffness 152 kN/m (a=0.2g, f=5 Hz, L_{rein}/H=0.7H, N_L=8)

Comparison of $\Delta\gamma_{oct}$ at reinforcement level in backfill for three model walls, with different reinforcement stiffness is shown in Fig. 4.45. The strain increments at an elevation of 6.0 m are decreased to negligible values at a distance of 8.0 m from facing for all three walls with different reinforcement stiffness. It can also be observed that at all elevations higher strain increments for wall with reinforcement stiffness of 5.2 kN/m. The strain increments for wall with reinforcement stiffness 100 kN/m and 152 kN/m are almost same at all elevations.

The variation of reinforcement strain increments ($\Delta\varepsilon_{a\_rein}$), along the length of reinforcement for walls with different reinforcement stiffness is shown in Fig. 4.46. The maximum $\Delta\varepsilon_{a\_rein}$ are 2.7%, 1.6% and 1.4% at 7th reinforcement layer for wall with reinforcement stiffness 5.2 kN/m, 100 kN/m and 152 kN/m, respectively. The reinforcement axial strains are inversely proportion to reinforcement stiffness values. The axial strain in reinforcement with lower stiffness is higher due to more elongation of weaker reinforcement than stronger reinforcement.

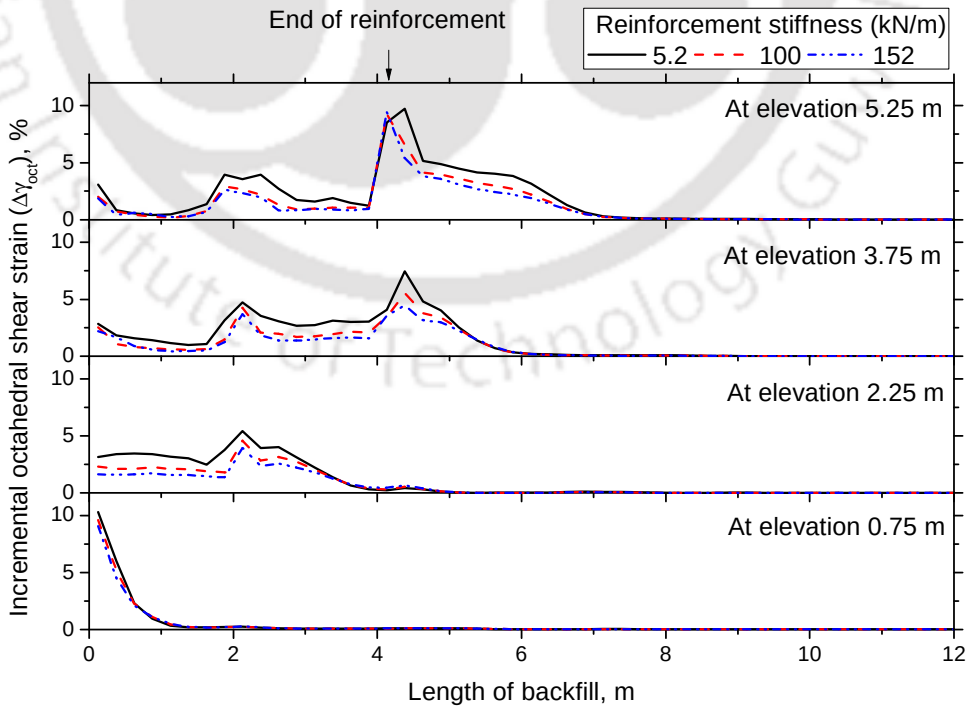

Fig. 4.45 Comparison of $\Delta\gamma_{oct}$ at backfill for wall with reinforcement stiffness subjected to dynamic excitation (a = 0.2g, f = 5Hz and L_{rein}/H = 0.7, N_L=8)

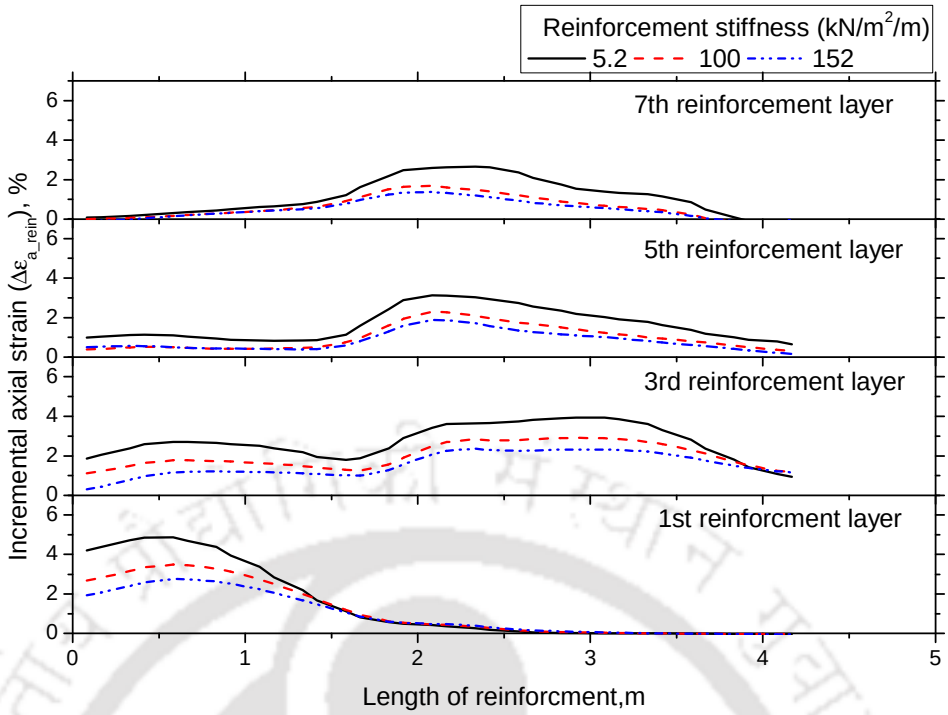

Fig. 4.46 Incremental axial strain on reinforcement after dynamic excitation (a=0.2g, f=5Hz, L_{rein}/H=0.7, N_L=8) with reinforcement stiffness 5.2, 100 and 152 kN/m

4.4.5 Effect of frequency of excitation

The wrap-faced reinforced soil walls are subjected to 3 Hz, 5 Hz and 7 Hz frequency of seismic excitation (a=0.2g). The horizontal displacement, vertical displacement, RMSA amplification factor and horizontal pressures are compared between walls subjected to different frequencies of excitation and are shown in Fig. 4.47.

From the figure it is observed that horizontal displacements near facing are 291.07 mm and 46.21 mm for wall subjected to seismic excitation of 3 Hz and 7 Hz respectively. The vertical displacements near the end of reinforcement are also maximum for wall subjected to 3 Hz seismic excitation. The RMSA amplification factors do not have significant variation for all three frequencies. The highest amount of horizontal pressures is acting on wall subjected to seismic excitation at 3 Hz

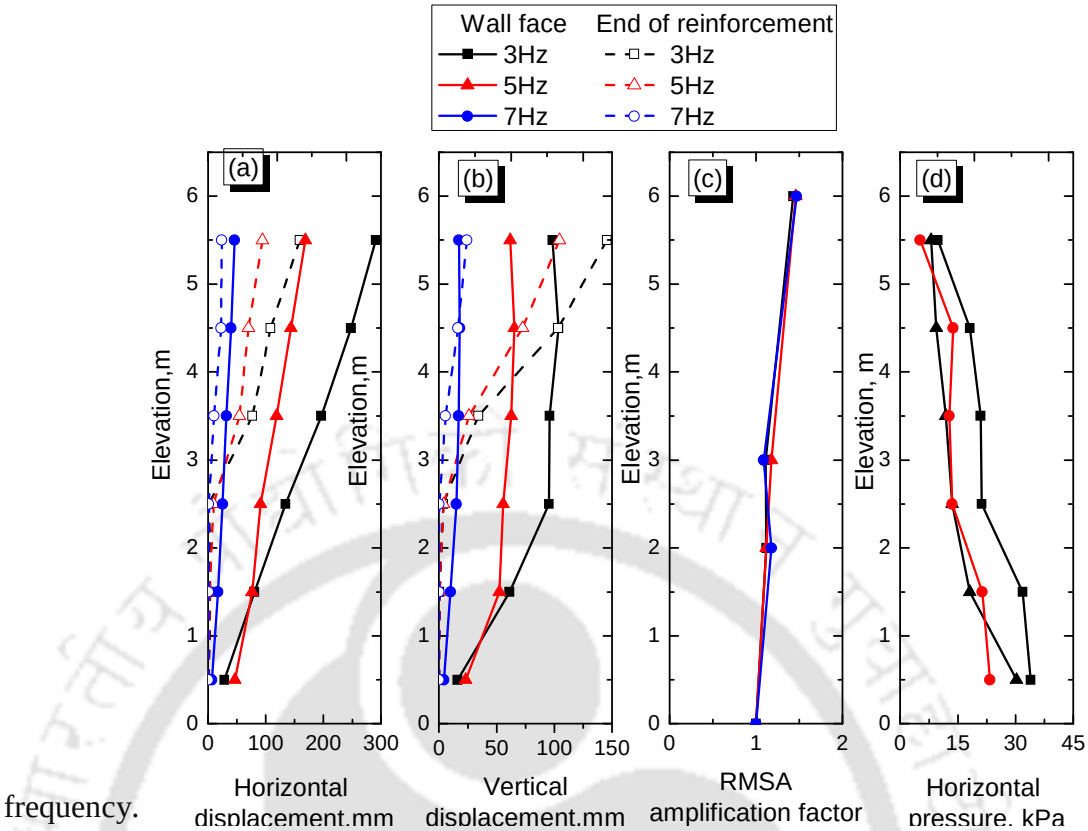

frequency.

Fig. 4.47 Response of model walls subjected to dynamic excitation at different frequencies (a = 0.2g, N_L = 6and L_{rein} = 0.7H)

Comparison of $\Delta\gamma_{oct}$ in the middle of two reinforcement layers, after dynamic excitation, is shown in Fig. 4.48. The maximum $\Delta\gamma_{oct}$ are 13.61%, 9.72% and 1.98% near the end of reinforcement at elevation 5.5 m for walls subjected to dynamic excitation of frequencies 3 Hz, 5 Hz and 7 Hz, respectively. The $\Delta\gamma_{oct}$ near the wall facing, are very small at elevations 5.5 m, 4.5 m and 3.5 m for all walls subjected to dynamic excitations of different frequencies. The intensity on increase in $\Delta\gamma_{oct}$ for wall subjected dynamic excitation of 3 Hz is more than other excitations (5 Hz and 7 Hz). But the extents of higher incremental octahedral shear strains are same for three excitations. Therefore, the extents of compound deformation zones are also same for three frequencies. The incremental axial strains ($\Delta\varepsilon_{a\_rein}$) developed in reinforcement members at different elevations are shown in Fig. 4.49.

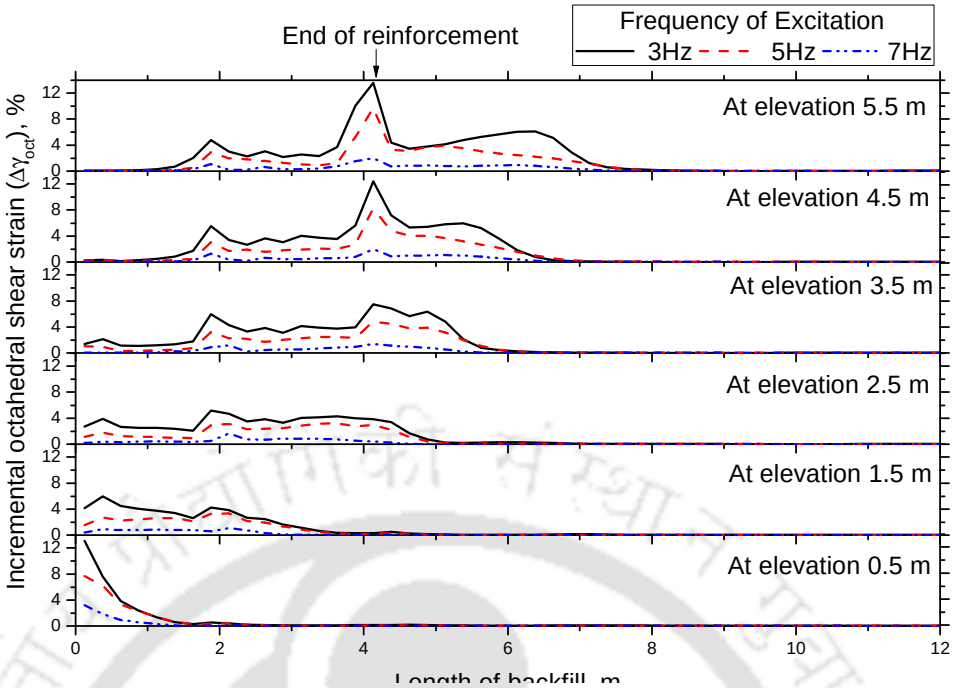

Fig. 4.48 Comparison of octahedral shear strain at backfill for walls subjected to dynamic excitations of frequency 3 Hz, 5 Hz and 7 Hz (a = 0.2g and L_{rein}/H = 0.7)

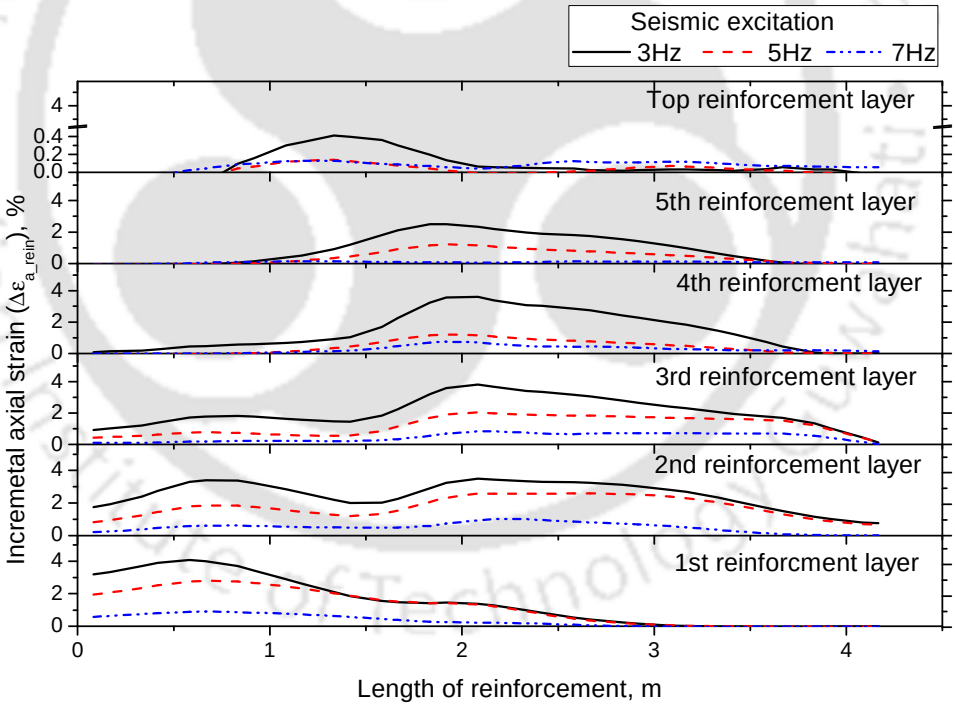

Fig. 4.49 Incremental axial strain on reinforcement for walls subjected to dynamic excitation of 3 Hz, 5Hz, and 7 Hz frequencies (a = 0.2g and N_L = 6)

The maximum $\Delta\varepsilon_{a\_rein}$ are 4%, 2.8% and 0.8% on first layer of reinforcement for walls subjected to frequency of excitation of 3 Hz, 5 Hz and 7 Hz respectively.

The maximum $\Delta\varepsilon_{a\_rein}$ at top layers are 0.4%, 0.13% and 0.12% for walls subjected to 3 Hz, 5Hz and 7 Hz respectively. The increments in reinforcement strains at top layer are more for wall subjected to lowest frequency of excitation due to higher soil strain developed resulting in more mobilization. So the frequency of earthquake effects the behavior of wrap-faced wall.

4.4.6 Effect of seismic acceleration

The wrap-faced walls subjected to 20 cycles of seismic excitation with accelerations of 0.2g, 0.3g and 0.4g at 5 Hz frequency are considered. Fig. 4.50 shows the response of the model subjected to different accelerations. The maximum horizontal displacement 168.8 mm and 380.27 mm for wall model subjected to seismic excitation of 0.2g and 0.4g, respectively. The vertical displacement at end of reinforcement is more than that near the facing for wall subjected to all three seismic excitations. The maximum vertical displacement at end of reinforcement is 227.36 mm for wall subjected to seismic excitation of 0.4g. The RMSA amplification factors at the top of wall are 1.46, 1.89 and 2.33 for wall subjected to seismic excitation of 0.2g, 0.3g and 0.4g, respectively. The lowest horizontal pressure is acting on wall subjected to seismic excitation of 0.2g.

The comparison of $\Delta\gamma_{oct}$ during dynamic excitation of 0.2g, 0.3g and 0.4g accelerations are shown in Fig. 4.51. The increases in octahedral shear strain are observed at a distance of 2 m (nearly at middle of reinforcement) from the facing depicting more shear movement for wall. The maximum octahedral shear strains are 17%, 14.5% and 9.7% near the end of reinforcements for wall subjected to base acceleration of 0.2g, 0.3g and 0.4g respectively at elevation 5.5 m. The octahedral shear strains reduce to negligible value at a distance of 8.0 m, 9.0 m and 10.0 m from facing for wall subjected to acceleration of 0.2g, 0.3g and 0.4g respectively. This

shows that the compound deformation zones extend deep into the backfill for walls subjected to higher excitation levels.

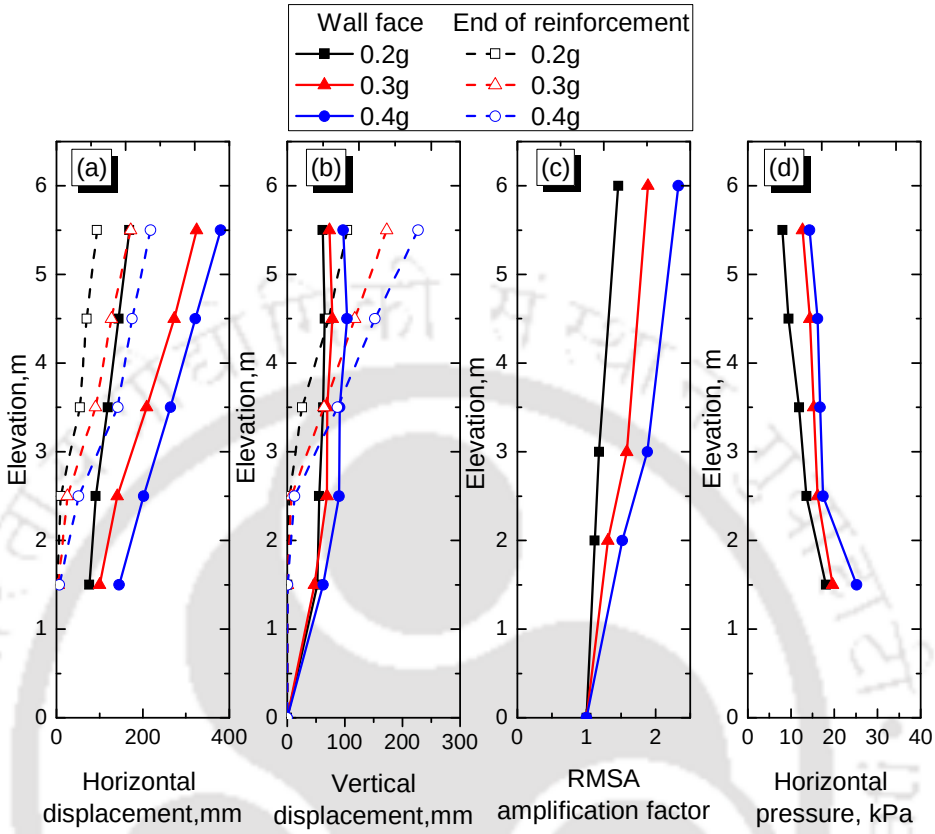

Fig. 4.50 Variation of (a) horizontal and (b) vertical displacement (c) RMSA amplification factor and (d) Horizontal pressure for walls subjected to dynamic excitation 0.2g, 0.3g and 0.4g (f=5 Hz, L_{rein}/H = 0.7, N_L = 6)

The incremental axial strain ($\Delta\varepsilon_{a\_rein}$) during the dynamic excitations of 0.2g, 0.3g and 0.4g accelerations is shown in Fig. 4.52. The maximum $\Delta\varepsilon_{a\_rein}$ are 2.8% and 5.3% at first layer of reinforcement for walls subjected to seismic excitation of 0.2g and 0.4g respectively. But at reinforcement at higher elevation (5th layer of reinforcement) the incremental axial strains are 1.2% and 1.6% for seismic excitation of 0.2g and 0.4g respectively. $\Delta\varepsilon_{a\_rein}$ at top level is lesser for higher excitation. This is due to longer compound deformation zones for walls subjected to higher excitations. Reinforcement strains are more at lower elevations (from 1st to 5th layer of reinforcements) due to more inertia force acting within reinforced zones.

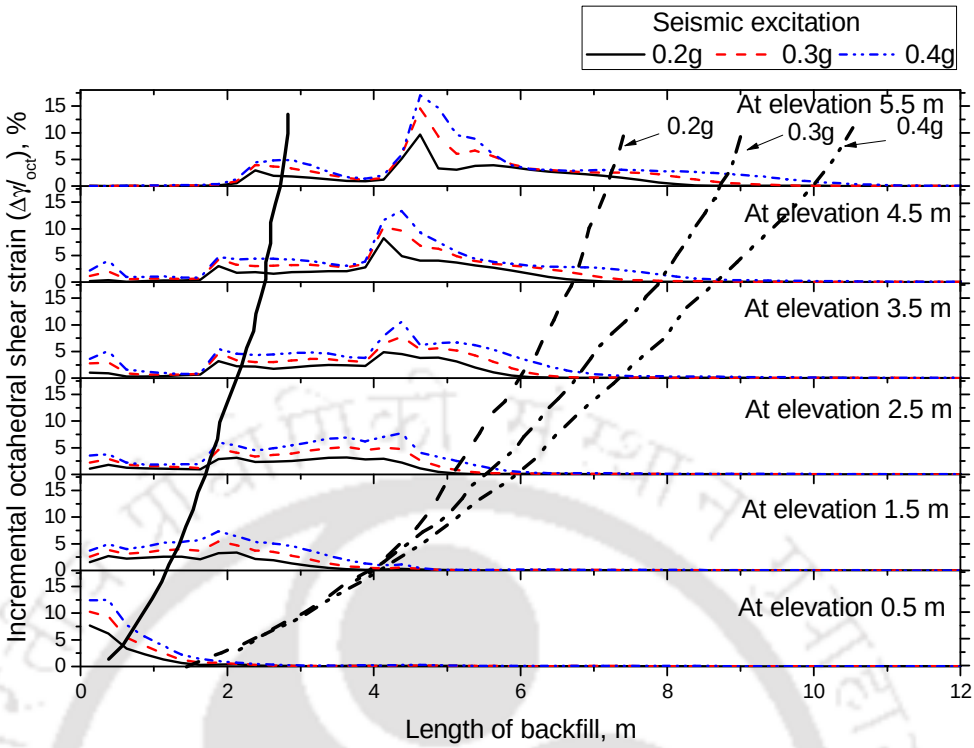

Fig. 4.51 Comparison of octahedral shear strain at backfill for walls subjected to dynamic excitations of acceleration 0.2g, 0.3g and 0.4g (f=5 Hz, L_{rein}/H = 0.7, N_L = 6)

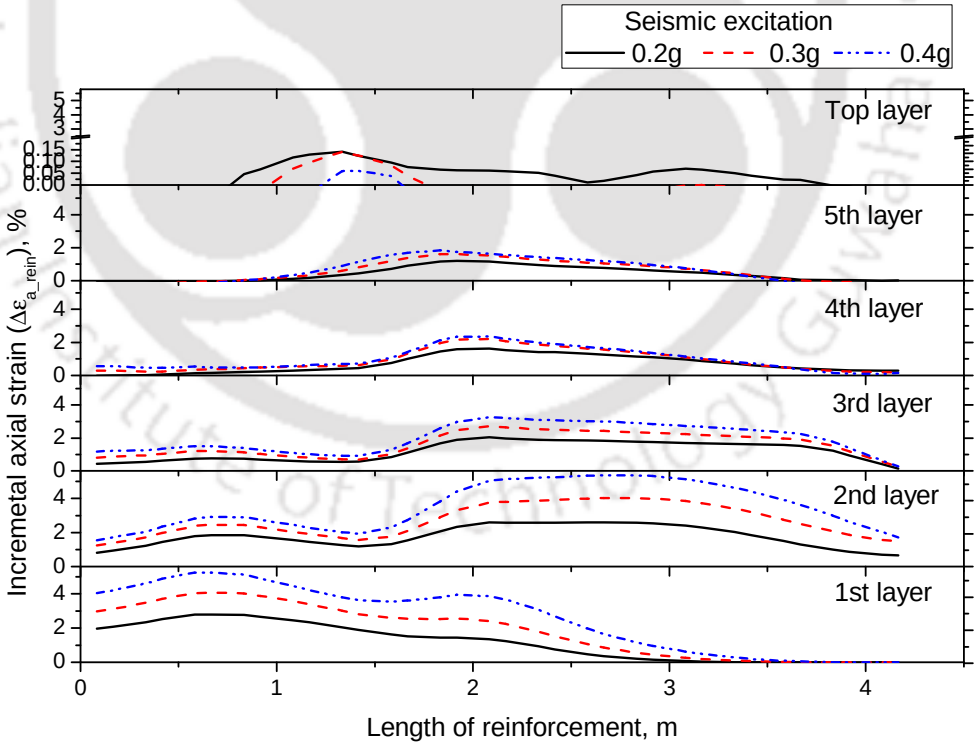

Fig. 4.52 Incremental axial strain on reinforcement for walls subjected to dynamic excitations of acceleration 0.2g, 0.3g and 0.4g (f=5 Hz, L_{rein}/H = 0.7, N_L = 6)

4.5 RESPONSE OF DESIGNED WRAP-FACED WALL MODEL

Hypothetical configurations of wrap-faced wall model walls were considered in earlier sections for observing the interdependency of soil strains, reinforcement strain and deformation zones. It is observed from the study that development of shear strains is effecting the formation of deformation zones. The strains on reinforcements are influenced by the soil reinforcement interaction and extent of compound deformation zone at backfill. To observe the wall response in terms of the influence of soil and reinforcement strains on wall response, a 6 m high wrap-faced wall is designed considering FHWA (2001) recommendations. The material parameters considered for the design are the same as that of model walls considered earlier. However, the spacing between two layers of reinforcement is adopted as 500 mm (maximum spacing as per FHWA 2001) and length of reinforcement as 0.7*H*. As part and design process various safety factors evaluated (Appendix B) for the design wall, subjected to 0.2 g acceleration, and listed in Table 4.4. The safety factors shown in Table 4.4 indicate that the wall considered is safe against external and internal stability for 0.2g acceleration.

Table 4.4 Static and dynamic Factors of safety values for full scale model

Loading condition	External stability		Internal stability	
	$FS_{sliding}$	$FS_{overturning}$	$FS_{rupture}$	$FS_{pullout}$
Static	4.16	5.34	4.98	8.69
Dynamic	1.80	1.78	4.90	8.27

Sinusoidal dynamic excitation of 0.2g acceleration at 5Hz frequency for 20 cycles is considered. Variations of octahedral shear strains, horizontal and vertical displacements along the length of backfill, after the dynamic excitation, are presented in Fig. 4.53. The horizontal displacement of soil element near the wall facing is 105.3

mm at an elevation of 6.25 m and remains almost constant upto end of reinforcement (upto 4.2 m) of wall. The vertical displacement of soil element is 41.7 mm near the wall facing at that elevation. The maximum vertical displacement of 77.8 mm is seen near the end of reinforcement (at 4.2 m distance from facing). The horizontal and vertical displacement decreased to negligible values at a distance of about 7.0 m from the facing. Higher strain values (in the range of 6 – 8%) are observed near the end of reinforcement at elevations + 3.5 m (above). The shear strains decreased to negligible value at 7 m from facing, at elevations 6.25 m, 5.25 m and 4.25 m, respectively. The $\Delta\gamma_{oct}$ is nearly 2% at a distance of 2.0 m from facing, at these elevations. Comparing the horizontal and vertical displacements and octahedral shear strains, three different deformation zones could be expected, as explained in the earlier sections. The less shear deformation within reinforced zone and more relative settlement at end of reinforcement indicate that reinforced soil zone is moving as single block.

$\Delta\varepsilon_{a\_rein}$ after dynamic excitation at different elevations are shown in Fig. 4.54. The maximum axial strain increments during dynamic excitation are 1%, 1.5% and 2.0% at 11th, 7th and 3rd layer of reinforcements, respectively, and occur nearly at middle of length of reinforcement. The maximum axial strain increment is near the facing at lower layer. The strain increments at middle of reinforcement are due to shear deformation of reinforced soil wall as explained earlier (Fig. 4.23).

Discussion

The comparisons of soil strains and reinforcement strains developed during the dynamic excitation show that, compound deformation extended to deep backfill resulting in more mobilization of soil; and lesser reinforcement strain development. The extent of compound deformation zones in backfill soil is, predominantly,

influenced by the reinforcement length (L_{rein}) and backfill friction angle (ϕ). It is also observed that the longer reinforcements, reduce the extent of compound deformation

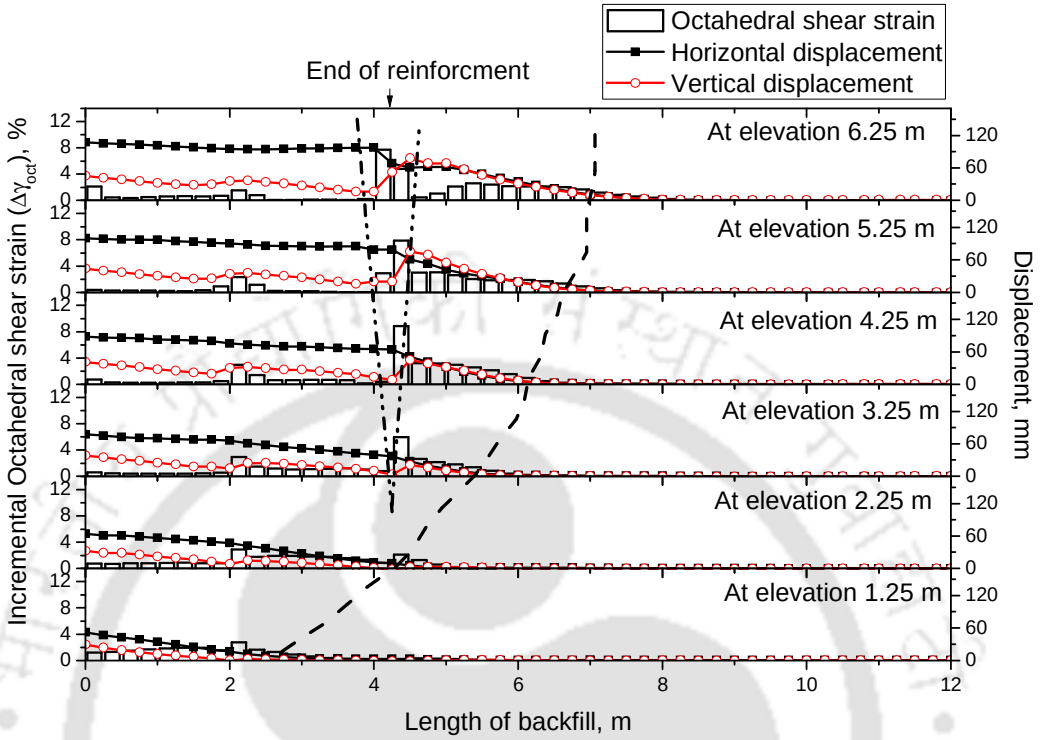

Fig. 4.53 Octahedral shear strain, horizontal displacement and vertical displacement along the length of backfill after 20 cycles of dynamic excitation (a=0.2g, f=5 Hz, L_{rein}/H=0.7H, N_L=12)

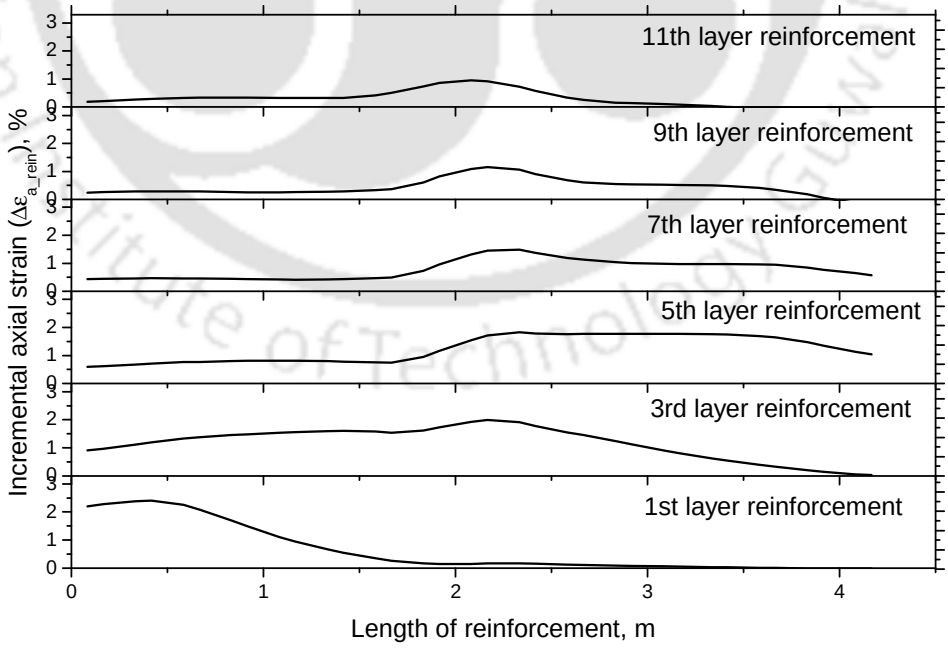

Fig. 4.54 Incremental axial strain on reinforcement after dynamic excitation (a=0.2g, f=5Hz, L_{rein}/H=0.7, N_L = 12)

zone into retained backfill and are more effective at higher layers. Hence, it can be concluded that providing the longer reinforcement at higher elevations and minimum reinforcement length at lower elevations will be beneficial. This may reduce the extent of compound deformation zone into retained backfill and balances the reinforcement strain to get optimum benefit. Increasing the number of reinforcement layers may reduce the facing displacement, but will not influence on extent of deformation zones within unreinforced backfill. Similarly reinforcement stiffness also influences the facing displacement, but have little influence on extent of deformation zones.

Wrap-faced wall with different reinforcement configurations

Four different wrap-faced wall reinforcement configurations, with 6 m high and reinforcement spacing of 500 mm (12 layers), are considered. They are (Fig. 4.55): i) Full height, 0.7H reinforcement length (L_{rein}); ii) Full height L_{rein} = 1.0H, iii) Top 1/6 H (two layers), L_{rein} = 1.0H and remaining L_{rein} = 0.7H; and iv) Top 1/2 H (6 layers), L_{rein} = 1.0H and remaining L_{rein} = 0.7H. Responses of the model walls after the dynamic excitation (20 cycles, a = 0.2g, f = 5Hz) are shown in Fig. 4.56. Different reinforcement configurations are denoted as, 0.7H, 1.0H, 2L-1.0H and 6L-1.0H, in the order.

The horizontal displacements near the facing at 5.5 m elevation are 100.83 mm, 60.44 mm, 73.62 mm and 60.65 mm for walls 0.7H, 1.0H, 2L-1.0H and 6L-1.0H, respectively. Maximum vertical displacements at 5.5 m elevation (near end of reinforcement) are 37.26 mm, 29.08 mm, 31.93 mm and 29.73 mm for the four configuration walls, respectively. It is seen from the displacement behaviour that the wall-2L-1.0H, could effectively reduce the deformations by about 17-30% of that of the wall-0.7H. Further, it is also observed that the displacements of wall-6L-1.0H are

almost identical to that of wall- 1.0*H* and reduced the deformations by about 20-45% from that of the wall-0.7*H*. The RMSA amplification factors and horizontal pressures did not show significant variation among different wall configurations. almost similar for all three types of wall with longer reinforcements.

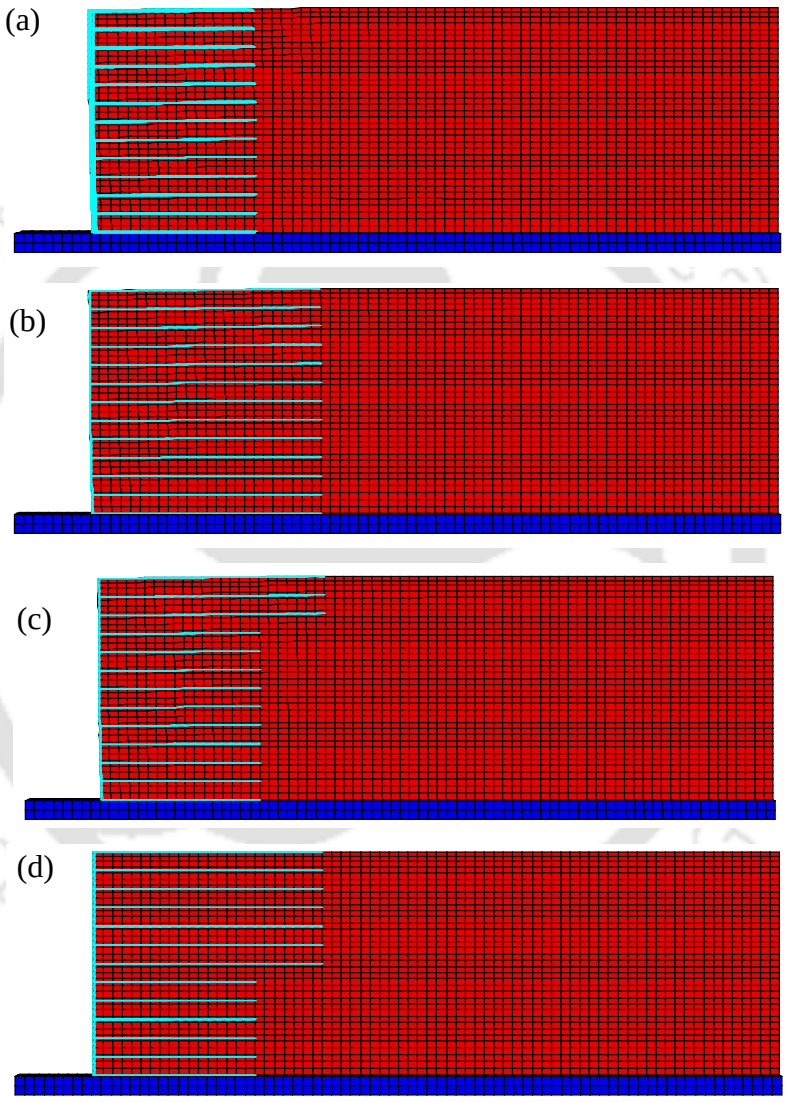

Fig. 4.55 Wrap-faced wall with reinforcement length (a) 0.7*H* (b) 1.0*H* and (c) top three layers 1.0*H* and other layers 0.7*H* (d) top seven layers 1.0*H* and others 0.7*H*

The $\Delta\gamma_{oct}$ during dynamic excitations are shown in Fig. 4.57. Maximum $\Delta\gamma_{oct}$ developed is 8% near the end of reinforcement for wall 0.7*H* at 5.75 m elevation. For other walls with longer reinforcement, the maximum $\Delta\gamma_{oct}$ are 3.7% near the end of

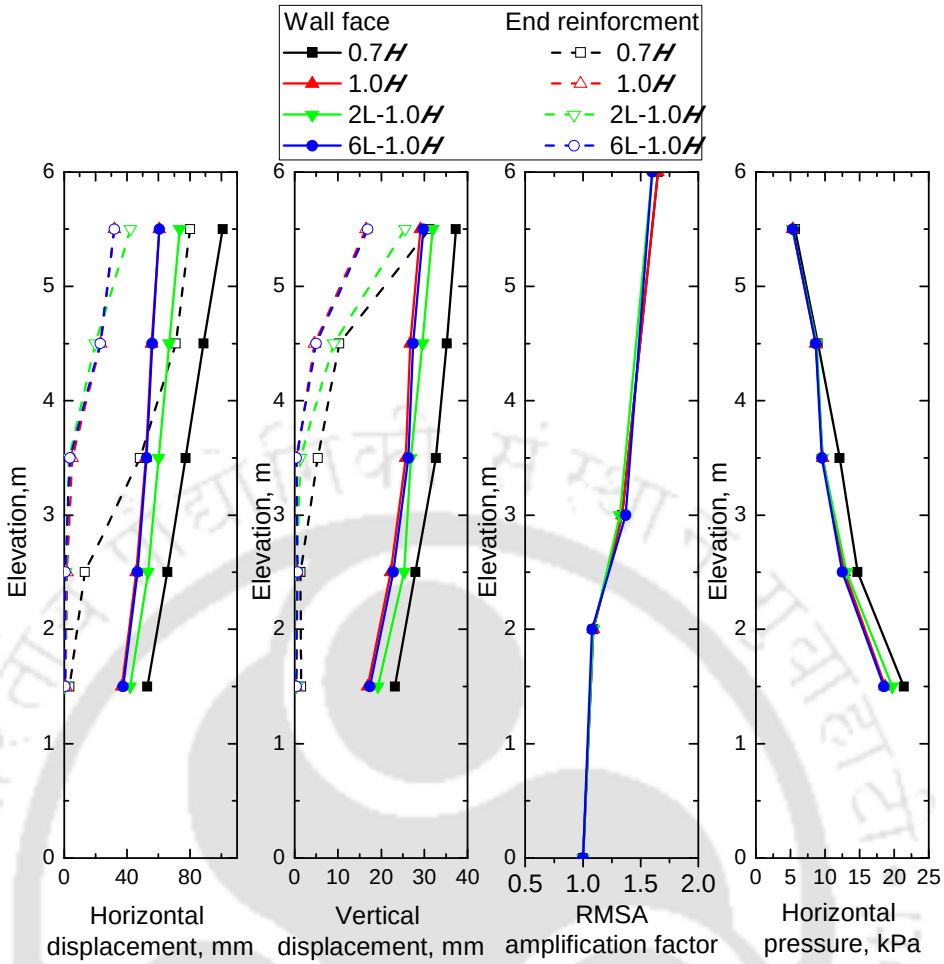

Fig. 4.56 Response of full height model walls with different reinforcement configurations subjected to dynamic excitation (a = 0.2g, f = 5Hz, N_L = 12)

reinforcement at an elevation of 5.75 m. The increase of octahedral shear strains are observed after end of reinforcement and reduces to negligible at a distance of 8 m from facing for all walls. So the extent of compound deformation can be reduced considerable by increasing the length top three layers of reinforcement to 1.0*H*. The same extent of compound deformation zone can be observed for wall with reinforcement length 1.0*H* and wall with reinforcement length 1.0*H* for top six layers and 0.7*H* for other layers (6L-1.0H). By considering the displacements discussed in Fig. 4.56 and extent of compound deformation zones, wall with top six layers of longer reinforcement (half of the height of wall) (i.e 6L-1.0H) are the best suitable for

wrap-faced wall with minimum facing displacement and vertical settlement near end of reinforcement.

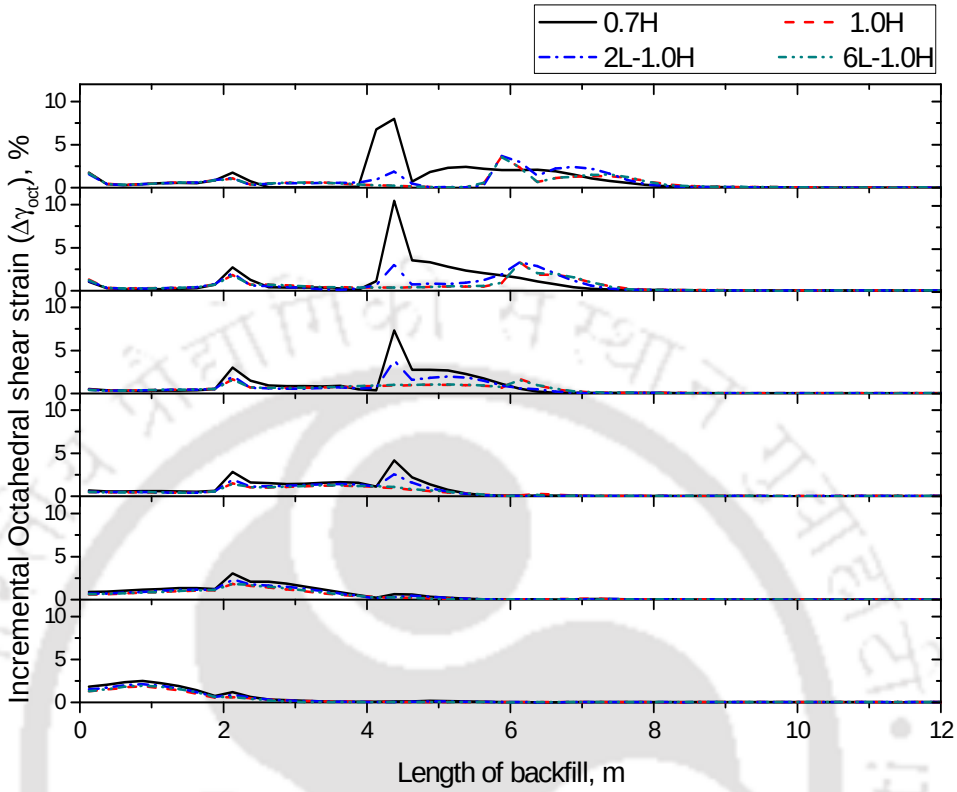

Fig. 4.57 Comparison of octahedral shear strain at backfill for wall with reinforcement 0.7*H*, 1.0*H* , 2L-1.0H and 6L-1.0H subjected to dynamic excitation (a = 0.2g, f = 5Hz)

4.6 SUMMARY

Numerical model was developed to simulate the shaking table tests of wrap-faced wall. The numerical model is validated with data obtained from reported physical model tests. The sensitivity analysis of numerical model is performed to observe the influences of different model parameters on model responses.

The calibrated numerical model is used to develop a full scale numerical model of a wrap-faced wall. Different numerical model studies are performed and the results analyzed in terms of horizontal, vertical displacement, incremental octahedral shear strains in soil, and axial strains in the reinforcement elements. The formation of

deformation zones in wrap-faced walls based on displacements, strains are discussed. Three distinct modes of deformation zones: shear deformation within reinforced zone, relative compaction near end of reinforcement and compound deformation zone extending to the backfill are observed.

The influences of parameters as length of reinforcement, number of layers of reinforcement, backfill soil, and reinforcement stiffness on deformation zones formation are also studied. The deformation zones formations are mainly influenced by reinforcement length, backfill soil and number of reinforcement layers. The wall with longer reinforcement at higher elevation and minimum reinforcement length at lower elevations reduce the extent of compound deformation zone in retained backfill.

Chapter 5. STUDIES ON RIGID-FACED WALLS

5.1 INTRODUCTION

As discussed in Chapter 1, reinforced soil walls will be constructed with different types of facing. Among various facing options, wrap facing provides highly flexible system while full height facing provides fully rigid system. Behavior of wrap-faced wall systems were discussed in the earlier chapter. In this chapter, simulation of full height rigid-faced reinforced soil walls subjected to seismic excitation are presented and discussed. After calibration of the numerical model, parametric studies are conducted to investigate the effect of different parameters. Results are presented in terms of variations of horizontal and vertical displacements, octahedral shear strain variations along the length of backfill, axial strains along the length of reinforcement at different layers. Accelerations (in terms of RMSA amplification factors), horizontal pressures and displacements are also presented along the full height of the wall. The results have been analyzed to predict the location of deformation zones.

5.2 DEVELOPEMENT OF NUMERICAL MODELS OF RIGID-FACED WALLS

Numerical models are developed using FLAC^{3D} to simulate the shaking table studies on rigid-faced reinforced soil wall models reported by Krishna and Latha (2009).

5.2.1 Target physical model

Laboratory model shaking table tests rigid-faced reinforced soil retaining walls described by Krishna and Latha (2009), are considered as reference case for

generating the numerical models. The shaking table tests were conducted on rigid-faced reinforced wall models of size 700 mm × 500 mm in plan and 600 mm deep. The facing was build from 12 hollow rectangular steel box sections that were bolted together using two vertical steel rods, to represent the 600 mm high rigid wall (Fig. 5.1). The facing was fixed to a bottom plywood sheet using the vertical steel rods to represent a fixed bottom condition. The model was constructed in a laminar box by backfilling the wall in equal lifts of sand pluviation and with a layer of reinforcing material laid after each lift. The reinforcement materials were run through the bolts of the facing system to obtain a rigid connection between the wall and reinforcement. Four layers of geotextile reinforcement of length (L_{rein}) 420 mm (i.e., 0.7H) were used in the model. The backfill material used in the model tests was poorly graded sand having dry unit weight of 16.2 kN/m^3 and friction angle of 43°. Four different reinforcement materials were used by Krishna and Latha (2009). The low strength geotextile is considered for the present study which is having ultimate tensile strength of 0.104 kN/m and secant modulus of 5.2 kN/m at 2% strain. The mass per unit area of the reinforcement material was reported as 110 g/m^2. A nominal surcharge of 0.5 kPa was applied after completion of all lifts. After removing the temporary supports on facing, model wall was subjected to 20 cycles of sinusoidal excitation at different frequencies. Results obtained through various instrumentations were discussed in terms of facing horizontal deformations, acceleration amplification values. The details of the test configuration and location of various instrumentations are shown in Fig. 5.1. An unreinforced wall was also considered to compare the results with that of reinforced wall. The unreinforced wall configuration was similar to that of rigid-faced wall but without reinforcement. Typical responses from physical model tests, in the

form of horizontal displacements for unreinforced wall and accelerations for a reinforced wall at different elevations are shown in Fig. 5.2 and Fig. 5.3, respectively.

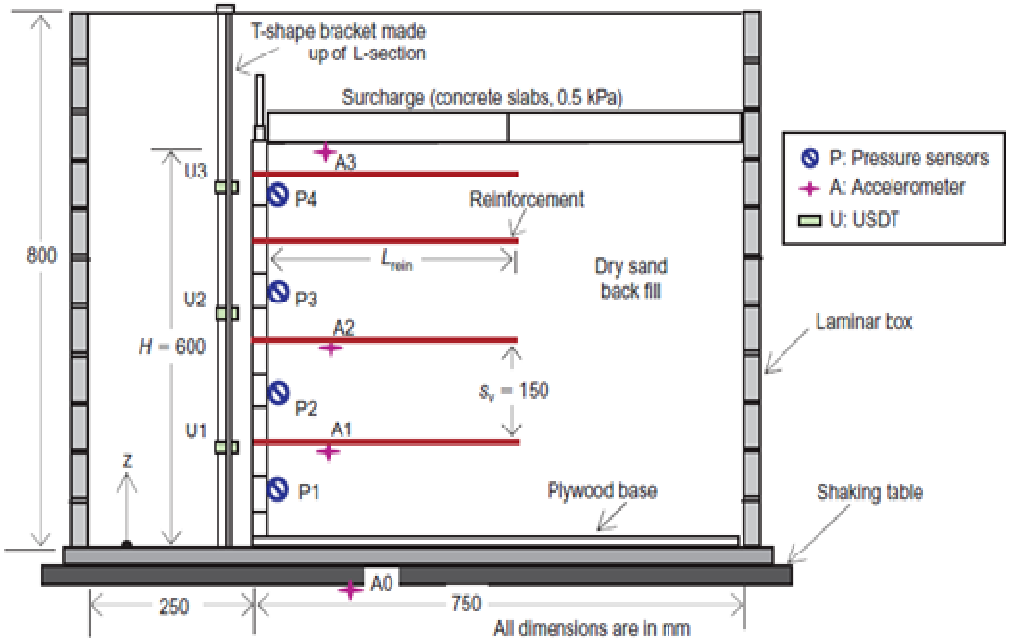

Fig. 5.1 Test arrangement of rigid face reinforced retaining wall in physical model tests (after Krishna and Latha 2009)

5.2.2 Development of numerical grid

The finite difference programme, FLAC^{3D}, is used for development of numerical model of rigid-faced reinforced soil walls. Physical model construction and testing sequence, implemented in experimental procedure, are followed in development of numerical model. The shaking table is first generated as rigid zone of 800 mm long and 50 mm thick. The backfill soil is built up in layers with same sequence as physical model and reinforcements are placed on each layer. The model grid of 25 mm wide and 600 mm high is considered to simulate the rigid wall and fixed at the bottom against lateral sliding. A grid of size 600 mm high and 750 mm long is generated to represent the backfill of rigid-faced retaining wall. Though the width of physical model is 500 mm, model of 100 mm lateral dimension is considered

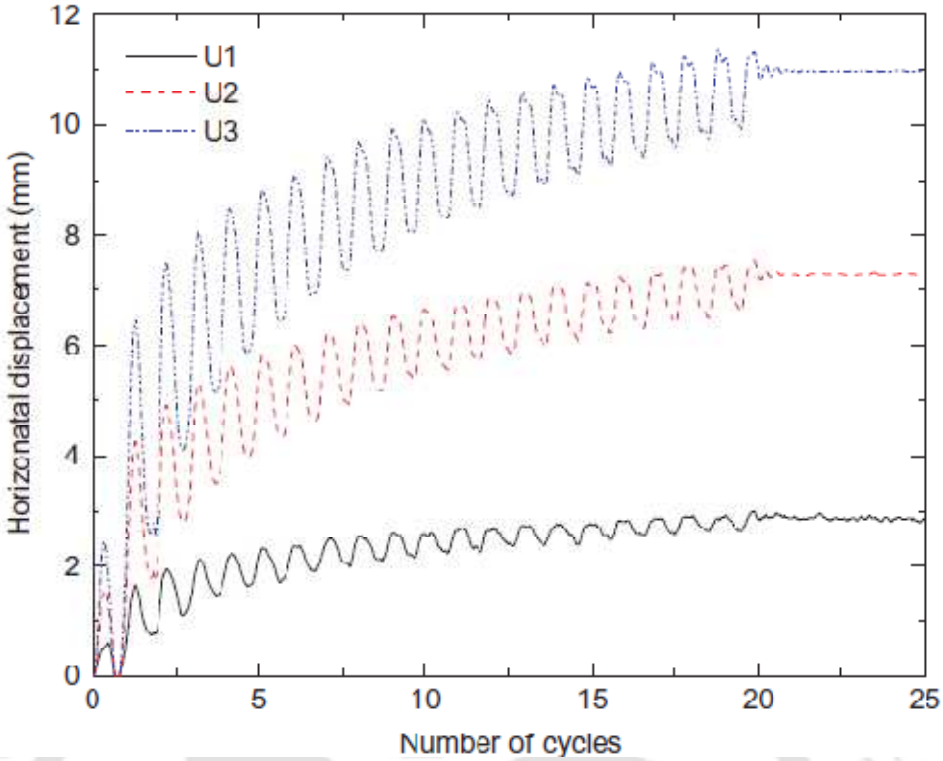

Fig. 5.2Typical horizontal displacements histories of unreinforced wall with number of cycles (after Krishna and Latha, 2009)

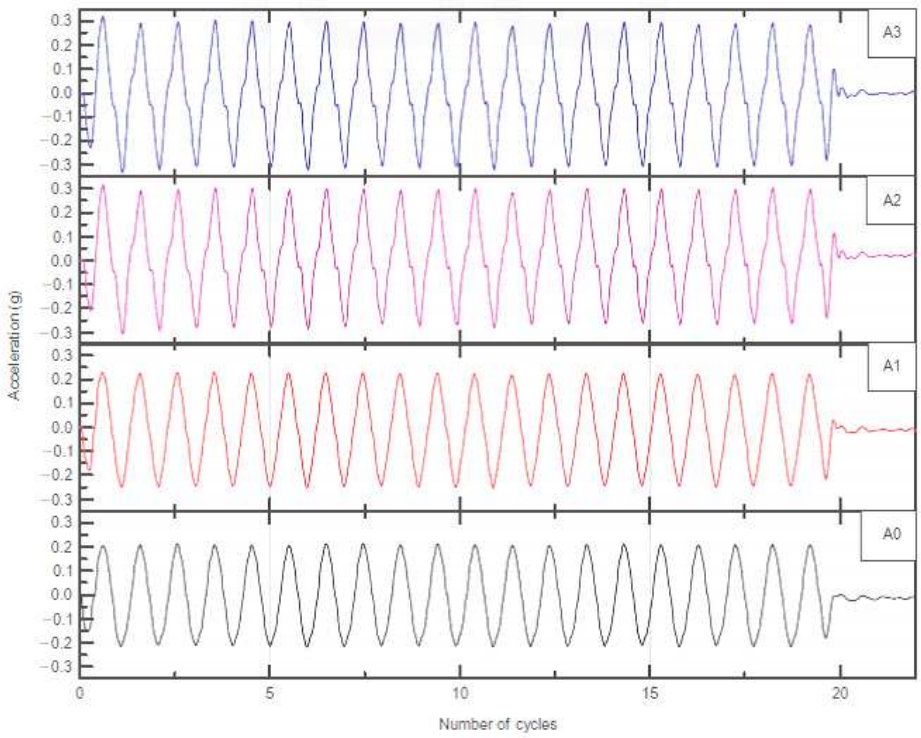

Fig. 5.3Typical acceleration histories of reinforced wall with number of cycles (after Krishna and Latha, 2009)

for ease of model solving in numerical simulation. The entire grid, representing shaking table, rigid wall and backfill is divided in number of zones of 25 mm each. Four layers of geotextile reinforcement of length (L_{rein}) 420 mm, (Krishna and Latha 2009) are used in the model. Various interfaces are also considered for proper interaction between dissimilar elements. Fig. 5.4(a) shows the numerical grid considered to simulate the rigid-faced retaining wall.

The construction sequence followed in the numerical model generation is similar to that of physical model. The foundation zone is first brought to static equilibrium before placing the rigid wall and backfill. The wall is then placed over the foundation zone and brought to static equilibrium. Horizontal movement of the wall is restricted to represent temporary support during construction. The backfill model is generated in equal lifts and reinforcement is placed after each lift. The reinforcements are extended to the wall and attached with the wall to represent rigid connection between wall and reinforcement. The structural elements in FLAC^{3D} interact with main grid only at structural nodes (Itasca 2008). The geogrid is rigidly attached to the wall. But at the interface between wall and soil, the geogrid nodes may arbitrarily select nodes either from wall or from soil. So the finer geogrid is considered for wall portion, so that more structural nodes interact with wall elements. The model is brought to static equilibrium after each lift. A surcharge of 0.5 kPa is applied at top and model is brought to static equilibrium. The supports of the walls are removed after the end of construction.

The material properties for backfill soil and reinforcements are assigned based on their respective constitutive models as described in Section 3.3.1 and Section 4.2.2. The rigid wall is modeled as elastic material. The elastic modulus, Poisson's ratio and density of concrete are considered for numerical simulation. Two different interfaces

are considered in the present model: interface between backfill soil and wall; and interface between soil and reinforcement. The interface between the backfill soil and wall is controlled by relative interface movement, that depend on interface normal stiffness (k_n) and shear stiffness (k_s) as explained in Section 3.3.4. The interface between the soil and reinforcement is modeled as linear spring-slider system (Section 3.3.4 and Section 4.2.2).

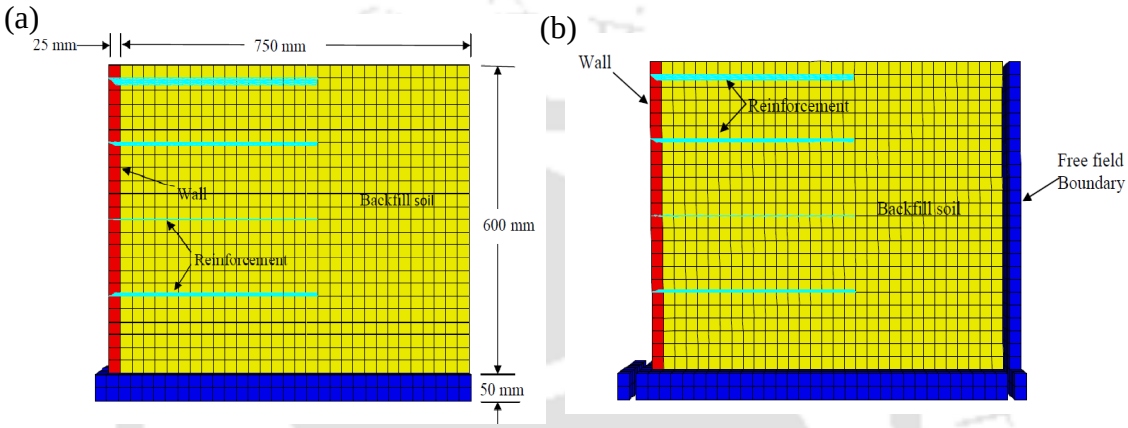

Fig. 5.4 Grid adopted for numerical simulation (a) static simulation (b) dynamic simulation

Boundary conditions

The boundary conditions applied to the model represent the actual boundary of the physical model tests (Krishna and Latha, 2009). The bottom boundary is completely fixed in vertical direction to represent the rigid boundary between the model wall and shaking table. The far end boundary elements are fixed in *x* direction to represent the fixed container. During the construction, the model wall is fixed in horizontal direction to represent the temporary facing support. The lateral boundaries are fixed in *y* direction to represent the lateral boundaries at the side of the physical model. After the completion of all the layers construction, and the model was brought to equilibrium, the facing boundaries are removed layer by layer representing the stage wise removal of temporary support. The boundary conditions after support removal are shown in Fig. 5.5.

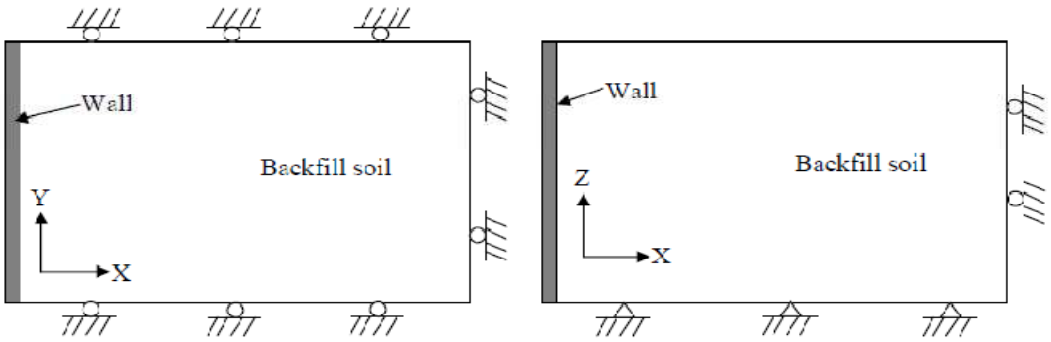

Fig. 5.5 Boundary conditions of the model (not to scale) in X-Y plane (plan) and Z-X plane (side elevation)

During dynamic modeling, free field boundary is applied at far end. The free field boundary conditions are applied to the lateral boundary grid points automatically. The cyclic hysteresis and damping are applied as described in Chapter 4. The dynamic excitation is applied at the stiff bottom in the form of velocity in horizontal direction (uni-axial shaking). The model considered for dynamic analysis with free field boundary is shown in Fig. 5.4(b).

Selection of grid size of model

Sensitivity analysis was carried out by considering three models with different grid sizes of 50 mm, 25 mm and 12.5 mm. The horizontal displacements after support removal, during static analysis, are 1.06 mm, 1.93 mm and 2.03 mm. The variation of horizontal displacements is within 5% for grid size of 25 mm and 12.5 mm. For dynamic analysis, the maximum range of frequency propagation for 25 mm and 12.5 mm grids are 38 Hz and 78 Hz, respectively (calculated for model with density 1600 kg/m^3 and average shear modulus of 150 kPa as mentioned in Section 3.2.1). The grid size of 25 mm is adopted for numerical simulation by considering the speed of calculation.

5.2.3 Validation of numerical model

Dynamic model studies are conducted for unreinforced and reinforced retaining walls subjected to 20 cycles of sinusoidal dynamic motion at 0.2g base input acceleration at a frequency of 3 Hz. The model parameters considered for the numerical model are listed in Table 5.1. The displacement histories at elevations of 150, 350 and 550 mm; acceleration histories at elevations of 150, 300 and 600 mm; and incremental pressures at 100, 230, 380 and 500 mm elevations, are recorded to compare the results of physical model tests.

Table 5.1 Material properties used in numerical simulation

Wall properties	
Mass density, kg/m^3	2500
Elastic modulus, kPa	2×10^7
Soil properties for Mohr model	
Mass density, kg/m^3	1630
Elastic modulus, kPa	1×10^4
Poisson's ratio	0.3
Friction angle, Degrees	43
Dilation angle, Degrees	15
Cohesion, kPa	0.1
Reinforcement (Geotextile) properties	
Mass density, g/m^2	230
Thickness, m	0.001
Reinforcement (Geotextile) interface properties	
Coupling spring cohesion, kPa	0.1
Coupling spring friction, Degrees	29
Coupling spring stiffness, kPa	1×10^6

A typical variation of displacements and accelerations with number of cycles of dynamic loading at different elevations of backfill soil for rigid-faced wall at 0.2g acceleration and 3 Hz frequency are shown in Fig. 5.6 and Fig. 5.7, respectively. The horizontal displacements increase nonlinearly with increase in number of cycles. The horizontal displacement of wall is greater at higher elevations of wall. The accelerations are amplified at higher elevations of wall.

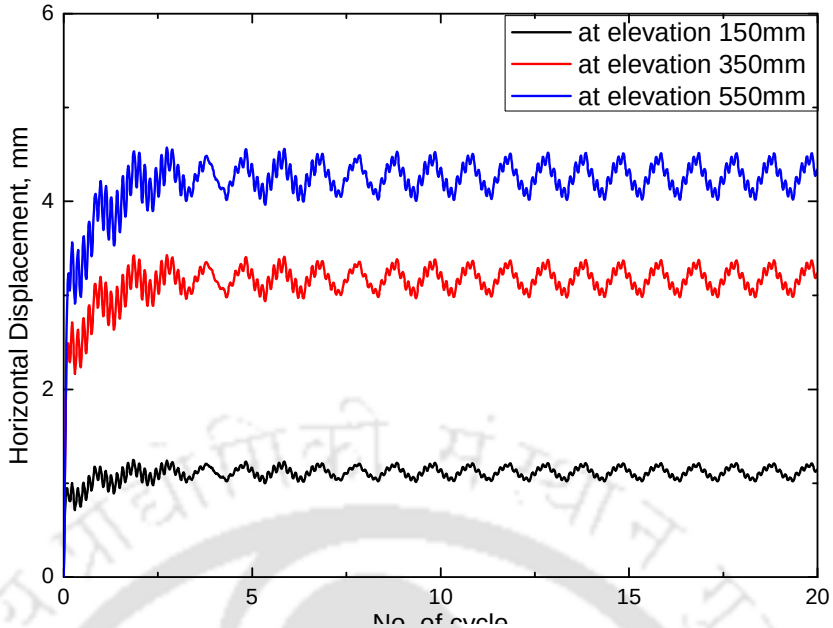

Fig. 5.6 Typical displacement histories at different elevations during dynamic excitation (a= 0.2g, f=3Hz, L_{rein}/H = 0.7 and N_L=4)

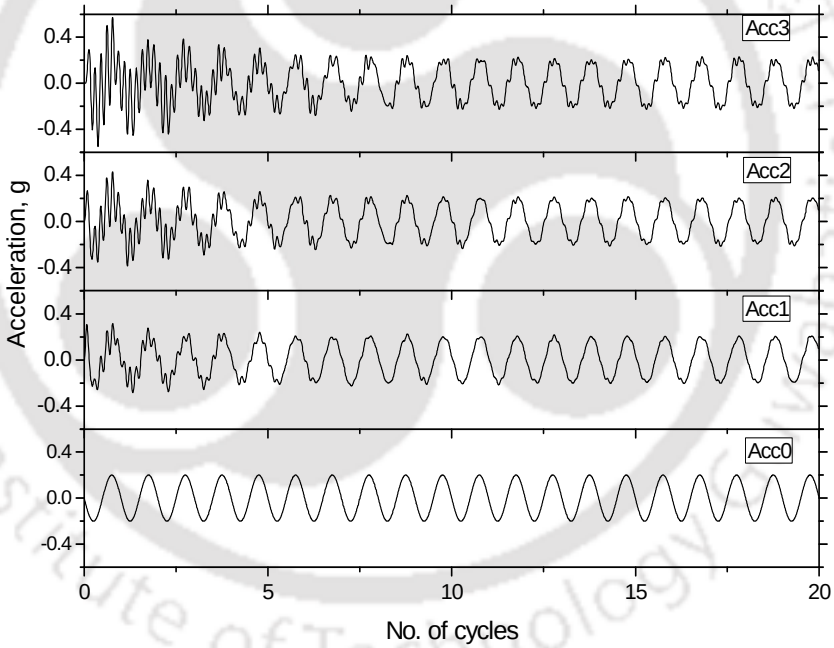

Fig. 5.7 Typical acceleration histories at different elevations in numerical simulation

The acceleration amplifications at different elevations are quantified as *root mean square acceleration* (RMSA) amplification factor as per Eq. 4.1. Fig. 5.8 compares the variation of horizontal displacements, RMSA amplification factors and horizontal pressure increments at different elevations obtained from physical tests and numerical simulations, for acceleration of 0.2g at 3 Hz frequency for reinforced (N_L =

4) and unreinforced walls. The maximum horizontal displacement (u) of unreinforced wall at an elevation of 500 mm is 12.1 mm for numerical model and that of physical model is 11.0 mm. For the reinforced wall the values of u are 4.3 mm and 4.00 mm, respectively, for numerical and physical models. The acceleration amplifications of unreinforced wall at an elevation of 600 mm are 1.25 and 1.21 for numerical and physical model, respectively. For reinforced wall, 1.09 for numerical model and 1.14 for physical model. The incremental pressure for unreinforced wall at an elevation of 100 mm is 0.19 kPa for numerical model and 0.06 kPa for physical model. While incremental pressure for reinforced wall is 0.33 kPa for numerical model and 0.23 kPa for physical model. The comparison of results from physical and numerical models and their percentage differences are tabulated in Table 5.2. The results show the ability of numerical model to capture the behavior of physical model with reasonable accuracy.

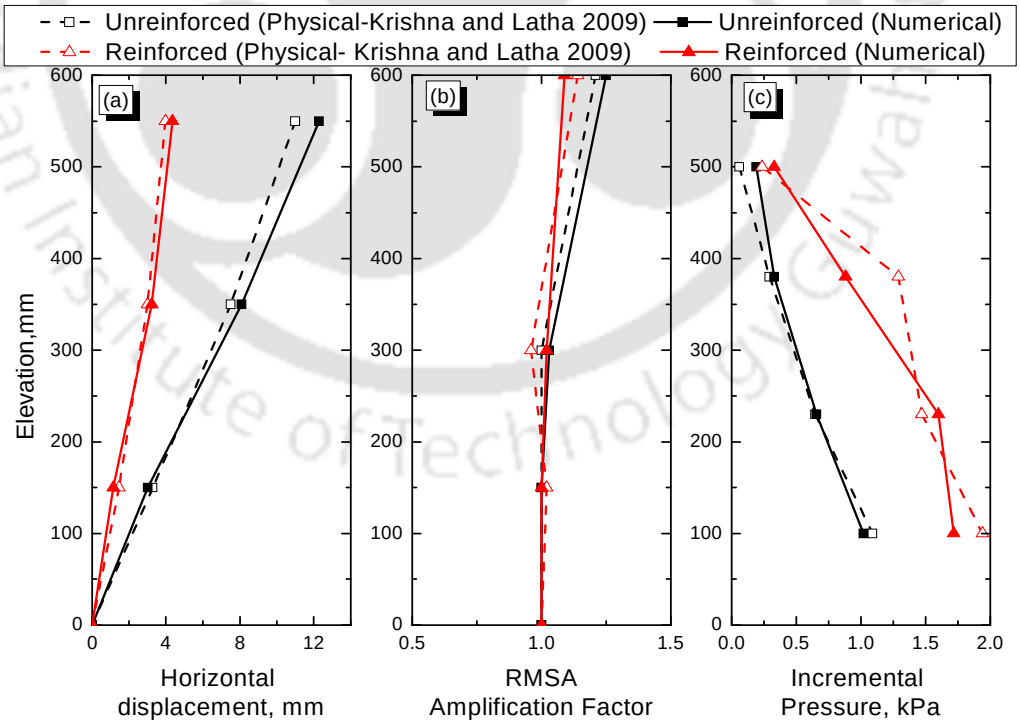

Fig. 5.8 Comparison of results from numerical and physical model tests on unreinforced and reinforced (a = 0.2g, f= 3 Hz and N_L = 4): a) Displacement profiles b) Acceleration amplification and c) Incremental pressure

Table 5.2 Comparison of results from physical and numerical model

Wall type	Horizontal displacement (mm)			RMSA amplification factors		
	Physical	Numerical	% difference	Physical	Numerical	% difference
Unreinforced	11.1	12.1	9.1%	1.25	1.21	3.2
Reinforced	4.3	4.0	6.7%	1.14	1.09	4.4%

5.2.4 Sensitivity analysis

Sensitivity analyses are conducted to understand the influence of different parameters on model behavior. The model parameters considered for sensitivity analysis are tabulated in **Error! Reference source not found.**.

Table 5.3 Material properties used for sensitivity analysis

Material properties	**Model parameters**
No. of reinforcing layers	3,4,6
Backfill friction angle, Degree	43, 38, 52
Dilation angle, Degree	10, 15, 20
Reinforcement Stiffness, kN/m	5.5, 150, 220

Comparative results are presented in terms of horizontal displacements, RMSA amplification factors and horizontal pressure increments at different elevations. Fig. 5.9, Fig. 5.10, Fig. 5.11 and Fig. 5.12 show effect of various parameters: backfill friction angle, dilation angle, reinforcement and number of reinforcing layers, respectively, on wall response. As discussed in Chapter 4, the model is observed to be sensitive to the variation of backfill friction angle, number of reinforcing layers and reinforcement stiffness. Fig. 5.11 and Fig. 5.12 also show the effectiveness of reinforcement by providing comparison with unreinforced wall.

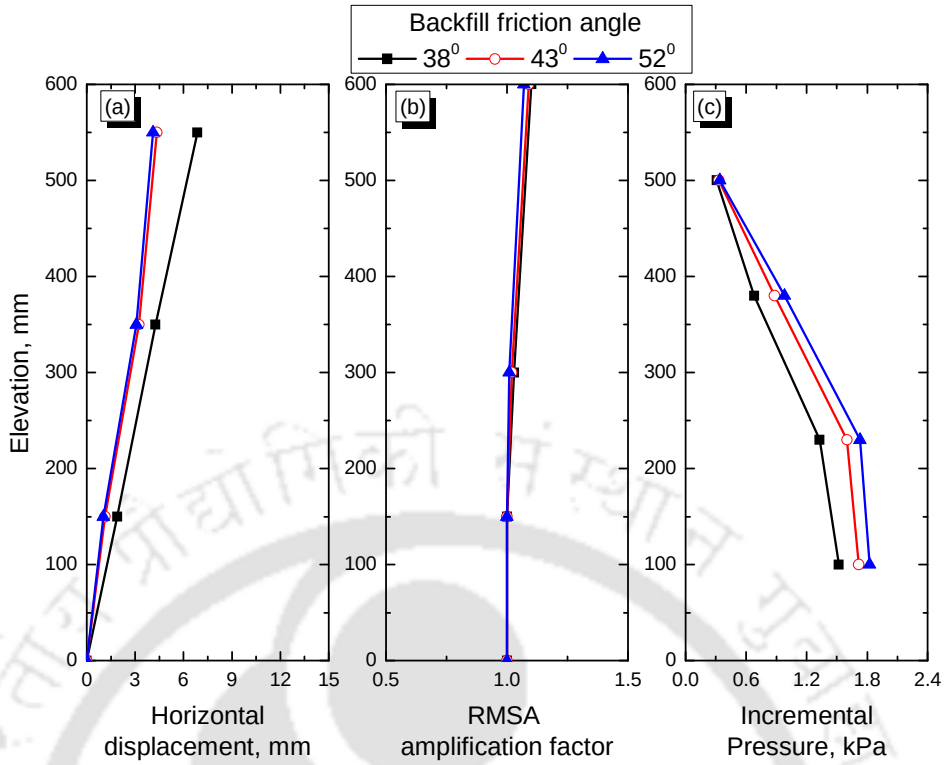

Fig. 5.9 Sensitivity of numerical model with respect to backfill friction angle: a) Displacement profiles b) Acceleration amplification c) Incremental pressure

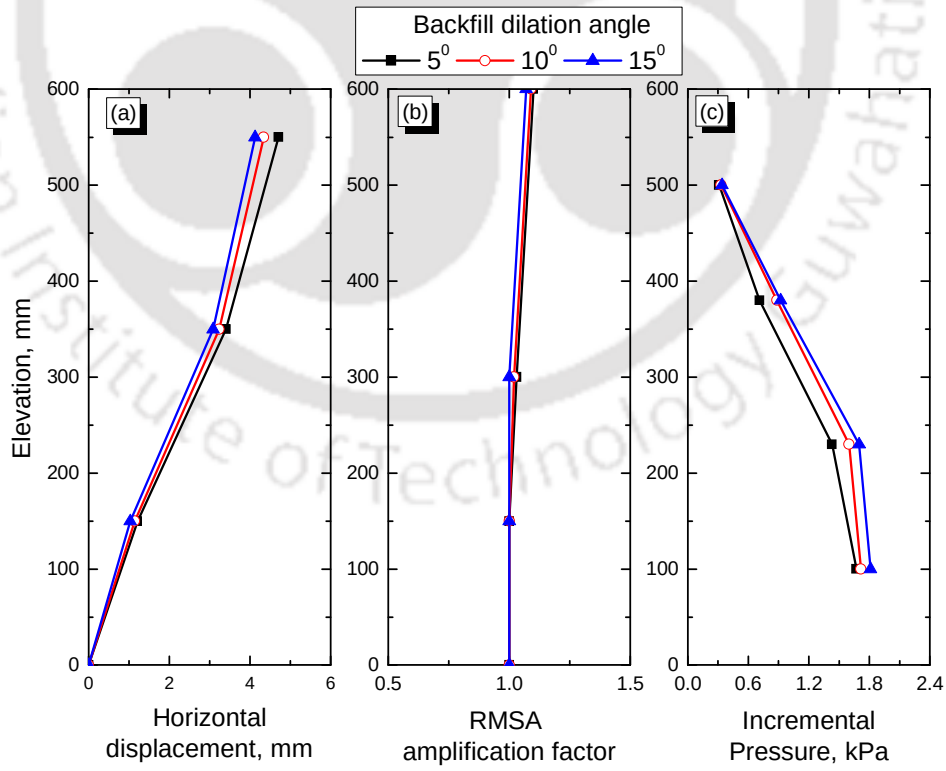

Fig. 5.10 Sensitivity of numerical model with respect to backfill dilation angle: a) Displacement profiles b) Acceleration amplification c) Incremental pressure

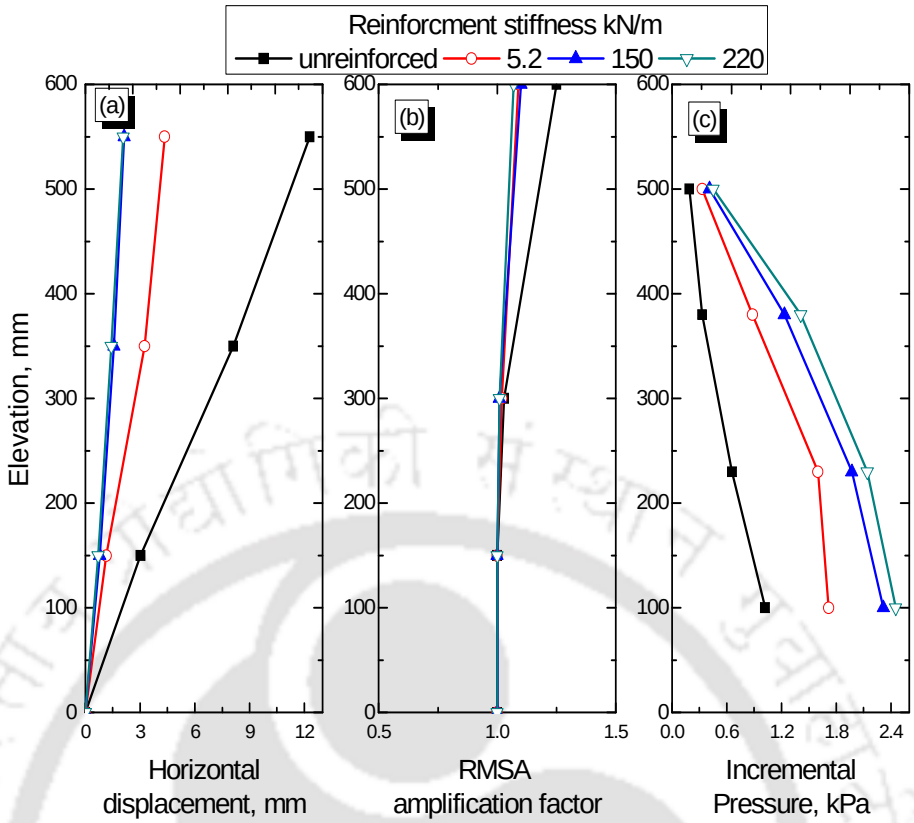

Fig. 5.11 Sensitivity of numerical model with respect to stiffness of reinforcement: a) Displacement profiles b) Acceleration amplification c)Horizontal pressure

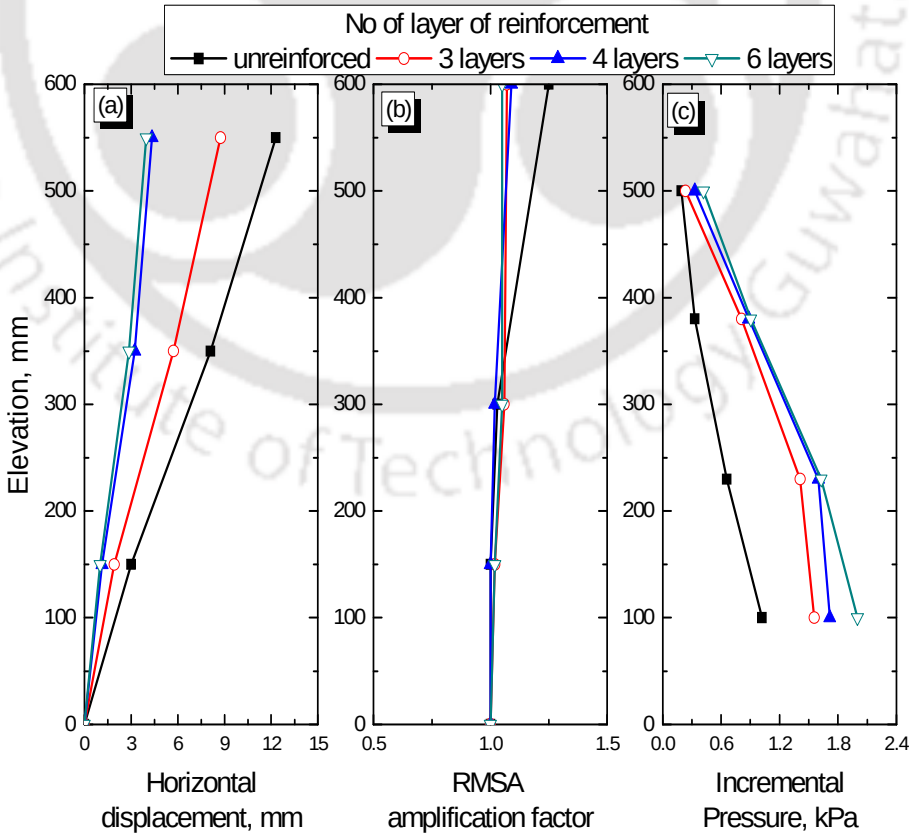

Fig. 5.12 Sensitivity of numerical model with respect to number of reinforcing layers: a) Displacement profiles b) Acceleration amplification c) Incremental pressure

5.2.5 Dynamic response of rigid-faced walls: Displacements and Strains

Variations of octahedral shear stains, horizontal and vertical displacements along the length of backfill are studied for unreinforced and reinforced (N_L = 4) wall models, subjected to dynamic excitation (a=0.2g; f=3 Hz), are being observed. Fig. 5.13 shows the shear strain, and displacements variations for unreinforced soil wall. In general, the maximum values of horizontal displacement (u) and vertical displacements (v) and incremental octahedral shear strain ($\Delta\gamma_{oct}$) are observed near the wall facing and they decrease gradually along the length of the backfill. Maximum horizontal displacements are 11.0 mm, 9.0 mm, 4.1 mm and 0.6 mm, at 525 mm, 375 mm, 225 mm and 75 mm elevations, respectively. The corresponding maximum vertical displacements (v) are in the range of 5.52 mm - 0.5 mm. The $\Delta\gamma_{oct}$ are 10.8% near the wall facing at 525 mm elevation and in the order of 4% at other elevations. Fig. 5.14 shows the similar results for a reinforced soil wall with four layers of reinforcement. The maximum u at 525 mm elevation is 4.0 mm near the wall face and it remains same upto the end of reinforcement (upto 420 mm length). From this point onwards a slight decrease in the u, upto the end of wall, is observed. Almost similar behavior has been observed at the other elevations also. The v are very low and almost uniform except, near the end of reinforcement, along the length of backfill at different elevations. The $\Delta\gamma_{oct}$ are less than 0.75% within reinforced zone but increase to 1.0% at the end of reinforcement. Comparisons of unreinforced and reinforced wall responses show significant reductions in $\Delta\gamma_{oct}$, u, and v values. Backfill soil, near the facing is subjected to more strains in unreinforced wall and decreases gradually, while the maximum strains are near the end of reinforcement for reinforced retaining wall. These observations indicate that, the whole reinforced zone acts together as rigid body in case of reinforced retaining wall. The horizontal displacements are not reduced to

minimum value near the far end boundary of wall. The model response is affected by far end boundary for both unreinforced and reinforced retaining wall and also reported in literature (Krishna and Latha 2009).

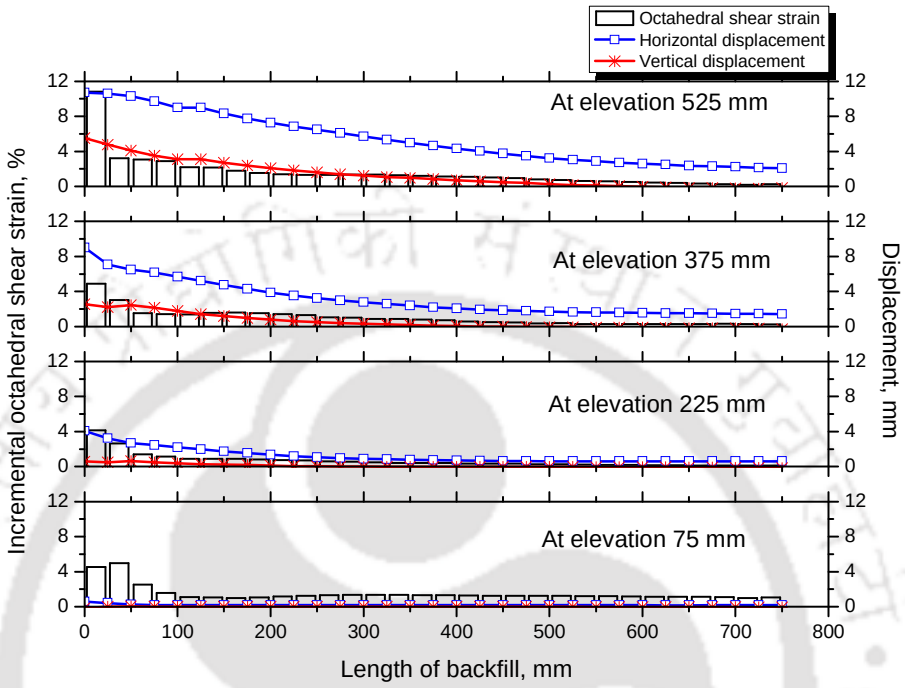

Fig. 5.13 $\Delta\gamma_{oct}$, u and v along length of backfill after dynamic excitation (a = 0.2g and f = 3Hz) for unreinforced wall

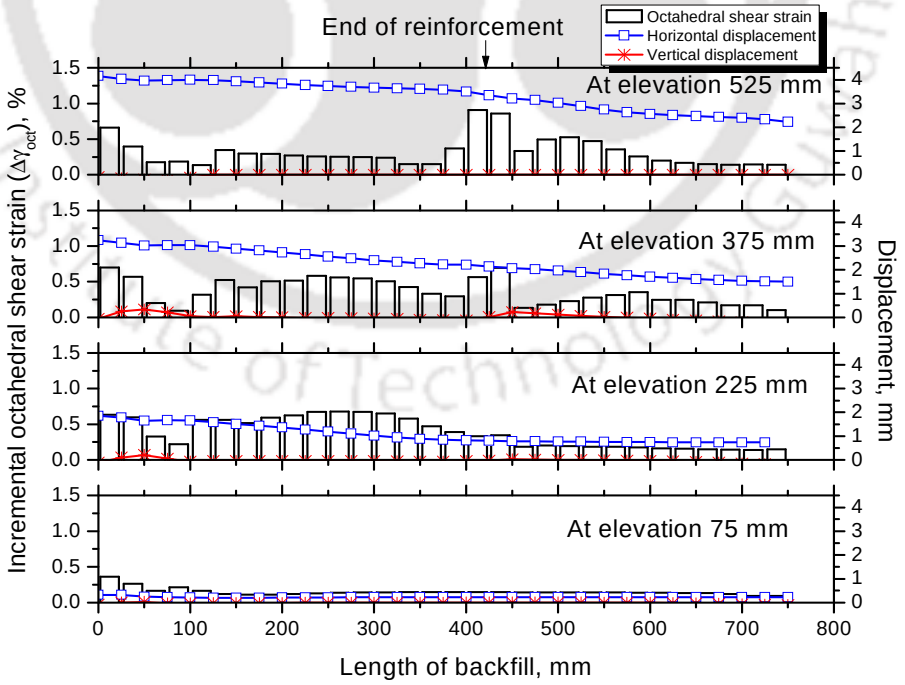

Fig. 5.14 $\Delta\gamma_{oct}$, u and v along length of backfill of dynamic excitation for reinforced wall (a = 0.2g and f = 3Hz, L_{rein}/H = 0.7 and N_L = 4)

5.3 SEISMIC RESPNSE OF FULL SCALE RIGID-FACED WALL MODELS

Seismic behavior of a full scale rigid-faced model of 6 m high (H), 18 m long and 1 m wide with four reinforcement layers is studied, using the validated numerical model. The model parameters are kept same as that of laboratory model, except the reinforcement parameters. A 1mm thick geotextile having mass per unit area of 230 g/m^2 with, about 152 kN/m ultimate tensile strength is adopted. The length of geotextile reinforcement (L_{rein}) is 4.2 m as per FHWA (2001). The base of wall is fixed against rotation and sliding. A surcharge of 5 kPa, resembling 20 cm thick cement concrete slab, is applied at the top of backfill. The foundation of wall is considered to be rigid hence, vertical displacements are restricted. Stability analysis has been carried out for full scale rigid-faced wall according to FHWA (2001). The factors of safety obtained for static and dynamic stability analyses are tabulated in Table 5.4. The safety factors shown in Table 5.4 indicate that the wall considered is safe against external and internal stability.

Table 5.4 Static and dynamic factors of safety for full scale rigid-faced model

Loading condition		External stability		Internal stability	
		$FS_{basesliding}$	$FS_{overturning}$	$FS_{rupture}$	$FS_{pullout}$
Static		4.16	5.34	2.00	4.34
Dynamic	0.2g	1.80	1.79	1.97	1.95

5.3.1 Rigid-faced wall subjected to dynamic excitation

The full scale rigid-faced wall model is subjected to 20 cycles of sinusoidal dynamic excitation of 0.2g acceleration (a) at 5 Hz frequency (f). Typical variations of displacements with number of cycles of dynamic loading, at different elevations of backfill, are shown in Fig. 5.15. It is observed that horizontal displacements increase with dynamic shaking. The horizontal displacement reached maximum within initial 5 cycles of dynamic excitation and remains almost constant after that.

The response of model, after 20 cycles of excitation (a = 0.2g and f = 5 Hz), in the form of horizontal displacements (u), vertical displacements (v), RMSA amplification factors and horizontal pressures, near the facing and at the end of reinforcement are shown in Fig. 5.16. The maximum u are 30.1 mm and 12.6 mm near the facing and at the end of reinforcement; and corresponding v are 16.2 mm and 0.97 mm, respectively. The RMSA amplification factors are 3.36 and 2.85 at wall facing and at the end of reinforcement respectively. The horizontal pressure variation near end of reinforcement follows typical earth pressure distribution.

The incremental octahedral shear strains ($\Delta\gamma_{oct}$), u and v displacements along the length of backfill between two reinforcement layers are presented in Fig. 5.17. The $\Delta\gamma_{oct}$ are 1.76% and 1.14% near the wall facing (confined to zone upto 0.4 m from facing) at elevation of 5.25 m and 3.75 m respectively. The $\Delta\gamma_{oct}$ at other part of backfill gradually goes down to 0.3% at a distance of 5.3 m and 2.7 m at elevation of 5.25 m and 3.75 m, respectively. The u near the facing are 29.5 mm and 19.45 mm at elevations of 5.25 m and 3.75 m, respectively. The u decrease gradually and become less than 10 mm, after the end of reinforcements. The v near the facing are 11.2 mm and 4.90 mm at an elevation of 5.25 m and 3.75 m respectively. The v also decreases gradually and less than 1mm within the reinforced zone.

The incremental axial strains ($\Delta\varepsilon_{a\_rein}$) in reinforcement, after dynamic excitation, are determined and shown in Fig. 5.18. From the figure it is observed that $\Delta\varepsilon_{a\_rein}$ are less than 1.0% at all the reinforcement layers. The reinforcement strain increments showed maximum values, near the facing which can be attributed to the soil movement ($\Delta\gamma_{oct}$ in Fig. 5.17) near the facing. Both reinforcement strains and soil strains are more near the rigid wall facing.

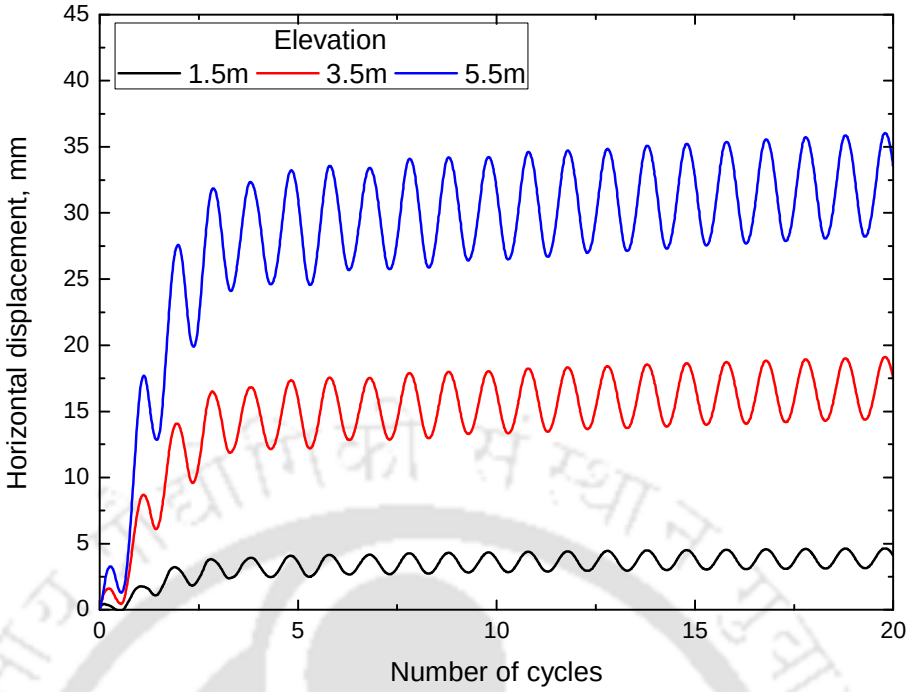

Fig. 5.15 Typical displacement histories at different elevation of rigid-faced wall

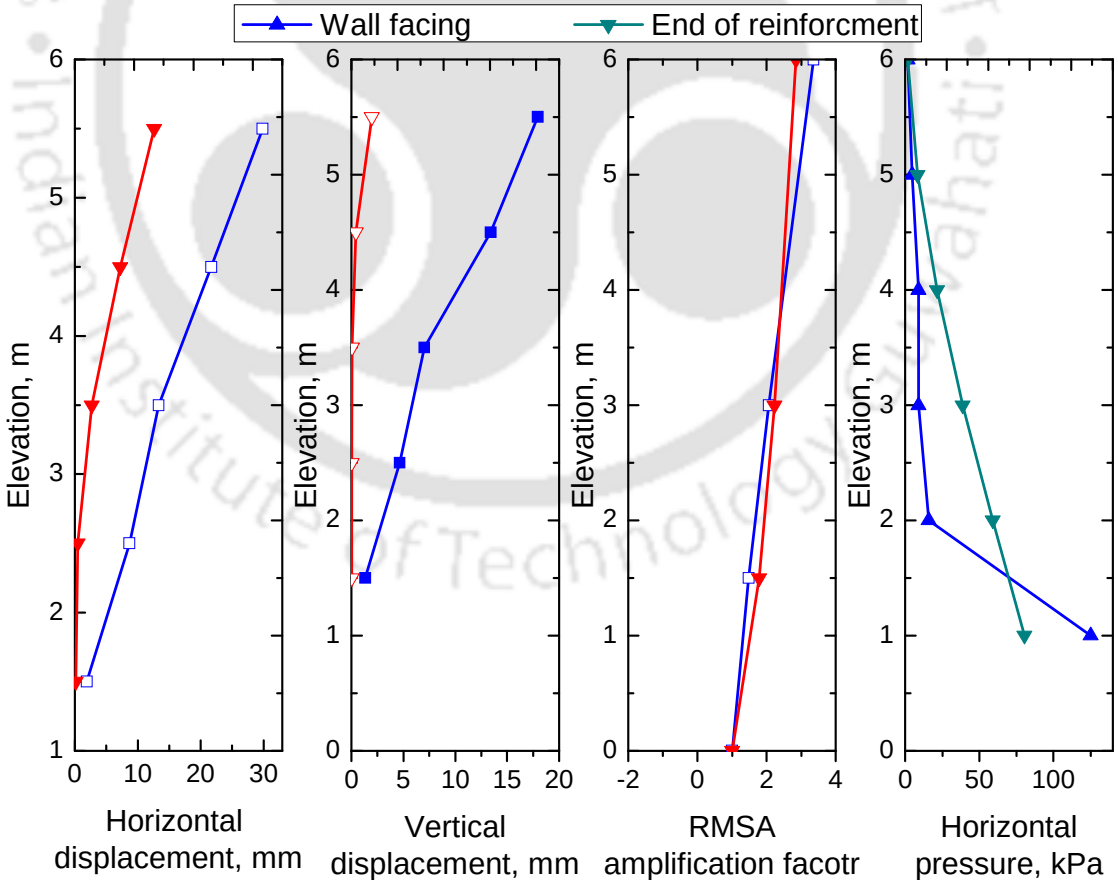

Fig. 5.16 Horizontal, vertical displacements, RMSA amplification factor and horizontal pressure at different elevations after dynamic excitation (a=0.2g, f = 5Hz L_{rein}/H=0.7, N_L=4)

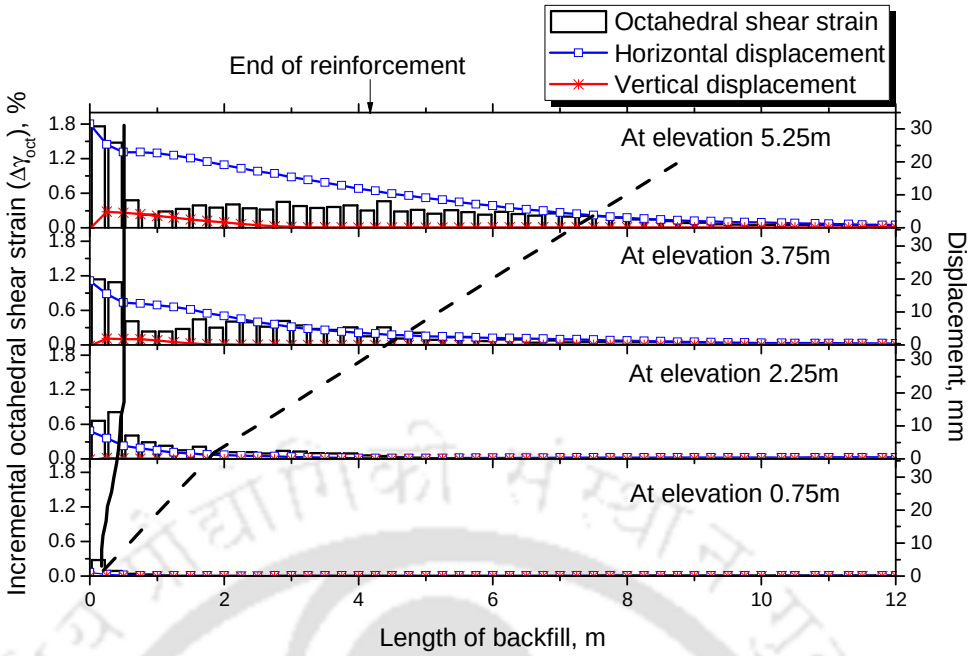

Fig. 5.17 $\Delta\gamma_{oct}$, u and v along the length of backfill after 20 cycles of dynamic excitation (a=0.2g, f=5Hz, L_{rein}/H=0.7, N_L=4)

The higher strain at 2nd, 3rd and 4th layer indicates higher load acting at these layers. The load acting on 1st layer of reinforcement is less due to lesser movement of reinforcement within backfill. This is due to limited extent of strained zone into the backfill.

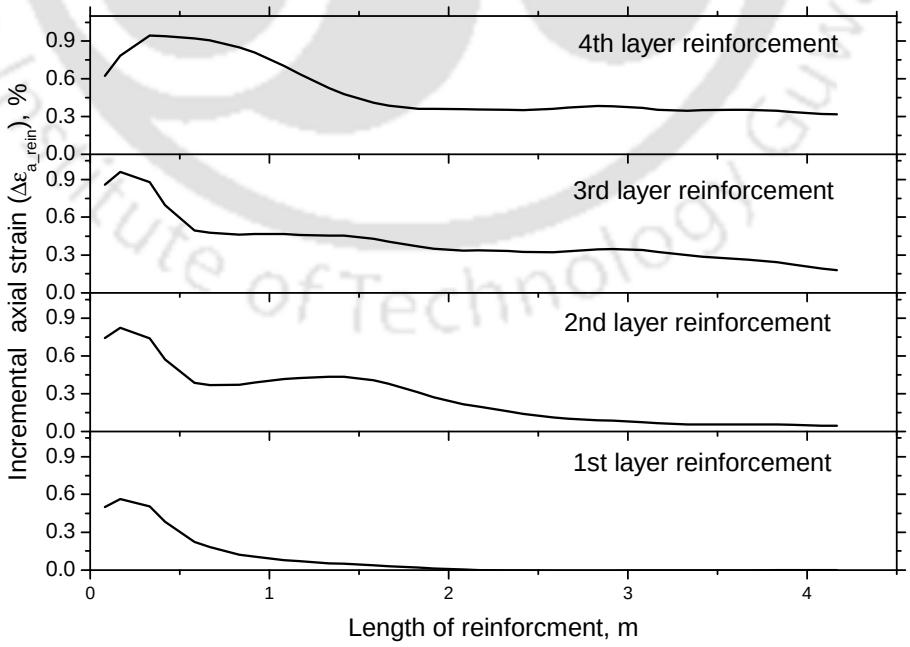

Fig. 5.18 Incremental axial strain along length of reinforcement after dynamic excitation (a = 0.2g, f = 5Hz, L_{rein}/H = 0.7 and N_L = 4)

By observing the variations of $\Delta\gamma_{oct}$, u and v, two deformation zones are identified. The first zone (solid line in Fig. 5.17) exists totally in reinforced zone and very close to the facing which can be considered as high strain zone and shows relative settlement of reinforced zone near wall facing. The second zone (dashed line in Fig. 5.17) is the constant strain zone which is extending beyond reinforced zone, formed due to shear deformation within reinforced zone at higher elevation. The boundary of this zone is obtained by joining points having $\Delta\gamma_{oct}$ of 0.3%, as the soil behave as elastic upto 0.3% octahedral shear strain (Section 3.3.1). The zones can also be viewed with reference to the transition (change in slope) in the variation in horizontal displacements. This type of deformation zones are also observed by El-Emam and Bathurst (2004) and Ling et al. (2005a) as surface deformations near the wall facing and some tension cracks in backfill.

The contours of octahedral shear strain in backfill soil of rigid-faced wall subjected to dynamic excitation of acceleration 0.2g and frequency 5 Hz are shown in Fig. 5.19. Both deformation zones, that were discussed earlier, are prominently seen the figure. It is observed that extent of high strain zones (strains above 0.5 %) are confined very near to the wall. The extent of constant shear zone or shear deformation zone is extended upto end of reinforcement at higher elevations. The deformation zones in backfill soil of rigid-faced wall are shown in Fig. 5.20, schematically. The high strain zone or zone of relative compaction is formed very near to the wall facing due to vertical settlement. The constant shear zones due to shear deformation extend beyond reinforced zone.

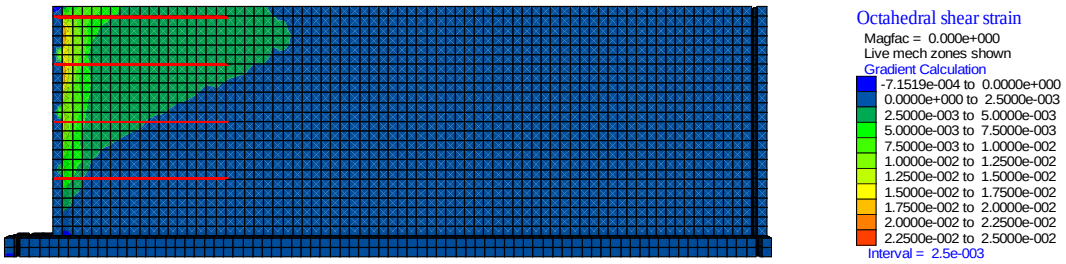

Fig. 5.19 Contour of octahedral shear strain after dynamic excitation

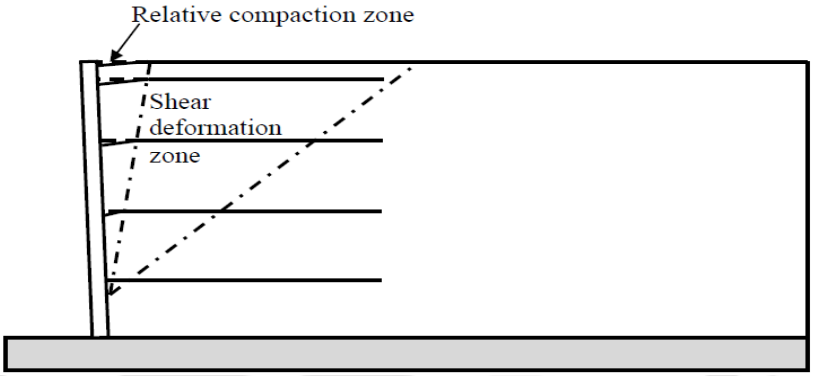

Fig. 5.20 Deformation zones of rigid-faced reinforced soil retaining wall after dynamic excitation

5.4 PARAMETRIC STUDIES

The influence of parameters such as reinforcement length, number of reinforcing layers and type of backfill (friction angle) are studied to observe the effect on $\Delta\gamma_{oct}$, $\Delta\varepsilon_{a\_rein}$ and location of deformation zones, after dynamic excitation. The parameters considered for this purpose are listed in Table 5.5.

Table 5.5 List of parameters considered for parametric studies

Soil properties	
Friction angles, degree	30, **38**, 43
Reinforcement configuration	
Length of reinforcement	**0.7H**, 1.0H, 1.2H
No. of reinforcement layers	**4**, 6, 8
Reinforcement stiffness (Secant modulus at 2% strain)(kN/m)	5.2, 100, **152**
Facing properties	
Facing stiffness (Elastic modulus) (GPa)	15.2 , **27.4**

Note: Parameters in Bold font indicate the common parameters

5.4.1 Effect of backfill friction angle

The rigid-faced wall models with three different backfill friction angles of 30°, 38° and 43° are considered. The comparative results after seismic excitation (a = 0.2g, f = 5Hz) are shown in Fig. 5.21. The maximum horizontal and vertical displacements of 38.44 mm and 18.59 mm observed near facing at elevation 5.5 m for wall with backfill friction angle 30°. About 27% and 45% reduction in horizontal and vertical displacements near the facing are observed for change in backfill friction angle to 43°. The RMSA amplification factors at top are 3.36 and 3.38 for wall with backfill friction angle 38° and 43°. The horizontal pressures do not have any appreciable variation for wall with different backfill friction angles. More than 27% reduction in horizontal displacement and about 17% reduction in vertical displacements near the facing are observed for similar changes in backfill friction angle from 30° to 43° for wrap-faced wall (Section 4.4.3). More reduction in vertical displacements near the facing for rigid-faced walls is due to friction developed between the wall and soil and rigid fixity between wall and reinforcement.

Comparison of incremental octahedral shear strain ($\Delta\gamma_{oct}$) developed within soil elements after dynamic excitation for wall with different backfill friction angles is shown in Fig. 5.22. The $\Delta\gamma_{oct}$ near the wall facing at elevation 5.25 m are 2.4%, 1.76% and 1.14% for wall with backfill friction angles of 30°, 38° and 43°, respectively. The $\Delta\gamma_{oct}$ are within the range of 0.7% - 0.3% in reinforced zone and decreases to negligible value at 8 m from facing. The increase in vertical settlements (v) near the wall facing causes higher strain near facing for three different backfill soils. In comparison with wrap-faced wall, $\Delta\gamma_{oct}$ are more near the end of reinforcement and strained zones are more extended in retained backfill for wrap-faced wall with backfill friction angle of 30° (Fig. 4.40).

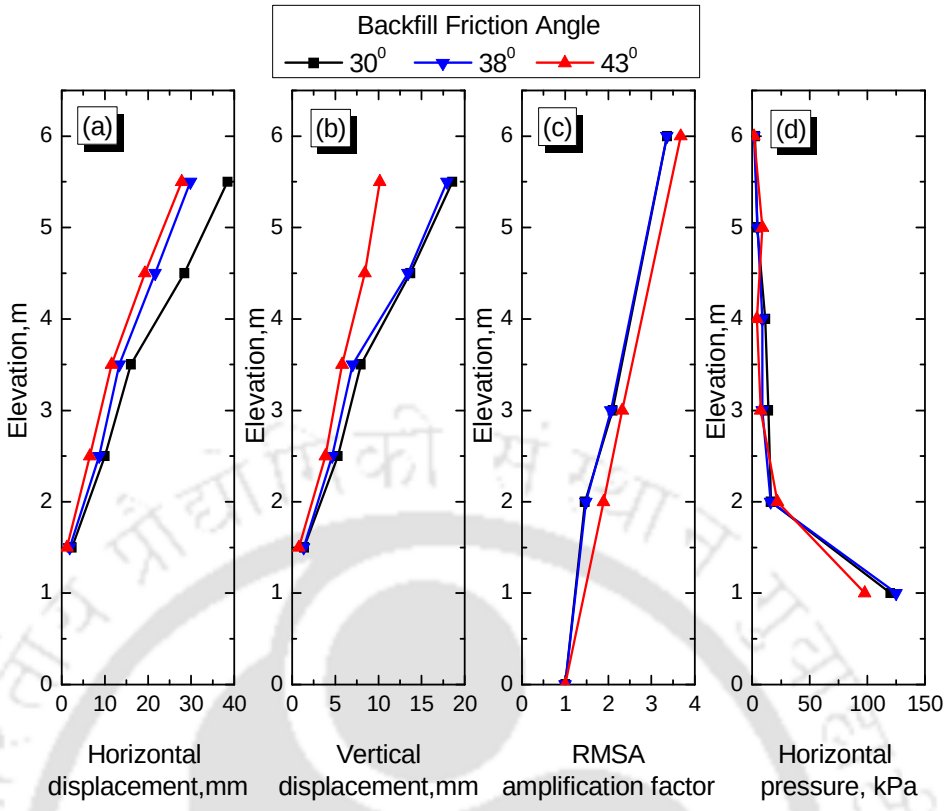

Fig. 5.21 Response of model walls with backfill friction angles 30°, 38° and 43° subjected to dynamic excitation (a = 0.2g, f = 5Hz and L_{rein}/H = 0.7, N_L=4)

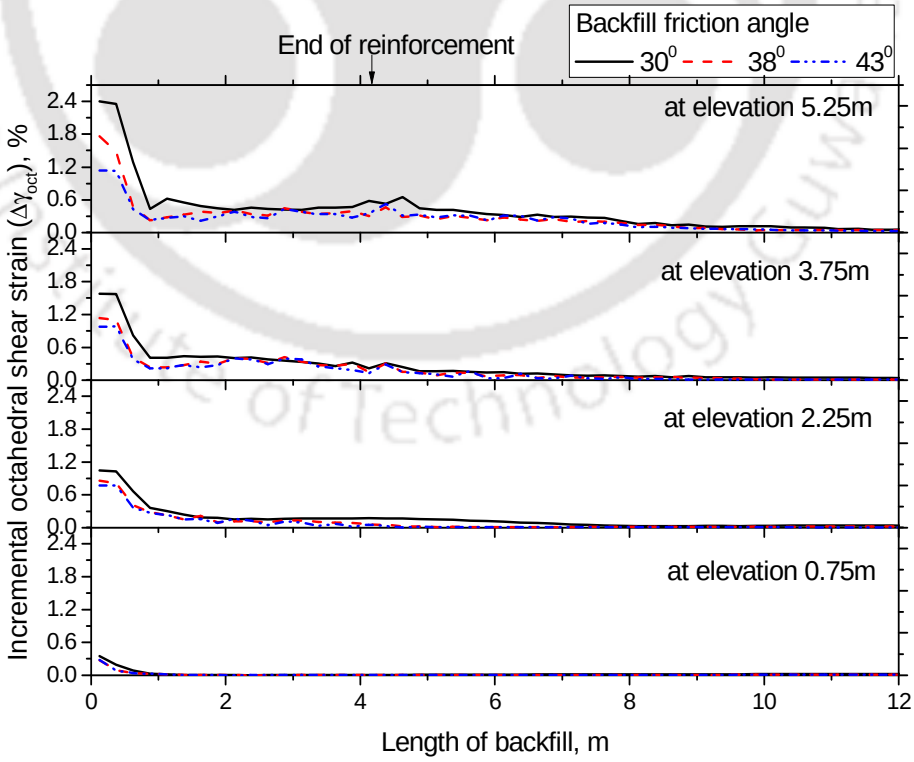

Fig. 5.22 Comparison of $\Delta\gamma_{oct}$ at backfill for wall with backfill friction angle 30°, 38° and 43° after dynamic excitation (a = 0.2g, f = 5Hz and L_{rein}/H = 0.7, N_L=4)

The variations in reinforcement strain increments ($\Delta\varepsilon_{a\_rein}$) for wall with different backfill soil (friction angle 30°, 38° and 43°) are shown in Fig. 5.23. A little variation is observed in reinforcement strain for wall with backfill friction angle 30°, 38° and 43°. This is due lesser horizontal displacement of wall causing lesser mobilization of soil- reinforcement interaction due to pullout of reinforcement.

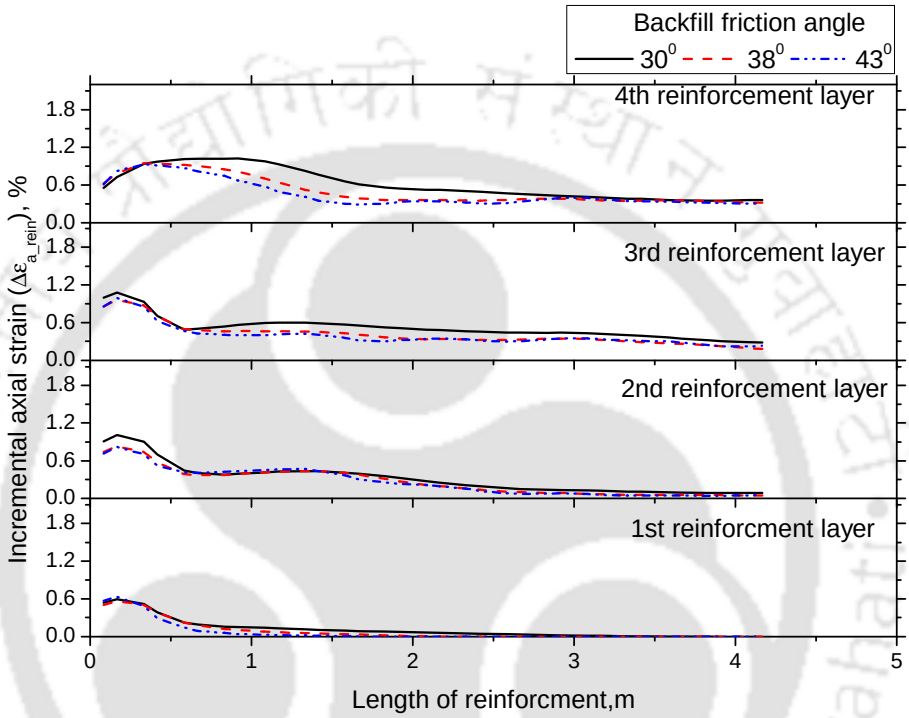

Fig. 5.23 $\Delta\varepsilon_{a\_rein}$ on reinforcement after dynamic excitation (a=0.2g, f=5Hz and L_{rein}/H = 0.7) with backfill friction angle 30°, 38° and 43°

5.4.2 Effect of reinforcement stiffness

The horizontal and vertical displacements and RMSA amplification factor and horizontal pressures are compared for wall with different reinforcement stiffness of 5.2, 100 and 152 kN/m and are shown in Fig. 5.24. About 25% and 20% reduction in u and v are observed for change in reinforcement stiffness 5.2 kN/m to 152 kN/m. But about for same variation of reinforcement stiffness 40% and 30% reduction in u and v are observed in wrap-faced walls.

Comparison of $\Delta\gamma_{oct}$ in backfill soil for the three model walls is shown in Fig. 5.25. The $\Delta\gamma_{oct}$ near the wall facing at elevation 5.25 m are 2.7%, 1.76% and 1.7% for

wall with reinforcement stiffness 5.2, 100 and 152 kN/m, respectively. At other elevations, almost same strain increments near the wall facing are observed for model walls with different reinforcement stiffness. The $\Delta\gamma_{oct}$ values did not affected much with reinforcement stiffness. A high strained zone showing relative settlement is formed near the facing for three model walls.

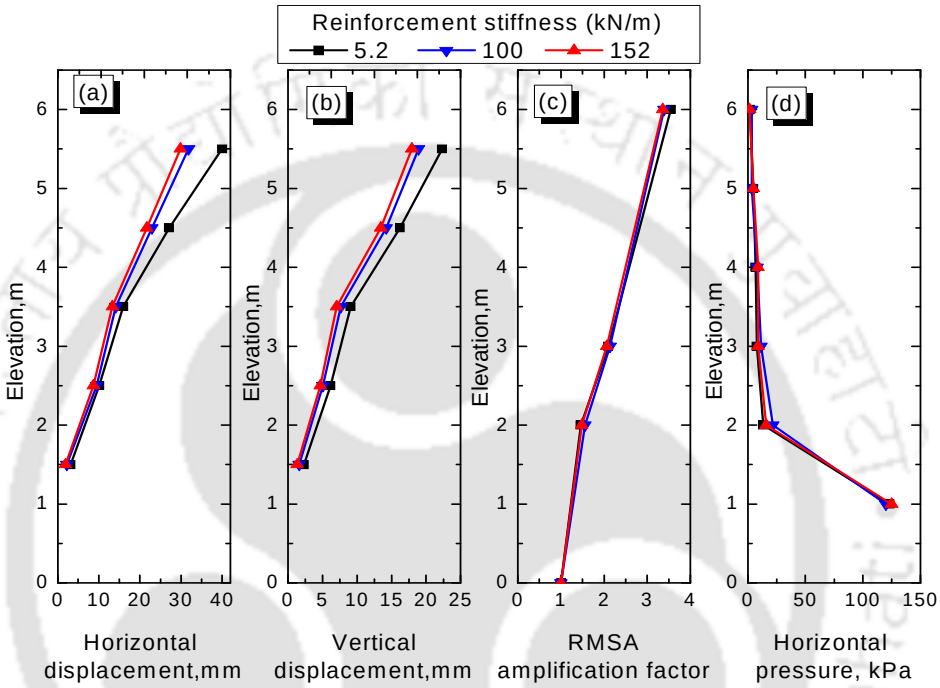

Fig. 5.24 Comparison of $\Delta\gamma_{oct}$ for walls with reinforcement stiffness 5.2, 100 and 152 kN/m after dynamic excitation (a = 0.2g, f = 5Hz and L_{rein}/H = 0.7)

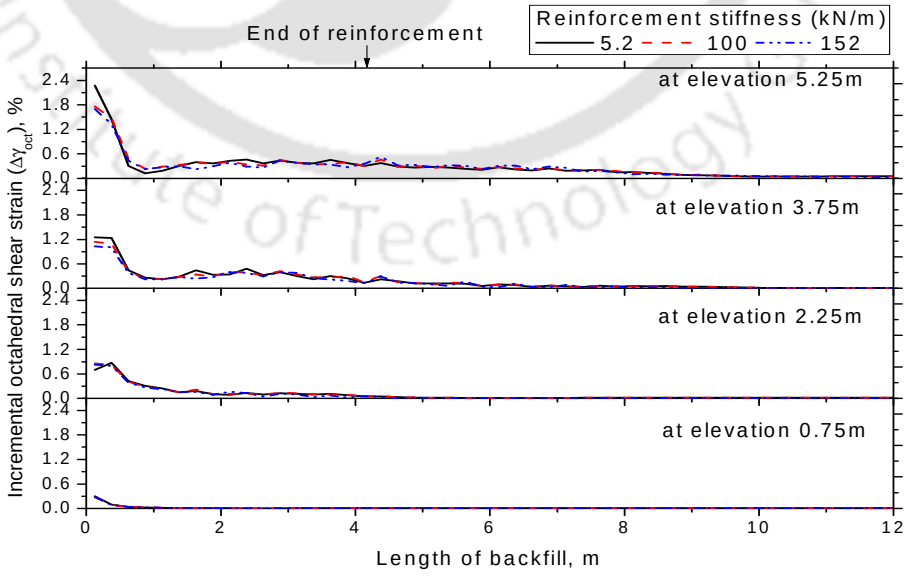

Fig. 5.25 Comparison of $\Delta\gamma_{oct}$ at backfill for wall with reinforcement stiffness 5.2, 100 and 152 kN/m after dynamic excitation (a = 0.2g, f = 5Hz and L_{rein}/H = 0.7, N_L=4)

Fig. 5.26 shows comparison of $\Delta\varepsilon_{a\_rein}$ for model walls with different reinforcement stiffness, after the seismic excitation. The maximum $\Delta\varepsilon_{a\_rein}$ is 0.9%, 0.6% and 0.6% at top layers for walls with reinforcement stiffness 5.2, 100 and 152 kN/m, respectively. The reinforcement strains are maximum near the facing and gradually decrease to negligible value.

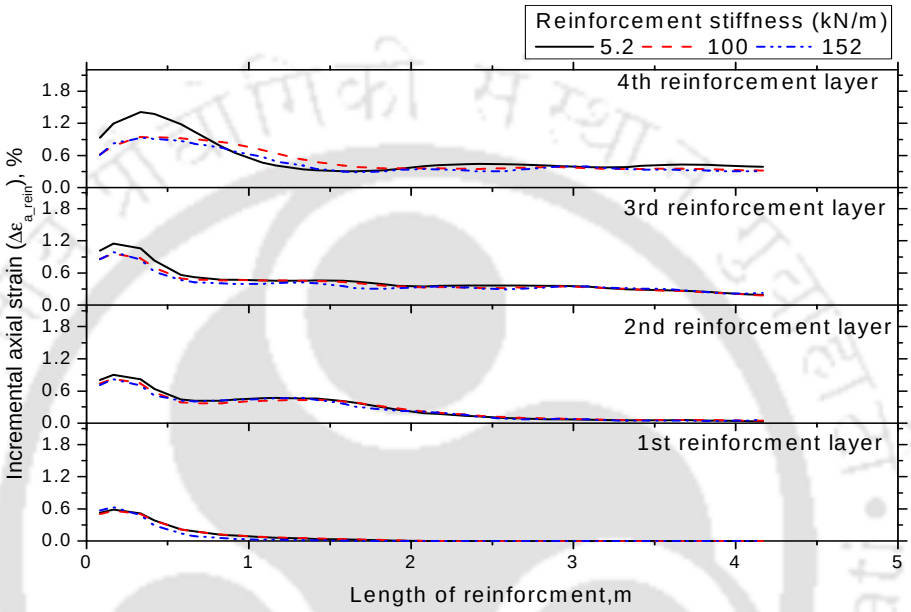

Fig. 5.26 $\Delta\varepsilon_{a\_rein}$ on reinforcement after dynamic excitation (a=0.2g, f=5Hz and L_{rein}/H = 0.7) with reinforcement stiffness 5.2, 100 and 152 kN/m

5.4.3 Effect of length of reinforcing layers

Three different reinforcement lengths (L_{rein}) 0.7H, 1.0H and 1.2H (H is the height of wall) are considered. The horizontal (u) and vertical (v) displacements, RMSA amplification factors and horizontal pressures are compared between wall models with different reinforcement lengths as shown in Fig. 5.27. The figure shows that u and v are influenced by change in reinforcement length from 0.7H to 1.0H. About 17% and 50% reduction in u and v, respectively, are observed for change in reinforcement length from 0.7H to 1.0H. More reduction in v is due to decrease in horizontal movement of rigid wall away from backfill. The RMSA amplification

factors and horizontal pressures are almost similar for wall with both reinforcement lengths.

Comparison of $\Delta\gamma_{oct}$ in backfill soil for three different reinforcement lengths (L_{rein} = 0.7H, 1.0H and 1.2H) is shown in Fig. 5.28. The $\Delta\gamma_{oct}$ near the facing is 1.76% and 1.14% for reinforcement length of 0.7H and 1.0H respectively. The strain variation in soil for wall with reinforcement length 1.0H and 1.2H are almost same. Comparisons of strain in soil depict more vertical settlement near the facing for wall with reinforcement length 0.7H. As zone of relative compaction is not formed near the end of reinforcement in rigid-faced wall as observed in wrap-faced wall (Chapter 4), wall with longer reinforcement only reduces displacement of wall and soil near facing.

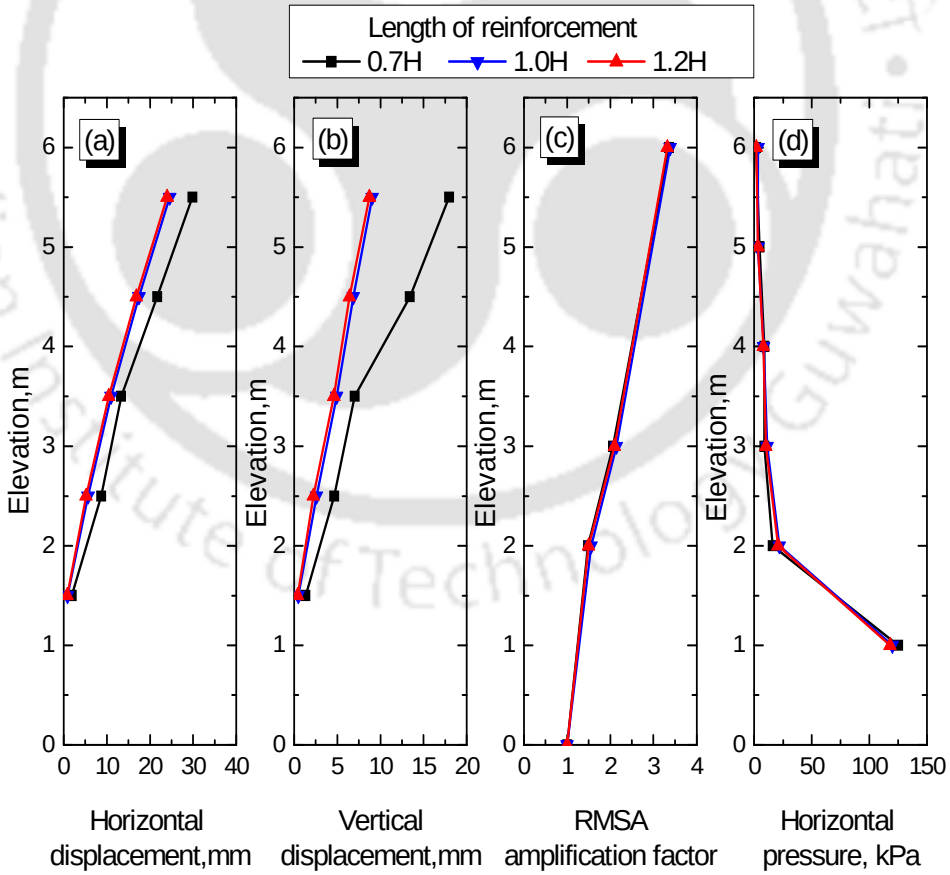

Fig. 5.27 Response of model walls with L_{rein}/H = 0.7, 1.0 and 1.2 subjected to dynamic excitation (a = 0.2g, f = 5 Hz and N_L=4)

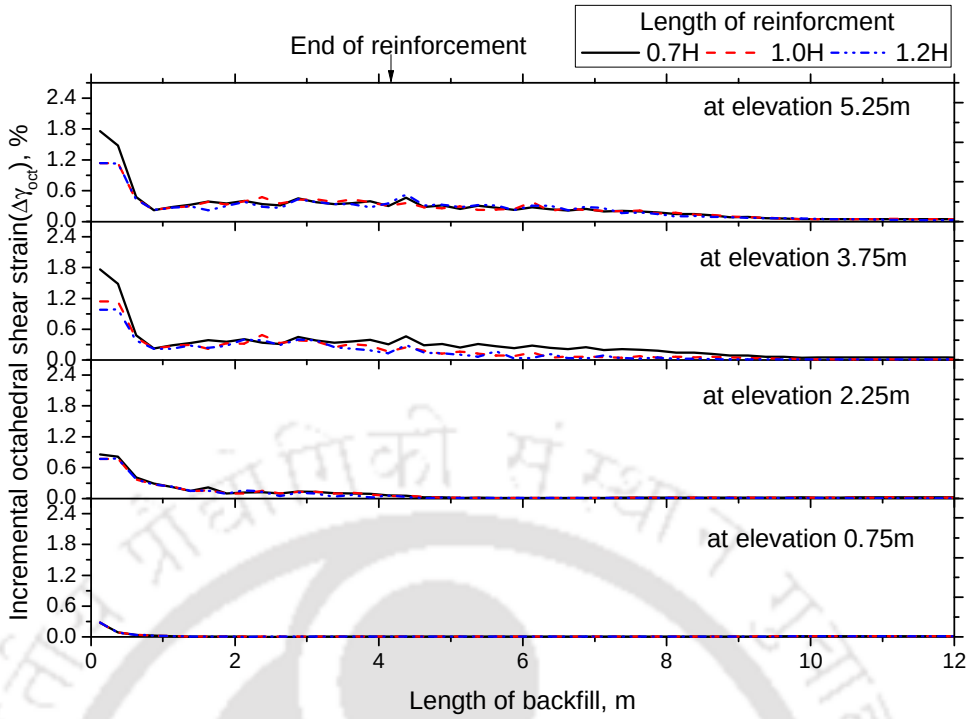

Fig. 5.28 Comparison of octahedral shear strain at backfill for wall with L_{rein}/H = 0.7 and 1.0 after dynamic excitation (a = 0.2g, f = 5 Hz and N_L=4)

5.4.4 Effect of number of reinforcing layers

The rigid-faced wall with 4, 6 and 8 numbers of reinforcing layers subjected to 20 cycles of dynamic excitation of 0.2g and frequency 5 Hz are considered. The horizontal and vertical displacements, RMSA amplification factor and horizontal pressures are compared between the wall models and is shown in Fig. 5.29. The horizontal displacements at top of wall are 29.87 mm, 24.77 mm and 24.59 mm for wall with 4, 6 and 8 numbers of reinforcement, respectively. The vertical displacements at top of wall are 17.96 mm, 9.74 mm and 9.06 mm for wall with 4, 6 and 8 numbers of reinforcement layers respectively. The variations of horizontal and vertical displacements are almost negligible for wall with 6 and 8 layers of reinforcements. The RMSA amplifications at top are 3.36, 3.12 and 3.0 for wall with 4, 6 and 8 layers of reinforcement, respectively. The horizontal pressures are almost same for wall with 4, 6 and 8 layers of reinforcement.

The $\Delta\gamma_{oct}$ away from reinforcement layer in backfill soil are compared for wall with 4, 6 and 8 layers of reinforcement in Fig. 5.30. Common elevations, which are not at reinforcement levels, are considered for determination of $\Delta\gamma_{oct}$. The maximum $\Delta\gamma_{oct}$ is near the wall and is almost remain constant after 0.4 m from facing within reinforced zone, then decrease to negligible value at a distance of 8 m from facing at higher elevation for wall with 4, 6 and 8 layers of reinforcement. The maximum incremental shear strain at elevation 5.7 m 2.52% for wall with 4 layers of reinforcement and 2.15%and 2.08% for wall with 6 and 8 layers of reinforcement. The variation of octahedral shear strain along backfill shows a zone of relative settlement near the facing and shear deformation within reinforced zone for wall with 4, 6 and 8 layers of reinforcement.

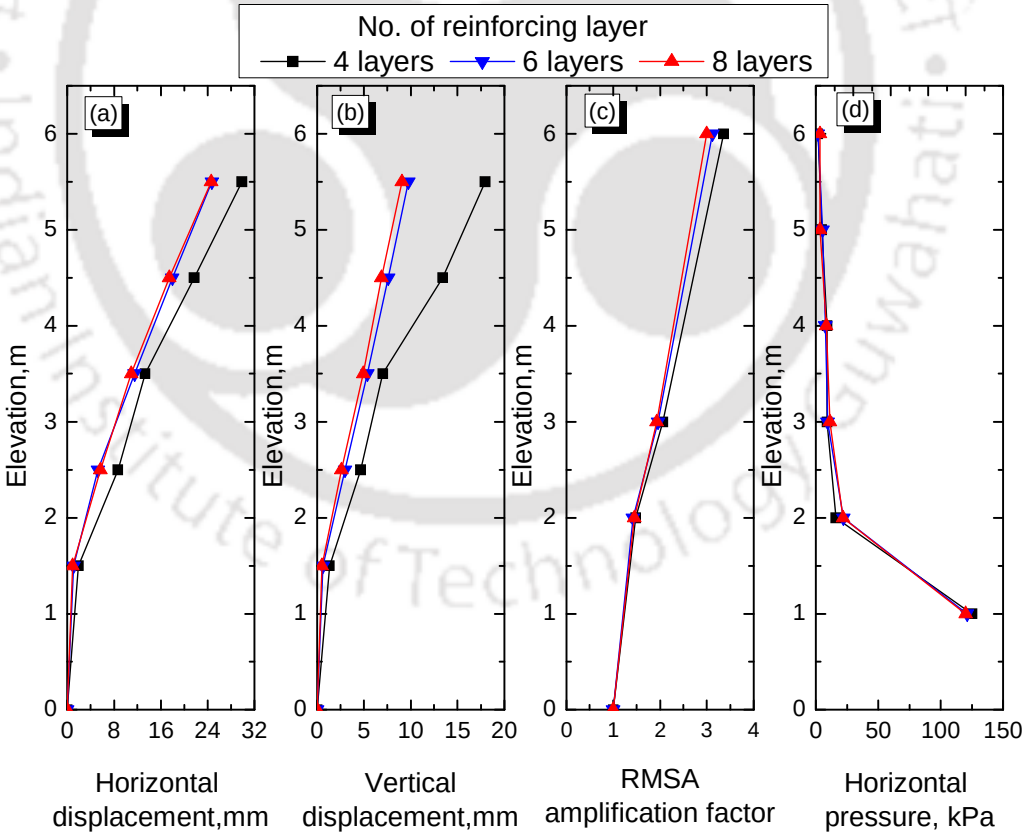

Fig. 5.29 Response of model walls for wall with 4, 6 and 8 layers of reinforcement subjected to dynamic excitation (a = 0.2g, f = 5Hz and L_{rein}/H = 0.7)

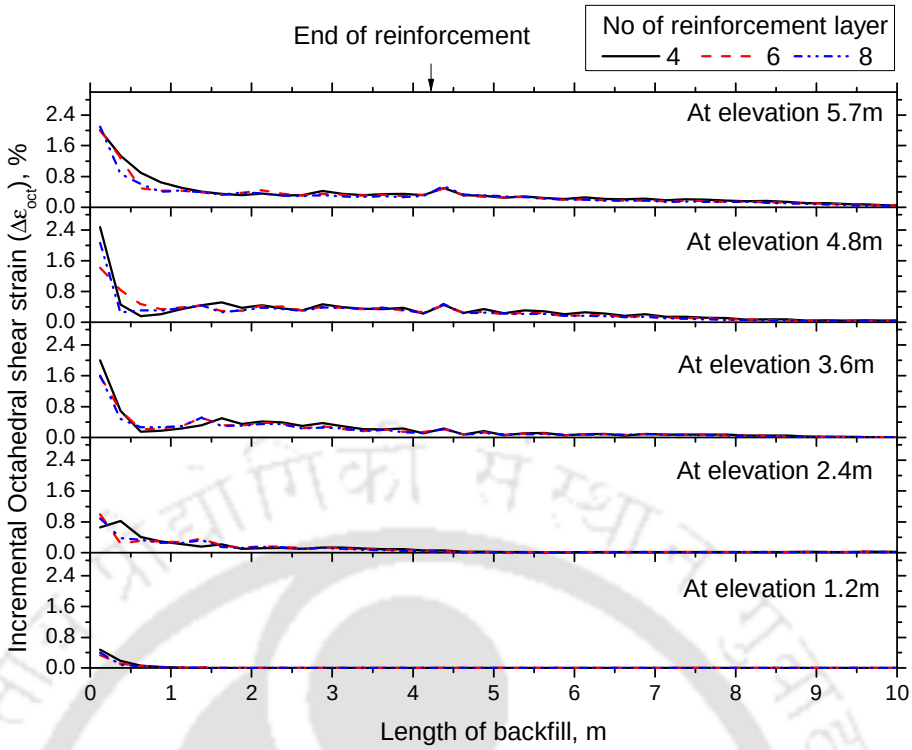

Fig. 5.30 Comparison of $\Delta\gamma_{oct}$ at backfill for wall with 4, 6 and 8 layers of reinforcement after dynamic excitation (a = 0.2g, f = 5Hz and L_{rein}/H = 0.7)

5.4.5 Effect of facing stiffness

Studies of reinforced soil walls with varying backfill soil, reinforcement length and stiffness show that formation of deformation zones of reinforced soil walls are affected by the flexibility of facing (wrap and rigid-faced walls). Wrap-faced walls are highly flexible in nature. Rigid-faced wall with different facing stiffness 27.4 GPa and 15.2 GPa, resembling M30 and M10 grade concrete, are considered for analysis. The results are compared between the wall models with facing stiffness 27.4 GPa and 15.2 GPa subjected to dynamic excitation of 0.2g acceleration and frequency 5 Hz and is shown in Fig. 5.31. The horizontal displacement at top of wall is 29.9 mm and 39.6 mm for wall with facing stiffness 27.4 GPa and 15.2 GPa respectively. The vertical displacements of backfill soil at top are 17.96 mm and 22.41 mm for wall with facing stiffness 27.4 GPa and 15.2 GPa respectively. About 32% and 25% change in horizontal and vertical displacement is observed for small change in facing

stiffness (27.4 GPa to 15.2 GPa). The RMSA amplification factors at the top of backfill are 3.12 and 2.81 for wall facing stiffness 27.4 GPa and 15.2 GPa, respectively. The horizontal pressure acting on wall with lesser stiffness is more than that of model with higher wall stiffness.

Fig. 5.32 shows comparison of $\Delta\gamma_{oct}$ between two reinforcement layers after dynamic excitation. The variation of octahedral shear strain along backfill shows a zone of relative settlement near the facing and shear deformation within reinforced zone for wall with facing stiffness 15.2 GPa and 27.4 GPa. The locations of deformation zones are different for rigid walls with different stiffness from that of warp faced walls.

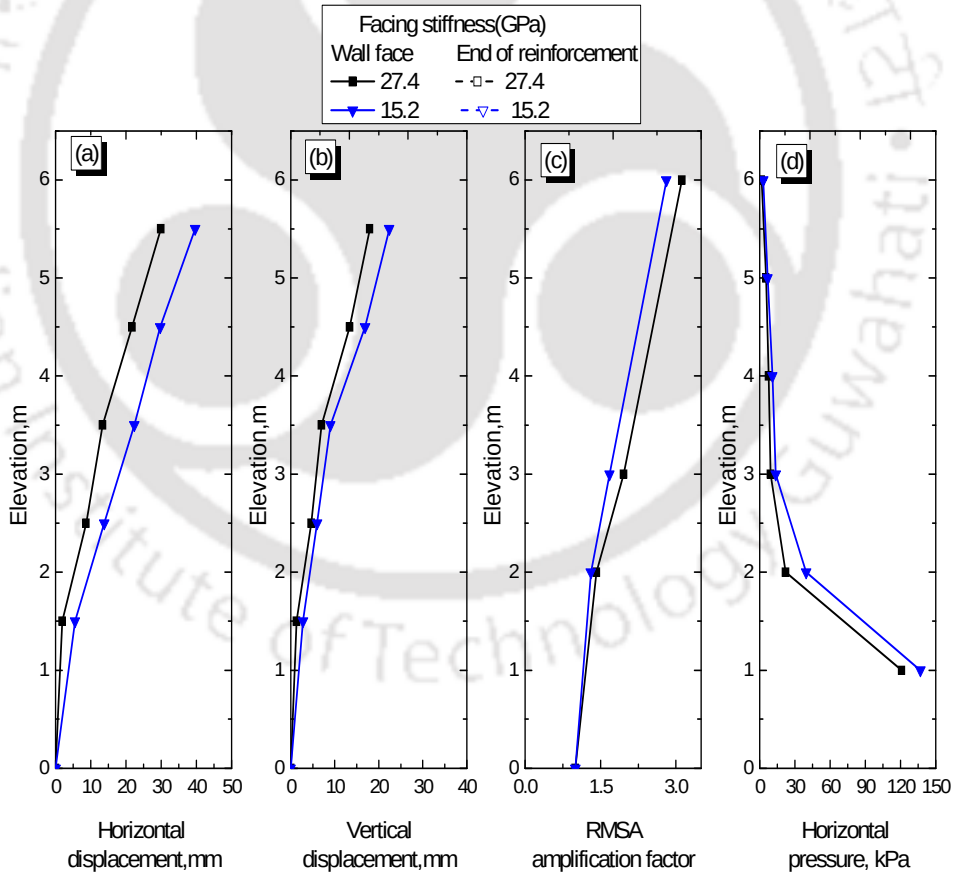

Fig. 5.31 Response of model walls with backfill different facing stiffness 27.4 GPa and 15.2 after dynamic excitation (a = 0.2g, f = 5 Hz and L_{rein}/H = 0.7)

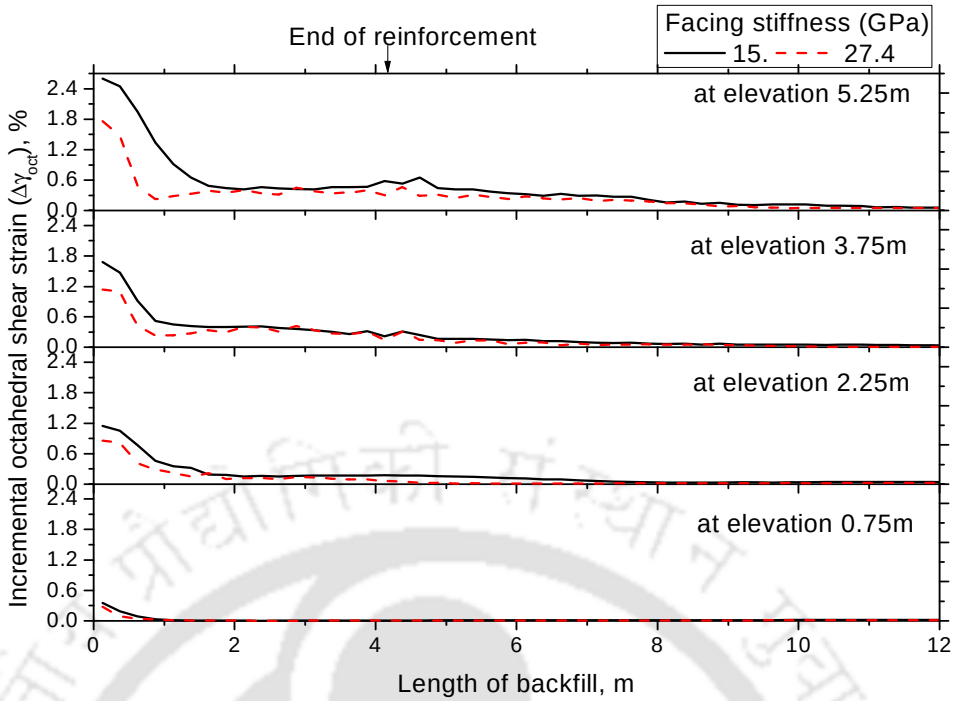

Fig. 5.32 Comparison of v at backfill for wall with facing stiffness 27.4 GPa and 15.2 GPa after dynamic excitation (a = 0.2g, f = 5Hz and L_{rein}/H = 0.7)

5.4.6 Effect of frequency of excitation

Seismic excitations of acceleration 0.2g at different frequencies 3 Hz, 5 Hz and 7 Hz are considered in this section. The results for the walls subjected to different excitation frequencies are shown in Fig. 5.33. The maximum u near the wall facing are 19.08 and 54.66 mm for wall subjected to seismic excitation of 3 Hz and 7 Hz, respectively. The v near wall facing is maximum for wall subjected to 7 Hz seismic excitation. The RMSA amplification factors at top of wall are 2.03, 3.36 and 3.82 for model walls subjected to 3 Hz, 5 Hz and 7 Hz respectively. The results indicate that frequency of excitation has significant effect on the response of the structure in all the parameters. Among the range of frequencies considered, 7 Hz frequency excitation showed larger response. But for the same range of frequencies, in case of wrap-faced walls, higher displacements are observed for model subjected to 3 Hz frequency of excitation.

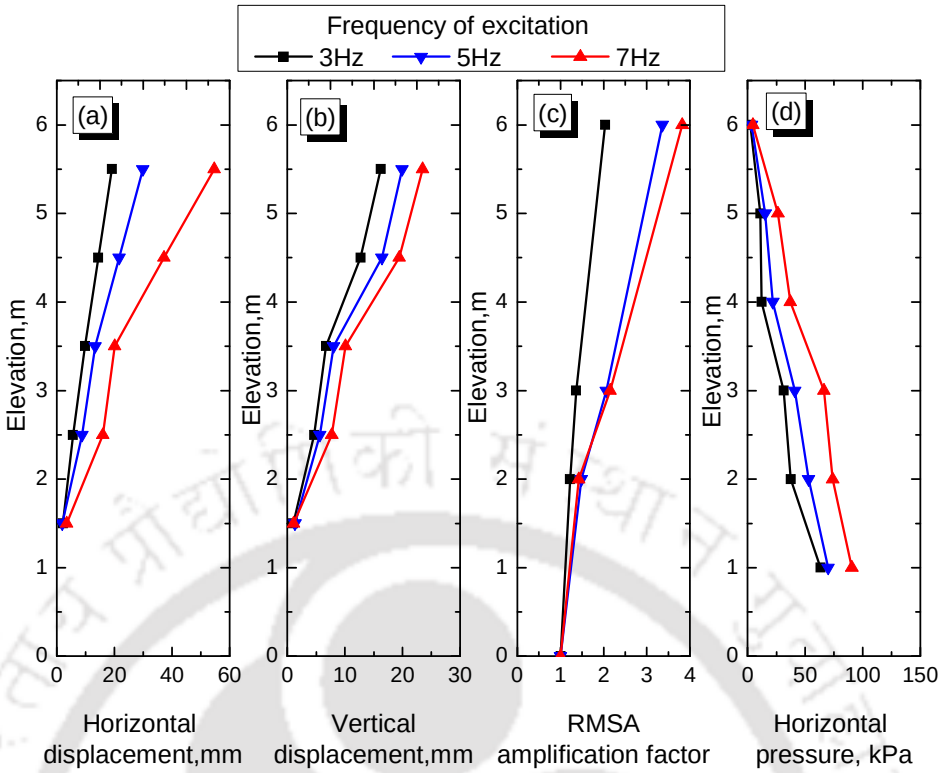

Fig. 5.33 Response of model walls with backfill different frequency of excitation (a = 0.2g and L_{rein}/H = 0.7)

The comparisons of $\Delta\gamma_{oct}$ in backfill soil (in the middle of reinforcing layer) after different dynamic excitations are shown in Fig. 5.34. The maximum $\Delta\gamma_{oct}$ near the facing are 1.22%, 1.76% and 2.97% at elevation 5.25 m for wall subjected to seismic excitation of 3 Hz, 5 Hz and 7 Hz frequencies, respectively. A small increase of 1.39% at 5.75 m elevation is observed near the end of reinforcement for wall subjected to seismic excitation of frequency 7 Hz. The strain reduces to negligible value at 10 m from the facing. A high strain compaction zone near the facing and shear deformation zone extending to 6 m into retained zone is observed for wall subjected to excitation of 7 Hz frequency. The $\Delta\gamma_{oct}$ increases near end of reinforcement and reduces to negligible value at 10 m from wall facing at elevation 5.25 m. The increase in $\Delta\gamma_{oct}$ after end of reinforcement shows formation of compound deformation zones as observed in wrap-faced walls (Fig. 4.21). The frequency of excitation effect the deformation zones of rigid-faced walls.

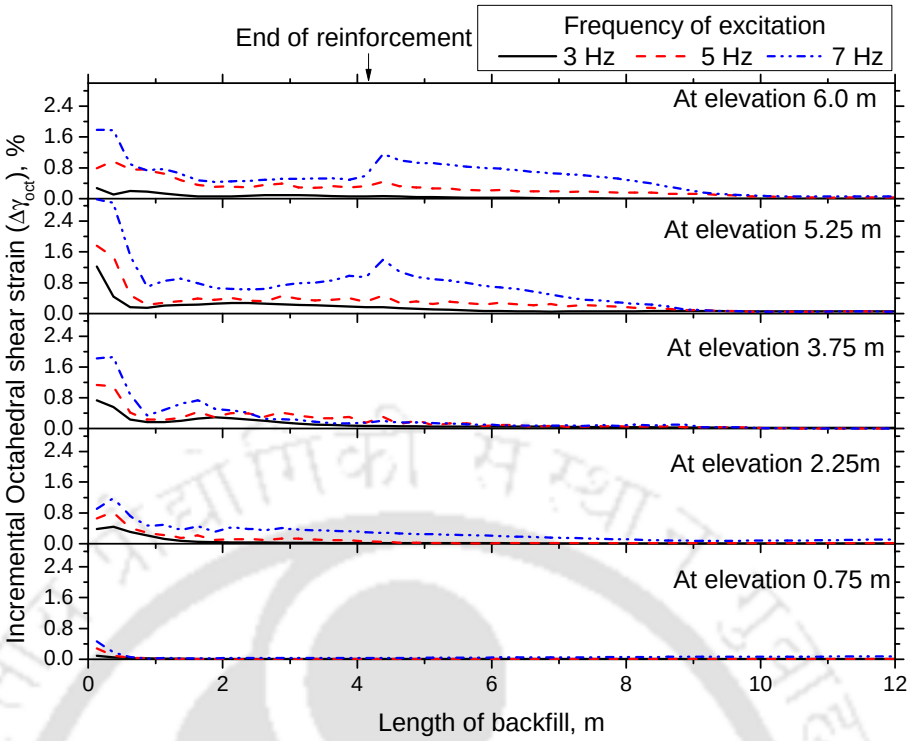

Fig. 5.34 Comparison of $\Delta\gamma_{oct}$ at backfill for walls subjected to dynamic excitations of frequency 3 Hz, 5 Hz and 7 Hz (a = 0.2g and L_{rein}/H = 0.7)

5.4.7 Effect of acceleration of dynamic excitation

A stepped amplitude sinusoidal function at 3 Hz frequency is considered to observe the behavior of rigid-faced wall at different acceleration levels. The amplitude is increased at 2 second interval (after 6 cycles) from 0.1g to 0.6g acceleration with 0.1 g step (Fig. 5.35).

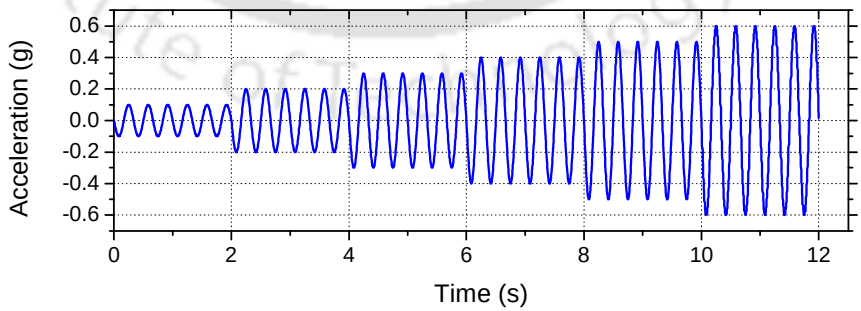

Fig. 5.35 Input base stepped acceleration

Comparison of the results at different acceleration levels for wall subjected to stepped excitation (a = 0.1g to 0.6g, f = 3Hz) is shown in Fig. 5.36. The horizontal

displacements are 18.4 mm, 36.0 mm 65.4 mm at top of wall near the facing at input accelerations of 0.2g, 0.4g and 0.6g, respectively. The horizontal displacements increase with increase in input acceleration. The vertical displacements are 12.2 mm, 17.0 mm and 18.35 mm at top of backfill near wall facing at input acceleration of 0.2g, 0.4g and 0.6g, respectively. About 2.5 times increase in horizontal displacement and 35% increase in vertical displacements are observed with increase in acceleration from 0.2g to 0.6g. The RMSA amplification factors are 1.68, 1.64 and 1.63 at top near wall facing at input acceleration of 0.2g, 0.4g and 0.6g respectively. The maximum horizontal pressures are 50.2 kPa, 89 kPa and 132 kPa at input acceleration of 0.2g, 0.4g and 0.6g respectively. The horizontal pressures on wall increase with increase in input accelerations, due more inertia force at higher acceleration.

The octahedral shear strain within backfill soil at different input acceleration is shown in Fig. 5.37. It is observed from the figure that at acceleration level of 0.2g and 0.4g, the strained zones are very near to the wall. But at 0.5g and 0.6g excitation levels, the strained zones are extended into the deep backfill. Similar increased deformation zones with increase in acceleration levels were reported by Watanabe et al. (2003), El-Emam and Bathurst (2004) and Nakajima et al. (2008).

Fig. 5.38 shows the variation of incremental octahedral shear strains ($\Delta\gamma_{oct}$) along the length of backfill soil at excitation level of 0.2g, 0.4g and 0.6g. The $\Delta\gamma_{oct}$ are determined in between two reinforcement layers. The $\Delta\gamma_{oct}$ are 2.68%, 2.0% and 1.25% near the facing at an excitation level of 0.6g, 0.4g and 0.2g, respectively, at an elevation of 5.25 m. The $\Delta\gamma_{oct}$ decreases to value as low as 0.5% at distance of 0.5 m from wall facing at elevations 5.25 m and 3.75 m at all excitation level. A small peak in $\Delta\gamma_{oct}$ is observed at the end of reinforcement for acceleration of 0.6g at elevation 5.25 m and 3.75 m. The $\Delta\gamma_{oct}$ reduce to negligible value beyond 8.0 m from wall face.

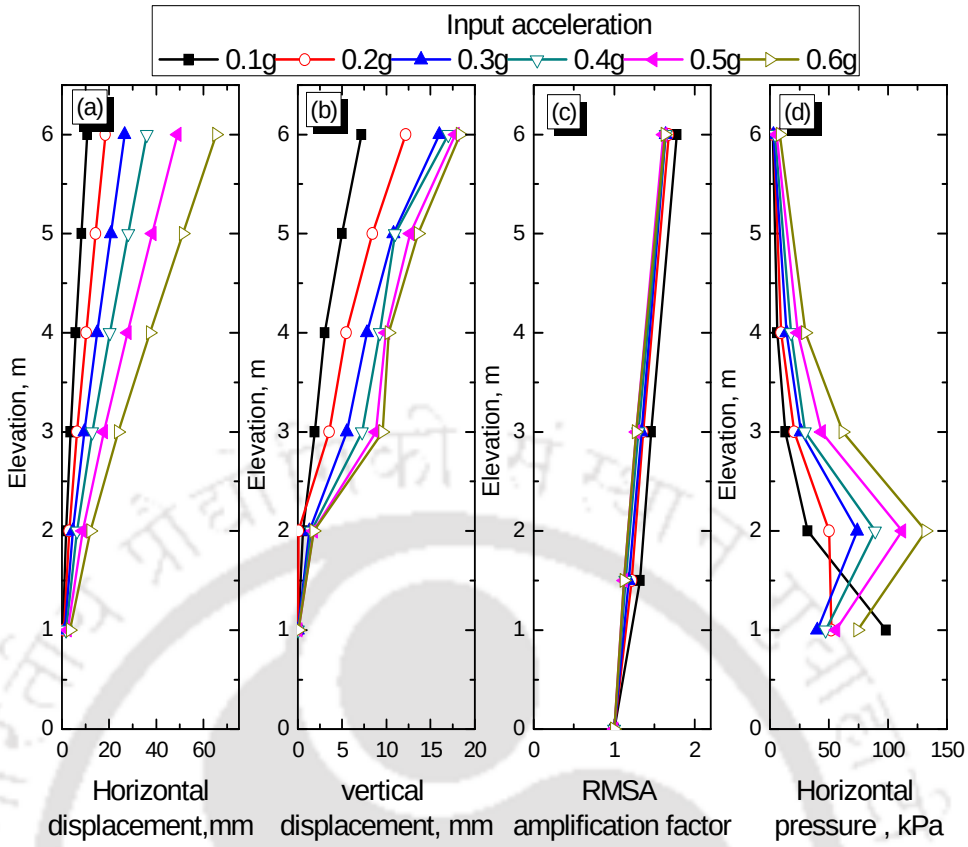

Fig. 5.36 Horizontal and vertical displacement at different elevation for different input acceleration

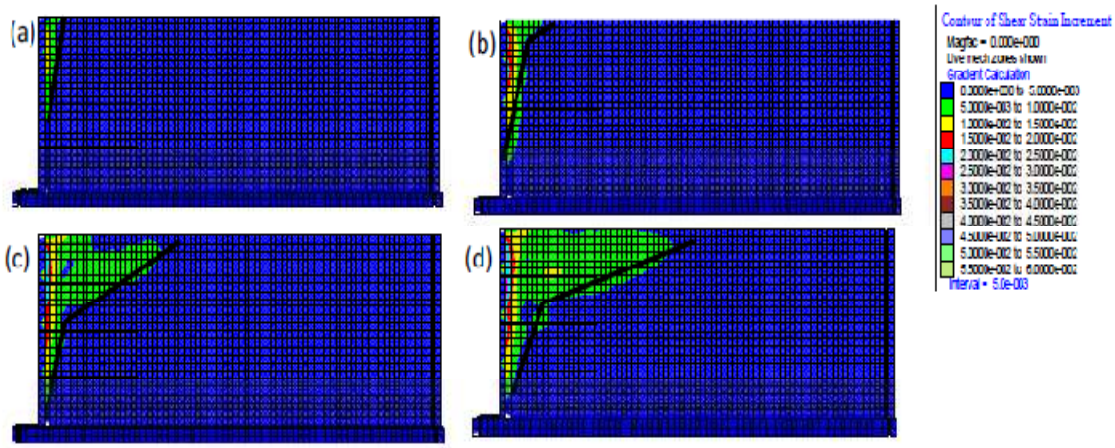

Fig. 5.37 The octahedral shear strain on backfill soil after 2 sec dynamic excitation of (a) 0.2g (b) 0.4g (c) 0.5g and (d) 0.6g. (f = 3 Hz, L_{rein}/H = 0.7 and N_L= 4)

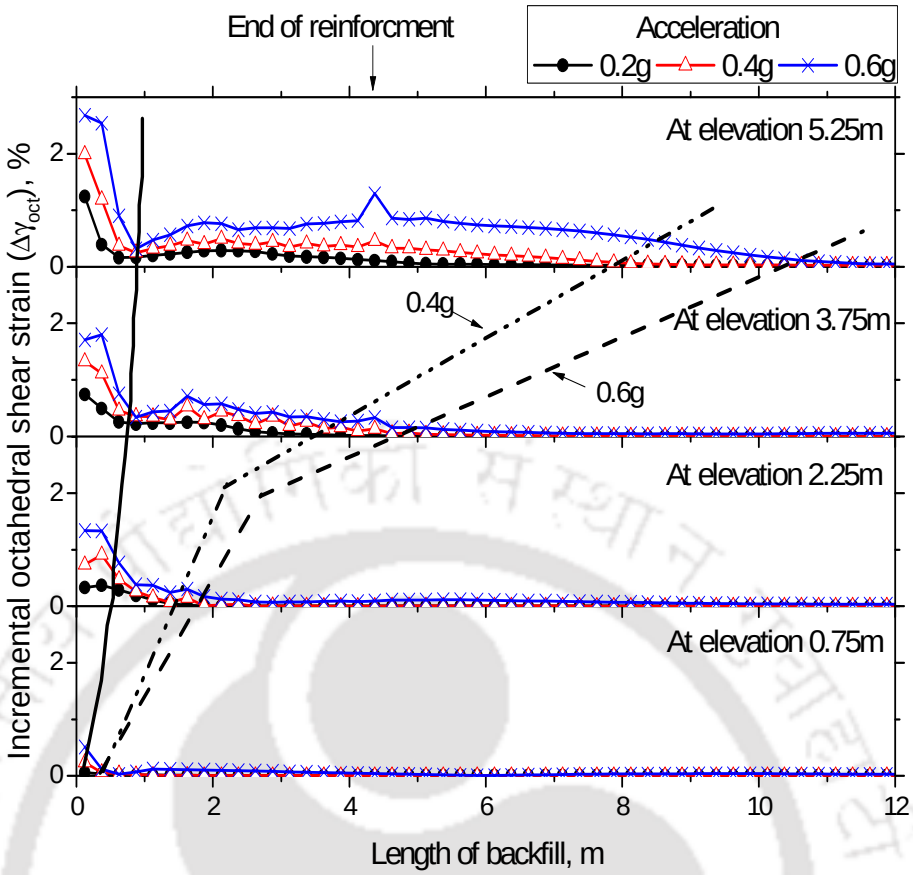

Fig. 5.38 $\Delta\gamma_{oct}$ along the length of backfill at different excitation level (f = 3 Hz, L_{rein}/H = 0.7 and N_L= 4)

The incremental axial strains in reinforcement members ($\Delta\varepsilon_{a\_rein}$) during dynamic excitation are determined along the reinforcement length and shown in Fig. 5.39. The $\Delta\varepsilon_{a\_rein}$ are 1.63%, 1.10% and 0.59% at an excitation level of 0.6g, 0.4g and 0.2g respectively at 3rd layer of reinforcement. The incremental axial strain decreases to negligible value near the end of reinforcement for wall subjected to excitation of 0.2g and 0.4g. The incremental axial strains are 0.43% and 0.40% at top and 3rd layer of reinforcement and negligible value for other layer of reinforcement for wall subjected to excitation of 0.6g. The top two layers of reinforcements are within the strained zone of soil at higher excitation level. The $\Delta\varepsilon_{a\_rein}$ increases depending on extent of soil strain zone.

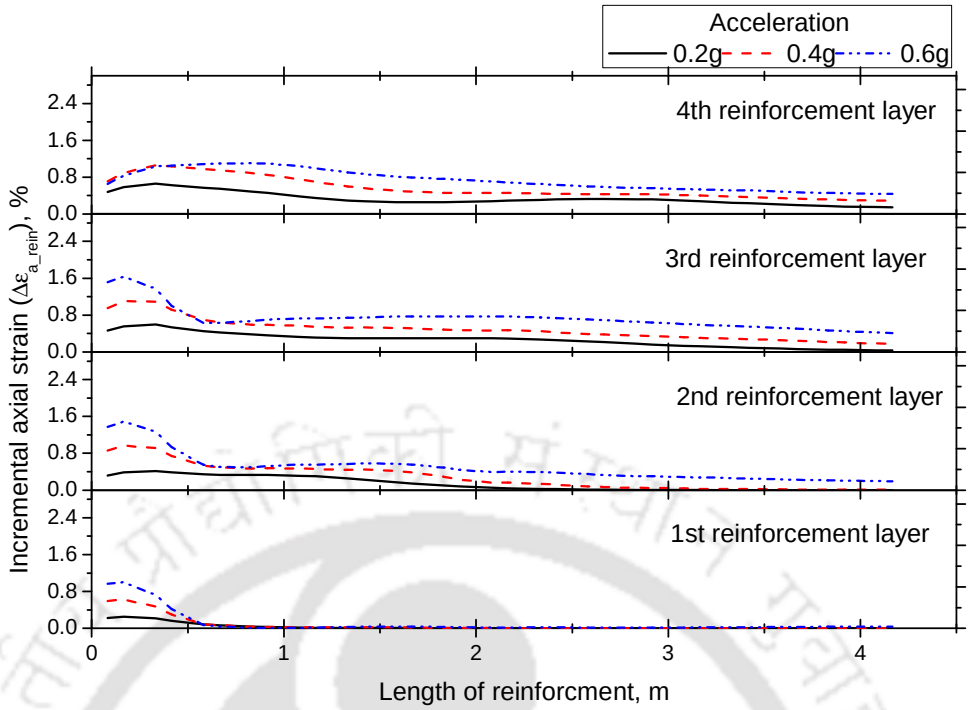

Fig. 5.39 $\Delta\varepsilon_{a\_rein}$ along the length of reinforcement at different excitation level (f = 3 Hz, L_{rein}/H = 0.7 and N_L= 4)

5.5 COMPARISON OF WRAP-FACED AND RIGID-FACED WALLS BEHAVIOUR

The behavior of wrap-faced and rigid-faced reinforced walls is compared to observe the effect of facing on wall behavior. A 6.0 m high wrap-faced and rigid-faced wall with 6 layers of reinforcement having vertical spacing of 1m each are considered for comparison. The length of reinforcement is kept as 0.7H for both walls. Both walls are subjected to dynamic excitation of acceleration 0.2g and 5 Hz frequency. The comparison in terms of horizontal and vertical displacements, RMSA amplification factors and horizontal pressures are shown in Fig. 5.40. In general, it is seen from the figure that the displacements are larger in wrap-faced walls and RMSA amplifications are larger in rigid-faced walls. The maximum horizontal displacement near wall facing is 24.77 mm and 173.16 mm for rigid-faced wall and warp-faced wall respectively. The vertical displacements near wall face and end of reinforcement for

wrap-faced wall are 55.81 mm and 106.44 mm respectively, while that for rigid-faced wall are 9.74 mm and 1.88 mm, respectively. The RMSA amplification factor is 1.46 and 3.12 at top near the wall edge for wrap-faced and rigid-faced wall respectively. The RMSA amplification factor decreases in wrap-faced wall due to more horizontal displacement and that decreases the stiffness of soil. The horizontal pressure is same for both wrap and rigid-faced wall upto elevation of 2.4m. The horizontal pressure at 1.2 m elevation is 28.6 kPa and 121 kPa for wrap-faced and rigid-faced wall, respectively. These higher pressures at lower elevations, in rigid-faced walls, are due to the fixed condition at the facing bottom.

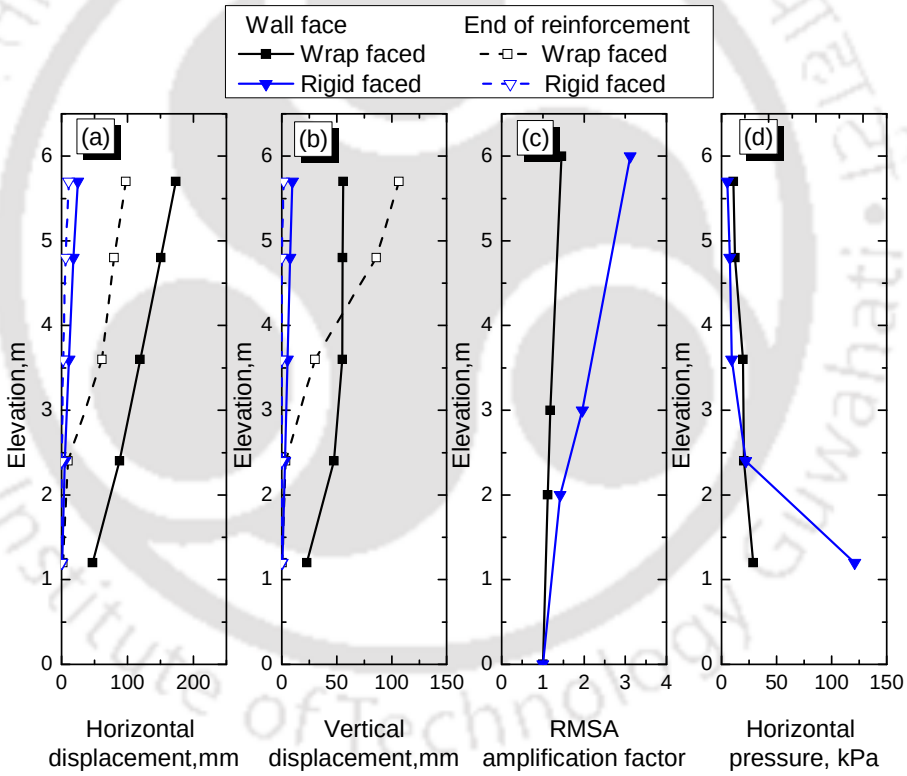

Fig. 5.40 Response of wrap and rigid-faced walls with after 20 cycles of dynamic excitation (a=0.2g, f = 5Hz L_{rein}/H=0.7, N_L=6)

The $\Delta\gamma_{oct}$, horizontal and vertical displacements along the length of backfill for wrap-faced and rigid-faced walls subjected to dynamic excitation of acceleration 0.2g and frequency 5 Hz are shown in Fig. 5.41. Fig. 5.41(a) shows strain increments of 2.9% at 2m from face of wall and more than 9.7% near the end of reinforcement at

elevation 5.5 m for wrap-faced wall. The horizontal displacements (u) of soil element within reinforced zone are maximum and they gradually reduce to negligible value. The vertical displacements (v) increases suddenly near the end of reinforcement. Fig. 5.41(b) shows that $\Delta\gamma_{oct}$ is 2.02% at elevation of 5.5 m near the facing (confined to zone upto 0.4 m from facing). The horizontal and vertical displacements are maximum near the facing and decrease gradually.

The deformations of wrap-faced wall subjected to dynamic excitation consist of three different modes: shear deformation within reinforced zone, relative compaction near end of reinforcement and shear zone extending to backfill zone. However, high strained deformation zone in rigid-faced wall is very close to the facing. The variation of location of probable deformation zones in wrap and rigid-faced wall is due to the flexibility of facing of reinforced soil wall.

The variation in $\Delta\varepsilon_{a\_rein}$ after dynamic excitation along the length of reinforcement for wrap-faced and a rigid-faced wall is shown in Fig. 5.42. The maximum $\Delta\varepsilon_{a\_rein}$ is nearly 0.2% at 1.4 m and 1% at 0.3 m from facing for wrap-faced and rigid-faced walls, respectively. The maximum $\Delta\varepsilon_{a\_rein}$ are within 1% near the facing for rigid-faced walls and within 2.5% at middle of reinforcement length for wrap-faced walls. The reinforcement strain is maximum near the facing for 1st layer of reinforcement for wrap-faced walls. The comparison of reinforcement strain in wrap and rigid-faced reinforced walls shows that shear deformation of soil occurs near the middle of reinforcement for wrap-faced wall and near the facing for rigid-faced walls.

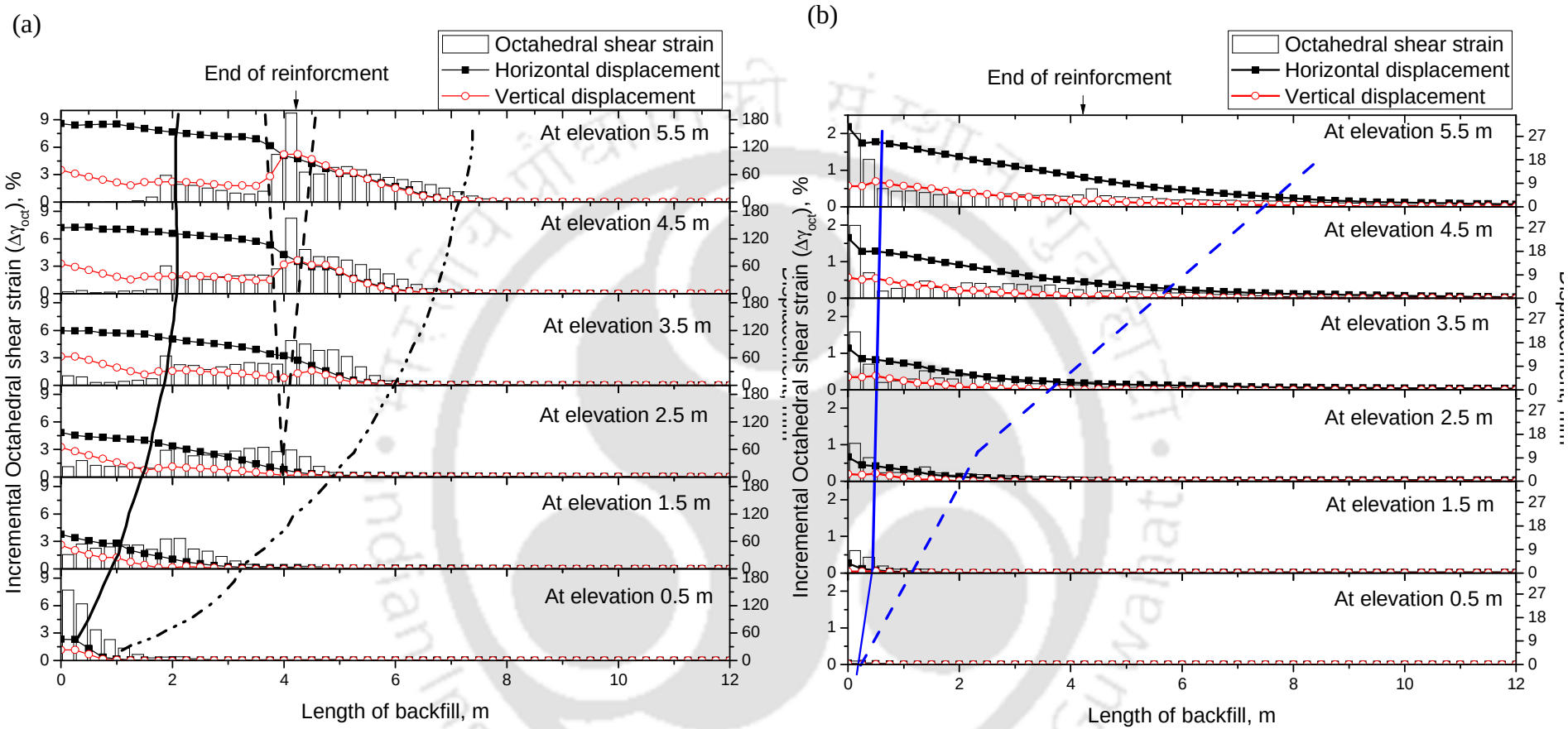

Fig. 5.41 Octahedral shear strain, horizontal displacement and vertical displacement along the length of backfill for (a) wrap-faced wall and (b) rigid-faced wall after 20 cycles of dynamic excitation of 0.2g and 5Hz (a=0.2g, f=5Hz, L_{rein}/H=0.7, N_L=6)

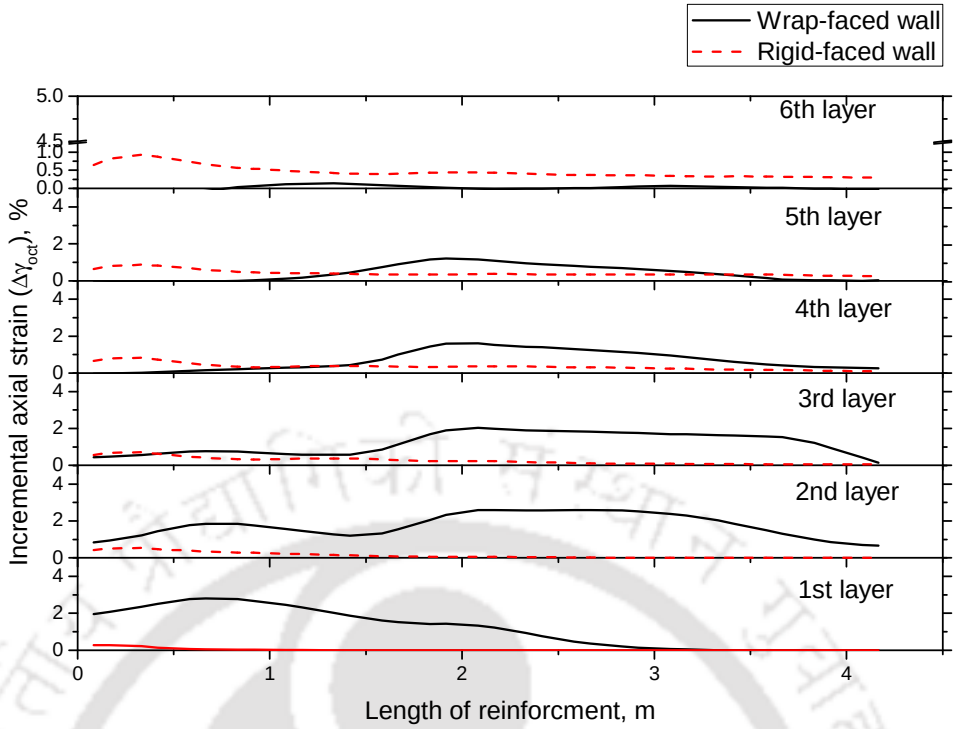

Fig. 5.42 Axial stress along the length of reinforcement at different excitation level (a=0.2g, f=5 Hz, L_{rein}/H = 0.7 and N_L= 6)

Discussion

Comparison of $\Delta\gamma_{oct}$, u, v and $\Delta\varepsilon_{a\_rein}$ and corresponding deformation zones for rigid-faced and wrap-faced walls are discussed. It is observed that reinforced wall with flexible facing as wrap-faced wall has completely different deformation zones from that of rigid-faced walls. The deformation for wrap-faced walls can be divided into three different zones. The shear deformation approximately at the middle of reinforcing layers, settlement at the end of reinforcement and compound deformation zone at the retained backfill. The strain developed in reinforcement during dynamic excitation depends on location of soil strain. In rigid-faced wall deformation zones are formed near the wall facing and strain developed within reinforced zone and at retained zones are very low. Therefore, no such deformation zone other than that near the wall facing is formed in rigid-faced wall. This variation in deformation zone is

due to facing flexibility. The design of reinforced soil wall considering the facing flexibility is important for proper evaluation of reinforcement loads.

5.6 SUMMARY

Numerical model was developed and validated to simulate the shaking table tests of rigid-faced walls. The calibrated numerical model was utilized to develop a full scale numerical model of rigid-faced wall. Dynamic behaviour of model wall subjected to sinusoidal excitation was discusses by varying different model and excitation parameters. The displacements and strains developed within model for full scale model are determined and analyzed. The changes strains and displacement within backfill soil signifies two deformation zones in the backfill: a) high strained zone near the wall facing and b) shear deformation extended to some part of retained backfill. The response of wrap and rigid-faced walls are compared to analyze the effect of facing. The formation of deformation zones, soil strains and reinforcement strains are different for wrap-faced and rigid-faced walls.

Chapter 6. MODEL WALLS SUBJECTED TO DIFFERENT EARTHQUAKE MOTIONS

6.1 INTRODUCTION

Seismic studies on the reinforced soil retaining wall models are being generally conducted for sinusoidal excitations at constant frequencies (Sakaguchi, 1996; Ramakrishna et al. 1998; El-Emam and Bathurst, 2005 and 2007; Sabermahani et al. 2009; Krishna and Latha 2007 and 2012; Liu and Ling, 2012). These idealized studies, only give relative behavioral aspects of the model structures. However, during the real earthquake excitation model behavior is significantly affected by various ground motion parameters, especially, the frequency content (Hatami and Bathurst, 2000; Cakir, 2013; Athanasopoulos et al. 2013). The real earthquake excitation contains wide range of frequency contents. In the light of importance of real earthquake motions, few researchers studied the behavior of structures using different recorded/modified ground motions (Cai and Bathurst 1995; Helwany and McCallen 2001; Ling 2005b; Liu 2009; Lee et al. 2010; Liu et al. 2011; Lee and Chang, 2012; Cakir, 2013; Lee and Chang 2012; Liu and Ling, 2014).

The frequency effects on response of wrap-faced and rigid-faced reinforced soil wall models are discussed in Section 4.4.5 and Section 5.4.6. It was discussed that responses of the model walls depend on the frequency of excitation. The influence of frequency on response of structures depends upon its proximity to the fundamental frequency of the system. This chapter presents numerical model studies on both the wrap-faced and rigid-faced reinforced soil retaining walls, subjected to different actual earthquake excitations which are rich in the frequency content.

The wrap-faced and rigid-faced walls described in Section 4.5 and Section 5.3, respectively, are considered for numerical simulation. Stability analyses have been carried out for full scale wrap and rigid-faced reinforced soil wall models according to FHWA (2001). The factors of safety (FS) obtained for static and dynamic stability are tabulated in Table 6.1. For internal stability, obtained among different internal stability FS values ($FS_{rupture}$ and $FS_{pullout}$) at different reinforcement layers, the lowest safety factors are reported. In FHWA (2001) external stability of reinforced soil walls depend on backfill soil type of reinforced and retained soil, length of reinforcement and loading if any. However, the internal stability depends additionally on reinforcement spacing. As reinforcements spacing are different for wrap faced and rigid faced walls, factor of safeties against internal stability are different. The safety factors shown in the Table 6.1 indicate that the walls considered are safe against external and internal stability for 0.2 g acceleration level, while for 0.3g acceleration level $FS_{overturning}$, are marginal.

Table 6.1 Static and dynamic Factors of safety values for wrap and rigid-faced walls

Loading condition			External stability		Internal stability	
			$FS_{basesliding}$	$FS_{overturning}$	$FS_{rupture}$	$FS_{pullout}$
Static	Wrap		4.16	5.34	4.98	8.69
	Rigid		4.16	5.34	2.00	4.34
Dynamic	Wrap	0.2 g	1.80	1.78	4.90	8.27
		0.3 g	1.48	1.43	4.87	7.94
	Rigid	0.2g	1.80	1.79	1.97	1.95
		0.3g	1.48	1.43	1.95	1.61

6.2 FUNDAMENTAL FREQUENCY OF MODEL WALLS

The fundamental frequency (FF) of the wall systems are estimated by theoretical and numerical methods. The theoretical fundamental frequency (f_{11}) for two dimensional models is estimated as per Equation 6.1 (Wu 1994) that introduces a shape factor (*GF*). f_1 is the fundamental frequency of equivalent one dimensional (1-D) linear elastic model which is estimated based on height (*H*), shear modulus (*G*) and density (ρ) of soil according to Equation 6.2. The shape factor (Eq. 6.3) takes into account the height (*H*) and width (*B*) of the two dimensional (2-D) model and Poisson's ratio of the (υ) of the medium

$$f_{11} = GF.f_1 \tag{6.1}$$

$$f_1 = \frac{1}{4H}\sqrt{\frac{G}{\rho}} \tag{6.2}$$

$$GF = \sqrt{1 + \left(\frac{1}{2-\vartheta}\right)\frac{H}{B}} \tag{6.3}$$

The average shear modulus of rigid faced wall is 3.50×10^4 kPa and that of wrap faced wall is 1.35×10^4 kPa. The reduction in shear modulus in wrap faced wall is due to low confining pressure developed in wrap-faced wall for its flexible facing. The fundamental frequency of wall for a height of 6 m has been evaluated as 7.07 Hz for rigid faced wall and 4.38 Hz for wrap faced wall as per Wu's (1994) equation. The fundamental frequency is also determined from free vibration response of the numerical model after a small dynamic excitation as suggested by Zarnani and Bathurst (2009). The FF values obtained by this method are 6.81 Hz and 3.98 Hz for rigid-faced and wrap-faced walls, respectively. The model wall parameters and fundamental frequency values are summarized in Table 6.2. For the rigid-faced walls of 3 m high is also considered and FF is found to be about 11.98 Hz.

Table 6.2 Fundamental frequency values of reinforced soil wall models

Type of wall	Height	Average shear modulus (kPa)	Density (kg/m^3)	Theoretical (Wu's method) Hz	Numerical ($FLAC^{3D}$) Hz
Rigid-faced	6m	3.50×10^4	1600	7.07	6.81
	3m	2.41×10^4	1600	11.74	11.98
Wrap-faced	6m	1.35×10^4	1600	4.38	3.98

6.3 EARTHQUAKE GROUND MOTIONS

The full scale wrap and rigid-faced reinforced soil retaining wall models are subjected to five real earthquake motions. Ground motions recorded during 1966 Parkfield, 1976 Friuli, 1989 Loma Prieta, 1995 Kobe, and 2001 Bhuj earthquakes, having moment magnitude values ranging from 6.1 to 7.6, are selected for the study. Fig. 6.1 shows actual acceleration time histories of earthquake ground motions. It can be seen from the figure that these different ground motions are with different peak ground acceleration (PGA) levels, durations and frequency contents. Details about all the five earthquake ground motion records are listed in Table 6.3. From the table it can be seen that PGA values are in the range of about 0.1 g to 0.82 g. It is also to be noted that, having the same moment magnitude (M_w) value of 6.9, Loma Prieta earthquake and Kobe earthquakes showed very different PGA values as 0.25 g and 0.82 g, respectively, as well different durations. This shows the importance of consideration of real earthquake ground motions which may be different with different frequency content and their magnitudes.

To study the frequency effects of real earthquake ground motions, on the seismic behavior of the full scale models, PGAs of all the five earthquake ground motions are scaled to one PGA value of 0.3g. Further, to eliminate the ground motions duration effect, equal duration of 10 s, comprising the significant acceleration

amplitudes (as shown within dotted lines in Fig. 6.1(a)) are considered for the simulations. The scaled ground motions of different earthquakes (with PGA of 0.3g and duration of 10 s) are shown in Fig. 6.1(b). Fig. 6.1(c) shows the frequency content of the scaled earthquake acceleration histories through FFTs (Fast Fourier Transformations). It can be observed from the figure that the ground motions exhibit different predominant frequencies ranging from 0.673 Hz for Loma Prieta EQ to 5.437 Hz for Parkfield EQ.

Table 6.3 Ground motion parameters of actual earthquake records

Sl No.	Earthquake	Date	Ground station	Duration (s)	PGA (g)	PGV (cm/sec)	PGD (cm)	M_w
01	Parkfield	28/06/1966	CMDS station 1014	43.89	0.138	6.84	2.67	6.1
02	Friuli	06/05/1976	Unknown	20.00	0.479	31.24	7.49	6.5
03	Loma Prieta	18/10/1989	Emeryville	20.53	0.249	43.30	9.60	6.9
04	Kobe	16/01/1995	Unknown	40.00	0.818	90.35	153.9	6.9
05	Bhuj	26/01/2001	Ahmedabad	133.525	0.099	13.06	7.94	7.6

6.4 MODEL RESPONSE FOR EARTHQUAKE MOTIONS

Scaled earthquake ground motions are applied as input excitations at the base of rigid-faced and wrap-faced reinforced soil wall models and responses are observed in terms of accelerations, displacements and strains. Fig. 6.2 presents input acceleration and acceleration history responses, obtained at top of backfill (at 6 m elevation and at 1 m away from the facing) for different earthquakes. Fig. 6.3 presents Fast Fourier Transformations (FFT) of input accelerations and FFTs of acceleration responses obtained at top of backfill for different earthquakes.

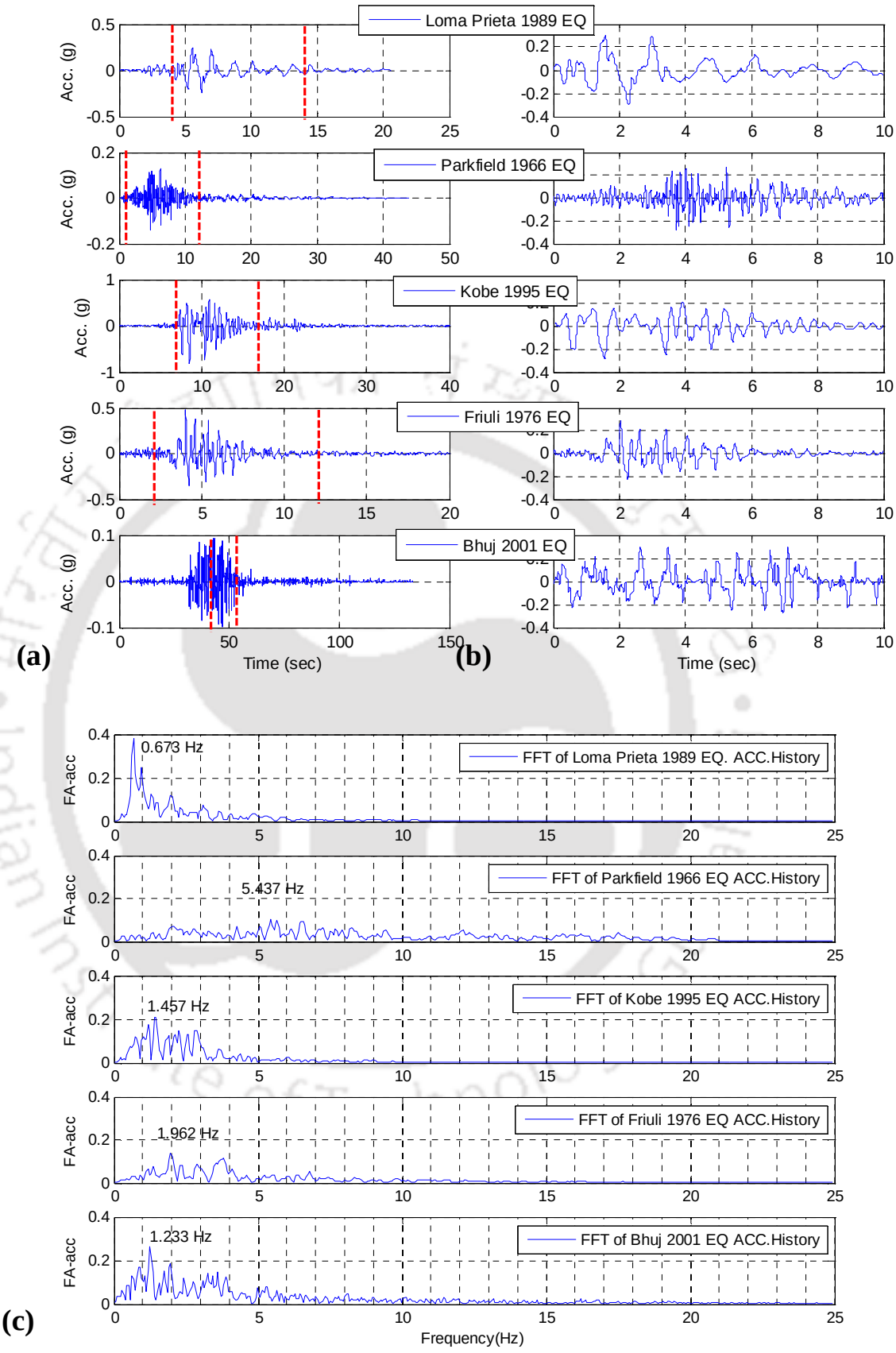

Fig. 6.1 Earthquake ground motion records (a) Actual histories; (b) Scaled histories for 10 second duration and 0.3 g PGA and, (c) FFTs of the scaled ground motions

It is seen from the figures that accelerations are significantly amplified at the top surface of both the walls. Peak accelerations observed at the surface, are within the range of 0.4 g to 1 g for different base earthquake motions having the same (0.3 g) peak acceleration. From the FFT spectra, it is noted that for rigid-faced walls the peak values of frequency curves are obtained almost in a narrow range of frequency values (6.5 to 6.8 Hz) against different predominant frequency values of the input motion at base of the wall. Similarly, the peak values of frequency curves for wrap-faced walls are in a narrow range of 3.7 to 4.0 Hz. With the fundamental frequency of the wall systems considered, it can be inferred that the narrow range of predominant frequency values are very close to the FF values. From this observations, it can be stated that frequency content close to the natural frequency of the system will be amplified the most and influence the response of the system. This can also be depicted in terms of transfer functions as shown in Fig. 6.4. Transfer function (TF) is a measure of amplification of amplitudes corresponding to different frequencies of input signal to the output signal. Mathematically, TF at a given frequency *(f)* is defined by Eq. 6.4 (Kay 1988) where P_{io} is the cross power spectral density (Welch 1967) of input signal (*i*, base acceleration) and output signal (*o*, acceleration at top); and P_{ii} is the power spectral density (PSD) of input signal (*i*, base acceleration).

$$TF_{io}(f) = \frac{P_{io}(f)}{P_{ii}(f)} \qquad 6.4$$

Fig. 6.4 shows the PSDs of input acceleration at base (A0) and at top of backfill (A3) along with its transfer function for Loma Prieta, Parkfield and Bhuj earthquakes, for rigid-faced walls. It is observed from the figure that frequency corresponding to the maximum amplification at top of backfill is 6.9 Hz for Loma Prieta EQ, 6.6 Hz for Parkfield EQ and 6.9 Hz for Bhuj EQ. Similarly results for wrap-faced walls

Earthquake	Input Ground motion	Response of rigid-faced walls	Response of wrap-faced walls
Parkfield	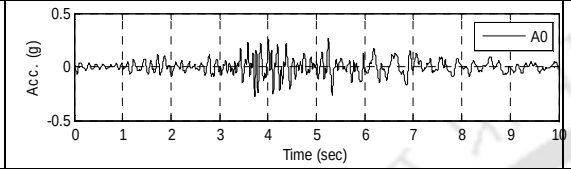	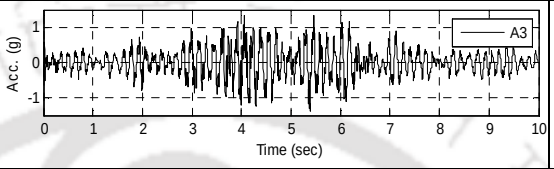	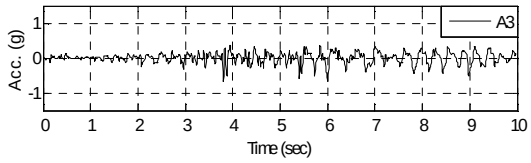
Friuli	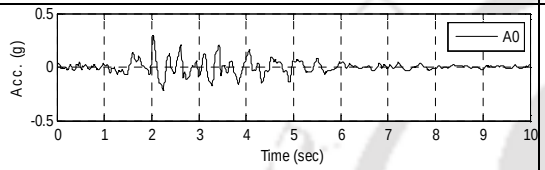	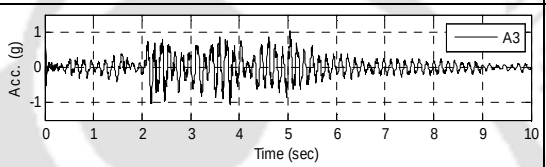	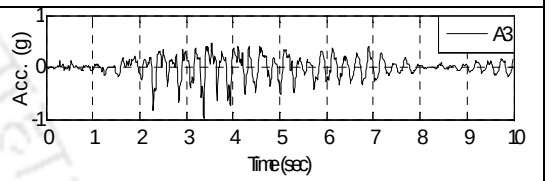
Loma Prieta	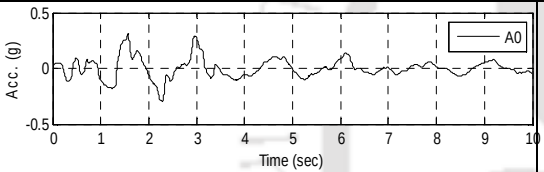	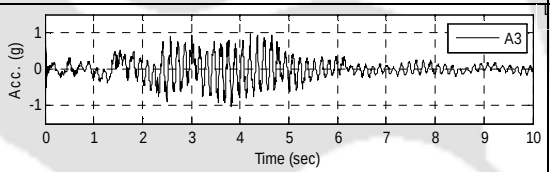	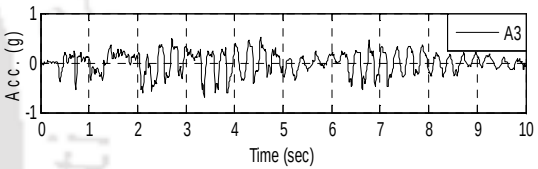
Kobe	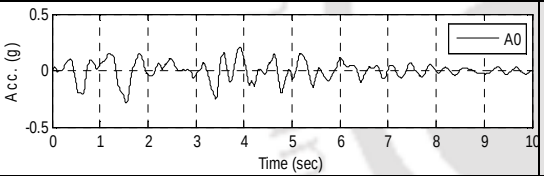	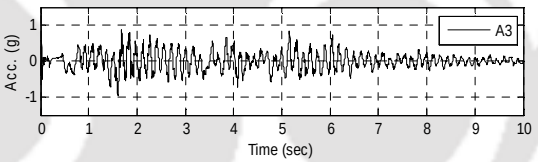	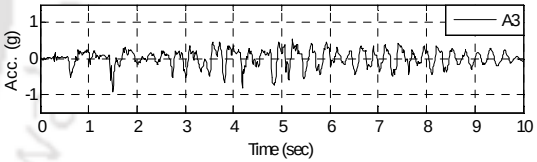
Bhuj	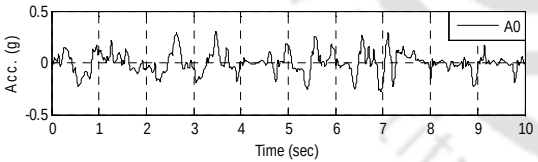	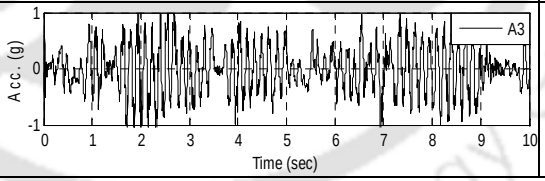	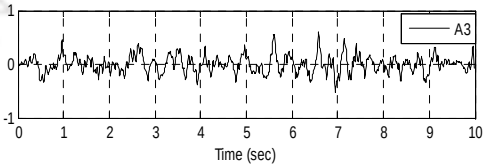

Fig. 6.2 Acceleration applied at base of model (A0) and acceleration recorded at top of backfill (A3) for rigid and wrap-faced walls for different earthquakes

Earthquake	FFT of input motion	FFT of response for rigid-faced walls	FFT of response for wrap-faced walls
Parkfield	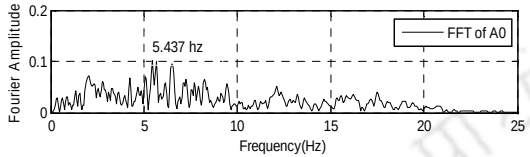	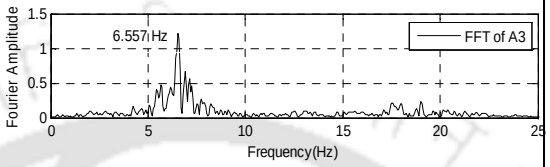	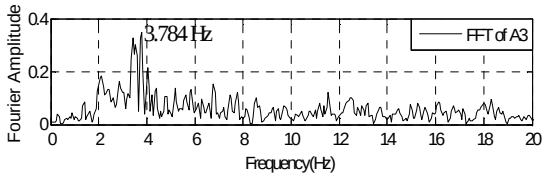
Friuli	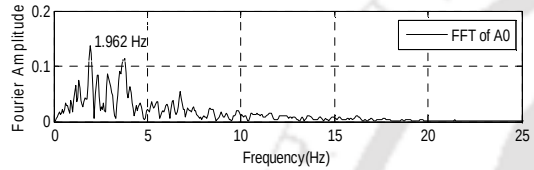	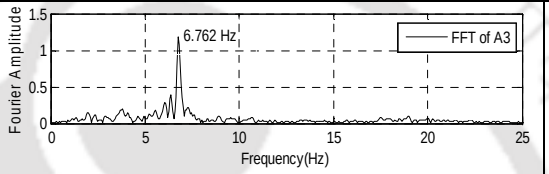	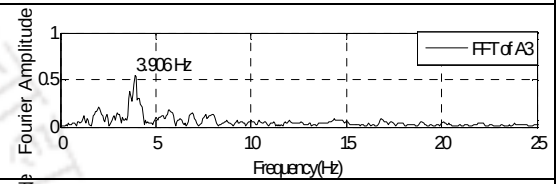
Loma Prieta	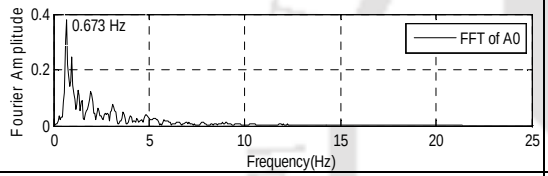	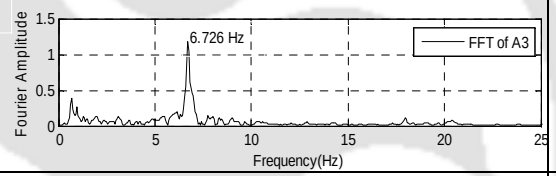	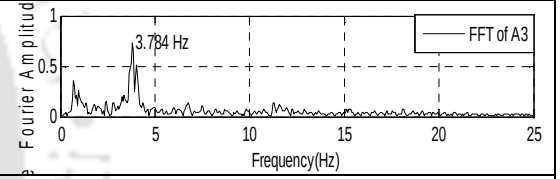
Kobe	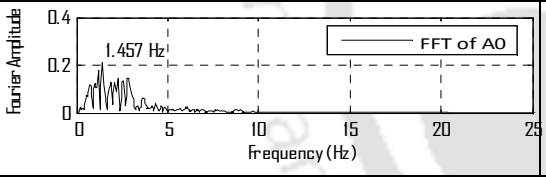	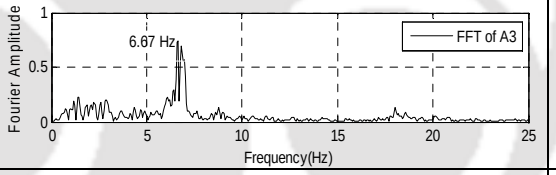	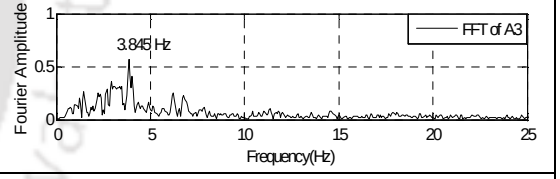
Bhuj	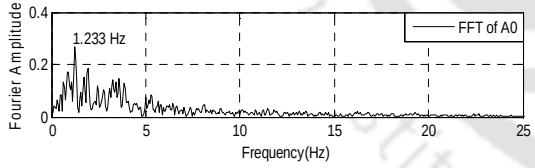	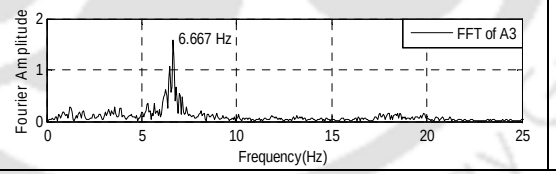	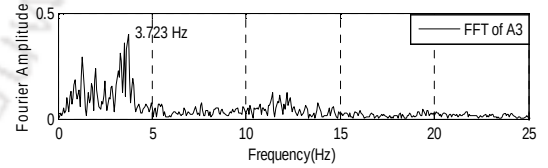

Fig. 6.3 Fast Fourier Transformation (FFT) of acceleration applied at base of model (A0); and recorded at top of backfill (A3) for rigid and wrap-faced walls for different earthquakes

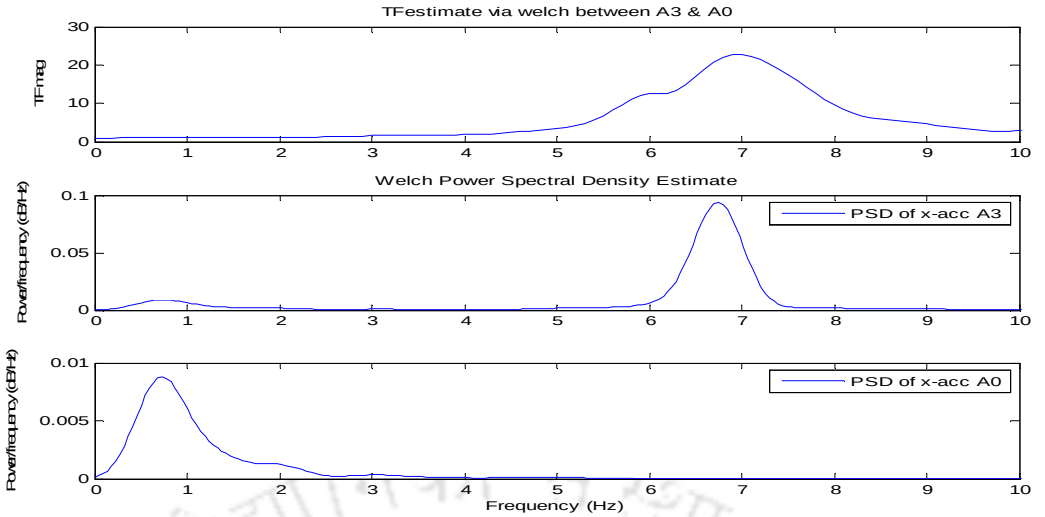

(a)

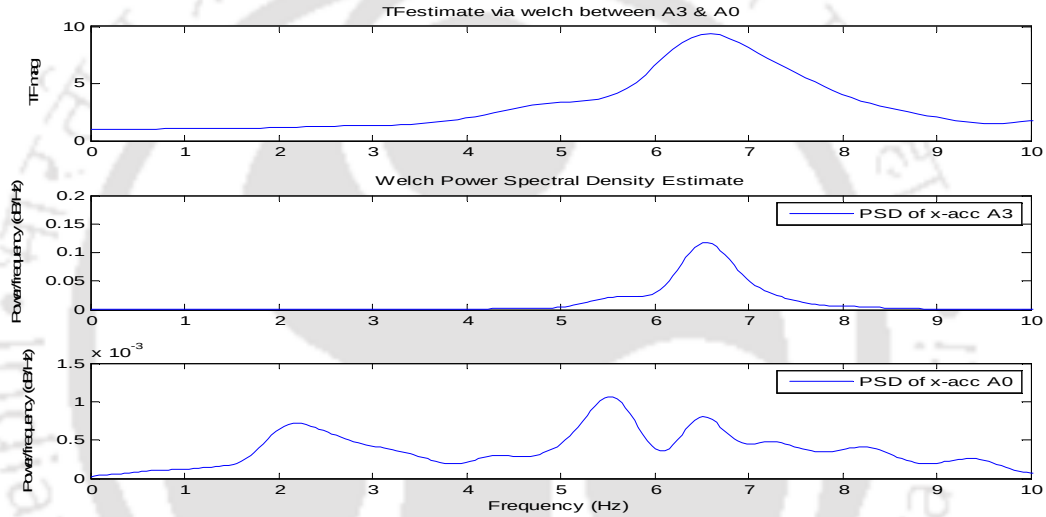

(b)

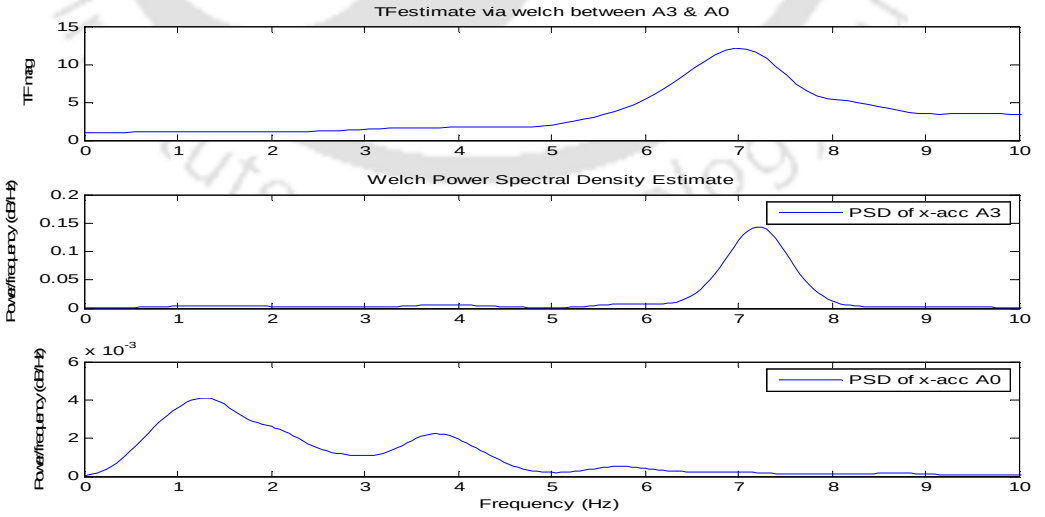

(c)

Fig. 6.4 Transfer functions between accelerations at base of wall (A0) and top of backfill (A3) for (a) Loma Prieta, (b) Parkfield and (c) Bhuj earthquakes

subjected to Parkfield and Bhuj earthquakes are shown in Fig. 6.5. The maximum amplification at top of backfill is at 3.7 Hz for Parkfield EQ and 3.6 Bhuj EQ. The amount of magnification of acceleration at the top of backfill is much higher for rigid-faced reinforced walls with respect to wrap-faced reinforced soil walls.

To verify the effect of natural frequency of the wall system, which is mainly depending on the height of model wall, a rigid-faced wall model is analyzed with 3 m height. Natural frequency of this model wall is about 12 Hz (Table 6.2).

Fig. 6.6 shows the input acceleration at base of wall and corresponding acceleration at top of backfill (at 3 m elevation) and their Fourier amplitude spectrum of 3 m high wall subjected to scaled Bhuj earthquake excitation. It is observed from the figure that the FFT at top of backfill shows higher amplification amplitude at a frequency of 11.92 Hz. This frequency value is very near to the fundamental frequency of 3m high wall model. Fig. 6.7 shows the PSDs of input acceleration at base (A0) and at top of backfill (A3) along with its transfer function in 3 m high rigid-faced wall for Bhuj earthquake. The maximum transfer function magnitude is observed near the fundamental frequency of the reinforced soil wall, i.e around 12 Hz. So, together with the observations presented in Fig. 6.2 to Fig. 6.7, it can be stated that, when a retaining wall is being subjected to real earthquake excitation, which contains different frequency content, amplitudes at frequency close to the fundamental frequency of the wall will be amplified the most.

Further, the results of rigid-faced walls, in the form of variations of horizontal displacement, RMSA amplification factors and horizontal pressures along height of the wall after different dynamic excitations are presented in Fig. 6.8(a). A general observation from the figure is that horizontal displacements and acceleration amplification (RMSA factors) profiles are different for different earthquake

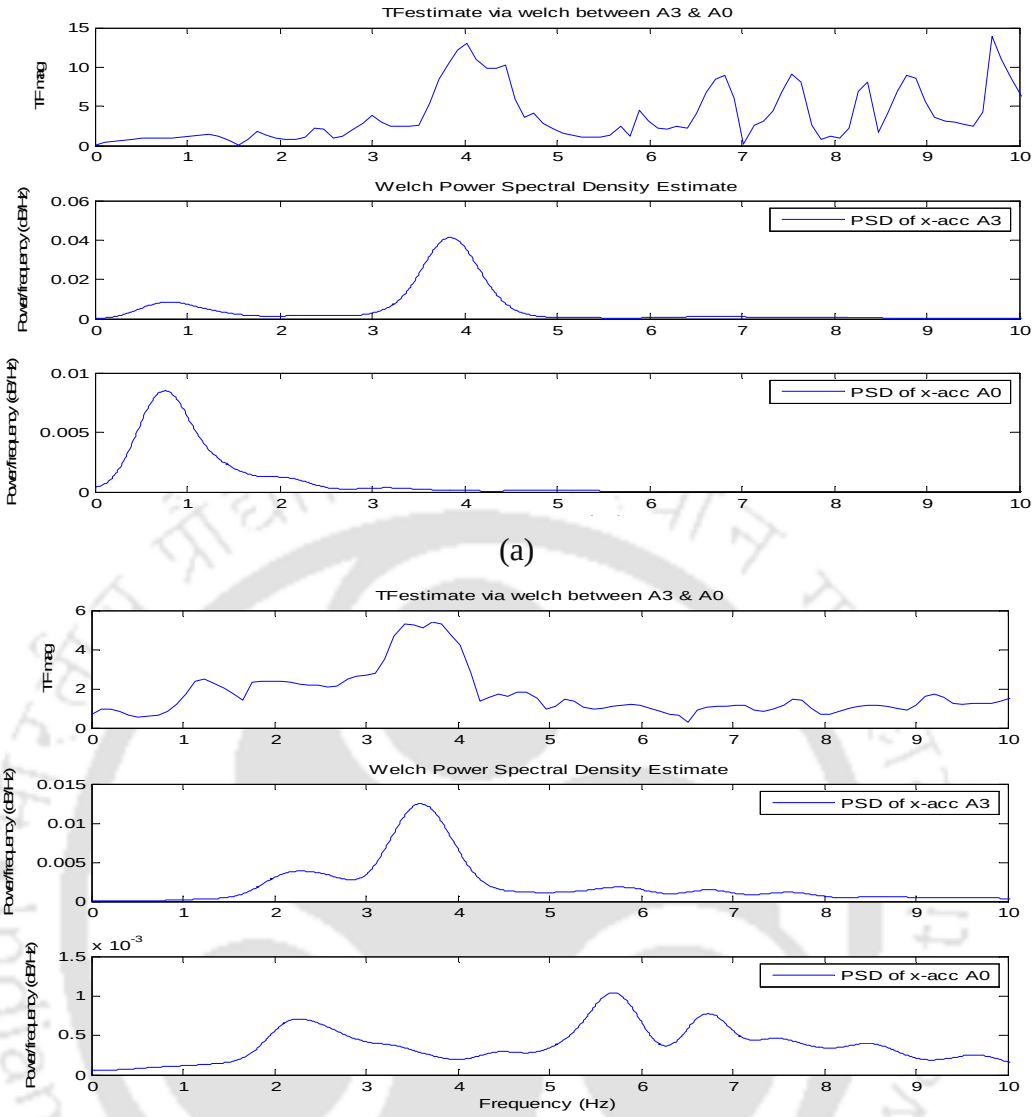

Fig. 6.5 Transfer function between accelerations at base of wrap-faced wall (A0) and top of backfill (A3) for (a) Loma Prieta and (b) Parkfield earthquakes

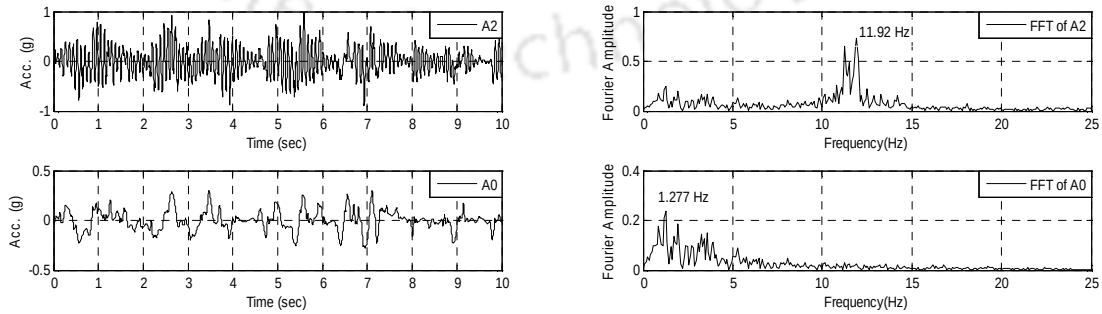

Fig. 6.6 Accelerations at base of model (A0) and at top of backfill (A2) and their corresponding FFTs of 3m high model subjected to scaled Bhuj earthquake motion

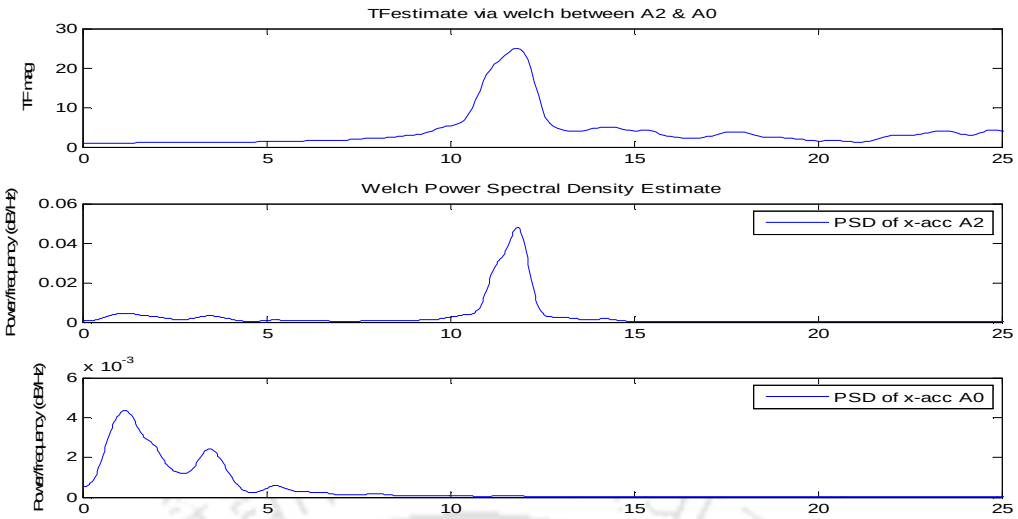

Fig. 6.7 Transfer function between accelerations at base of wall (A0) and top of backfill (A2) of 3 m high model subjected to scaled Bhuj earthquake motion

excitations; while horizontal pressures are more or less identical. Maximum horizontal displacements at the top of wall are ranged within 42.38 mm for Parkfield and 24.48 mm for Kobe earthquake. The maximum horizontal displacements are 39.32 mm, 31.34 mm and 30.52 mm observed respectively for Bhuj, Friuli and Loma Prieta earthquakes. From the plot, it is also observed that maximum RMSA amplification factor is 4.74 for Parkfield earthquake; and the minimum value is 2.19 for Kobe earthquake. The RMSA factors for Friuli, Bhuj and Loma Prieta earthquake are 3.74, 3.95 and 3.14, respectively. The reason for getting the maximum response for Parkfield earthquake can be justified with its predominant frequency which is 5.45 Hz. This is close to the fundamental frequency of the model considered. However, it could not be figured out reason for the relative responses with the other excitations.

No single ground motion parameter (predominant frequency, PGA, PGV, and PGA/PGV) is proportionally related to structure response as shown in Table 6.4. The transfer function gives the amplification of amplitudes at top of wall. It is observed from Fig. 6.4 that maximum transfer function magnitude is observed within a range of 5-9 Hz for rigid-faced walls. To establish possible relation with the frequency content

of the excitation, cumulative Fourier amplitudes of accelerations within the range of 5-9 Hz frequency (the zone of maximum transfer function magnitude) are evaluated, which are also presented in Table 6.4. It is observed that this parameter indicating the frequency content within 5 to 9 Hz is proportional to the response of the structure in terms of maximum displacement and PGA at the surface. This indicates that frequency content of the earthquake ground motion within the range of frequencies close to the fundamental frequency of the structure will influence the structure response. Further it is also to be noted that amplitudes corresponding to the natural frequency of the system will be amplified the most resulting higher amplification factors.

To verify the above statement, the horizontal displacements, RMSA amplification factors and horizontal pressures along the height of wall after different dynamic excitation for wrap-faced walls are plotted in Fig. 6.8(b). The cumulative Fourier amplitude near the fundamental frequency, within a range of 3-5 Hz (the zone of maximum transfer function) are evaluated from Fig. 6.5 and shown in Table 6.4. From the table it is observed that cumulative Fourier amplitudes are 0.77, 1.53 and 1.08 for Parkfield, Bhuj and Kobe earthquakes and corresponding horizontal displacements are 81.99 mm, 307.9 mm and 207.9 mm, respectively. So the amplitudes for the frequency content nearest to the fundamental frequency and within a range of increase in transfer function magnification are affecting the response of reinforcement soil walls.

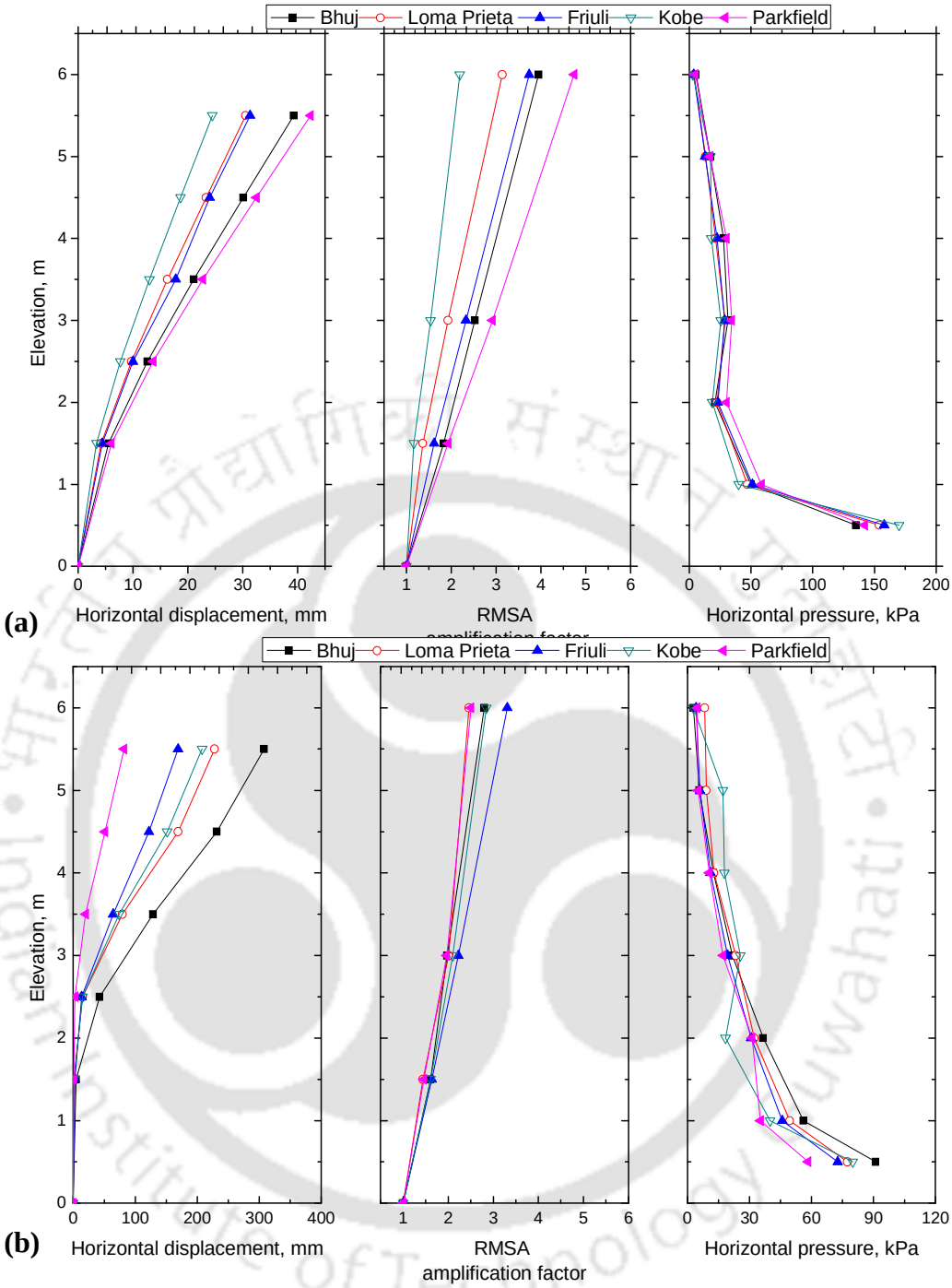

Fig. 6.8 Horizontal displacement, RMSA amplification factor and horizontal pressure for (a)rigid-faced wall (b)wrap-faced wall subjected to different scaled earthquake excitations

Table 6.4 Ground motion parameters and responses of scaled earthquake excitations

Earthquakes	Ground motion parameters						Responses					
	Predominant Frequency (Hz)	PGA (g)	PGV (m/sec)	PGA/ PGV	Cumulative FFT amplitudes within frequency		Predominant Frequency (Hz) of Acc. History at top of wall		Max. RMSA amplification factor		Horizontal displacement (mm)	
					5-9 Hz (RF)	3-5 Hz (WF)	RF	WF	RF	WF	RF	WF
Parkfield	5.437	0.3	0.137	2.190	1.795	0.77	6.557	3.784	4.74	2.51	42.38	81.99
Bhuj	1.233	0.3	0.353	0.850	1.183	1.526	6.667	3.723	3.95	2.8	39.32	307.9
Friuli	1.962	0.3	0.211	1.422	0.82	1.129	6.762	3.906	3.74	3.31	31.34	169.2
Loma Prieta	0.673	0.3	0.458	0.655	0.395	0.627	6.762	3.784	3.14	2.46	30.52	228.0
Kobe	1.457	0.3	0.291	1.031	0.456	1.081	6.670	3.845	2.19	2.85	24.48	207.9

RF: Rigid-faced wall

WF: Wrap-faced wall

Fig. 6.9(a) shows displacement histories at top of wall during dynamic excitation of different earthquakes of rigid-faced wall. The maximum displacements are ranging from 47.09 mm for Parkfield earthquake at 6.186 s, to 27.54 mm at 6.04 s for Kobe earthquake excitation. The maximum displacement and its time of occurrence for different earthquakes are different depending on frequency content of earthquake. The highest wall displacement is due to highest frequency content within 5-9 Hz frequency of Parkfiled earthquake. In similar way Fig. 6.9(b) shows displacement histories at top of wrap-faced wall during dynamic excitation of different earthquakes. The maximum displacements are 308 mm at 9.99 s for Bhuj earthquake and 83.51 mm at 9.417s for Parkfield earthquake. The highest wall displacement for wrap-faced wall is due to highest frequency content within range of 2.5-4.5 Hz for Bhuj earthquake.

The histories of incremental lateral pressures, at 0.125 m from base and near the wall for rigid-faced walls, during different earthquake excitations are shown in Fig. 6.10(a). The maximum incremental lateral pressure for Parkfield earthquake is 50 kPa at 5.38 s , for Friuli earthquake is 27.5 kPa and at 2.38 s, for Loma Prieta 30.9 kPa at 2.98 s, for Kobe earthquake is 28.7 kPa and at 3.97 s and for Bhuj earthquake 34.6 kPa at 2.67 s. The histories of incremental pressures acting at same location for wrap-faced walls, during different earthquake excitations are shown in Fig. 6.10(b). The maximum incremental lateral pressure for Bhuj earthquake is 22.32 kPa at 0.99s and for Parkfiled earthquake is 6.015 kPa at 7.107s.

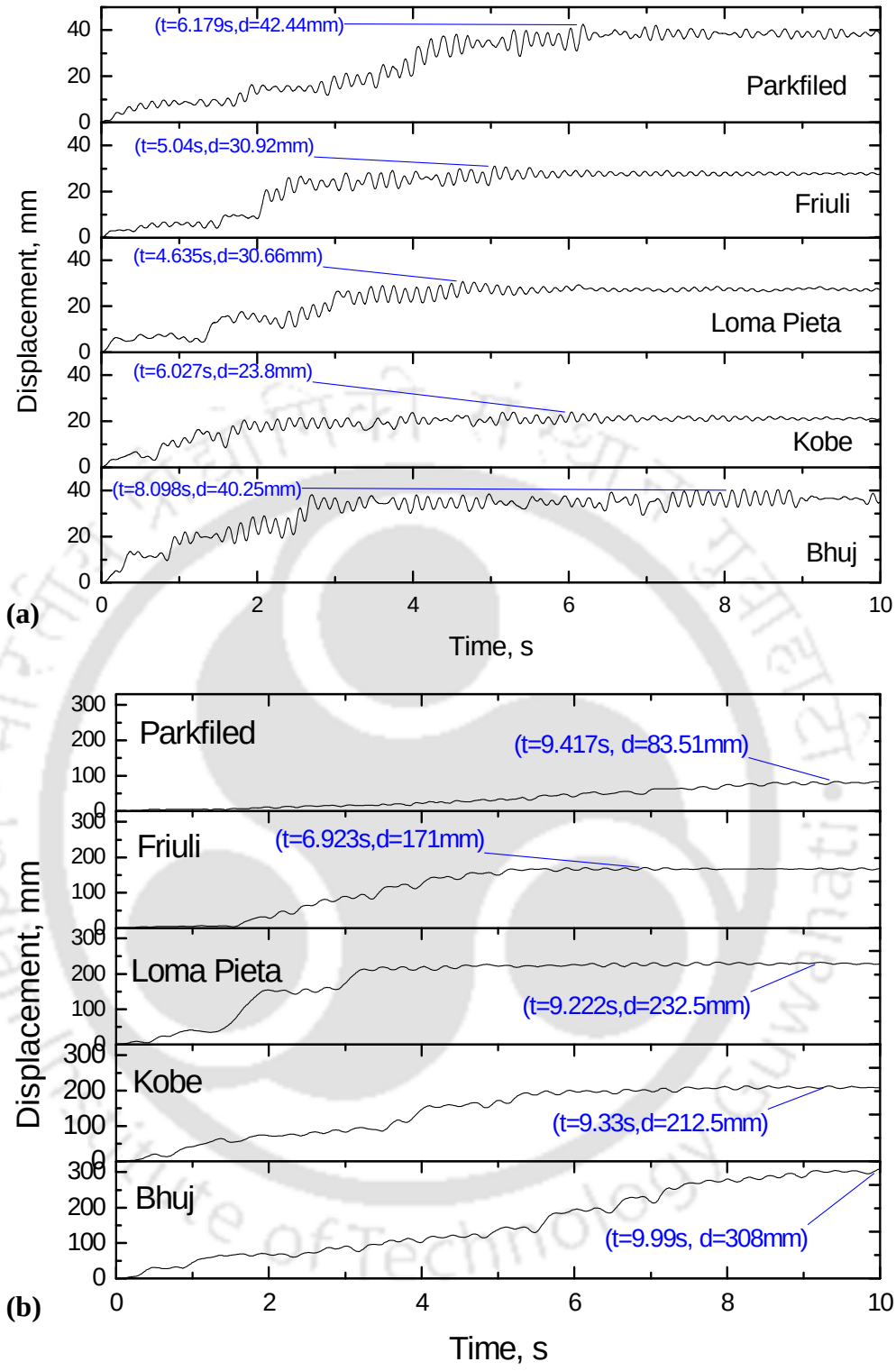

Fig. 6.9 Comparison of displacement histories during dynamic excitation of different earthquakes for (a) rigid-faced walls (b) wrap-faced walls

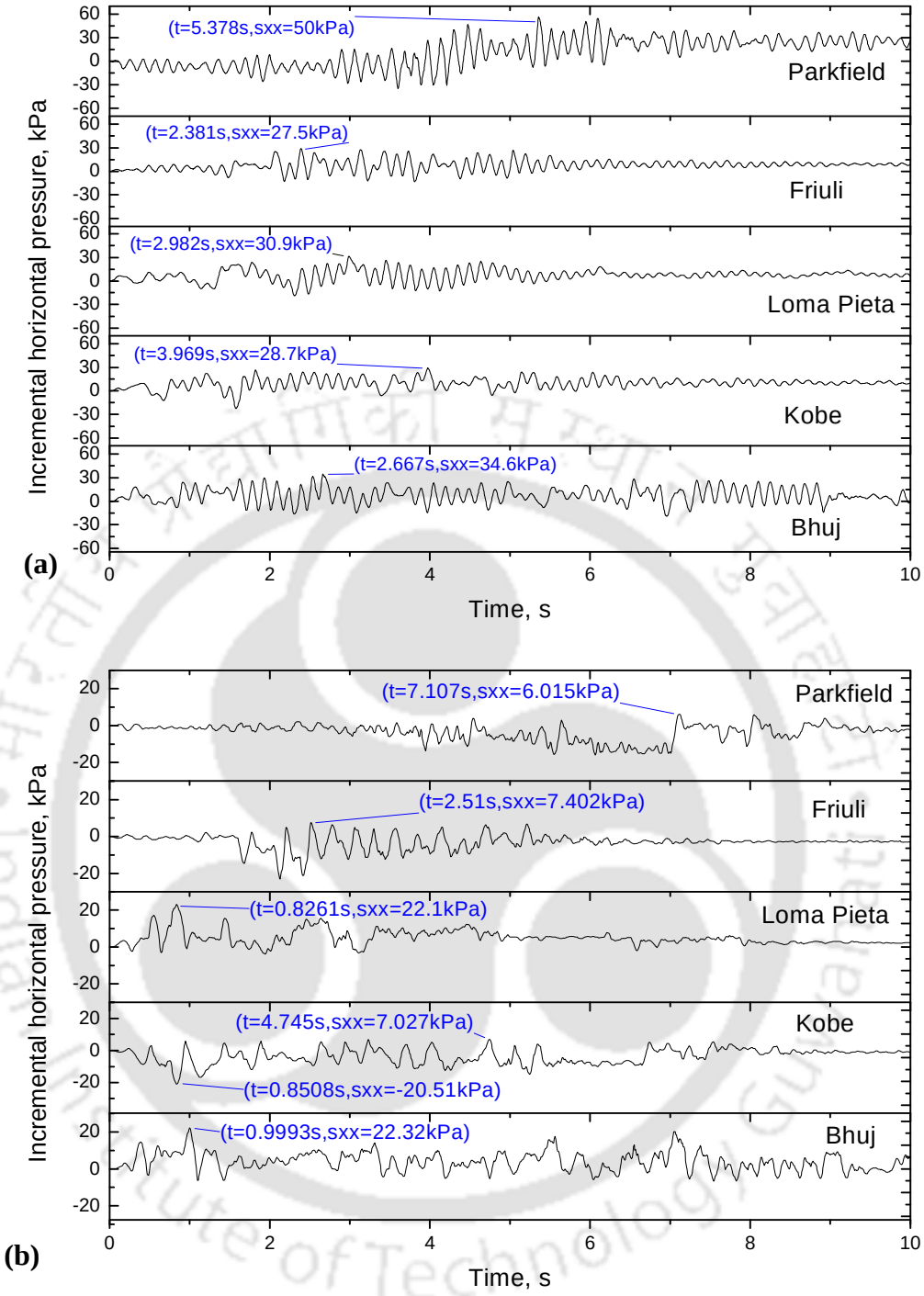

Fig. 6.10 Comparison of incremental horizontal pressure on (a) rigid-faced wall (b) wrap-faced wall during dynamic excitation for different earthquakes

It is seen from Fig. 6.9 and Fig. 6.10 that occurrence of peak values of displacement and incremental earth pressures are different for the same excitations. Similar such observations were also reported by Cakir (2013) and Athanasopoulos et

al. (2013). Further, it is also noted that lateral dynamic earth pressures are varied significantly, in spite of equal PGA values.

Comparison of contours of octahedral shear strains of rigid-faced walls subjected to different earthquake ground motions are presented in Fig. 6.11. It is observed that for same scaled ground acceleration of 0.3g the length of strained zones are different for different earthquake excitations. The incremental octahedral shear strains ($\Delta\gamma_{oct}$) along the length of backfill soil, between two reinforcing layers at different elevations for wall subjected to Kobe, Bhuj and Parkfield earthquake motions are shown in Fig. 6.12. Maximum $\Delta\gamma_{oct}$ near the wall facing are 0.89%, 1.16% and 1.30% for wall model subjected to Kobe, Bhuj and Parkfield earthquake, respectively, at elevations 5.25 m and similar higher soil strains near wall facing are also observed for other elevations. Another strain boundary is obtained by joining points having $\Delta\gamma_{oct}$ 0.3%. Two strained zones, as discussed in Chapter 5, can be seen in the Fig. 6.12 for different earthquake motions. The length of shear deformation zone in the backfill is different for wall model subjected to different earthquakes. The minimum and maximum length of shear deformation zones are observed for Kobe and Parkfiled earthquakes, respectively.

Similarly octahedral shear strain contour for wrap-faced walls subjected to different earthquake ground motions are presented in Fig. 6.13. The $\Delta\gamma_{oct}$, for wall subjected to Kobe, Bhuj and Parkfield earthquake motions are shown in Fig. 6.14.

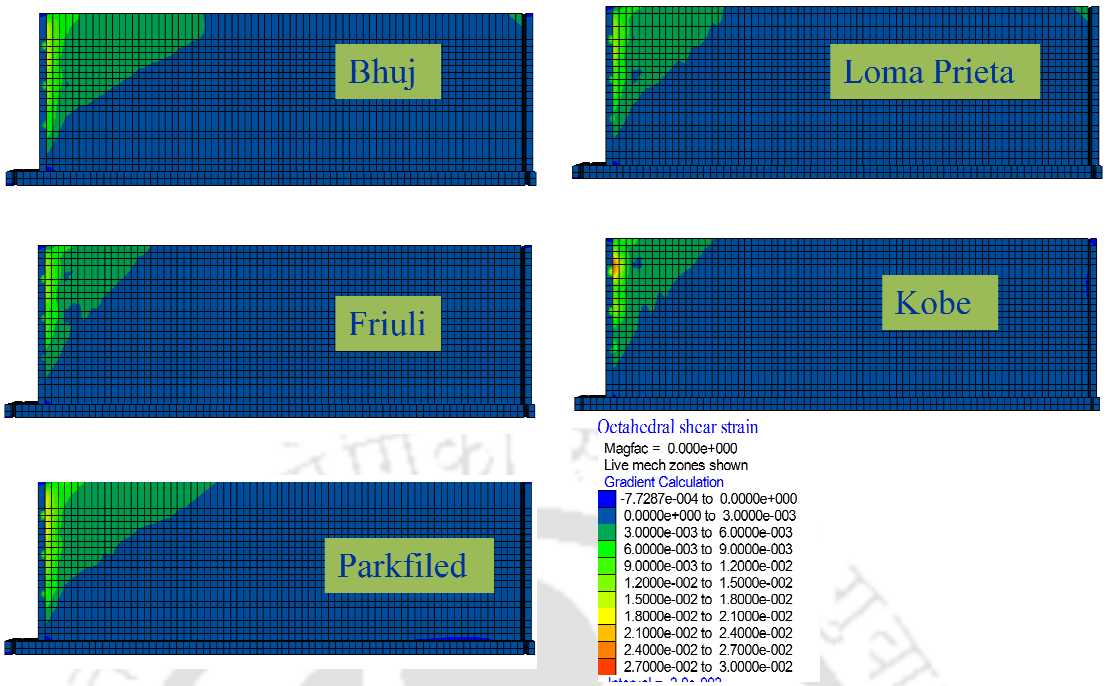

Fig. 6.11 Contours octahedral shear strains at the end of different excitations

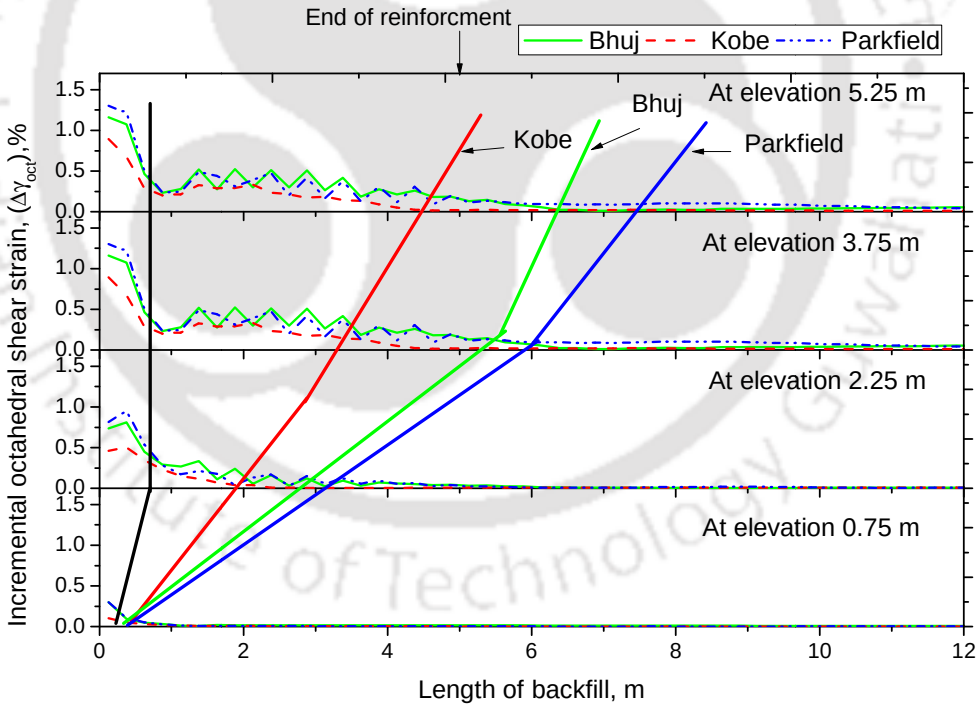

Fig. 6.12 $\Delta\gamma_{oct}$ along the length of backfill of rigid-faced wall subjected to Kobe EQ and Parkfield EQ

The increase in soil strain is observed at a distance of 2.0m from facing for wall subjected to three earthquakes. The increase in strain also observed near the end of reinforcement for three earthquakes. The maximum increase in soil strain near end

of reinforcement is observed for Bhuj and minimum for Parkfield earthquake. The extent of compound zone is the longest for Bhuj earthquake among three earthquakes. It is observed that for same excitation the extent of strained zones are different based on frequency content of excitation.

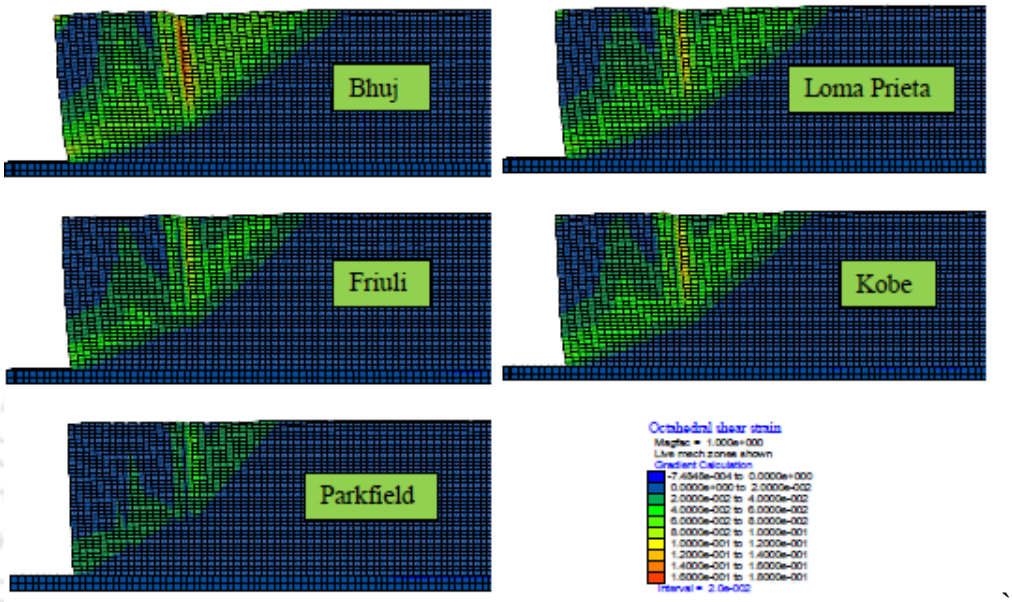

Fig. 6.13 Contours octahedral shear strains at the end of different excitations

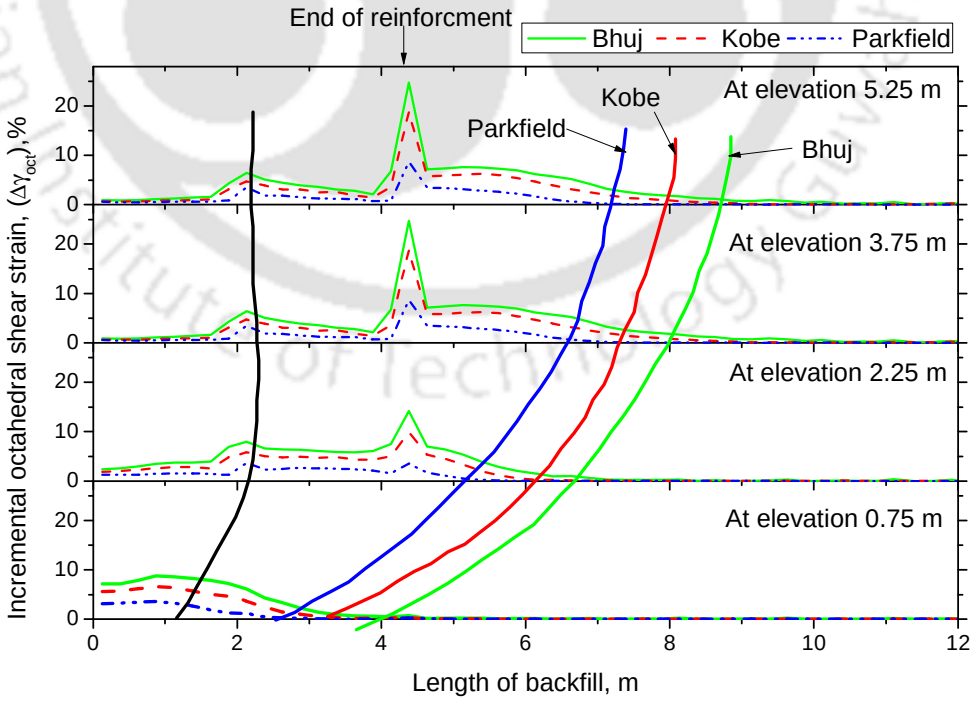

Fig. 6.14 $\Delta\gamma_{oct}$ along the length of backfill of wrap-faced wall subjected to Kobe EQ and Parkfield EQ

6.5 SUMMARY

Behaviors of rigid-faced and wrap-faced wall models subjected to scaled earthquake motions were discussed. The fundamental frequency rigid and wrap-faced walls were evaluated. Five Scaled earthquake ground motions are applied to numerical models of wrap-faced and rigid-faced reinforced soil walls and corresponding responses are studied. Response of the model walls were analysed in terms frequency content of the earthquake motion in relation to the fundamental frequency of the model walls. In spite of, same PGA value (0.3 g) and duration (10 s) different ground motions resulted in different displacements, acceleration and strains. No single ground motion parameter could relate the relative response of the model for different earthquakes. The maximum values of displacements and acceleration amplifications were observed for the earthquake motions having significant frequency content nearer to the fundamental frequency of the model wall. Cumulative Fourier amplitudes of input accelerations, within the frequency range of 0.7 to 1.3 times the FF of the model, could proportionally relate the response of the model.

Chapter 7. CONCLUDING REMARKS

7.1 SUMMARY OF THE THESIS

The thesis presented the numerical model studies of reinforced soil retaining walls and their dynamic behavior. The objective was to investigate the behavioral aspects of model walls with main focus on strains and displacements along with formation of deformation zone under variety of loading and wall configurations. Two types of GRS walls, flexible wrap-faced and full height rigid-faced reinforced soil walls were considered. Numerical models of the same were developed using FLAC^{3D} and validated with the identical physical model tests reported in literature. A chapter was devoted to provide the description of FLAC^{3D} and various model parameters adopted to simulate the wall models. The calibrated numerical models were used to develop full scale models different parametric studies were conducted. The results are analyzed in terms of horizontal, vertical displacement, octahedral shear strain and axial strain in reinforcement at end of dynamic excitations. The formation of deformation zones in reinforced soil walls based on displacements and strains were discussed. Two chapters, one on wrap-faced walls and the other on rigid-faced walls were presented with sinusoidal dynamic excitations. One other chapter considered both the walls together and using different earthquake ground motions which are rich in frequency content. The following section summarizes the conclusions drawn from this research work.

Limitations associated with rigid foundation base; extreme cases of flexible wrap facing and full height rigid facing; fixed surcharge pressure; pure cohesionless dry soil; fixed height; and limited excitation parameters etc. shall be taken into account while adopting/analysing the conclusions.

7.2 CONCLUSIONS

7.2.1 Studies on Wrap-Faced Reinforced Soil Walls

- The wrap-faced wall numerical model developed has been reasonably validated with the laboratory scale physical model results. The model was sensitive to different material properties like backfill friction and dilation angles, stiffness of reinforcement material and soil-reinforcement interface parameters.
- Laboratory scale numerical model (0.6m high, *H*) showed almost uniform horizontal displacements within the reinforced zone and high vertical settlements at the end of reinforcement. This indicated the rigid block movement of the reinforced zone during dynamic excitation.
- Full scale numerical model (H = 6 m) subjected to sinusoidal excitation, showed three distinct modes of deformation: shear deformation within reinforced zones, relative compaction near the end of reinforcement and compound deformation zones extending to the retained backfill.
- Peak values of octahedral shear strain in soil and axial strain in reinforcement confirms the formation of shear deformation zone. Increased vertical displacements at the end of reinforcement zone show the relative compaction zone, limited to the depth of 1/3 to 1/2 H from top. The compound deformation zone is the mobilized retained backfill that has been strained along with the reinforced zone.
- The strain developed in reinforcements during dynamic excitation, depends on overburden pressure on each layer of reinforcement and the extent of compound deformation zone into the retained backfill.

- From the parametric studies it is observed that all the parameters, i.e. backfill friction angle; stiffness of reinforcing material; number and length of reinforcement layer; are effected the displacements significantly. But, acceleration amplifications and horizontal pressures were less affected.
- The backfill friction angles affect the length of compound deformation zone in backfill soil. A deeper compound deformation zones for wrap-faced wall with lesser friction angle (softer backfill). As the higher friction angle backfill showed effective performance even in terms of effective reinforcement functioning, it is recommended to make sure of good compactive frictional backfill.
- The wall with longer reinforcement length restricts deformation due to lesser relative compaction near the end of reinforcement and less extent of compound deformation zone into unreinforced backfill. However, The longer reinforcement throughout height of the wall is not effective/economical. The wall with longer reinforcement (L_{rein}/H = 1.0H, H is height of wall) upto half of height at higher elevations and minimum reinforcement length (L_{rein}/H = 0.7H) at remaining height showed effective performance similar to the full height longer reinforcement.
- The wall with more numbers of reinforcing layers causing less shear deformation within reinforced zone and lesser horizontal displacements. But showed more relative settlement near end of reinforcement, which is due to the rigid block movement of the reinforced zone.
- The extent of compound deformation zones into the retained backfill is not affected by reinforcement stiffness. However, the shear deformations within

reinforced zone and reinforcement strains are more for wall with low reinforcement stiffness representing weak geotextile.

- The strains developed in reinforcements are influenced by strains developed within soil element, extent of compound deformation zones into retained backfill, interaction between soil and reinforcement, reinforcement stiffness and inertia force developed within reinforced zone.
- For the range of frequencies (3, 5, and 7 Hz) considered with 0.2 g acceleration, 3 Hz frequency excitation showed larger displacements and strains but equal extent of compound deformation zone. Further, higher excitations (larger acceleration) also showed increased displacements and strains along with deeper extent of compound deformation zone.

7.2.2 Studies on Rigid-Faced Reinforced Soil Walls

- The numerical model of laboratory scale rigid-faced walls developed is reasonably good in simulating dynamic responses and sensitive to the different material properties.
- In laboratory models, maximum shear strain developed was about 12%) near the facing for unreinforced wall, while it is about 1 %, near the end of reinforcement for reinforced wall. Displacements were significantly reduced by about 50-75% by reinforcing layers.
- Studies on full scale rigid-faced reinforced wall models showed two types of strained zones: high strain zone near the wall facing; and low strained zone extending into the retained backfill. Larger localised vertical and horizontal displacements near the wall facing indicate high strain zone (about 1 to 2%); Low strain zone was marked by the extent of the retained

backfill experiencing elastic strain level (around 0.3%). These zones differ from the zones identified in flexible wrap-faced wall model.

- The variation of length and stiffness of reinforcement, number of reinforcement layers; and backfill soil could marginally effect the strained zones, other than small changes near the wall facing at acceleration of 0.2g.
- The extent of deformation zones in reinforced and unreinforced backfill and development of reinforcement depends on level of seismic excitation.
- The facing stiffness affects the response of the rigid-faced wall. The horizontal displacement of wall and vertical displacement of the backfill increases with decrease in wall stiffness. The strain increments in soil are higher for model with lesser wall stiffness.
- Location of maximum strain varies depending on type of facing. The maximum axial tension developed in rigid-faced wall is near the facing. But in case of wrap-faced wall maximum axial tension is developed near the middle of reinforcement in all layers except lowest layer. The maximum axial tension developed near the facing at the lowest layer of reinforcement.
- Type of facing plays significant role on the response of reinforced soil retailing structures. The results compared for wrap-faced and rigid-faced walls; and rigid-faced walls with different facing stiffness values support this observation.

7.2.3 Reinforced soil wall subjected to different earthquake motions

- When a reinforced retaining wall is being subjected to real earthquake excitation, which contains different frequency content, amplitudes at

frequency close to the fundamental frequency of the wall will be amplified by the most.

- The response of the structure cannot be predicted by any single ground motion parameters such as predominant frequency, PGA, PGV and PGA/PGV. The amplitudes corresponding to the range of frequencies close to the fundamental frequency (FF) of the structure amplified the most, resulting higher amplification factors. Frequency content of earthquake ground motion close to the fundamental frequency (0.7 to 1.3 times FF) of the structure influence the structure response.
- The maximum displacement of the structure and horizontal pressure on wall and its time of occurrence during earthquake excitation for different earthquakes, having same PGA values, are different depending on frequency content of earthquake.
- The deformation zones formed for reinforced soil walls (wrap-faced and rigid-faced walls) subjected to different earthquake excitation is different based on frequency content of the earthquakes.
- The study reemphasizes the importance and complexity of actual earthquake ground excitations in analyzing the seismic behavior of important public infrastructure facilities. PGA or predominant frequency alone will not aid to predict the structures' performance. Different performance parameters like displacements, accelerations, strains, and pressures will attain their peak values at different time.

7.3 MAJOR CONTRIBUTIONS OF THE PRESENT STUDY

Major contributions from the study are summarized as below:

1. Investigation of location of deformations zones based on horizontal and vertical displacements and octahedral shear strains within backfill.
2. The study of variations of soil and reinforcement strains along the length of backfill and reinforcement and its influence on formation of deformation zones.
3. Type of facing plays significant role on the response of reinforced soil retaining structures. Location of maximum strains and deformation zones are influenced by facing stiffness.
4. The study reemphasizes that the response of the structure cannot be predicted by any single ground motion parameters such as predominant frequency, PGA, PGV and PGA/PGV of an earthquake. Frequency content of earthquake ground motion close to the fundamental frequency of the structure influence the structure response.

7.4 LIMITATIONS OF PRESENT STUDY

1. The foundation base was considered as rigid.
2. The surcharge pressure was fixed. The models with different surcharge pressures are not considered.
3. Pure dry cohesionless soil was considered as backfill soil.
4. Limited duration and PGA of earthquake excitations were considered.
5. The walls with other types of reinforcements are not considered for the present study.
6. Full scale model simulations were conducted only for one selected height.

7.5 SCOPE FOR FUTURE RESEARCH

There is a scope for more detailed studies on the topic and further analysis to be done for the data presented in this thesis. The following are the recommendations for future work:

- Critical analyses of model studies (physical or numerical) with different types of facing (like modular block facing and panel facing which are semi-rigid in nature) to suggest design guidelines for incorporating facing stiffness component in the design.
- The model studies on reinforced soil walls resting on deformable foundations, with different facing systems, with higher surcharges and with different height can be performed to observe complete behavioural aspects and to generalise the conclusions.
- The backfill soil properties considered for reinforced and retained backfill are same. The model studies with different reinforced and retained backfill can be modelled and analysed.

REFERENCES

1. AASHTO (2002). *Standard specifications for highway bridges*, (17th Edition 2002), American Association of State Highway and Transportation Officials, Washington, DC, USA.

2. AASHTO (2004). *LRFD bridge design specifications*, SI units (3rd Edition), American Association of State Highway and Transportation Officials, Washington, DC, USA.

3. Ahmad, S.M., and Choudhury, D. (2008). Pseudo-dynamic approach of seismic design for waterfront reinforced soil-wall. *Geotextile and Geomembranes*, 26, pp. 291-301.

4. Ahmad, S.M. and Choudhury, D. (2012). Seismic internal stability analysis of waterfront reinforced-soil wall using pseudo-static approach. *Ocean Engineering*, Vol. 52, pp. 83-90.

5. ASTM D 4595 (2005*). Standard Test Method For Tensile Properties of Geotextiles by the Wide Width Strip Method*. ASTM standard. West Conshohocken, Pennsylvania, USA.

6. ASTM D5261 (1996). *Standard Test Method for Measuring Mass per Unit Area of Geotextiles.* ASTM Standards, West Conshohocken, Pennsylvania, USA.

7. ASTM D6706-01 (2007). *Standard test method for measuring geosynthetic pullout resistance in soil.* ASTM standards, West Conshohocken, Pennsylvania, USA.

8. ASTM D6913-04(2009). *Standard test method for particle-size distribution of soils using sieve analysis.* ASTM Standards, West Conshohocken, Pennsylvania, USA.

9. Athansopoulos-Zekkos A, Vlachakis VS, Athansopoulos GA.(2013). Phasing-issues in the seimic response of yielding, gravity-type earth retaining walls- overview and result from a FEM study. *Soil Dynamics and Earthquake Engineering*; Vol. 55 pp.59-70.

10. Basha, B.M. and Babu, G.L.S. (2009). Seismic reliability assessment of external stability of reinforced soil wall using pseudo-dynamic method. *Geosynthetic International*, Vol. 16, No. 3, pp. 199-215.

11. Basha, B.M. and Babu, G.L.S. (2010). Optimum Design for External Seismic Stability of Geosynthetic Reinforced Soil Walls: A Reliability Based Approach. *Journal of Geotechnical and Geoenvironmental Engineering ASCE*. Vol. 136, No. 6, pp.797-812.

12. Basha, B.M. and Babu, G.L.S. (2011). Seismic reliability assessment of internal stability of reinforced soil walls using pseudo-dynamic method. *Geosynthetics International* Vol.18 No.5, pp.221-241.

13. Bathurst, R.J., Cai, Z. (1995). Pseudo-static seismic analysis of geosynthetic-reinforced segmental retaining wall, *Geosynthetic International*, Vol. 2, No. 5, pp. 787-830.

14. Bathurst, R.J., Hatami, K. (1998). Seismic response analysis of a geosynthetic-reinforced soil retaining wall. *Geosynthetic International*, Vol. 5, No. 1-2, pp. 127-166.

15. Bathurst, R. J., Hatami, K. and Alfaro, M. C. (2002). Geosynthetic reinforced soil walls and slopes: seismic aspects. *Chapter 14, Geosynthetics and Their Applications*, S. K. Shukla, (ed.), Thomas Telford, London, pp. 327–392.

16. Bathurst, R.J, Allen. T.M. and Walters, D.L. (2005). Reinforcement Loads in Geosynthetic Walls and the Case for a New Working Stress Design Method, *Geotextiles and Geomembranes*, Vol. 23, pp. 287-322.

17. Bergado, D.T., Bukkanasuta, A. and Balasubramaniam, A.S. (1986). Laboratory pull-out tests using bamboo and polymer geogrids including a case study. *Geotextiles and Geomembranes* 5, pp.153-189.

18. BS 8006 (1995). *Code of practice for strengthened/reinforced soils and other fills*. Publication no. BS8006-1995, British Standards Publication.

19. BS 8006 (2010). *Code of practice for strengthened/reinforced soils and other fills*. Publication no. BS8006-1-2010, British Standards Publication.

20. Burke, C., Ling H.I. and Liu H. (2004). Seismic response analysis of a full scale reinforced soil retaining wall, *Proc. 17th ASCE Engineering Mechanics conference*, June 13-16, 2004, pp. 1-6.

21. Cai Z., Bathurst R.J. (1995). Seismic response analysis of geosynthetic reinforced soil segmental retaining walls by finite element method. *Computers and Geotechnics*, 17, pp. 523-546.

22. Cai, Z. ,and Bathurst, R.J. (1996). Seismic induced permanent displacement of geosynthetic-reinforced segmental retaining walls, *Canadian Geotechnical Journal*, 33, pp. 937-955.

23. Cakir T. (2013). Evaluation of the effect of earthquake frequency content on seismic behavior of cantilever retaining wall including soil-structure interaction. *Soil Dynamics and Earthquake Engineering;* Vol. 45, pp.96-111.

24. Canadian Foundation Engineering Manual (CEFM) (2006), Canadian Geotechnical Society.

25. Canadian Highway Bridge Design Code (CHBDC)(2000). *Report No. CAN/CSAS6-00.2000*. The Canadian Standards Association (CSA International), Toronto, Ontario.

26. Chen, W.F and Mizuno, E. (1990).*Non-linear analysis in soil mechanics: theory and implementation.* Elsevier.

27. Choudhury, D., Nimbalkar S.S. and Mandal, J.N. (2007). External stability of reinforced soil walls under seismic conditions. *Geosynthetic International*, Vol. 14, No. 4: pp. 211-218.

28. Choudhury, D. and Ahmad, S. M. (2009). External stability of waterfront reinforced soil structures under seismic conditions using a pseudo-static approach. *Geosynthetics International*, Vol. 16, No. 1: pp. 1-10.

29. Coduto, D.P. (2002). *Geotechnical Engineering Principles and Practices*, Pearson Education Asia. 590 p.

30. Collin, J. G., Chouery-Curtis, V. E., and Berg, R. R. (1992). Field observations of reinforced soil structures under seismic loading. *Proc.,Int. Symp. on Earth Reinforcement Pract., Earth reinforcement practice*, H. Ochiai, N. Yasufuku, and K. Omine, eds., Vol. 1, Balkema,Rotterdam, The Netherlands, pp.223–228.

31. Coulomb C.A. (1776). Essai sur une application des regles des maximis et minimis a quelques problemes de statique relatifs a l'architecture. *Memoires de l'Academie Royale pres Divers Savants*, Vol. 7.

32. Duncan, J.M., Byrne, P., Wong, K.S. and Mabry, P. (1980). Strength, stress, strain and bulk modulus parameters for finite element analyses of stresses and movements in soil masses. *Report No. UCB/GT/80-01*, Department of Civil Engineering, University of California, Berkeley.

33. El-Emam, M.M., Bathurst, R.J., Hatami, K., Mashhour, M.M. (2001). Shaking table and numerical modeling of reinforced soil walls. *Proc. of the International Symposium on Earth Reinforcement*, Vol.1, Kyushu, Japan, pp.329-334.

34. El-Emam M.M. and Bathurst R.J. (2004), Experimental design, instrumentation and interpretation of reinforced soil wall response using a shaking table, *International Journal of Physical Modeling in Geotechnics*, 4, pp. 13-32.

35. El-Emam, M.M., Bathurst R.J. and Hatami K.(2004). Numerical modeling of reinforced soil retaining walls subjected to base acceleration. *Proc. of 13th World Conference on Earthquake Engineering,*Vancouver, B.C., Canada, paper no. 2621.

36. El-Emam, M. M. and Bathurst, R. J. (2005). Facing contribution to seismic response of reduced-scale reinforced soil walls. *Geosynthetics International*, Vol. 12, No. 3, pp. 215–238.

37. El-Emam, M. M. and Bathurst, R. J. (2007). Influence of reinforcement parameters on the seismic response of reduced-scale reinforced soil retaining walls. *Geotextiles and Geomembranes*, Vol. 25, No. 1, pp. 33-49.

38. Eliahu, U., and Watt, S. (1991). Geogrid-reinforced wall withstands earthquake. *Geotech. Fabrics Rep.*, 9(2), pp.8–13.

39. Eurocode 8. *Design of structures for earthquake resistance*. BS EN 1998.

40. Fakharian, K. and Attar, I.H. (2007). Static and seismic numerical modeling of geosynthetic-reinforced soil segmental bridge abutments. *Geosynthetics International*, Vol.14, No.4, pp.228-243.

41. Farrag, K., Juran, I. and Yalcin, B. (1993). Pullout resistance of geogrid reinforcements. *Geotextiles and Geomembranes*, 17, pp.157-170.

42. FHWA (2001). *Mechanically Stabilized Earth Walls and Reinforced Soil Slopes Design and Construction Guidelines*. Publication No. FHWA-NHI-00-043, US Department of Federal Highway Administration (FHWA).

43. FHWA (2010). *Mechanically Stabilized Earth Walls and Reinforced Soil Slopes Design and Construction Guidelines*, Vol. I & II. Publication No. FHWA-NHI-10-024, US Department of Federal Highway Administration (FHWA).

44. Gurung, N. and Iwao, Y. (1999). Pull-out test analysis for geo-reinforcement. *Geotextiles and Geomembranes* 17, pp. 157-170.

45. Hatami K., Bathurst R.J. (2000). Effect of structural design on fundamental frequency of reinforced-soil retaining walls. *Soil Dynamics and earthquake Engineering* , 19(2000), pp. 137-157.

46. Hatami, K. and Bathurst, R. J. (2005). Development and verification of a numerical model for the analysis of geosynthetic-reinforced soil segmental walls under working stress conditions. *Canadian Geotechnical Journal*, Vol. 42, No. 4, pp 1066-1085.

47. Hatami, K. and Bathurst, R. J., (2006). Numerical model for reinforced soil segmental walls under surcharge loading, *Journal of Geotechnical and Geoenvironmental Engineering*, Vol. 132, No. 6, pp 673-684.

48. Helwany, M.B. and McCallen, D. (2001). Seismic analysis of segmental retaining walls.II: Effects of facing details. *Journal of Geotechnical Engineering*, ASCE, 127(9), pp. 750-756.

49. Helwany, M.B., Budhu,M. and McCallen, D. (2001). Seismic analysis of segmental retaining walls.I: Model Verification. *Journal of Geotechnical Engineering*, ASCE, 127(9), pp. 741-749.

50. Ho, S. K. and Rowe, R. K. (1996). Effect of wall geometry on the behavior of reinforced soil walls. *Geotextiles and Geomembranes*, Vol. 14, No. 10, pp. 521–541.

51. Holtz, R.D. (2001). *Geosynthetic for soil reinforcement,* Ninth Spencer J. Buchanan Lecturer, College Station, Texas, November 9,2001, p.20.

52. Huang B., Bathurst R.J. and Hatami K. (2009). Numerical study of reinforced soil segmental walls using three different constitutive models, *Journal of Geotechnical and Geoenvironmental Engineering, ASCE,* Vol.135, No.10, pp.1486-1498.

53. Huang, C.C. (2000). Investigation of soil retaining structures damaged during Chi-Chi (Taiwan) Earthquake. *Journal of the Chinese Institute of Engineers,* Vol. 23, No. 4, pp. 417-428.

54. Huang, C. C., Chou, L. H. and Tatsuoka, F. (2003). Seismic displacements of geosynthetic-reinforced soil modular block walls. *Geosynthetics International*, Vol. 10, No. 1, pp. 2–23.

55. Huang, C.C. and Wang, W.C. (2005). Seismic displacement chart for the performance-based assessment of reinforced soil wall, *Geosynthetic International*, 12, No.4, pp.176-190.

56. Huang, C.-C and Wu, S.-H. (2006). Simplified approach for assessing seismic displacement of soil retaining walls. Part I : *Geosynthetic-reinforced modular block walls, Geosynthetic international*, 13, No.6, pp. 219-232.

57. Huang, C.-C., Wu, S.-H. and Wu, H.-J. (2009). Seismic displacement criterion for soil retaining walls based on soil strength mobilization. J*ournal of Geotechnical and Geoenvironmantal Engineering*, Vol. 135, No. 1, pp. 74-83.

58. Huang, C.-C. and Chen, Y.-S. (2012). Stability analysis of reinforced walls subjected to toe scouring. *Geosynthetic International*, Vol. 19, No. 4, pp. 284-291.

59. Huang, C.-C. (2013). Vertical acceleration response of horizontally excited reinforced soil walls. Geosynthetic International, 20, No. 1, pp.1-12.

60. IS 1893: Part-I (2002). Criteria for earthquake resistant design of structures. *Bureau of Indian Standards*, New Delhi.

61. IS: 2720 (Part-II)-1971. *Methods of tests for soils: Determination of shear strength parameters of a specimen in triaxial compression test*. Bureau of Indian Standards, New Delhi.

62. IS: 2720 (Part-IV)-1985. *Methods of test for soils: Grain size analysis*. Bureau of Indian Standards, New Delhi.

63. Ismeik, M. and Guler, E. (1998). Effect of Wall Facing on the Seismic Stability of Geosynthetic-Reinforced Retaining Walls. *Geosynthetics International*, Vol. 5, No. 2, pp. 41-53.

64. Itasca (2008). *Fast Lagrangian Analysis of Continua3D Version 3.1*, Itasca Consulting Group Inc., Minneapolis.

65. Juran, I., Knochenmus, G., Acar, Y. B. and Arman, A. (1988). Pull-out response of geotextiles and geogrids (Synthesis of Available Experimental Data).*Proc. of Symposium on Geotextiles for Soil Improvement, ASCE, Geotech. Special Publication* 18, pp. 92-111.

66. Karpurapu, R. and Bathurst, R. J. (1992). Numerical investigation of controlled yielding of soil-retaining wall structures. *Geotextiles and Geomembranes*, Vol. 11, No. 2, pp. 115-131.

67. Kay SM. (1988). Modern spectral estimation. Englewood Cliffs NJ; Prentice-hall.

68. Koerner, R.M. (1999). *Designing with Geosynthetics*. 4th Edition, Prenstice Hall Inc. NJ, 761 P.

69. Koerner, R.M. and Soong, Ye-Yang (2001). Geosynthetic reinforced segmental retaining walls, *Geotextile and Geomembranes*, Vol.19, pp 359-386.

70. Koerner, R.M. and Koerner, G.R. (2013). A database, statistics and recommendations regarding 171 failed geosynthetic reinforced mechanically stabilized earth (MSE) walls. *Geotextiles and Geomembranes* , 40, pp. 20-27.

71. Koga, Y., Ito, Y., Washida, S. and Shimazu, T., (1988). Seismic resistance of reinforced embankment by model shaking table tests. *Proc. International Geotechnical Symposium on Theory and Practice of Earth Reinforcement*, Fukuoka, Japan, pp. 413–418.

72. Koseki, J., Munaf,Y., Tatsuoka, F., Tateyama, M., Kojima, K. and Sato, T. (1998). Shaking and Tilt Table Tests of Geosynthetic-Reinforced Soil and Conventional-Type Retaining Walls. *Geosynthetics International*, Vol. 5, Nos. 1-2, pp. 73-96.

73. Koseki J., Bathurst, R.J., Güler, E., Kuwano, J. and Maugeri, M. (2006). Seismic stability of reinforced soil walls. *Proc. 8th International Conference. on Geosynthetics*, pp. 51 -78.

74. Koseki J., Tateyama, M., Watanabe, K. and Nakajima, S. (2007). Stability of earth structures against high seismic loads. Keynote Lecture, *Proc. 13th Asian Regional Conference on Soil Mechanics and Geotechnical Engineering*, Kolkata, India, Keynote Lecture, 23p.

75. Kramer, S.L. (1996). *Geotechnical Earthquake Engineering*, Prentice Hall Upper Saddle River, NJ. 653 p.

76. Kramer, S.L. and Paulsen, S.B.(2004). Seismic performance evaluation of reinforced slopes. *Geosynthetic International*, Vol.11 No.6, pp. 429-438.

77. Krishna, A.M., and Latha, G.M. (2007). Seismic response of warp-faced reinforced soil-retaining wall models using shaking table tests. *Geosynthetic International*, 14(6),pp. 355-364.

78. Krishna, A.M. (2008). *Seismic response of geosynthetic reinforced soil wall models using shaking table*. PhD Thesis, Department of Civil Engineering, Indian Institute of Science, Bangalore, India.

79. Krishna, A.M. and Latha, G.M. (2009). Seismic behavior of rigid-faced reinforced soil retaining wall models: reinforcement effect. *Geosynthetic International*, 16(5), pp. 364-371.

80. Krishna, A.M. and Latha, G.M. (2012). Modeling of dynamic response of wrap faced reinforced soil retaining wall. *International Journal of Geomechanics, ASCE*, Vol.12, No.4, pp. 437-450.

81. Kuhlemeyer, R.L and Lysmer, J. (1973). Finite element method accuracy for wave propagation problems, *Journal Soil Mechanics and Foundations Div.* ASCE, Vol. 99, No. SM5, pp. 421-427.

82. Latha, G.M. and Krishna, A.M. (2008). Seismic response of reinforced soil retaining wall models: Influence of backfill relative density. *Geotextiles and Geomembranes*, Vol.26, No.4, pp 335-349.

83. Lee, K.Z.Z., Chang, N.Y., and Ho, H.Y. (2010). Numerical simulation of geosynthetic-reinforced soil walls under seismic shaking. *Geotextile and Geomembranes*, 28, pp. 317-334.

84. Lee, K.Z.Z. and Chang, N.Y. (2012). Predictive modeling of seismic performances of geosynthetic-reinforced soil walls. *Geotextiles and Geomembranes*, 35, pp. 25-40.

85. Ling, H.I., Leshchinsky, D. and Perry, E.B. (1997). Seismic design and performance of geosynthetic –reinforced soil structures. *Geotechnique* 47(5), pp. 933-952.

86. Ling, H.I. (2001). Recent applications of sliding block theory to geotechnical design. *Soil Dynamics and Earthquake Engineering*, 21, pp. 189-197.

87. Ling, H.I., Leshchinsky, D. and Chou, N.N.S. (2001). Post-earthquake investigation on several geosynthetics-reinforced soil retaining walls and slopes during Ji Ji earthquake of Taiwan. *Soil Dynamics and Earthquake Engineering*, Vol 21, pp.297-313.

88. Ling, H. I. (2003). Chapter 25. A critical review of full-scale shaking table tests conducted on reinforced soil retaining walls. *Reinforced soil engineering: Advances in research and practice*, Marcel Dekker, New York, 491–510.

89. Ling, H.I., and Leshchinsky, D. (2003). Finite element parameter studies of the behavior of segmental block reinforced soil retaining walls. *Geosynthetics International*, Vol. 10, No. 3, pp. 77–94.

90. Ling, H.I., Liu, H., Kaliakin, V.N., Leshchinsky, D. (2004). Analyzing dynamic behavior of geosynthetic-reinforced soil retaining walls. *Journal of*

Geotechnical and Geoenvironmental Engineering, ASCE, 130(8), pp.911-920.

91. Ling, H.I. and Leshchinsky, D. (2005). Failure analysis of modular-block reinforced–soil walls during earthquake. *Journal of Performance of Constructed Facilities, ASCE,* Vol.19, No.2, pp.117-123.

92. Ling, H.I., Mohri,Y., Leshchinsky, D., Burke, C., Matsushima, K. and Liu, H. (2005a). Large scale shaking table tests on modular-block reinforced soil retaining walls. *Journal of Geotechnical and Geoenvironmental Engineering*, ASCE, Vol. 131 No.4, pp. 465-476.

93. Ling, H.I., Liu, H. and Mohri, Y. (2005b). Parametric studies on behavior of reinforced soil retaining walls under earthquake loading. *Journal of Engineering Mechanics, ASCE,* Vol.131, No. 10, pp. 1056-1065.

94. Ling, H.I., Yang, S., Leshchinsky, D., Liu, H. and Burke, C.(2010). Finite-element simulations of full scale modulur-block reinforced soil retaining walls under earthqu*ake loading. Journal of Engineering Mechanics, ASCE, Vol*. 136, No. 5, pp.653-661.

95. Liu, H. (2009). Analyzing the reinforcement loads of geosynthetics-reinforced soil walls subject to seismic loading during service life. *Journal of Performance of Constructed Facilities, ASCE,* Vol.23, No.5, pp.292-302.

96. Liu, H. and Ling, H.I. (2012). Seismic response of reinforced soil retaining walls and strain-softening of backfill soil. *International Journal of Geomechanics, ASCE,* Vol. 12, No.4, pp.351-36.

97. Liu, H., Wang X. and Song, E. (2011). Reinforcement load and deformation mode of geosynthetics-reinforced soil walls subject to seismic loading during service life. *Geotextiles and Geomembranes*, 29,pp.1-16.

98. Liu, H., Yang, G. and Ling, H.I. (2014). Seismic response of multi-tiered soil retaining walls. Soil Dynamics and Earthquake Engineering, 61-62, pp. 1-14.

99. Lo Grasso A.S., Maugeri M. and Recalcati, P. (2005). Seismic behaviour of geosynthetic-reinforced slopes with overload by shaking table tests. *Slopes and Retaining Structures under Seismic and Static Conditions*, ASCE Geotechnical Special Publication No. 140, CDROM.

100. Masing, G.(1926). Eignespannungen und verfestigung beim messing. *In: Second International Congress on Applied Mechanics, Zurich, Switzerland*, pp. 332–335.

101. Matsuo, O., Tsutsumi, T., Yokoyama, K. and Saito, Y. (1998). Shaking table tests and analyses of geosynthetic-reinforced soil retaining walls, *Geosynthetics International*, Vol. 5, Nos. 1-2, pp. 97-126.

102. Mojallal, M., Ghanbari, A. and Askari, F. (2012). A new analytical method for calculating seismic displacements in reinforced retaining walls. *Geosynthetic International*, Vol. 19, No. 3, pp. 212-231.

103. Mononobe N. and Matsuo H. (1929). Earthquake proof construction of masonry dam.. *Proceedings World Engineering Conference*, Vol.9, pp. 176.

104. Murata, O., Tateyama, M. and Tatsuoka, F. (1994). Shaking table tests on a large geosynthetic-reinforced soil retaining wall model. *Recent case histories of permanent geosynthetic-reinforced soil retaining walls*, F. Tatsuoka and D. Leshchinsky (eds.), Balkema, Rotterdam, The Netherlands, pp. 259–264.

105. Nakajima, S., Hong, K., Mulmi, S., Koseki, J., Watanabe, K. and Tateyama, M. (2008). Study on seismic performance of geogrid reinforced soil retaining walls and deformation characteristics of backfill. Proc. Of 4th Asian Regional Conference on Geosynthetics, Shanghai, China.

106. Nakanishi, A. and Sakaguchi, M. (1990). Seismic behavior of reinforced embankments by geotextiles. *Proc. of the 4th International Conference on Geotextiles, Geomembranes and Related Products*, The Hague, Netherlands, May 1990, Balkema, Vol. 1, pp.121.

107. NCMA (1997). Design Manual for Segmental Retaining Walls. *National Concrete Masonry Association*, Collin, J., Editor, Second Edition, Herndon, Virginia, USA.

108. NCMA (1998). Segmental Retaining Walls Seismic Design Manual. *National Concrete Masonry Association*, Bathurst, R.J., Editor, First Edition, Herndon, Virginia, USA.

109. Nimbalkar, S. S., Choudhury, D. and Mandal, J. N. (2006). Seismic stability of reinforced-soil wall by pseudo-dynamic method. *Geosynthetics International*, Vol. 13, No. 3, pp. 111–119.

110. Nishimura, J., Hirai, T., Iwasaki, K., Saito, Y., and Morikshima, M. (1996). Earthquake resistance of geogrid reinforced soil walls based on a study conducted following the southern Hyogo earthquake. *Proc., Int. Symp. on Earth Reinforcement Pract., IS-Kyushu '96, Earth Reinforcement Pract.*, H. Ochiai, N. Yasufuku, and K. Omine, eds., Balkema, Rotterdam, The Netherlands.

111. Nouri, H., Fakher, A. and Jones, C.J.F.P. (2008). Evaluating the effects of the magnitude and amplification of pseudo-static acceleration on reinforced soil slopes and walls using the limit equilibrium horizontal slices method, *Geotextile and Geomembranes*, 26, pp. 263-278.

112. Nova-Roessig, L. and Sitar, N. (2006). Centrifuge model studies of the seismic response of reinforced soil slopes. *Journal of Geotechnical and Geoenvironmental Engineering*,Vol.132,No.3,pp.388-400.

113. Okabe, S. (1924). General theory of earth pressure and seismic stability of retaining walls and dams. *Journal of Japanese Society of Civil Engineers,Tokyo*, Vol.12, No. 1.

114. Palmeira, E. M. and Gomes, R. C. (1996). Comparisons of Predicted and Observed Failure Mechanisms in Model Reinforced Soil Walls. *Geosynthetics International*, Vol. 3, No. 3, pp. 329-347.

115. Palmeira, E.M. (2004). Bearing force mobilization in pull-out tests in geogrids. *Geotextiles and Geomembranes*, Vol. 22, pp. 481-509.

116. Pamuk, A., Ling, H.I., Leshchinsky, D., Kalkan, E. and Adalier, K.(2004). Behavior of reinforced wall system during the 1999 Kocaeli (Izmit), Turkey, Earthquake, *Proc. of Fifth International Conference on Case Histories in Geotechnical Engineering*, New York, pp.3.45.

117. Perez, A. (1999). *Seismic Response of Geosynthetic Reinforced Steep Slopes*. Master of Science Thesis, University of Washington.

118. Perez, A. and Holtz, R. D. (2004). Seismic Response of Reinforced Steep Soil Slopes: Results of a Shaking Table Study. *Geotechnical Engineering for Transportation Projects*, ASCE Geotechnical Special Publication No. 126, pp. 1664-1672.

119. Prashanth, V., Bhattacharjee, A. and Krishna, A.M. (2011). Soil-Geosynthetics Interaction Behaviour in Oblique Direction. *Proc. International Conference on Advances in Geotechnical Engineering*, 7-9 November 2011, Perth, Australia.

120. PWRC. 2000. Design and construction manual for geotextile reinforced soil structures, Publics Works Research Center, Japan (in Japanese).

121. Race, R., and del Cid, H. (2001). Seismic performance of modular block retaining wall structures during the January 2001 El Salvador Earthquake. *Proc., Int. Geosynthetic Engineering Forum 2001*, Taipei, Taiwan, pp. 125–144.

122. Ramakrishnan, K., Budhu, M., and Britto, A. (1998). Laboratory Seismic Tests on Geotextile Wrap-Faced and Geotextile-Reinforced Segmental Retaining Walls. *Geosynthetics International*, Vol. 5, No. 1-2, pp. 55-71.

123. Rankine, W. (1857). On the stability of loose earth. *Philosophical Transactions of the Royal Society of London*, Vol. 147.

124. Reddy, G.V.N., Madhav, M.R., and Reddy, E.S. (2008). Pseudo-static seismic analysis of reinforced soil wall- effect of oblique displacement. *Geotextile and Geomembranes*, 26(2008), pp. 393-408.

125. Richardson G.N. and Lee K.L., (1975). Seismic design of reinforced earth walls, *Journal of Geotechnical Engineering Division*, ASCE, Vol. 101, No. GT2, pp. 167-188.

126. Richardson, G. N., Feger, D., Fong, A. and Lee, K. L. (1977). Seismic testing of reinforced earth walls. *Journal of the Geotechnical Engineering Division, ASCE*, Vol. 103, No. 1, pp. 1–17.

127. Rowe R. K. and Ho. S. K (1997). Continuous panel reinforced soil walls on rigid foundations. *Journal of Geotechnical and Geoenvironmental engineering*, Vol. 123, No. 10, pp. 912-920.

128. Rowe R. K. and Skinner G. D. (2001). Numerical analysis of geosynthetic reinforced retaining wall constructed on a layered soil foundation. *Geotextiles and Geomembranes*, Vol. 19, pp. 387–412.

129. RTA (2005). Design of reinforced soil walls, *QA specification R57*, Roads and Traffic Authority, New South Wales, Australia.

130. RTRI (2006). Design standard for railway earth structures, Railway Technical Research Institute, Japan (in Japanese).

131. Sabermahandi, M., Ghalandarzadeh, A. and Fakher, A. (2009), Experimental study on seismic deformation modes of reinforced-soil walls, *Geotextiles and Geomembranes* 27, pp. 121–136.

132. Sakaguchi, M., Muramatsu, M. and Nagura, K. (1992). A discussion on reinforced embankment structures having high earthquake resistance. *Proc. Of the International Symposium on Earth Reinforcement Practice*, IS-Kyushu '92, Fukuoka, Japan, Vol. 1, pp. 287–292.

133. Sakaguchi, M., Yamada, K. and Tanaka, M. (1994). Prediction of deformation of geotextile reinforced walls subjected to earthquakes. *Proc. of the 5th International Conference on Geotextiles, Geomembranes and Related Products*, Singapore, September 1994, Vol. 1, pp 521-524.

134. Sakaguchi, M. (1996). A study of the seismic behaviour of geosynthetic reinforced walls in Japan, *Geosynthetic International*, Vol. 3 No. 1 pp 13-30.

135. Sandri, D. (1994). Retaining walls stand up to the Northridge Earthquake. *Geotechnical Fabrics Report*, vol. 12, no. 4, pp. 30-31.

136. Sandri, D. (1997). A performance summery of reinforced soil structures in the greater Los Angeles area after the Northbridge earthquake. *Geotextile and Geomembranes*, Vol.15, No. 4-6, pp.235-253.

137. Shahu, J.T. (2007). "Pullout response of inextensible sheet reinforcement subject to oblique end-force". *Journal Geotechnical Geoenvironmental Engg.* 133(11), pp. 1440–48.

138. Shekarian, S., Ghanbari, A. and Farhadi, A. (2008), New Seismic parameters in the analysis of retaining walls with reinforced backfill. Geotextile and Geomembranes, 26, pp. 350-356.

139. Skinner, G.D. and Rowe, R.K. (2005). Design and behavior of a geosynthetic reinforced retaining wall and bridge abutment on a yielding foundation. *Geotextiles and Geomembranes*, Vol. 23, No. 3, pp. 234–260.

140. Subaida, E.A., Chandrakaran S. and Sankar, N. (2008). Experimental investigations on tensile and pullout behaviour of woven coir geotextiles. *Geotextiles and Geomembranes* 26, pp.384–392.

141. Tatsuoka, F., Koseki, J. and Tateyama, M. (1995). Performance of geogrid reinforced soil retaining walls during the Great Hanshin-Awaii Earthquake, January 17, 1995. *Proc. Of the 1st International Conference on Earthquake Geotechnical Engineering,* IS-Tokyo'95, Tokyo, Japan, pp 55-62.

142. Tatsuoka, F., Koseki, J. and Tateyama, M. (1996). Performance of reinforced soil structures during the 1995 Hyogo-ken Nanbu Earthquake. Earth Reinforcement, *Third International Symposium on Earth Reinforcement*, IS Kyushu '96, A.A. Balkema, H. Ochiai, N. Yasufuku and K. Omine eds., November 12-14, 1996, Fukuoka, Kyushu, Japan, vol. 2, pp. 973-1008.

143. Tatsuoka, F., Tateyama, M., Uchimura, T. and Koseki, J. (1997). Geosynthetic Reinforced Soil Retaining Walls as Important Permanent Structures, *Geosynthetic International*, Vol4, No.2, pp 81-136.

144. Tatsuoka, F. (2002). Geosynthetic-reinforced soil retaining walls as permanent structures. *Proc. Indian Geotechnical Conference 2002*, Allahabad, India, pp. 681-699.

145. Tatsuoka, F., Tataeyama, M., Mohri, Y. and Matsushima, K. (2007). Remedial treatment of soil structures using geosynthetic-reinforcing technology. *Geotextile and Geomembranes*, Vol. 25, No. 4-5, pp. 204-220.

146. Telekes, G., Sugimoto, M. and Agawa, S. (1994). Shaking table tests on reinforced embankment models. *Proc. 13th International Conference on Soil Mechanics and Foundation Engineering*, New Delhi, India, 2, pp. 649-654.

147. Vidal, H. (1966): La Térré armée (un nouvéau matériau pour lvs travaux pblics). *Annalés de l'ITBTP*, pp. 223-224, Juillet-Aout .

148. Watanabe, K., Munuf, Y., Koseki, J., Tateyama, M. and Kojima, K. (2003). Behaviors of several types of retaining walls subjected to irregular excitation. *Soils and Foundations*, Vol.43, No. 5, pp.13-27.

149. Welch PD. (1967). The use of fast Fourier transform for the estimation of power spectra: a method based on time averaging over short, modified periodograms. *IEEE Transactions on Audio and Electroacoustics*, 15(2):70-3.

150. White, D. M., and Holtz, R. D. (1996). Performance of geosynthetic reinforced slopes and walls during the Northridge, California earthquake of January 17, 1994. *Proc., Int. Symp. on Earth Reinforcement Pract., IS-*

Kyushu '96, Earth Reinforcement Pract., H. Ochiai, N. Yasufuku, and K. Omine, eds., Balkema, Rotterdam, The Netherlands, Vol. 2, pp. 965–972.

151. Wu G. (1994). *Dynamic soil-structure interaction: pile foundations and retaining structures*. PhD thesis, University of British Columbia, Vancouver, Canada.

152. Yogendrakumar, M., Bathurst, R.J., Finn, W.D.L.(1992) Dynamic response analysis of reinforced soil retaining wall. *Journal of Geotechnical Engineering, ASCE*, 118(8), pp.1158-1167.

153. Yoo, C. and Kim, S. (2008). Performance of two-tier geosynthetic reinforced segmental retaining wall under a surcharge load : Full scale load test and 3D finite element analysis, *Geotextiles and Geomembranes*, 26, pp. 460-472.

154. Zarnani S, Bathurst RJ. (2009) Influence of constitutive model on numerical simulation of EPS seismic buffer shaking table tests. *Geotextiles and Geomembranes*, Vol. 27, pp.308-12.

155. Zarnani, S., El-Emam, M.M. and Bathurst, R.J. (2011). Comparison of numerical and analytical solutions for reinforced soil wall shaking table tests. *Geomechanics and Engineering*, Vol.3, No.4, pp.291-321.

Appendix A. HYPERBOLIC MODEL PARAMETERS OF SAND

A.1 INTRODUCTION

The behaviour of sand is nonlinear and dependent on stress acting on it. The stiffness of sand is high at higher confining pressures and low at lower confining pressures. The stress dependent behaviour of sand can be simulated in the numerical models by stress dependent constitutive model using hyperbolic model proposed by Duncan and Chang (1970) following previous works of Kondner (1963) and Jambu (1963). The determination of hyperbolic parameters for the sand by using the procedure suggested by Duncan et al. (1980) is discussed in this appendix.

A.2 NON-LINEARITY AND STRESS-DEPENDENCY OF SOIL

The stress-strain curves of many soils was approximated as hyperbolic by Kondner (1963) who represented the axial strain and deviator stress by the following relationship:

$$(\sigma_1 - \sigma_3) = \frac{\varepsilon}{a + b\varepsilon} \quad \text{(A.1)}$$

in which σ_1 and σ_3 are the major and minor principal stress; ε is the axial strain and a and b are constants whose values could be determined from laboratory triaxial compression test results. The triaxial test results are plotted on transformed axes by taking axial strain ε on x-axis and $\varepsilon/(\sigma_1 - \sigma_3)$ on y-axis, the plot will be linear for soils with truly hyperbolic stress-strain curve. The equation for this line is:

$$\frac{\varepsilon}{(\sigma_1 - \sigma_3)} = a + b\varepsilon \quad \text{(A.2)}$$

The intercept and the slope of the resulting line will give the values of the constants a and b respectively. The parameters a and b physically represent reciprocal of the initial tangent modulus (E_i) and reciprocal of the ultimate (asymptotic) value of the deviator stress $(\sigma_1 - \sigma_3)$ of the soil respectively. The hyperbolic representation of the actual stress-strain curve and transformed plots are shown in Fig.A.1. The values of tangent modulus (E_i) and $(\sigma_1 - \sigma_3)$ are increased with increase in confining pressure. Jambu (1963) showed the relation between tangent modulus and confining pressure by the following relationship:

$$E_i = KP_a\left(\frac{\sigma_3}{P_a}\right)^n \qquad \text{(A.3)}$$

Where σ_3 is the minor principal effective stress in the soil, P_a is the atmospheric pressure expressed in the same pressure units as E_i and σ_3, K is the modulus number and n is the modulus exponent and both are dimensionless numbers.

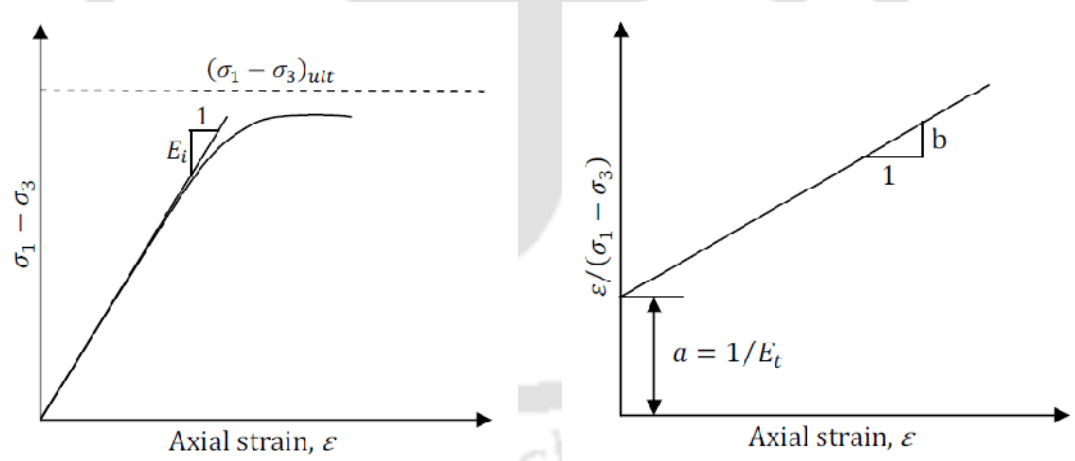

(a) Actual (b) Transformed

Fig.A. 1 Hyperbolic representation of stress-strain curve (after Duncan et al. 1980)

Duncan and Chang (1970) was derived expression for the tangent modulus of soil at any stress level by eliminating the strain term in equation of modulus and by incorporating the Mohr-Coulomb yield criteria and expressed as:

$$E_t = \left[1 - \frac{R_f(1-\sin\phi)(\sigma_1-\sigma_3)}{2(c.\cos\phi+\sigma_3\sin\phi)}\right]^2 K_n.P_a\left(\frac{\sigma_3}{P_a}\right)^n \quad \text{(A.4)}$$

where K_n is the modulus number; n is the modulus exponent; c is the cohesion; σ_1 and σ_3 are the major and minor effective confining stress respectively; ϕ is the angle of internal friction; R_f is the failure ratio; p_a is atmospheric pressure. The failure ratio (R_f) is defined as the ratio between the failure shear stress observed in the laboratory and ultimate (asymptotic) value and expressed as below. R_f is usually considered as the average value from tests at different confining pressures.

$$R_f = \frac{(\sigma_1-\sigma_3)_f}{(\sigma_1-\sigma_3)_{ult}} \quad \text{(A.5)}$$

A.3 HYPERBOLIC MODEL PARAMETERS

This section presents, determination of hyperbolic parameters K, n and R_f for the sand used in pullout test of geotextiles. The data obtained from the triaxial tests are used to obtain these parameters according to procedure described by Duncan et al. (1980).

The real stress stress-strain relationship of a soil usually differs from a hyperbola that causes that causes the transformed plot to diverge from straight line, both at low and high strain values. Duncan et al. (1980) suggested that the values of parameters *a* and *b* can be determined from the straight line passing through the points in hyperbola which matches the stress-strain curve at the 70% and 95% points.

The transformed stress-strain plot of sand used in pullout test is shown in Fig. A. 2 for which actual stress-strain plot is shown in Fig. 3.8. The stress-strain values at 70% and 90% levels are presented in Table A. 1. Table A. 2 presents the values of different parameters evaluated based on transformed plot shown in Fig. A. 2. The hyperbolic model parameter average R_f are determined from the initial modulus (E_i)

obtained from the transformed plot. The other hyperbolic model parameters K and n obtained from Fig. A. 3.

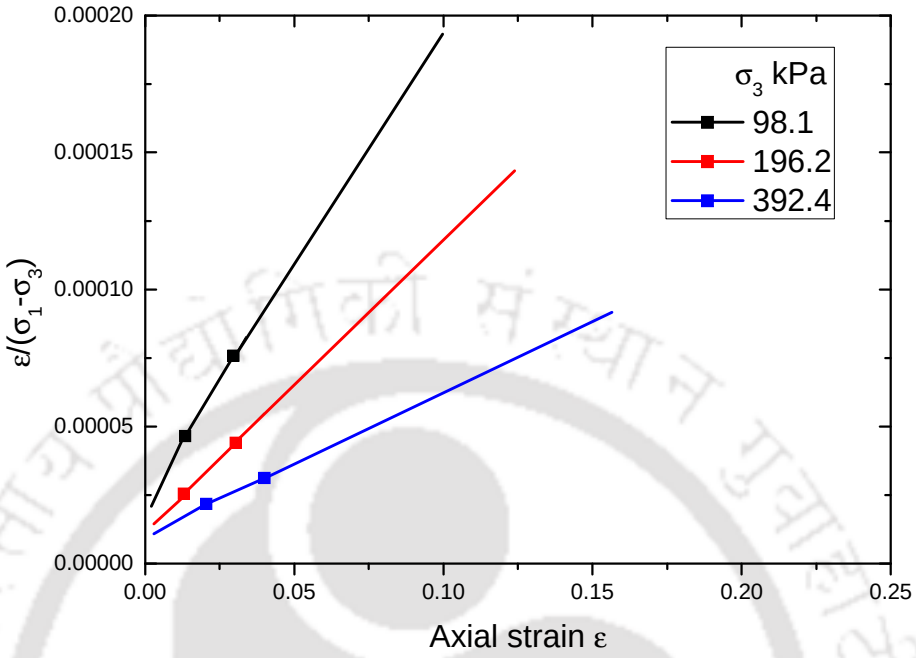

Fig. A. 2 Transformed stress-strain plot for sand

Table A. 1 Stress-strain values corresponding to 70% and 90% stress level

σ_3	$(\sigma_1-\sigma_3)_f$	70% stress level			90% stress level		
		$(\sigma_1-\sigma_3)$	ε_a	$\varepsilon_a/(\sigma_1-\sigma_3)$	$(\sigma_1-\sigma_3)$	ε_a	$\varepsilon_a/(\sigma_1-\sigma_3)$
98.1	412.32	288.624	0.013	4.64E-05	391.705	0.0297	7.58E-05
196.2	726.305	508.414	0.013	2.56E-05	689.990	0.0304	4.41E-05
392.4	1353.428	947.399	0.021	2.17E-05	1285.756	0.0400	3.11E-05

Table A. 2 Hyperbolic parameters value

σ_3	a	b	$E_i=1/a$	$(\sigma_1-\sigma_3)_{ult}$	$(\sigma_1-\sigma_3)_f$	R_f
98.1	0.0000186	0.0018	53763.44	555.556	412.32	0.742
196.2	0.000014	0.0011	71428.57	909.091	726.305	0.799
392.4	0.0000105	0.0005	95238.1	2000	1353.428	0.677
					Average R_f	0.739

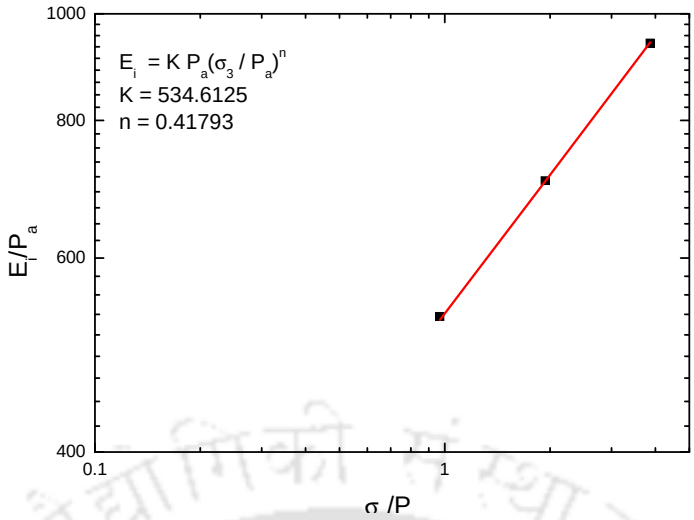

Fig. A. 3 Determination of hyperbolic model parameters

Appendix B. STABILITY ANALYSIS OF REINFORCED SOIL WALLS

B.1. INTRODUCTION

Design and stability analysis of reinforced soil walls is based on various codes as referred in

. For for design of reinforced soil walls, FHWA (2001) recommendations are followed in the study to check the stability of reinforced soil walls. Detail of the analysis is presented in this appendix.

B.2. STABILITY ANALYSIS BASED ON FHWA(2001) RECOMMENDATIONS

The stability analysis of reinforced soil walls comprises two parts (FHWA 2001): external stability and internal stability of wall. External stability analysis involves overall stability of soil mass considering the slip surface outside the reinforced soil. Internal stability consists of evaluating potential slip surface within the reinforced soil mass. External and internal stability analyses are carried out for both static and seismic design of reinforced soil walls.

External stability of reinforced soil walls

The static earth pressures acting on reinforced backfill, due to retained backfill and surcharge acting on retained backfill, and are calculated from Rankine's (1857) earth pressure theory.

The Factors of safety for sliding along base is calculated as below:

$$FS_{sliding} = \frac{\sum Horizontal\ resisting\ forces\ (P_R)}{\sum Horizontal\ driving\ forces\ (P_D)}$$

where horizontal driving forces (P_D) are earth pressures due to retained backfill and surcharge acting over it (Fig.B.1). The horizontal resisting forces (P_R) are the frictional forces developed at the base of the reinforced backfill. The Factors of safety for sliding is calculated at bottom most reinforcement level near the base. For stable reinforced wall Factors of safety for sliding should be more than 1.5.

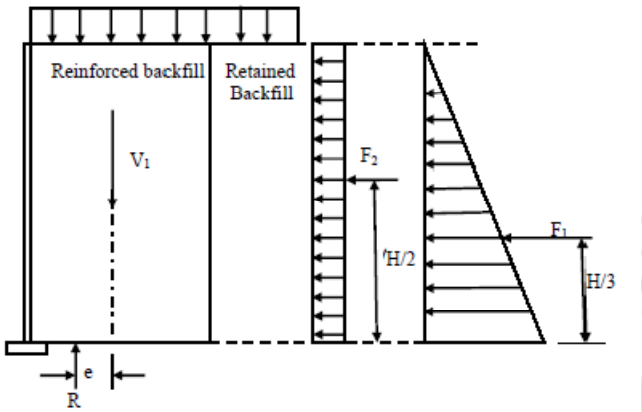

Fig. B.1 Earth pressures due to backfill and surcharge

The Factors of safety due to overturning is calculated from the following relationship:

$$FS_{overturning} = \frac{\sum Resisitng\ moment M_R}{\sum Overturning\ moment M_O}$$

where resisting moment is sum of moments of weight of reinforced backfill about toe of wall and overturning moment is sum of moments of earth pressures due to retained backfill and surcharge over it about toe. The Factors of safety for overturning should more than 2.0.

As the models considered in Chapter 4 are assumed to be resting over hard stratum and foundation settlements are not allowed. The Factors of safety due to bearing capacity failure is not considered.

During an earthquake, the retained backfill exerts an additional horizontal thrust on the reinforced backfill. The horizontal thrust (P_{AE}) due to earthquake is

calculated from pseudo-static Mononobe-Okabe (1929) analysis. Moreover, the reinforced backfill is also subjected to a horizontal inertia force (P_{IR}) due to mass of active portion of the reinforced wall section assumed to be with a base width of 0.5H (Fig.B.2), where H is the height of reinforced soil wall.

$P_{IR} = 0.5A_m\gamma_r H^2$

where

A_m = Maximum ground acceleration coefficient at centroid of reinforced backfill = $(1.45 - A)A_m$

A = Maximum ground acceleration coefficient.

γ_r = Unit weight of reinforced backfill

H = Height of reinforced soil wall.

The 50 percent of seismic thrust (P_{AE}) and full inertial force (P_{IR}) are considered in addition to static forces in seismic design. The reduced P_{AE} is considered because two seismic forces horizontal thrust and inertial forces unlikely to peak simultaneously.

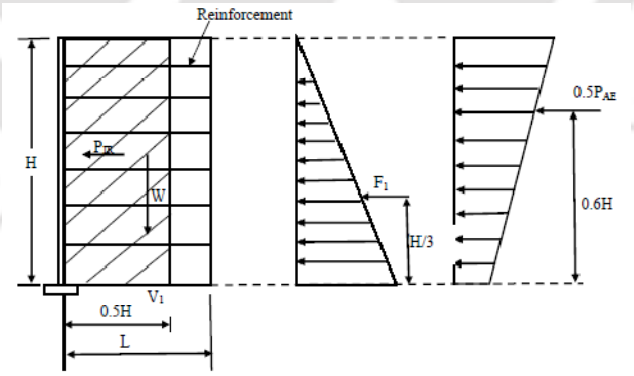

Fig.B.2 Seismic external stability of reinforced soil wall

The factors of safety for sliding and overturning for seismic design are calculated in similar manner as that of static design, considering the dynamic forces in

addition to static forces. The computed Factors of safety for seismic consideration should be equal to greater than 75% of minimum static Factors of safety.

Internal stability of reinforced soil wall

In internal stability design, the potential failure surface assumed to act within reinforced backfill is shown in Fig B.3. The total reinforcement length is divided into two parts. The tensile force acting on each layer of reinforcement is determined from the horizontal stress acting over tributary area of geosynthetic and compared with allowable tensile strength of reinforcement. The force required to pullout out of reinforcements for the soil is calculated and compared with resisting force developed on each layer of reinforcement. The resisting forces developed on each layer of reinforcement are dependent on reinforcement length beyond the potential failure surface. The maximum tension T_{max} per unit width in each layer of reinforcement is:

$T_{max} = \sigma_H A_t$

Where

σ_H = horizontal stress along potential failure line calculated from weight of retained backfill and surcharge acting on it.

A_t = tributary area which is equal to vertical spacing between reinforcing layers.

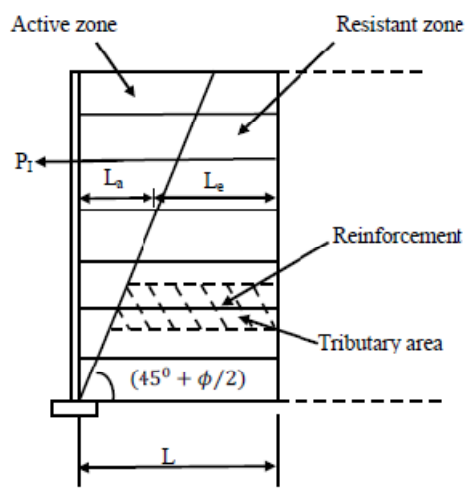

Fig. B.3 Potential failure surface considered for internal stability analysis

By knowing the allowable tensile strength of reinforcement, Factors of safety for rupture is calculated from the following relation:

$$FS_{rupture} = \frac{Allowable\ tensile\ strength\ of\ reinforcement(T_{al})}{Maximum\ tension\ developed\ in\ reinforcement(T_{max})}$$

The resisting force developed on length of reinforcement within resisting zone is as follows:

$$T_{res} = F^{*}\gamma_r Z_p L_e C R_c \alpha$$

Where

F^{*} = Pullout resistance factor

$\gamma_r Z_p$ = The overburden pressure including dead load surcharges and neglecting traffic surcharges

L_e = Embedded length of reinforcement in resisting zone

R_c = Coverage ratio = 1.0 (for mat reinforcement)

α = Scale correction factor

The Factors of safety for pullout is calculated as follows:

$$FS_{pullout} = \frac{Resisting\ force\ on\ reinforcment\ within\ resisting\ zone\ (T_{res})}{Maximum\ tension\ developed\ in\ reinforcment\ (T_{max})}$$

During an earthquake, the dynamic increments (T_{md}) developed within reinforcement due to inertial force (P_I) developed within reinforced zone and is distributed in different reinforcement layer depending on their proportional area within resisting zone.

$$T_{md} = P_I \frac{L_{ei}}{\sum_1^n L_{ei}}$$

where L_{ei} is length of reinforcement within resisting zone.

The total tensile force (T_{total}) is calculated by adding maximum tension (T_{max}) developed and dynamic increment (T_{md}). The dynamic factor of safeties for rupture

and pullout are calculated in similar manner as that of static factor of safeties considering the dynamic increments in addition to static forces.

B.3. STABILITY ANALYSIS OF WRAP-FACED WALL

A 6.0 m high wrap-faced reinforced soil wall as mentioned in Section 4.5 is considered. The model parameters considered for design are list in Table B.1. Factors of safety calculations for external stability and internal stability are shown in Tables B.2 to B.4. As there is no consideration for facing contributions in (FHWA 2001) similar procedure wall followed for stability analysis of rigid faced wall.

Table B.1 Data for stability analysis of wrap-faced reinforced soil wall

Design parameters	Design data
Height of wall	6.0m
Surcharge	5 kPa
Length of reinforcement	4.2m
Spacing between reinforcement	0.5m
Angle of friction for reinforced and retained backfill	38°
Unit weight of soil for reinforced and retained backfill	16 kN/m^3
Ultimate strength of reinforcement	150 kN/m
Maximum ground acceleration coefficient	0.2g
FOS for creep reduction	4
FOS for installation damage	1.1
FOS for durability reduction	1.1
Interaction coefficient	0.8
Coverage ratio (for mat reinforcement)	1.0
Interaction coefficient	0.8
Minimum $FS_{pullout}$	1.5
Minimum $FS_{rupture}$	1.3

Table B.2 External stability calculation for static and seismic design

Horizontal Earth pressures				Vertical Pressure		Point of action					FS (Static)		FS (dynamic)	
Static		Dynamic		Reinf-orced soil, V_1	Surch arge, V_2	Height from base			Distance from facing		$FS_{sliding}$	$FS_{overturning}$	$FS_{sliding}$	$FS_{overturning}$
Retained backfill, F_1	Surchar-ge, F_2	Seismic thrust, P_{AE}	Inertia force, P_{IR}			For F_1	For F_2	For P_{AE}	For V_1	For V_2				
68.51	7.14	54	72	403.2	21.0	2.0	3.0	3.6	2.1	2.1	4.16	5.34	1.80	1.78

Table B.3 Internal stability calculations for static design

No of layer	Height of reinforcement from bottom	Tributary area	T_{max} kN/m	$T_{allowable}$ kN/m	$L_{a(calculated)}$	$L_{e(calculated)}$	$L_{calculted}$	$L_{provided}$	$L_{e(provided)}$	$FS_{rupture}$	$FS_{pullout}$
1	0.5	0.75	16.59	82.64	0.24	0.23	1.24	4.2	3.96	4.98	26.23
2	1	0.5	10.11	82.64	0.49	0.15	1.49	4.2	3.71	8.17	36.72
3	1.5	0.5	9.16	82.64	0.73	0.15	1.73	4.2	3.47	9.02	34.09
4	2	0.5	8.21	82.64	0.98	0.15	1.98	4.2	3.22	10.07	31.43
5	2.5	0.5	7.26	82.64	1.22	0.16	2.22	4.2	2.98	11.39	28.76
6	3	0.5	6.30	82.64	1.46	0.16	2.46	4.2	2.74	13.11	26.05
7	3.5	0.5	5.35	82.64	1.71	0.16	2.71	4.2	2.49	15.44	23.29
8	4	0.5	4.40	82.64	1.95	0.17	2.95	4.2	2.25	18.78	20.44
9	4.5	0.5	3.45	82.64	2.19	0.17	3.19	4.2	2.01	23.96	17.44
10	5	0.5	2.50	82.64	2.44	0.19	3.44	4.2	1.76	33.09	14.10
11	5.5	0.375	1.16	82.64	2.68	0.17	3.68	4.2	1.52	71.27	13.09
12	5.75	0.375	0.80	82.64	2.80	0.24	3.80	4.2	1.40	102.94	8.69

Minimum length of L_e =1.0m

Table B.4 Internal stability calculations for seismic design

No of layer	T_{max} kN/m	T_{md} kN/m	T_{total} kN/m	$T_{allowable}$ kN/m	$L_{a(calculated)}$	$L_{e(calculated)}$	$L_{required}$	$L_{provided}$	$L_{e(provided)}$	$FS_{rupture}$	$FS_{pullout}$
1	16.59	0.28	16.87	82.64	0.24	0.22	0.24	4.2	3.96	4.90	27.52
2	10.11	0.26	10.37	82.64	0.49	0.15	0.49	4.2	3.71	7.97	38.19
3	9.16	0.24	9.40	82.64	0.73	0.15	0.73	4.2	3.47	8.79	35.42
4	8.21	0.22	8.43	82.64	0.98	0.15	0.98	4.2	3.22	9.80	32.64
5	7.26	0.21	7.46	82.64	1.22	0.15	1.22	4.2	2.98	11.07	29.82
6	6.30	0.19	6.49	82.64	1.46	0.15	1.46	4.2	2.74	12.73	26.97
7	5.35	0.17	5.53	82.64	1.71	0.16	1.71	4.2	2.49	14.96	24.06
8	4.40	0.16	4.56	82.64	1.95	0.16	1.95	4.2	2.25	18.13	21.06
9	3.45	0.14	3.59	82.64	2.19	0.17	2.19	4.2	2.01	23.03	17.88
10	2.50	0.12	2.62	82.64	2.44	0.18	2.44	4.2	1.76	31.54	14.34
11	1.16	0.11	1.27	82.64	2.68	0.18	2.68	4.2	1.52	65.31	12.79
12	0.80	0.10	0.90	82.64	2.80	0.25	2.80	4.2	1.40	91.82	8.27

Appendix C. LIST OF PUBLICATIONS

Journals:

1. Bhattacharjee, A. and Krishna A.M. (2014). Strain behavior of soil and reinforcement in wrap faced reinforced soil walls subjected to seismic excitation. *Indian Geotechnical Journal*, DOI 10.1007/s40098-014-0139-x (Accepted).
2. Bhattacharjee, A. and Krishna, A.M., (2014). Effect of backfill on wrap faced reinforced soil wall subjected to seismic excitation. *International Journal of Innovative Research in Science, Engineering and Technology*, Vol. 3(4), pp. 37-42.
3. Bhattacharjee, A., and Krishna, A.M., (2012). Development of numerical model of wrap faced walls subjected to seismic excitation. *Geosynthetics International*, Vol. 19, No. 5, pp. 354-369. DOI: 10.1680/gein.12.00022
4. Bhattacharjee, A., and Krishna, A.M., (2012). Seismic response of rigid faced reinforced soil retaining walls. *International Journal of Geotechnical Earthquake Engineering*, Vol. 3, N o. 2, pp. 1-14. doi:10.4018/jgee.2012070101.
5. Bhattacharjee, A. and Krishna, A.M. (2011), "Behavior of gravity retaining wall subjected to seismic excitation using FLAC 3D", *International Journal of Earth Science and Engineering*, Vol. 04, No 06 SPL, pp 71-74.

Conferences:

1. Bhattacharjee, A. and Krishna, A.M. (2014). Strain localization in rigid faced walls under seismic excitation. *Proc. Indian Geotechnical Conference 2014*, Kakinada, India, 18-20 December 2014, pp. 445-452.
2. Bhattacharjee, A. and Krishna, A.M. (2013). Strain behavior in backfill soil of rigid faced reinforced soil walls under seismic shaking *Proc. Indian Geotechnical Conference 2013*, Roorkee, India, 22-24 December 2013.
3. Bhattachajee, A. and Krishna, A.M. (2013). Strain behaviour of backfill soil of wrap faced reinforced soil walls: A numerical study. *Advances in Geotechnical Infrastructure*, Edited by C. F. Leung, S. H. Goh & R. F. Shen, ISBN: 978-981-07-4948-4 :: doi:10.3850/978-981-07-4948-4 104 (accepted)

4. Bhattacharjee, A. and Krishna, A.M. (2012). Behaviour of rigid faced reinforced walls with strip reinforcement using 3D models. *Proc. Indian Geotechnical Conference 2012*, Delhi, India,13-15 December 2012, Vol. 2, pp. 684-687.
5. Prashanth, V., Bhattacharjee, A. and Krishna, A.M. (2011). Soil-Geosynthetics Interaction Behaviour in Oblique Direction. *Proc. International Conference on Advances in Geotechnical Engineering*, 7-9 November 2011, Perth, Australia (Accepted).
6. Bhattacharjee, A. and Krishna, A.M. (2011). Numerical modelling of wrap faced reinforced soil walls under seismic shaking. *Proc. 14th Asian Regional Conference on Soil Mechanics and Geotechnical Engineering*, 23-27 May, 2011, Hong Kong, China.
7. Bhattacharjee, A., Prashant V. and Krishna, A.M. (2011). Numerical modelling of pull out test for reinforcement in oblique direction. *Proc. of Indian geotechnical Conference*, December 15-17, Kochi (paper No. N-246), Vol.II, pp 891-894.
8. Bhattacharjee, A. and Krishna, A.M. (2010). Numerical modeling of rigid faced reinforced soil walls under seismic shaking. *Proc. of Indian Geotechnical Conference 2010*, Geotrendz, IIT Bombay, Dec.16-18, 2010, pp.869-872.
9. Bhattacharjee, A. and Krishna, A. M. (2009), "Study of seismically induced permanent displacement of gravity retaining wall", Proc. of Indian Geotechnical Conference 2009, Geotide, Guntur, Dec.17-19 2009, pp. 627-631.